INVESTIGATIONS ON LOW DIELECTRIC LOSS LITHIUM BASED CERAMICS AND THEIR COMPOSITES FOR MICROWAVE AND EMBEDDED PASSIVE APPLICATIONS

THESIS SUBMITTED TO THE UNIVERSITY OF KERALA IN PARTIAL FULFILMENT OF THE REQUIREMENT FOR THE DEGREE OF

DOCTOR OF PHILOSOPHY IN PHYSICS

BY

SUMESH GEORGE

Under the Guidance of

Dr. M. T. Sebastian

NATIONAL INSTITUTE FOR INTERDISCIPLINARY SCIENCE AND TECHNOLOGY
THIRUVANANTHAPURAM-695 019
KERALA, INDIA

DECEMBER 2009

Dedicated to my Parents…

DECLARATION

I hereby declare that the matter presented in the thesis entitled **"INVESTIGATIONS ON LOW DIELECTRIC LOSS LITHIUM BASED CERAMICS AND THEIR COMPOSITES FOR MICROWAVE AND EMBEDDED PASSIVE APPLICATIONS"** *is the outcome of investigations carried out by me under the supervision of Dr. M. T. Sebastian, Scientist 'G', Materials and Minerals Division, National Institute for Interdisciplinary Science and Technology (Formerly Regional Research Laboratory) (CSIR), Thiruvananthapuram, India and the results embodied here has not been submitted elsewhere for the award of any other degree.*

Thiruvananthapuram *Sumesh George*

http://w3.rrlt.csir.res.in

Fax: ++91-(0) 471-2491712
Phone: 4712515294 (O), 471-2446901 (R)
E-Mail: mailadils@yahoo.com.
mtsebastian@niist.res.in.
Council of Scientific & Industrial Research
NATIONAL INSTITUTE FOR INTERDISCIPLINARY SCIENCE AND TECHNOLOGY
THIRUVANANTHAPURAM- 695019. INDIA

Dr. M. T. SEBASTIAN
Scientist-G & Deputy Director

CERTIFICATE

This is to certify that this thesis entitled "INVESTIGATIONS ON LOW DIELECTRIC LOSS LITHIUM BASED CERAMICS AND THEIR COMPOSITES FOR MICROWAVE AND EMBEDDED PASSIVE APPLICATIONS" is an authentic record of the investigations carried out by Mr. Sumesh George at the Materials and Minerals Division of National Institute for Interdisciplinary Science and Technology (Formerly Regional Research Laboratory) (CSIR), Thiruvananthapuram, India, under my supervision and guidance. This thesis or any part thereof has not been submitted elsewhere for the award of any other degree.

Thiruvananthapuram

Dr. M. T. Sebastian
(Supervisor)

CONTENTS

CHAPTER 2

Synthesis and Characterization of Dielectric Substrates, Resonators, and Composites

CHAPTER 3

Low Temperature Sintering and Microwave Dielectric Properties of Li_2ASiO_4 (A = Mg And Ca) Ceramics for LTCC Substrate Applications.

CHAPTER 4

Microwave Dielectric Properties of Novel Temperature Stable High Q $Li_2Mg_{1-X}Zn_xTi_3O_8$ and $Li_2A_{1-X}Ca_xTi_3O_8$ (A=Mg, Zn) Ceramics

CHAPTER 5

Effect of Borosilicate Glass Fluxing in $Ca[(Li_{1/3}A_{2/3})_{1-x}Ti_x]O_{3-\delta}$ (A=Nb,Ta) Complex Perovskite Ceramics

CHAPTER 6

Dielectric Response of $Ca[(Li_{1/3}Nb_{2/3})_{0.8}Ti_{0.2}]O_{3-\delta}$ Ceramic Filled Polymer Composites

Preface

The rapid developments in the microelectronic industry accelerate the search for new material with innovative properties which can fulfill the requirements of technological advances. The dielectric ceramics play a prominent role in telecommunication and satellite broadcasting industry for its potential advantages such as reliability, ease of integration, good dielectric properties and excellent performance. The basic requirements of materials for RF applications are low dielectric loss, optimum relative permittivity and nearly zero temperature coefficient of resonant frequency. In electronic industry, dielectric materials are being used as electronic packages, substrates, dielectric resonators, waveguides, dielectric antennas and capacitors etc. The distinction between these applications is basically based on the permittivity value of the dielectric material. The thesis entitled "**INVESTIGATIONS ON LOW DIELECTRIC LOSS LITHIUM BASED CERAMICS AND THEIR COMPOSITES FOR MICROWAVE AND EMBEDDED PASSIVE APPLICATIONS"** divided into 8 chapters. It is the outcome of a detailed investigation carried out on the synthesis and characterization of several low loss ceramics and composites for substrate, LTCC, dielectric resonator and capacitor applications.

The first chapter of the thesis gives a general introduction to dielectric substrates, resonators and composites. Emerging technologies such as low temperature co-fired ceramic and embedded capacitor technology for miniaturization and its requirements and advantages are also discussed in this chapter. The preparation and characterization techniques used for the microwave dielectric ceramics and polymer ceramic composite are given in the chapter 2.

The chapter 3 discusses the synthesis, characterization and microwave dielectric properties of novel low loss low permittivity Li_2ASiO_4

(A=Mg and Ca) ceramics for microwave substrate applications. The effects of synthesis condition on the microwave dielectric properties of both the ceramics are discussed. The influence of different borosilicate glass additions on the sinterability, densification, structure, microstructure and the microwave dielectric properties of the Li_2ASiO_4 (A=Mg and Ca) dielectric ceramics has been investigated. These ceramics show relative permittivity in the range 4-9 with low dielectric loss (tan $\delta \approx 10^{-4}$). Compared to LCS-glass composites, the LMS-glass composites show excellent microwave dielectric properties at a low sintering temperature and can be a promising candidate for substrate and LTCC based devices.

Fourth chapter discusses the synthesis, characterization and microwave dielectric properties of novel temperature stable high Q dielectric ceramics ($Li_2Mg_{1-x}Zn_xTi_3O_8$ (x=0 to 1) and $Li_2A_{1-x}Ca_xTi_3O_8$ (A=Mg, Zn, and x= 0 to 0.2) which can be sintered at a low sintering temperature of 1075 ^oC/4hrs. An attempt has also been made to lower the sintering of $Li_2MgTi_3O_8$ and $Li_2ZnTi_3O_8$ ceramics for possible application in LTCC based devices. Among all the compositions of $Li_2Mg_{1-x}Zn_xTi_3O_8$ ceramics, the $Li_2Mg_{0.9}Zn_{0.1}Ti_3O_8$ dielectric ceramic composition shows the best dielectric properties such as ε_r = 27, Q_u x f = 62000 GHz, and τ_f = (+) 1.2 ppm/^oC when sintered at 1075 ^oC/4hrs. The effect of Ca substitution on the structure and microwave dielectric properties of $Li_2A_{1-x}Ca_xTi_3O_8$ (A=Mg, Zn, and x= 0 to 0.2) has been investigated and it is found that formation of second phase degrades the microwave dielectric properties slightly. Effect of LMZBS glass addition on the sinterability and microwave dielectric properties of $Li_2MgZnTi_3O_8$, $Li_2MgZnTi_3O_8$ dielectric ceramics has been investigated for LTCC applications. The microwave dielectric materials presented in this chapter are superior in terms of cost of raw materials, sintering temperature and microwave dielectric properties compared to the already known

dielectric ceramics and these materials may be a major milestone in microwave dielectric resonator research.

The development of low temperature sintered low loss high permittivity microwave ceramics for resonator applications are discussed in the fifth chapter. The influence of various borosilicate glasses on the sinterability, densification, structure and microstructure and the microwave dielectric properties of the $Ca[(Li_{1/3}A_{2/3})_{1-x}Ti_x]O_{3-\delta}$ (A=Nb,Ta) dielectric ceramics is investigated. The temperature coefficient of the CLNT-glass and CLTT-glass system are tuned in the range ± 10 ppm/^oC by increasing the rutile content in the CLNT and CLTT ceramics. Compared to CLTT-glass system, the CLNT-glass system shows excellent temperature stable microwave dielectric properties when sintered at a relatively low temperature of about 950 ^oC.

Sixth chapter discusses the preparation and dielectric properties $Ca[(Li_{1/3}Nb_{2/3})_{0.8}Ti_{0.2}]O_{3-\delta}$ ceramic filled polymer composites for substrate applications. The physical and dielectric properties of the composites are investigated in terms of volume fraction of filler, frequency, and temperature. The experimentally observed relative permittivity and dielectric loss are compared with different theoretical models. The predicted relative permittivity of this composite using Lichtenecker and EMT model is in agreement with experimentally observed results. Coplanar Waveguide Fed monopole Antenna was designed and fabricated using epoxy-CLNT polymer-ceramic composite and compared the return loss characteristics with standard FR-4 epoxy.

The high permittivity ceramic-metal and polymer-ceramic-metal composites for capacitor applications are discussed in chapter seven. The effect of sintering temperature on the percolation threshold and the dielectric properties of $Ca[(Li_{1/3}Nb_{2/3})_{0.8}Ti_{0.2}]O_{3-\delta}$ (CLNT) – Ag composite

for LTCC based high permittivity application is discussed in the first section and the polymer based CLNT-epoxy-Ag three phase composite for printed wiring board compatible embedded capacitor application is discussed in the next section. The experimentally observed relative permittivity of ceramic-metal and polymer-ceramic-metal composites is in agreement with power law.

The major results of the present investigation and the scope for future work is presented in chapter eight. Tape casting of the LTCC ceramics for multilayered structures and the design and fabrication of microstrip antenna using the tape would be of great scientific and technological importance. Present work reports several temperature stable, low loss, high permittivity ceramics. The Design and fabrication of dielectric resonator antennas having different geometries (Hemispherical and Conical) using these ceramics and polymer-ceramic composite are the hot topics to be pursued.

✯----------*ACKNOWLEDGEMENTS* ----------✯

I present this thesis, in the name of God, the Almighty, and my Source of Wisdom, who showers HIS unperturbed blessings undeservingly upon me throughout my life.

I would like to express my unfathomable gratitude to my supervisor, Dr.M.T. Sebastian (Scientist G, National Institute for Interdisciplinary Science and Technology (NIIST), Thiruvananthapuram). His wide knowledge, dedication, serious research attitude and logical way of thinking have been of great value for me. His constant inspiration, effective guidance, creative discussions, timely advice and support helped me a lot in formulating the thesis in time.

I am grateful to Prof. T. K. Chandrasekhar, Dr. B. C. Pai, (former Directors) and Dr. Suresh Das, Director, NIIST for kindly providing the facilities for the research work.

I am gratefully acknowledge Dr. Jose James (Scientist F, NIIST), Dr. Manoj Raama Varma (Scientist E-II, NIIST), and Dr. N. Santha for fruitful scientific discussions and advices during my work.

I am deeply indebted to Dr. K. G. K. Warrier (Head, Materials and Minerals Division, NIIST, Thiruvananthapuram), Dr. U. Syamaprasad, Dr. Peter Koshy and Dr. P. Prabhakar Rao (Scientists, MMD, NIIST, Thiruvananthapuram) for their help given during the course of this work.

The creative suggestions, valuable advice and help given by my seniors in the lab, Dr. H. Sreemoolanadhan (Scientist, VSSC), Dr. K. P. Surendran (University of Aviero, Portugal), Dr. P. V. Bijumon (Research in Motion, Canada), Dr. L. A. Khalam (Sel. Grade Lecturer, Iqbal College, Thiruvananthapuram), Dr. P. S. Anjana, (Lecturer, All Saints College, Thiruvananthapuram), and Dr. G. Subodh (University of Stuttgart, Germany) are greatly acknowledged.

I thank my fellow labmates in Fine Ceramic group: Ms. Sherin Thomas, Mr. Tony Joseph, Ms. T. S. Sasikala, Mr. Dhanesh Thomas, Mr. M. A. Sanoj, Mr. K. M. Manu, Ms. K. S. Deepa, Mr. K. Jithesh, Ms. J. Chameswary, Ms. P. Nisha, Ms. C. P. Reshmi, Ms. P. Neenu Lekshmi, Ms .V. Madhumitha, and Mr. V. Jobin for their support and stimulating discussions. I am also thankful to my former colleagues in fine ceramics, Dr. P. C. Rajath Varma, Mr. V. K Sajith, Ms. R. Rejini, Ms. B. R. Priya Rani, K. S. Sandhya, Ms. Ali Fathima and Ms. S. Renjini for their love and support. I cherish the companionship of Mr. Alex Andrews, who made my days at NIIST and Thiruvananthapuram a memorable one.

I would like to thank Defence Research Development Organization (DRDO) and Council of Scientific and Industrial Research (CSIR), Government of India for providing me the research fellowship.

I am indebted to Mr. M. R. Chandran, Mr. P. Gurusamy, Mr. S. G. K. Pillai, Mr. Veluswamy and Mr. P. Mukundan for extending the SEM, XRD and thermal measurement facility for my research work. I am thankful to all the office and library staff at NIIST for all their help and cooperation.

I wish to express my deep sense of gratitude to Prof. P. Mohanan (Department of Electronics, CUSAT, Cochin) and Dr. Jacob Philip (Sophisticates Test Instrument Centre, CUSAT, Cochin) for creative scientific discussions on dielectric and thermal conductivity measurements.

I would like to extend my sincere gratitude to Dr. R. Ratheesh, Scientist, and Dr. S. Rajesh (C-MET, Thrissur) for the valuable help in my research.

I would like to express my thanks to Prof. J. Krupka, Warsaw Institute of Technology, Poland, for microwave measurements.

The favors rendered by Mr. V. Deepu and Mr. Sujith Raman (Department of Electronics, CUSAT), are greatly acknowledged.

I owe an unlimited debt of gratitude to my parents, who stood with me and supported me in my thick and thin times, with understandability, love, encouragements and prayers when it needed most. A special gratitude goes to my brother, my sister and their families for the unending support and encouragement in the successful completion of this thesis. I also extent my heart felt thanks to all my relatives, especially to Mr. M. D. Sebastian, who had enlightened my path with valuable advice, support and encouragements.

I do express my deepest gratitude to my grand parents for their prayers and love. At this time of happiness a special acknowledge is rendered to my grandma who is no more with me.

Last but not least, I need to express my appreciation to all those who have helped and inspired me during my doctoral study. The support from all these people gave me a lot of confidence throughout those countless hard-working days.

Sumesh George

Chapter-1

Microwave Dielectric Ceramics and Composites

This chapter discusses how the dielectrics are pivotal to the applications in microwave and embedded passive devices. A general introduction about the scientific and technological aspects of low permittivity dielectrics for substrate applications and the fundamental aspects, working principle and applications of dielectric resonators are discussed. Emerging technologies such as low temperature co-fired ceramic and embedded capacitor technology and their requirements and advantages are also discussed in this chapter.

1.1 Introduction to Microwave Communication

The ability to communicate with people while on the move has evolved remarkably since Marconi first demonstrated radio ability to provide continuous contact with ship sailing the English channel. This was in 1897, and since then new wireless communications methods and services have been enthusiastically adopted throughout the world. Particularly during the last two decades, the mobile radio communication industry has grown orders of magnitude, fueled by digital and RF circuit fabrication improvements, new large scale circuit integration, and other miniaturization technologies [1]. Historically the mobile communication has come slowly, and has been coupled closely to technological improvements [2]. The ability to provide wireless communication to an entire population was not even conceived until BEL laboratories developed the cellular concept in 1970's and wireless communication era was born in the 1970's. Wireless communication network have now become much more pervasive than anyone could have imagined when the cellular concept was first developed in the 1970's. Wireless technology is a truly revolutionary paradigm shift, enabling multimedia communications between people and devices from any location.

Wireless is a term used to describe telecommunications in which electromagnetic waves carry the signal over part of the entire communication. For wireless communication, a high frequency is desirable since the amount of information communicated directly scales with frequency. Today, microwave techniques have been increasingly adopted in radio astronomy, long distance communications, space navigation radar systems, medical equipments and missile electronic systems. With the increase in demand for exchanges of information via wireless communications, needs for communication systems using microwaves are

increasing. The term microwave seems to have first appeared in the paper by Nello Carrara in the first issue of Alta Frequenza in 1932. A credible definition came from Pozar's text microwave engineering, which states that the term microwave refers to alternating current signals with frequencies between 300 MHz to 300 GHz [3]. The existence of electromagnetic waves of which microwaves are part of the higher frequency spectrum, was predicted by James Clark Maxwell in 1868. In 1888, Heinrich Hertz was the first to demonstrate the existence of electromagnetic waves by building apparatus to produce radio waves. Microwaves are easier to control because small antenna could direct the waves as well. One advantage of such control is that the energy could be easily confined to tight beam. This beam could be focused on another antenna several kilometers away, making it difficult for someone to intercept the conversation. Another characteristic is that because of their high frequency, greater amount of information could be put on them. Both these advantageous (narrow beam width and modulation bandwidth) make microwaves very useful for RADAR as well as communications [4]. The telecommunication industry is one of the largest and rapidly growing industries with more than 1.5 trillion dollars in annual revenues for services and equipment. There are about 3.6 billion mobile phone subscribers worldwide which is more than half of the world population. The mobile phones operate in the range of 0.8 to 2 GHz. Frequencies from about 100 MHz to 2 GHz are used for communicating with low earth orbit satellites (LEOs) and 6-24 GHz are useful frequencies for geostationary satcoms. With continuing advances in microwave devices, more systems are being developed for millimeter portion of the microwave band. Figure 1.1 shows the microwave spectra and its applications.

The recent explosive growth in the wireless communication industry led to tremendous demand for novel low dielectric loss microwave

components. In wireless communication systems, a variety of dielectric ceramics have been utilized for microwave dielectric applications [5].

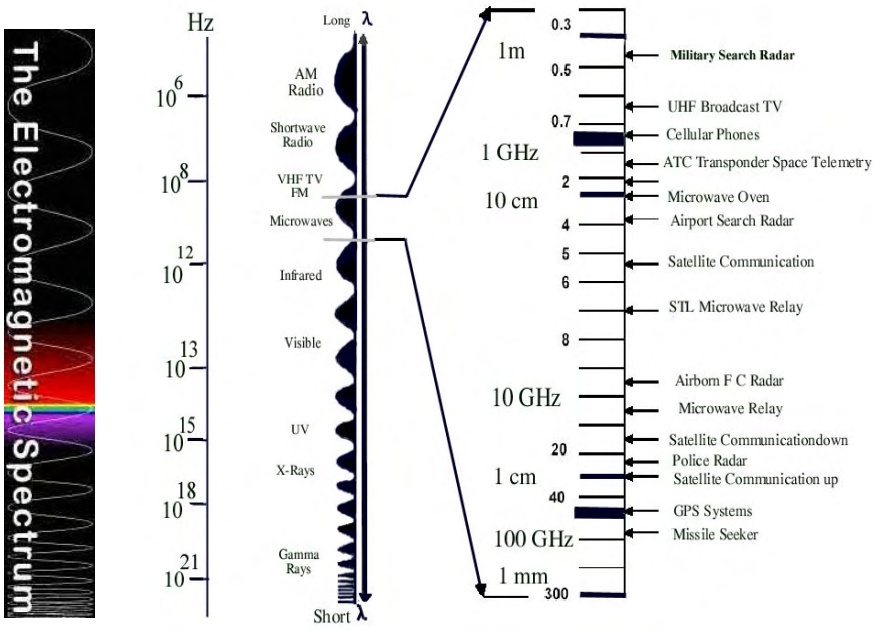

Fig. 1.1 microwave spectra and its applications (Ref. 5)

1.2 Role of Dielectrics in Microwave Applications

From a historical perspective, guided electromagnetic wave propagation in dielectric media received much attention in the early days of researching microwaves. The dielectric ceramics play a prominent role in telecommunication and satellite broadcasting industry for its potential advantages such as reliability, ease of integration, good dielectric properties and excellent performance [6]. In electronic industry, dielectric materials are being used as electronic packages, substrates, dielectric resonators, dielectric waveguides, dielectric antennas, capacitors etc.

1.2.1 Electronic packaging applications

The international technology roadmap for semiconductor (ITRS) predicts the necessity of low permittivity materials for interlayer dielectrics

as the components in the electronic modules increases according to Moor's law. The ITRS lists the development of low permittivity materials as one of the key five difficult challenges through 2009 for the semiconductor industry [7]. Moor's law predicts that the number of components in a module doubles in two years. The propagation delay time (t_d) of electromagnetic waves in a dielectric is given by the equation,

$$t_d = \frac{l\sqrt{\varepsilon_r}}{c} \text{------(1.1)}$$

where l is the line length, ε_r is the relative permittivity of the substrate and c is the speed of light [5]. For electronic packaging application the relative permittivity should be as low as possible. The relative permittivity less than 3 is generally accepted for packaging applications.

1.2.2 Substrate application

Microstrip patch antennas are resonant radiating structures that can be printed on circuit boards. Microstrip antennas comprise a radiator element commonly referred to as a patch. Microstrip patch antennas usually comprise just one square or circular metal antenna element attached to a low-loss dielectric substrate. The equations of electromagnetic waves derived from Maxwell equations is

$$\nabla^2 E = \frac{1}{c^2}\frac{\partial^2 E}{\partial t^2} \text{------(1.2)} \qquad \nabla^2 H = \frac{1}{c^2}\frac{\partial^2 H}{\partial t^2} \text{------(1.3)}$$

where E is the electric field, H is the magnetic field strength and c is the velocity of electromagnetic wave in vacuum [8].

If the medium is dielectric, then the velocity of electromagnetic waves through a dielectric medium is given by $v \propto (\mu\varepsilon_r)^{-1/2}$. Hence the value of relative permittivity (ε_r) greatly affects the speed of electromagnetic waves in a dielectric medium. Hence low permittivity is preferred in this aspect.

However, the width of the microstrip patch antenna [9], is given by the equation ,

$$w = \frac{c}{2 f_o \sqrt{\frac{(1+\varepsilon_r)}{2}}} \text{------(1.4)}$$

where ε_r is the permittivity of the substrate.

Hence as a compromise between the speed and the dimension, for a substrate material, the relative permittivity should be in the range of 4-15 is preferred.

1.2.3 Dielectric resonator application

A dielectric resonator is an electronic component that exhibits resonance for a narrow range of frequencies, generally in the microwave band. Dielectric ceramics are widely used as dielectric resonators and dielectric filters which are mounted to electronic devices such as in mobile phones, personal radios and satellite receivers. The use of dielectrics in microwave communication reduces substantially the overall dimensions of microwave circuits [5]. A high ε_r facilitates circuit miniaturization because the wavelength inside the DR is inversely proportional to the square root of its permittivity as given by the equation.

$$\lambda_d = \frac{\lambda_o}{\sqrt{\varepsilon_r}} \text{------(1.5)}$$

where λ_d is the wavelength in the dielectric, λ_0 is the wavelength in air (actually in vacuum). The dimension of the dielectric sample must be an integral multiple of half-wavelength in the dielectric to resonate in the simplest fundamental mode. If that wavelength is reduced, then the physical dimensions of the resonator must be reduced as well. When microwaves enter a dielectric material, they are slowed down by a factor roughly equal to the square root of the permittivity which implies that the wavelength

decreases by the same amount and the frequency is unaffected as shown in Fig. 1.2.

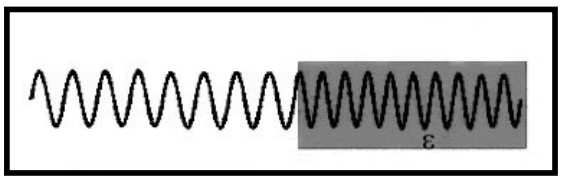

Fig. 1.2. The wave length reduced by a factor $(\varepsilon_r)^{1/2}$ when the wave enters in the dielectric medium. (Ref. 5)

1.2.4 Capacitor application

Capacitors are the indispensable components in all the electronic devices. Basic function of the capacitor is to charge and discharge during its operation. The value of permittivity determines the charge storage capacity of the capacitor. The capacitance C is given by the equation,

$$C = \frac{\varepsilon_o \varepsilon_r A}{d} \text{------(1.6)}$$

where ε_o and ε_r are the permittivity of the vacuum and relative permittivity of the dielectric material, A is the area of the electrode material and d is the thickness of the dielectric material. Hence, high permittivity dielectric material is preferred for miniaturization of the electronic devices [10].

The scope and breadth of dielectric ceramic material usage in electrical circuitry related electronic packaging and allied electro ceramics applications have expanded significantly during the last decades and the dielectric ceramic is an essential components in the microelectronic industry.

1.3 Physics of Dielectrics

Fundamentally, a dielectric is an insulating but polarizable material in an applied electric field. Such materials usually find uses as either capacitors or microwave resonators. The dielectric is characterized by relative permittivity (ε_r). The relative permittivity is the measure of the polarizability of the materials [11]. Important applications of microwaves result from their interaction with various types of materials. The interaction

of electromagnetic waves with dielectric materials causes a net polarization of the substance. There are several mechanisms which are responsible for this occurrence, including: interfacial (space-charge), molecular (dipole), ionic and electronic polarization. For a given material, the sum of the contributions from each mechanism determines the net polarization, P, of the dielectric material.

$$P=P_{electronic}+P_{ionic}+P_{molecular}+P_{interfacial}$$

Interfacial (space charge) polarization: Piling up of mobile charge carriers at physical barriers such as grain boundaries is the cause of interfacial polarization (space charge). At low frequency the mechanism give rise to high relative permittivity and in some cases may extend up to ~10^3 Hz.

Dipolar (molecular) polarization: In zero fields the dipoles will be randomly oriented and thus carry a polarization. When an electric field is applied, the dipoles will tend to align in the direction of applied field and the materials will acquire a net dipole moment. This is called orientational polarization. It is temperature dependent. With increase in temperature the thermal energy tends to randomize the alignment.

Ionic polarization: During chemical bonding the atom may acquire an excess of positive or negative charge and form an ionic bond. The displacement of positive and negative ions with respect to each other due to the application of electric field gives rise to ionic polarization.

Electronic polarization: When an electric field is applied the valence electron cloud shifts with respect to nucleus. This occurs at high frequency (~10^{15} Hz). It is independent of temperature. Electronic polarization is present in all materials and it does not contribute to conductivity or dielectric loss in most dielectrics. Electronic polarization is responsible for the optical refractive index, η and is a part of relative permittivity in all materials.

Figure 1.3 shows the frequency dependence of polarization. It is clear that the ionic and electronic polarization contributes to dielectric properties at microwave frequencies.

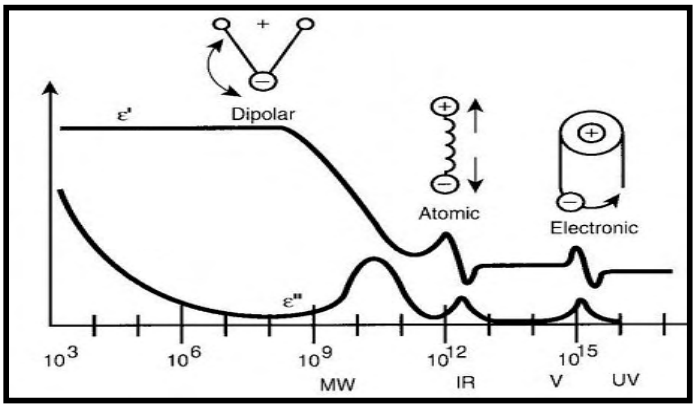

Fig. 1.3 The frequency dependence of polarization. (http://en.wikipedia.org/wiki/Dielectric_spectroscopy)

1.4 Microwave Dielectric Substrates; a Brief History

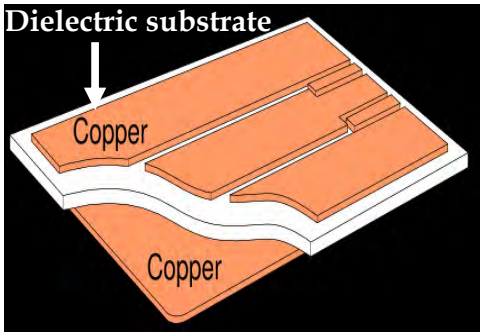

Fig. 1.4 Schematic representation of a substrate. (en.wikipedia.org)

A substrate is composed of ceramic or a composite material, on or within which electronic components are placed. Substrates have been used for hybrid integrated circuits (HIC) and for packaging semiconductor IC chips [10, 12]. Dielectric substrates are also used for fabricating transmission line media, including microstrip, strip line, coax and even waveguide. Important characteristics required for substrate applications are (i) low

relative permittivity (to increase signal speed) (ii) Low dielectric loss (for selectivity) (iii) high thermal conductivity (to dissipate heat) (iv) low or matching coefficient of thermal expansion to that of the materials attached to it, and (iv) low temperature coefficient of relative permittivity [13]. Dielectric substrate materials are classified into hard substrates and soft substrates. Fig. 1.4 shows the schematic representation of a substrate.

1.4.1 Hard Substrates

Hard substrates are ceramics such as alumina, aluminum nitride and beryllium oxide which can withstand extreme heat during wirebonding [10]. The market for these ceramic substrates has increased in recent years with the development of electronic industry. The development of hybrid circuits has given rise to the need for a substrate with a very smooth surface, available as thin flat plates and mechanically strong. A high thermal conductivity is also necessary since the miniaturization of components leads to high energy densities. For electronic applications steatite and alumina have been used as the substrate for its high mechanical strength and lower dielectric losses. The physical and dielectric properties of various dielectric substrates are shown in Table 1.1.

Alumina: Alumina and aluminous porcelain have good mechanical strength, resistivity, low dielectric loss and particularly thermal conductivity. Their thermal stability and freedom from crystallographic transitions enable them to survive the heat treatment involved in metallization and component formation with negligible dimensional distortion and without degradation of surface smoothness. One disadvantage of pure alumina is its high sintering temperature. Alumina containing small amount of manganese, chromium, or cobalt oxide can be sintered at a lower sintering temperature (1400 ^{o}C) in air and is widely used for packaging applications.

Beryllia: Beryllium oxide is well known as a ceramic having high thermal conductivity about eight times as high as alumina ceramics. Its main disadvantages are its high cost, toxicity while processing, lack of adequately smooth flat surface. Beryllia has found considerable use as substrate for high power semiconducting devices such as rectifier but is not widely used as a substrate for hybrid circuits.

Steatite: Steatite of which the principle constituent is magnesium silicate has a high thermal conductivity and thermal expansion close to that of commonly used metals. It can also be pressed directly into complex shapes which meet dimensional tolerances. It has low dissipation factor and low temperature coefficient of capacitance. Steatite has been widely used as a structural material in electronic devices and as dielectric.

Aluminium Nitride: Aluminium nitride is now available commercially in the form of substrates. Its thermal conductivity is intermediate between those of alumina and beryllia. Its thermal expansion is low and close to that of silicon. It may therefore find applications as base for silicon integrated circuits with high power dissipations.

Quartz: Thin slice of single crystal quartz is used as substrates for hybrid circuits operating at higher frequencies. Low permittivity minimizes the coupling between the components and conductors on the surface and low dissipation factor is essential at their frequencies.

Last two decades have witnessed an immense research on the development of low permittivity materials. Forsterite (Mg_2SiO_4), Cordierite ($Mg_2Al_4Si_5O_{18}$), Mullite (Al_2SiO_5), Wollastonite ($CaSiO_3$), and Spinel aluminates ($MgAl_2O_4$ and $ZnAl_2O_4$) has been developed as hard substrates [5, 10, 14-16].

Table 1.1. The physical and dielectric properties of various dielectric substrates. (Ref. 10)

Materials	Permittivity	Dissipation factor (10^{-4})	Resistivity (Ωm)	Thermal Conductivity ($Wm^{-1}K^{-1}$)	Thermal Expansion (10^{-6} K^{-1})
Alumina	9.9	1	$>10^{12}$	37	6.6
Beryllia K 120	6.6	2	10^{13}	208	9.2
Steatite	6	8 to 40	10^{15}	3.5	7.8 to 10.4
Aluminium Nitride	10	20	10^{9}	155	2.7
Quartz	4.5	2	10^{12} to 10^{14}	8.5	10
Forsterite Mg_2SiO_4	5.8 to 6.7	4 to 10	10^{15}	1.6 to 4.2	10.6
Spinel $MgAl_2O_4$	7.5	4	10^{9} to 10^{10}	7.6	6.6

1.4.2 Soft Substrates

Soft substrates are used in applications where packaged parts are soldered on the board [12]. Generally, the polymers are used as soft substrates. Polymers like polytetrafluroethylene (PTFE), polyethylene, polystyrene, poly-ether-ether-ketone and epoxy shows excellent dielectric properties. However, their low thermal conductivity and high thermal expansion limits their application as substrate in electronic modules. A third category of substrate materials is the composites in which the soft substrates are loaded with particles of hard ceramics.

1.5 Composites

Composite materials are engineered materials made from two or more constituent materials with significantly different physical or chemical properties and which remain separate and distinct on a macroscopic level

within the finished structure [17]. There are two categories of constituent materials: matrix and reinforcement. At least one portion of each type is required. The matrix material surrounds and supports the reinforcement materials by maintaining their relative positions. The reinforcements impart their special mechanical and physical properties to enhance the matrix properties. The major advantages of composites are attainment of unique combination of properties and properties can be made to vary continuously over a range. Another important property is that the composite can achieve some physical properties which are not attainable independently by its constituents.

1.5.1 Connectivity

Making ceramic polymer composites not only involves choosing of right material but also coupling them with best possible design. The concept of connectivity was first established by Newnham et al.[18]. Connectivity is a key feature in the development of multi phase solids since the physical properties can be changed in different orders of magnitude depending on how the connections are made [19]. The interspatial relationship in a multiphase material has maximum importance because it controls the mechanical, electrical, magnetic and thermal fluxes between the phases. In a composite each phase may be self-connected in either one, two or three dimensions. In a two phase composite there are 10 different combinations of connectivity and they are 0-0, 0-1, 0-2, 0-3, 1-1, 1-2, 1-3, 2-2, 2-3 and 3-3 connectivity. These connectivity patterns are illustrated in Fig. 1.5 using cube as building block. The most commonly studied composites are 0-3 and 1-3 configurations. 0-3 configuration can be easily prepared at relatively low cost [20].

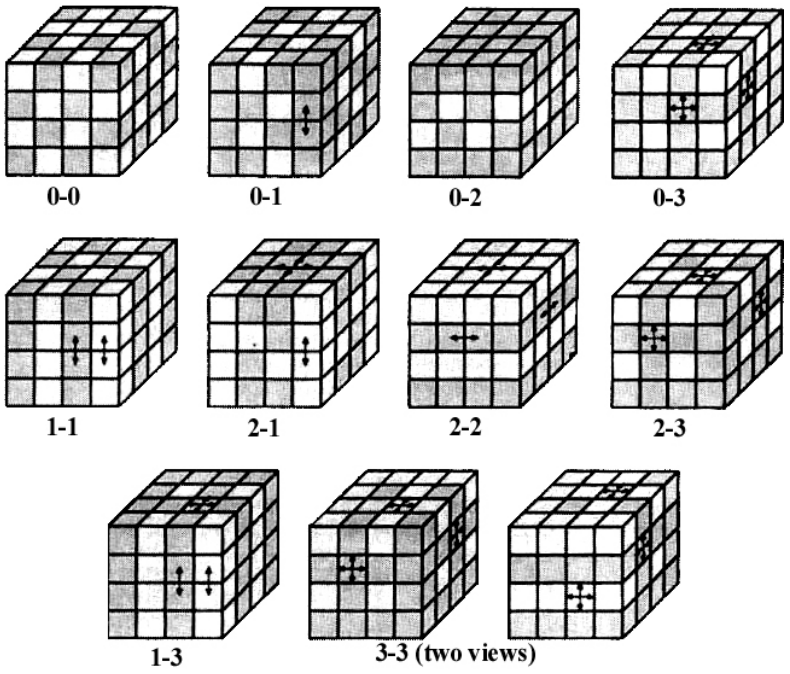

Fig. 1.5 Connectivity patterns in a di-phasic composites systems. (Ref. 18)

1.5.2 Polymer matrix composites

Polymeric composites are one of the most prominent classes of composites. Polymeric composites were introduced in early 1940s. Gradually the applications of the polymer composites continued to grow over years finding applications in aircrafts, ships, electronic industry etc. In a polymer based composites, physical properties of the polymer is modified using various fillers like ceramic, metal etc. Depending on the polymers used polymer composites can be classified in to two [21], (i) thermoplastic matrices (ii) thermoset matrices. Thermosetting plastics are polymer materials that irreversibly cure to a stronger form. The cure may be done through heat, through a chemical reaction (two-part epoxy, for example), or irradiation such as electron beam processing. A thermoplastic is a plastic that melts to a liquid when heated and freezes to a brittle, very glassy state when cooled sufficiently. Most thermoplastics are high-molecular-weight polymers whose chains associate through weak Van der Waals forces

(polyethylene); stronger dipole-dipole interactions and hydrogen bonding (nylon); or even stacking of aromatic rings (polystyrene). Thermoplastic polymers differ from thermosetting polymers as they can be re-melted and remolded. Thermoplastics are elastic and flexible above a glass transition temperature T_g. There are number thermoplastic polymers like; polyethylene, polystyrene, polypropylene, poly-ether-ether-ketone (PEEK) etc used for making composites. Thermoset materials are usually liquid or malleable prior to curing and designed to be molded into their final form. The curing process transforms the resin into a plastic or rubber by a cross-linking process. The cross-linking process forms a molecule with a larger molecular weight, resulting in a material with a higher melting point. Thermoset materials are generally stronger than thermoplastic materials due to this 3-D network of bonds, and are also better suited to high-temperature applications up to the decomposition temperature of the material. The most commonly used thermoset matrices are, epoxy resins, Polyimide, bakelite etc [21].

1.5.2.1 Polymer-ceramic composites for electronic applications.

Polymeric materials play a vital role in electronic substrates and microelectronic packages as a result of their ease of processing, low cost, low relative permittivity, adhesive properties, high electrically insulating properties etc [22]. The polymers show low permittivity and low dielectric loss but high coefficient of thermal expansion and low thermal conductivity precludes their immediate applications [22]. Further, for substrate application the relative permittivity should be in the range of 3-15. Hence, the monolithic polymers are limited in electronic applications. On the other hand, low dielectric loss ceramics have low coefficient of thermal expansion and average thermal conductivity. Thus the dielectric and thermal properties required for a substrate can be easily achieved by making ceramic polymer composites. In polymer-ceramic composites the dielectric

properties are controlled by the amount of filler, particle size and distribution of the filler, shape and orientation of the filler and finally dispersion of the filler in the polymer matrix [23]. The particle size of the filler has extreme importance in determining the permittivity of the composite. Extremely fine particles may exhibit lower permittivity compared to larger fillers. The shape of the particle plays a key role in determining the final permittivity of the composites through depolarization and volume loading effects. Non-spheroidal particles exhibit orientation effect with respect to measurement direction [24].

1.6 Dielectric Resonator; an Overview

The growth of satellite communication and cellular radio systems has led to the requirement of compact, temperature stable, and low cost filters. In the early seventies, it was difficult to find a device which could perform as filter, oscillator, and antenna with weight and size features suitable for integration in miniature circuits. For instance, for frequency stabilization, one has to rely upon the bulky expensive metallic cavities which were not integrable. These problems were alleviated with the advent of ceramic microwave dielectric resonators and have been essential in eliminating metallic cavities and waveguides. The past 25 years have seen a rapid development in the miniaturization of microwave circuitry and this has led to the development of dielectric resonators which can replace the bulky metallic cavities. The dielectric resonators used in filters oscillators and antennas have become indispensable component in microwave communication systems for its integration potential, size reduction, reliability and temperature stability [5]. The materials for dielectric resonators are required to excel in three characteristics, a high relative permittivity, a high quality factor, and a nearly zero temperature coefficient of resonant frequency. High relative permittivity is essential since it is the

key factor for miniaturization and can thus lower the cost of production. The higher the quality factor, the lower is the insertion loss and steeper the cut off. Moreover, a high quality factor provides a narrow band width and hence enables the allocation of more number of channels within a given frequency range [5, 25, 26].

The possibility of using unmetallized dielectrics as resonators was first proposed by Ritchmyer [27] in 1939. The search for dielectrics for microwave applications started from 1960. The first reported work on the adaptability of a high relative permittivity dielectric rod to generate standing wave resonance phenomena was proposed by Schlike [28]. Okaya reported that a piece of rutile (TiO_2) acted as a resonator and subsequently Okaya and Barash analyzed the different modes of a dielectric resonator [29, 30]. The first microwave filter proposed by Cohn [31] in 1968 where TiO_2 was used as the dielectric resonator. The rutile TiO_2 has a high relative permittivity (ε_r = 100), high quality factor (Qxf = 10000 GHz), and high temperature coefficient of resonant frequency (τ_f = +450 ppm/^{O}C). This filter was not put into practical use because of its large τ_f. A real breakthrough in microwave ceramic technology occurred when the first temperature stable ceramic dielectric barium tetratitanate developed by Raytheon [32] in 1970. Later, a modified barium titanate with improved performance was reported from BEL laboratories [33]. The next major breakthrough came from Japan when the Murata Manufacturing Company produced (Zr-Sn) TiO_4 ceramics with excellent microwave dielectric properties [34, 35]. These positive results led to an intensive research and actual implementation of dielectric resonator as the indispensable component in the microwave communications. In 2008, the current trend and the state of the art of microwave dielectric materials for telecommunication applications is discussed in the book "Dielectric materials for wireless communications" [5]. This book reports the sintering temperature and microwave dielectric

properties of more than 2000 low loss dielectric ceramic compositions and explains the ways to tailor their properties by possible substitution, dopant and glass additions.

The extensive research in the last three decades provides several extremely low loss ceramics suitable for resonator applications. The main DR families currenty used for practical applications are $MgTiO_3$–$CaTiO_3$ [5, 36], $BaTi_4O_9$ [37, 38], $BaTi_9O_{20}$ [33], $(Zr_{1-x}Sn_x)TiO_4$ [5, 34, 35], $Ba(Zn_{1/3}Ta_{2/3})O_3$ and $Ba(Mg_{1/3}Ta_{2/3})O_3$ [39], BaO-RE_2O_3-TiO_2 [40], $SrTiO_3$-$LaAlO_3$, $CaTiO_3$-$LaAlO_3$ [41-44].

With the revolution in mobile phone and satellite communication systems using microwave as propagation media, the research and development in the field of microwave dielectrics for device miniaturization and excellent performance has been one of the biggest challenges in the contemporary area of materials science. Hence search for new materials and tailoring the properties of existing materials are going on.

1.6.1 Working principle of DRs

A piece of dielectric can confine microwave energy at a few discrete frequencies through multiple internal reflections, provided energy is fed in the appropriate directions [27]. An electromagnetic wave moving from high permittivity region to low permittivity region encounters very high impedance at the dielectric–air interface and reflects back to the dielectric. As the permittivity of the dielectric increases the impedance offered by the boundary will also increase which enhances confinement of microwave energy (see Fig. 1.6). The reflection coefficient approaches unity when the permittivity approaches infinity. The trapped electromagnetic waves will form standing waves to generate resonance. If the transverse dimensions of the dielectric are comparable to the wavelength of the microwave, then certain modes satisfying Maxwell equations and boundary conditions will

be excited. The frequency of resonance depends on the physical dimensions and permittivity of the dielectric specimen.

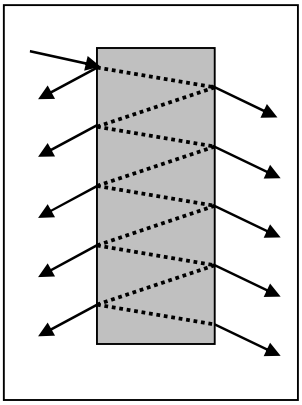

Fig. 1.6 Sketch of multiple internal reflections in DR

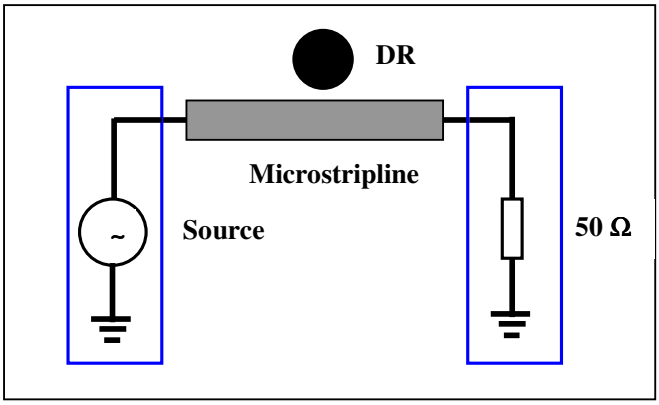

Fig.1.7 DR as circuit element coupled to a microstripline

Figure 1.7 shows a schematic representation of DR coupled to a microstripline. This coupling is a result of field interaction due to the microstrip line and DR. The fundamental $TE_{01\delta}$ resonance mode, is excited due to electromagnetic coupling between DR and microstripline. The quality factor (Q), which is the ability to confine energy in a certain mode is to be calculated at resonant frequency [5]. Hence,

$$Q = 2\pi \left[\frac{W_{\max}}{W_d} \right]_{\omega=\omega_{res}} \quad -------(1.7)$$

where W_{max} is the maximum energy stored in the resonator. W_d is the dissipated energy in the resonator during one period given by $W_d = P_d T$, where $T = \frac{2\pi}{\omega}$, P_d is the average power dissipated in the resonator and ω is the angular velocity. Thus eqn. (1.7) can be rewritten as

$$Q = \left[\frac{\omega W_{\max}}{P_d} \right]_{\omega=\omega_{res}} \quad -------(1.8)$$

A bulk dielectric material excited for resonance using microwave energy is equivalent to a parallel *LCR* resonant circuit. Hence the alternating field will have inductive, capacitive and resistive components. From the fundamental rules of resonant electrical circuits, the electric energy stored in the capacitor is given as

$$W_e(t) = \frac{C[v(t)]^2}{2} = \frac{C|V|^2 \cos^2(\omega t)}{2} \text{-------(1.9)}$$

and magnetic energy stored in the inductor is

$$W_m(t) = \frac{L[I(t)]^2}{2} = \frac{|V|^2 \cos^2(\omega t)}{2\omega^2 L} \text{-------(1.10)}$$

At resonance, capacitive and inductive reactance become equal and opposite to vanish. Hence the impedance of the circuit equals the ohmic resistance and maximum energy storage takes place within the body of the dielectric resonator. At this condition,

$$\omega = \omega_{res} \frac{1}{\sqrt{LC}} \text{------(1.11)}$$

The maximum stored energy W_{max} will be the sum of that stored in capacitor (W_e) and inductor (W_m). Since the average energy values are equal to one half of their peak values,

$$W_{\max} = 2W_e = 2W_m = W_e + W_m \text{------(1.12)}$$

Now using Eqn. (1.11) in (1.7), the definition of *Q* at resonance becomes [45]

$$Q = \left[\frac{\omega(W_e + W_m)}{P_d} \right]_{\omega=\omega_{res}} \text{------(1.13)}$$

If the operational frequency is not equal to the resonant frequency, the peak of the stored electric energy is not equal to the peak of the stored

magnetic energy. Therefore the definition of Q is not unique at any frequency other than ω_{res}.

1.6.2 Modes in DRs

A microwave resonator has infinite number of resonant modes, each of them corresponding to a particular resonant frequency, at which the electric stored energy is equal to the magnetic one. The excited modes can be classified into three distinct types: *TE, TM* and hybrid. The fields for *TE* and *TM* modes are axisymmetric whereas hybrid modes are azimuthally dependent. The hybrid modes can again be categorized into *HE* and *EH*.

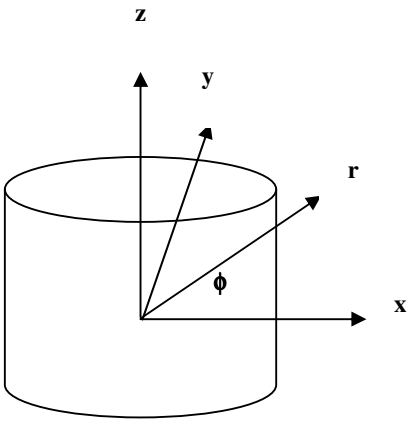

Fig. 1.8 Three dimensional view of an isolated cylindrical dielectric resonator.

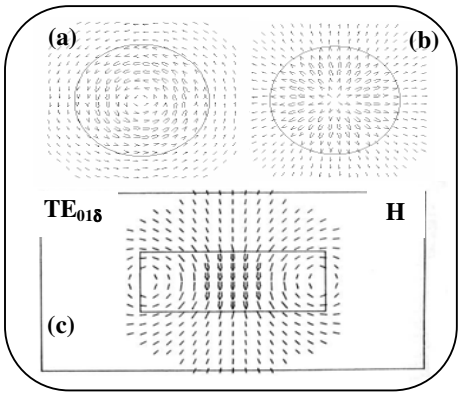

Fig. 1.9 Fields inside a cylindrical DR for $TE_{01\delta}$ mode with (a) Top view of E – Field (b) Top view of H – Field (c) H-Field in side view.

According to the mode nomenclature described by Kobayashi *et al.*[46, 47], the variation of fields along the azimuthal, radial and z-direction inside the resonator, are denoted by adding mode indices as subscripts to each family of modes. This nomenclature is historically based on the mode nomenclature of cylindrical dielectric waveguides. The *TE*, *TM, HE* and *EH* modes are classified as $TE_{nmp+\delta}$, $TM_{nmp+\delta}$, $HE_{nmp+\delta}$ and $EH_{nmp+\delta}$, respectively. The first index denotes the number of full-period field variations in azimuthal direction, the index m (m = 1, 2, 3 …..) denotes the order of variation of the

field along the radial direction and the index $p+\delta$ (p = 0, 1, 2……) denotes the order of variation of the fields along the *Z*-direction.

An interesting feature of DR is the variation in field distribution of different modes, because the modes behave like electric and magnetic multipoles such as dipole, quadrupole, octupole etc. The mode nomenclature makes it congenial the accurate prediction of far field radiation of dielectric resonators in their application as antennas. For example, the $TE_{01\delta}$ mode radiates like magnetic dipole oriented along its axis and $TE_{011+\delta}$ radiates like an axial magnetic quadrupole. Similarly, the *TM* counterparts radiate like electric dipole and quadrupole respectively. Three dimensional view of the isolated cylindrical dielectric resonator is shown in Fig. 1.8 and pictorial representations of the field distribution for various modes are shown in Figs. 1.9 - 1.11. In the cross sectional view, the field lines can be either concentric circles (like *E* field of the $TE_{01\delta}$ mode), or the radial straight line (like *H* field of the same mode).

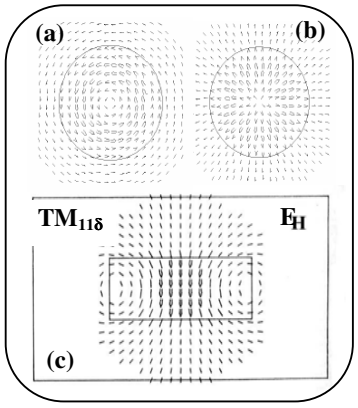

Fig.1.10 Fields inside a cylindrical DR for $TM_{11\delta}$ mode with (a) Top view of H – Field (b) Top view of E – Field (c) E-Field in side view (Ref. 26).

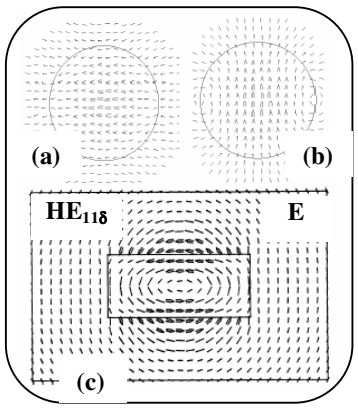

Fig. 1.11 Fields inside a cylindrical DR for $HE_{11\delta}$ mode with (a) Top view of E – Field (b) Top view of H – Field (c) E-Field in side view (Ref. 26).

The resonant mode most often used in shielded microwave circuits is $TE_{01\delta}$. In classical waveguide cavities, the third index is used to denote the number of half-wavelength variations in the axial direction of the waveguide. Here, the third index, denotes the fact that the dielectric resonator is shorter than one-half wavelength. The actual value of δ depends on the relative permittivity of the resonator and the substrate, and on the proximity to the top and bottom conductor planes. Practically a part of the field in the z-direction will decay exponentially outwards to the flat surface of the DR and is termed as evanescent field. Hence it is customary to denote the fraction of the half cycle variation in the z-direction [48] with δ, which takes values between 0.5 to 1. For higher modes, the pure transverse electric or transverse magnetic fields cannot exist, so that both electric and magnetic field must have nonvanishing longitudinal components. Such modes are termed as hybrid modes and the lowest being $HE_{11\delta}$. Hybrid modes are frequently used in dielectric resonator filters and whispering gallery mode resonators at millimeter wave frequencies. One of the main draw back of DR is that resonant frequencies of the modes are close to each other. For practical applications the design of the resonators is done in such a way that there is maximum separation of modes. The DR aspect ratio (D/L) of 1.8 to 2.1 is reported for optimum quality factor and minimum interference of spurious modes [5].

1.6.3 Types of Dielectric Resonators

A typical dielectric resonator for use in the microwave band is formed using a rectangular or cylindrical dielectric block having a coaxial through-hole wherein an inner conductor is formed on the inner surface of the through-hole and an outer conductor is formed on the outer surface of the dielectric block. Dielectric resonators are smaller than air cavity resonators having equivalent resonant frequencies because wavelengths in the

dielectric resonator are divided by the square root of the resonator's relative permittivity. The shape of a DR is usually a solid cylinder but can also be tubular, spherical and paralellopiped (Fig. 1.12).

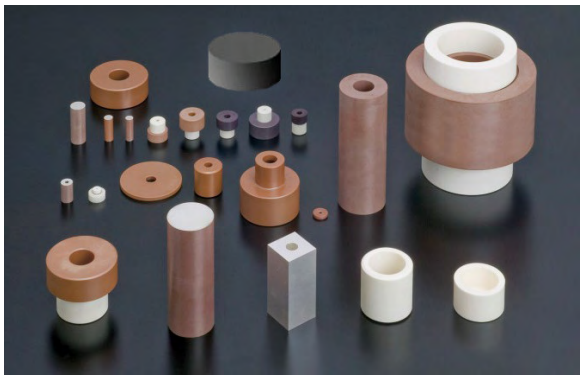

Fig. 1.12 Different types of Dielectric Resonators (courtesy: www.ntktech.com/product_detail.asp.productid=91)

The resonant frequency of modes can be tuned by inserting metal or ferrite screws into the central hole of a ring resonator. Similar techniques are used to avoid interference of unwanted modes with the desired mode in a DR by suppressing the modes and thereby reducing the dielectric loss. The mode spectrum and resonant frequencies of DRs greatly depend on the aspect ratio (diameter D/length L). The dimensions of the specimen are important to achieve wide separation of modes. The proper aspect ratios are 1.0 to 1.3 and 1.9 to 2.3. In practice the specimen diameters in the range 7 to 25 mm have been found most suitable.

1.6.4 Material requirements

Dielectric resonators utilizing a dielectric as a material for constructing the resonator have been widely used so as to miniaturize the resonant system of an electric circuit which handles high-frequency waves such as microwaves. The important characteristics required for a dielectric resonator material are high permittivity (ε_r) for miniaturization, high quality factor for selectivity and low temperature variation of resonant frequency for thermal stability [5].

1.6.4.1 Relative permittivity (ε_r)

The relative permittivity of material is its energy storing capacity when an electric potential is applied across it. The main contribution to the relative permittivity at microwave frequencies is the ionic polarization. Hence, materials containing ions with large ionic polarizabilities are required for sufficiently high ε_r. In order to achieve circuit miniaturization the permittivity of the ceramic must be high. A high ε_r material facilitates miniaturization because the wavelength inside the DR is inversely proportional to square root of its permittivity. The experimental determination of ε_r at microwave frequency is done by resonance method and will be described in the next chapter. It should be noted that, in polycrystalline ceramics, the experimental ε_r deviates more from the theoretical value because, the polarizability of the ceramics are affected by porosity, impurities and secondary phases.

1.6.4.1.1 Claussius mossotti equation

The relative permittivity of an insulator is related to the polarizability of atoms comprising it. The permittivity ε_r can be calculated theoretically using Clausius–Mossotti equation for cubic or isotropic materials [49]

$$\frac{\varepsilon_r - 1}{\varepsilon_r + 2} = \left(\frac{4\pi}{3}\right)\left(\frac{\alpha_D}{V_m}\right) \text{------(1.14)}$$

Rearranging we get

$$\varepsilon_r = \frac{3V_m + 8\pi\alpha_D}{3V_m - 4\pi\alpha_D} \text{------(1.15)}$$

where V_m is the molar volume and α_D is the sum of the dielectric polarizabilities of individual ions. The V_m of the dielectric material can be obtained from X-ray diffraction studies. Based on the additivity rule, Shannon states that the molecular polarizabilities α_D of a complex material

can be broken up into the molecular polarizabilities of simpler compounds by [50]

$$\alpha_D(A_2A'O_4) = 2\alpha_D(AO) + \alpha_D(A'O_2) ------(1.16)$$

where A are the cations. Furthermore, it is possible to break up the molecular polarizabilities of complex compounds in to ions according to

$$\alpha(A_2A'O_4) = 2\alpha(A^{2+}) + \alpha(A^{4+}) + 4\alpha(O^{2-}) ------(1.17)$$

The dielectric polarizabilities of several ions are reported by Shannon [50]. The calculated ε_r usually agree well with porosity-corrected experimental values for well-behaved ceramics [50]. It may be noted that deviations from calculated values can occur due to deviations from cubic symmetry, and also the fact that the sample is ceramic and not a single crystal. Presence of ionic or electronic conductivity, H_2O or CO_2 in channels, rattling of ions, presence of dipolar impurities or ferroelectric behavior also cause deviations from the calculated values [50].

1.6.4.2 High quality factor ($Q_u$xf)

The dielectric loss tangent of a material denotes quantitatively the dissipation of electrical energy due to different physical phenomenon such as electrical conduction, dielectric resonance, and loss from non linear-process. For describing microwave systems quality factor is commonly used instead of loss tangent. The efficiency of a resonant circuit to confine electromagnetic energy is termed as its quality factor (Q - factor). This is the figure of merit for assessing the performance or quality of a resonator. In the case of bulk ceramics energized by electromagnetic wave, quality factor is roughly the inverse of dielectric loss of the material. Q factor is defined as a ratio of the energy stored in the fields inside the resonator to energy loss or dissipation per cycle. If W_0 is the stored energy per cycle, P is power

dissipation and $\omega_o = 2\pi f_r$ is the angular velocity of the electromagnetic wave at resonant frequency f_r, then Q- factor is given by [51].

$$Q = 2\pi \frac{Maximum\quad Energy\quad Stored\quad per\quad cycle}{Average\quad Energy\quad Dissipated\quad per\quad cycle} \text{-------(1.18)}$$

$$Q = \frac{2\pi W_0}{PT} = \frac{\omega_o W_o}{P} \text{- - - - - - (1 . 19)}$$

In practical experiments the Q – factor is determined from the sharpness of the resonance curve, when the DR is connected in the transmission mode. If Δf is the 3 dB band width of the resonant curve, then from the resonant frequency,

$$Q = \frac{\omega_o}{\Delta\omega} = \frac{f_r}{\Delta f} \text{------(1.20)}$$

Hence, the sharper the resonance curve the higher the Q – factor.

The total Q-factor of a DR loaded on a circuit is termed as loaded quality factor (Q_L) given as

$$\frac{1}{Q_L} = \frac{1}{Q_e} + \frac{1}{Q_u} \text{------(1.21)}$$

where Q_e and Q_u represents the external and unloaded Q-factor of the DR respectively.

The unloaded Q-factor arises due to three individual components such as conductor loss ($1/Q_c$), dielectric loss ($1/Q_d$) and radiation loss ($1/Q_r$). The conductor loss is due to the contact between the metallic cavity and DR, radiation loss is due to the evanescent field decaying out from the DR surface and dielectric loss is the intrinsic loss of the material.

Hence, the total unloaded Q-factor (Q_u) of a DR can be represented as

$$\frac{1}{Q_u} = \frac{1}{Q_c} + \frac{1}{Q_d} + \frac{1}{Q_r} \text{------(1.22)}$$

In polycrystalline ceramics, defects such as grain boundaries, stacking faults, chemical or structural disorder, point defects, planar defects, line defects, inclusions, secondary phases, twinning, porosity etc. contribute towards the extrinsic dielectric loss. For an ideal DR devoid of all such intrinsic losses, an approximation can be made as

$$Q_d = \frac{1}{\tan \delta} \text{------(1.23)}$$

It should also be noted that in the case of an isolated DR, Q_d = Q_u as a general convention. However, the quality factor of a DR can only be measured as the loaded value (Q_L) by keeping in an external circuit. Hence it is necessary to have a relation between the two forms of quality factor (Q_u and Q_L) and is represented as

$$Q_u = Q_L(1+\beta) \text{------(1.24)}$$

where β is termed as the coupling coefficient given by

$$\beta = \frac{P_e}{P_u} \text{------(1.25)}$$

P_e is the power loss due to external factors and P_u is the sum of power losses due to conductor, dielectric and radiation.

According to Classical dispersion theory, [52, 53] in the microwave region, the loss is mainly due to the interaction of the applied field with phonons. The microwave energy is transferred to transverse optical phonons. These optical phonons can then generate thermal phonons. This leads to damping of the optical lattice vibrations and therefore causes dielectric loss. There is a linear increase of loss with frequency which is a characteristic phonon effect. Hence the quality factor of a DR is normally represented as $Q_u$xf instead of Q_u as a general convention. In general the losses are lower for centro-symmetric crystals than the non centro-

symmetric crystals. Normally a quality factor greater than 2000 is required for better selectivity and hence improved power handling capacity of the device comprising DR.

1.6.4.3 Low temperature coefficient of resonant frequency (τ_f)

The temperature coefficient of resonant frequency (τ_f) decides thermal stability of the dielectric resonator. The electronic devices employing microwave resonators require near zero τ_f values. The τ_f is defined as

$$\tau_f = \frac{1}{f_r}\frac{\Delta f}{\Delta T} \text{------(1.26)}$$

where f_r is the resonant frequency at room temperature, Δf is the variation of resonant frequency from room temperature for a change in temperature ΔT. The τ_f depends on the temperature variation of ε_r (τ_ε) and coefficient of linear thermal expansion (α_L) according to the expression

$$\tau_f = -\alpha_L - \frac{\tau_\varepsilon}{2} \text{------(1.27)}$$

For most of the ceramics α_L is about 10 ppm/^{o}C, indicating a major control of τ_ε on τ_f. The value of τ_f should be near to zero for practical applications. However, often the device engineer requires a small positive or negative τ_f to compensate for the temperature variation of the resonant frequency due to the external circuit connected to DR.

1.7 Factors Affecting Microwave Dielectric Properties

Microwave dielectric properties are influenced by a number of factors such as processing conditions, phase transitions, raw material impurities and crystal defects and porosity [54-61]. The three important parameters that affect the performance of the microwave components are ε_r, $Q_u x f$, and τ_f. The dielectric loss is the result of a combined contribution of the degree of crystal structure imperfection, microstructural inhomogenity and interaction of

phonons. Ceramics with microstructural inhomogenities such as relaxation of space charges or dipoles which lie either between matrix grains and inclusions, or at grain boundaries have higher losses (low Q_u). Such inhomogenities may arise due to secondary phases, impurity segregation, incomplete densification etc.

The structural factors that are involved in loss mechanism include lattice defects, distortion of symmetry, mass of ions, cation ordering etc. The dielectric loss tangent of microwave dielectrics (tan δ) is brought about by the effect of anharmonic terms in the potential energy on the mean separation of a pair of atoms and is increased by lattice imperfections in the crystal. The dielectric loss caused by the anharmonic terms increases at higher temperatures. The random distribution of ions also is considered to be a kind of imperfection in the atomic ordering. The Q factor of the ordered ceramics would be much greater than the less ordered ceramics. Any type of defects such as grain boundaries, stacking faults, chemical or structural disorder, point defects, planar defects, line defects, inclusions, secondary phases, twinning, porosity etc. contribute losses. In the microwave region, the intrinsic loss is mainly due to the interaction of the applied field with phonons. This leads to dampening of the phonon modes of fundamental lattice.

Because of the natural difficulties involved in getting ceramics with reproducible microstructures, it is essential that the ceramic is at least composed of a single phase with homogeneous microstructure to have as high Q_u as possible.

1.7.1 Effect of humidity

The tan δ increases with increasing porosity due to collection of moisture in the pores. Humidity effects on low frequency dielectric properties of porous materials have been studied [62, 63]. Jonscher [60]

identified low frequency loss mechanism in porous materials in the presence of moisture, and Tinga *et al*. [64] studied the effect in some materials at microwaves. It is clear that the relaxation process centered at low frequency is responsible for high dielectric loss over a wide frequency range extending into the microwave range. The humidity effects on low frequency dielectric properties of porous materials have been associated with the liberation of ions tightly bound in the dry condition. In contact with an adsorbed water film, these ions become free to move over extended regions. This mechanism would produce an interfacial polarization process giving rise to a low frequency peak.

1.7.2 Effect of porosity

(a) Relative permittivity

The dielectric is a composite system of two dielectrics (dielectric material and porosity) with different relative permittivities. Consider the dielectric as parallel layers of two dielectrics having volume fractions V_m and V_d and relative permittivities ε_1 ($\varepsilon_1 = \varepsilon_m$, dielectric phase) and ε_2 ($\varepsilon_2 = 1$, porosity) respectively. There are two possible configurations

(a) Electric field is perpendicular to the plane of the plates [65]. Then

$$\varepsilon' = \varepsilon_m - P(\varepsilon_m - 1) \text{------(1.28)}$$

(b) If electric field is parallel to the plane of the plates,

$$\varepsilon' = \frac{\varepsilon_m}{P(\varepsilon_m - 1) + 1} \text{------(1.29)}$$

Where P is the fractional porosity.

Maxwell [65] derived a realistic model of spherical particles of relative permittivity ε_d in a dielectric matrix ε_m. The relative permittivity of the mixture is given by

$$\varepsilon' = \frac{V_m \varepsilon_m \left(\frac{2}{3} + \frac{\varepsilon_d}{3\varepsilon_m}\right) + V_d \varepsilon_d}{V_m \left(\frac{2}{3} + \frac{\varepsilon_d}{3\varepsilon_m}\right) + V_d} \text{------(1.30)}$$

If the spheres are pores and applying a linearized approximation for $(\varepsilon_m - \varepsilon') \langle\langle \varepsilon_m$, then the above equation becomes

(b) Dielectric loss (tan δ)

The complex permittivity of a material is given by

$$\varepsilon = \varepsilon' - i\varepsilon'' \text{------(1.32)}$$

Real component ε' is relative permittivity and imaginary component ε'' describes the dissipation of the electric field.

Dielectric loss tangent, $\tan\delta = \frac{\varepsilon''}{\varepsilon'}$ ------(1.33)

Quality factor, $Q = \frac{1}{\tan\delta}$ ------(1.34)

The loss increases with porosity and an additional term to loss is introduced. Plot of tan δ against porosity on a log-log plot suggested a straight line which would give a dependence of the form,

$$\tan\delta = (1-P)\tan\delta_o + AP^n \text{------(1.35)}$$

tan δ_o is the loss tangent of fully dense material which depends on the amount of material present i.e., it should depend on the porosity. A = 1.298 x 10^{-2} and n = 2.73. The above equation can be put in the form of law of mixtures as

$$\tan\delta = (1-P)\tan\delta_o + P(AP^{n-1}) \text{------(1.36)}$$

The loss may be related to the surface area of the pore volume, *S*

$$\tan\delta = (1-P)\tan\delta_o + P(A^{'}S) \text{------(1.37)}$$

From sintering theory, surface area of the pores varies with porosity as

$$S \propto \left(\frac{P}{1-P}\right)^{2/3} \text{------(1.38)}$$

Substituting the above equation in equation. (1.37), we get [61]

$$\tan\delta = (1-P)\tan\delta_o + A^{'}P\left[\frac{P}{1-P}\right]^{2/3} \text{------(1.39)}$$

1.8 Applications of Dielectric Resonators

Dielectric Resonators are useful in RF communication devices in connection with filters, low noise oscillators, and resonator antennas [26]. Dielectric resonators are inevitable components in microwave subsystems which are used in the range of military to consumer products. These products include satellite receiver modules and cellular telephones. DRs find applications in Low Noise Block converters (LNB) for digital broadcasting systems, direct broadcast satellite (DBS) receivers, microwave filters, security systems, detectors, auto cruise control (ACC) radar systems, wireless communication equipments, cellular base stations, collision avoidance systems, global positioning systems, satellite multiplexing filter devices, high stability dielectric resonator oscillators, microwave duplexers, radio links, WiMAX filters, wideband networks LMDS, GSM, etc. In all the above mentioned applications DRs can be categorized based on their ability to determine and stabilize the frequency of a microwave oscillator or as a resonant element in a microwave filter.

1.8.1 Dielectric resonator oscillators

Dielectric resonator oscillators (DROs) are very popular devices in the radio frequency (RF) or microwave electronic field. These oscillators are typically employed in communication systems, radar systems, navigation

systems and other signal receiving and/or transmitting systems. Their popularity has been attributed to their high-Q, low loss, and conveniently sized devices for various applications in the RF and microwave fields. The oscillation frequency of a dielectric resonator oscillator depends on its dimensions and on the electromagnetic properties of its environment. Dielectric resonator oscillators have been used in radars, transponders, and communication systems, among other systems, to generate microwave signals with extremely low phase noise and good temperature stability. Generally, in these systems, the DRO is used to generate a frequency that is locked to a reference oscillator within a phase-locked loop circuit. The application of DR as oscillator element was first proposed by Day [66] in 1970. Subsequently, in 1977, a 4 GHz $Ba_2Ti_9O_{20}$ resonator integrated with Si bipolar transistor was used as a fixed frequency oscillator [33]. These fundamental fixed frequency oscillators are significantly simpler and efficient with 10–20 dB lower phase noise than conventional electronic oscillators. Later efforts were made to design tunable frequency DR oscillators functioning in the *X*-band using metallic/dielectric rod to perturb the evanescent fields, by optical methods or by varactor connected circuits [67]. A mechanical tunable DRO is shown in Fig. 1.13

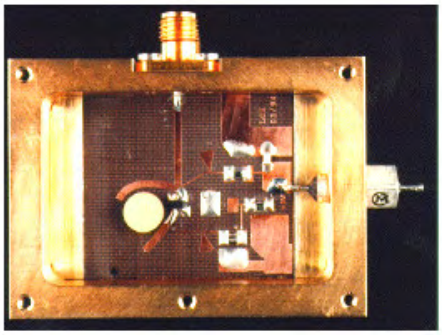

Fig. 1.13 Silicon bipolar mechanically tunable DRO at 10 GHz with parallel feed back stability. (londonmet.ac.uk)

1.8.2 Dielectric resonator filters

Owing to the superior performance characteristics of dielectric resonators, the use of dielectric resonators has become widespread, particularly in highly selective bandpass filters. Dielectric resonator filters are a class of stable microwave filters that are frequently used in radar and communications systems. A typical dielectric resonator filter consists of a ceramic resonator disc mounted in a particular way inside a metal cavity. Dielectric resonators are often utilized in filter circuits because of an intrinsically high Q value. The dielectric resonator, operating at a particular frequency, is tunable over a narrow bandwidth and frequency, fine tuning must be accomplished without affecting the high Q of the resonator. These characteristics allow a filter employing a dielectric resonator to have excellent frequency stability with only a small amount of frequency drift over a wide range of temperatures and environmental conditions. There are a variety of configurations regarding the filter design, including single mode, dual mode etc. The first DR filter was reported in 1975 by Wakino *et al.*[68]. In its basic structure, a DR filter consists of a high ε_r material suspended remote from a metal enclosure. At the resonant frequency, most of the electromagnetic energy is stored within the dielectric. The enclosure stops radiation and since the enclosure is remote, the resonant frequency is mainly controlled by the ε_r and dimensions of the DR sample. Practical filters are constructed by arranging coupled DRs to achieve specified frequency selective transfer function. The most commonly used DR structure is cylindrical one operated in $TE_{01\delta}$ mode. Consequent to the wide applications in wireless devices, a wide variety of DR structures and modes such as $TM_{01\delta}$, $HE_{11\delta}$ etc. are currently in use [69] to improve the rate of change of attenuation from passband to stopband (selectivity) and passband insertion loss. The major disadvantage of DR band pass filters is that the necessary encapsulation in a metal case to minimize radiation loss which

makes them bulky, especially for medium and low frequencies. Fig. 1.14 shows some of the DR geometries used to fabricate filters and Fig. 1.15 shows silver cavity and ceramic pucks used in filter.

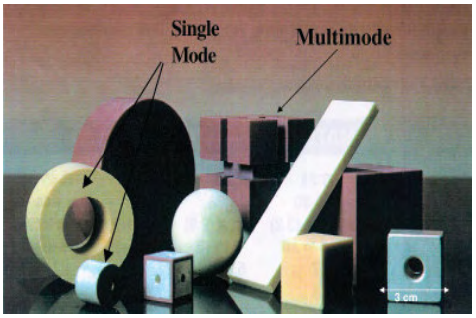

Fig. 1. 14 Various geometries of ceramic pucks to be used as single and multi mode resonators and filters (Ref. 70).

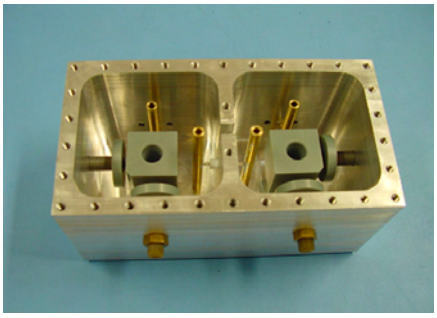

Fig. 1. 15 Silver coated cavity with ceramic pucks used in filter technology. (innovexpo.itee.uq.edu.au)

1.8.3 Dielectric resonators antennas

Dielectric resonator antennas (DRAs) are miniaturized antennas of ceramics or another dielectric medium for microwave frequencies. The radiation properties of dielectric resonator are known earlier, the use of DR as an antenna was first published in 1983 [71, 72]. Dielectric resonator antennas are fabricated entirely from low loss dielectric materials and are typically mounted on ground planes. Their radiation characteristics are a function of the mode of operation excited in the DRA. The mode is generally chosen based upon the operational requirement. Dielectric resonator antennas offer several advantages over other antennas, such as small size, high radiation efficiency, and simplified coupling schemes for various transmission lines. The DRA radiates through the whole surface except the ground part [72] and hence the surface can be avoided. The bandwidth can be controlled over a wide range by the choice of relative permittivity, and the geometric parameters of the resonator. Fig. 1.16 shows various ceramic geometries used in DRAs and Fig. 1.17 shows a dielectric resonator antenna with a cap for measuring radiation efficiency

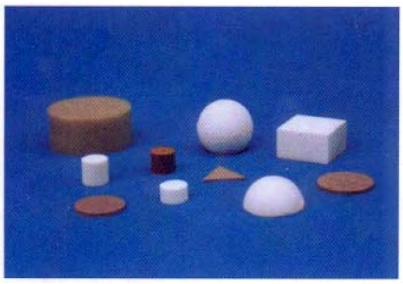

Fig. 1.16 Various DRA geometries. (Ref. 72)

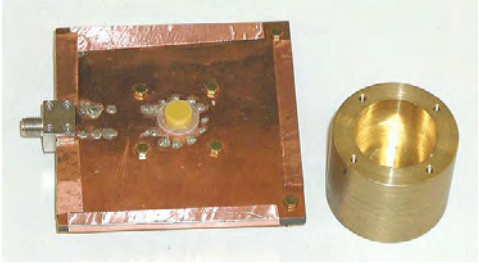

Fig. 1.17 A dielectric resonator antenna with a cap. (www.ee.olemiss.edu)

1.9 Low Temperature Co-fired Ceramics: an Overview

The ever widening range of microwave products in the consumer electronic market is continuously pushing device and component manufactures to seek new advanced integration, packaging and interconnection technologies, as size, cost, and performance are critical factors for the success of the microwave products [73]. Majority of ceramic component used in the system remain discrete. Transition from surface mount discrete components to integrated components in substrate requires low temperature firing ceramics co-firable with metallic electrodes. LTCC can be applied for the integration of passive elements into monolithic highly reliable and robust LTCC module [74]. These modules consist of several layers of substrate material with integrated elements inductors, capacitors, resonators, filters that are interconnected with 3-D stripline technology. The benefits of LTCC technology are cost efficiency for high volumes, high packaging density, reliability, the ability to utilise highly conductive and inexpensive metallization, good dielectric thickness control, high print resolution of conductors, low permittivity dielectric material, environmental stability, compact structures, integration [75-77] etc. Integrating resistors and capacitors into the LTCC substrate eliminates any solder joints and wire bonds. Because of the excellent insulation provided by the thin layers of

ceramic material, circuits can be alternately stacked, allowing digital, analog and microwave assemblies to be embedded in the same LTCC structure. This eliminates the need for separate housings and provides significant space and weight reductions. The schematic diagram describing the process of LTCC technology is shown in Fig. 1.18.

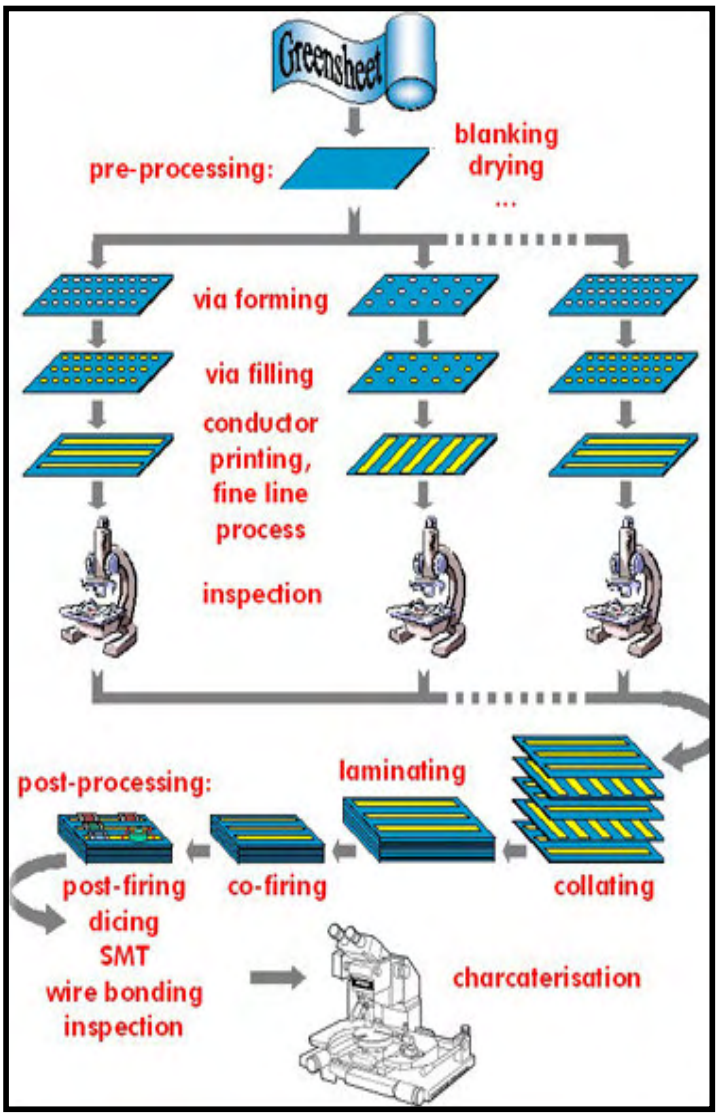

Fig. 1.18. Schematic diagram describing the process of LTCC technology. (www.ltcc.de/en/services_man.php)

The low sintering temperature provided by the LTCC technology is the key issue enabling its advantageous utilization for today's packaging concepts in microelectronic and microsystems and in microwave modules. This technology enables fabrication of 3-dimensional ceramic modules with embedded silver or copper electrodes, and LTCCs with relative permittivity from about 3 up to over 100 have been developed showing low dielectric loss. These advantages make the LTCC technology suitable for the high frequency circuits required for high-speed data communications. Although there are also other high-density, multilayer substrate technologies available, such as organic laminates, LTCC has a unique set of combined characteristics, which makes it a more attractive alternative as the frequencies shift into the microwave region.

1.9.1 A Brief history of LTCC

The origin of multilayer ceramic substrate technology was at RCA Corporation in the late 1950's and the basis of current process technologies (green sheet fabrication technology and multilayer laminate technology using the doctor blade method) was discovered at this time [78]. Progress was made using these technologies with IBM taking the lead, and the circuit board for IBM's mainframe computer commercialized in the early 1980's was the inheritance [79]. Since this multilayer board was cofired at the high temperature of 1600 ^{o}C with the alumina insulating material and conductor material (Mo, W, Mo-Mn), it is called High Temperature Cofired Ceramic. From the middle of the 1980's, efforts to increase the speed of mainframe computers accelerated, and as the key to increasing computer performance, further improvements are made to multilayer ceramic substrates for high density mounting applications. Fine wires were used in order to increase wiring density in circuit boards for high density mounting. But the attenuation of signal occurs due to the electrical resistance of the wiring. Hence it is necessary to use materials with low electrical resistance (like Cu

or Au). In addition, with the flip chip method of connecting bare LSI components directly, poor connection of the interconnects may result if the thermal expansion of the board is not close to that of the silicon (3.5 ppm/^{o}C). Hence an insulating material with low thermal expansion (ceramic) is desirable. Further, to achieve high speed transmission of signals, it is necessary that the ceramic has a low relative permittivity. In the early 1990's, many Japanese and American electronics and ceramics manufacturers had developed multilayer boards (LTCC) that met these requirements [74]. Among them, Fujitsu and IBM were the first to succeed with commercial applications of multilayer substrates using copper wiring material and low relative permittivity ceramics. From the latter half of the 1990's to the present, the focus of applications has shifted to high frequency wireless for the electronic components, modules and so on used in mobile communication devices. For the multilayer circuit board, the low thermal expansion of ceramics was its biggest merit for the purpose of high density mounting of LSI components. For high frequency applications, its low transmission loss is its key feature, and the low dielectric loss of ceramic gives it an advantage over other materials.

During the late 1980's, U.S. and Japanese manufacturers of computers and ceramic materials conducted extensive research and development of LTCC technology that is crucial to present day and future communication technologies. During the past 15 years scientists world over have developed a large number of new dielectric LTCCs (about 400) for high frequency applications with low sintering temperature or improved the properties of known materials. About 1000 papers and about 500 patents are filed in the area of LTCC materials and related technologies. Next-generation electronics systems will demand the performance, reliability, light weight and affordability that LTCC technology can provide. Low-temperature co-fired ceramics (LTCCs) has entered the mainstream of electronic design. The

process, design aspects and requirements for LTCC technology is discussed in the review "Low loss dielectric materials for LTCC applications: A review" authored by Sebastian and Jantunen [73].

1.9.2 Materials selection and requirements

Although the LTCC technology for high frequency applications demonstrates some very advantageous features, its development is still in the early stages. The main problems relate to the rigorous demands placed on the materials requirement. In general it is believed that the main difficulties in the development of new LTCC materials are not related to their dielectric properties but to their sintering behaviour, thermomechanical properties, chemical compatibility, production cost and the range of variation of each parameter [73].

1.9.2.1 Densification temperature

To produce a module, the LTCC materials are co-fired with an inner electrode structure and, as a consequence, the sintering temperature must be lower than the melting point of the electrode. In addition, a chemical compatibility between the LTCC material and the electrode must exist. Silver is a usual choice for the electrode, which means the sintering temperature is commonly adjusted to about 900 ^{o}C. It should be noted that any densification or crystallisation of the composite at lower temperatures, such as below 800 ^{o}C, is undesirable as this can prevent the evaporation of the organics and solvents used in conductive pastes and binder and plasticizers causing residual carbon traces in the microstructure. Any residual carbon that may form during binder decomposition if left in the LTCC would adversely affect the dielectric properties. This means that the densification of the ceramic should start above this temperature.

1.9.2.2 Dielectric properties

The dielectric properties of the LTCC materials determine its functionality. Low relative permittivity materials with ε_r = 4 -14 are used for substrate layers while high permittivity materials are used mainly for capacitor layers. Low temperature processing of ceramics affect the dielectric losses of LTCC ceramics and the dielectric loss significantly affects the performance of the LTCC based devices. The dielectric loss value of common LTCC materials, as expressed with the Q value (= 1/tanδ) multiplied by the measurement frequency, which should be greater than 1000 for a good LTCC material. The temperature dependence of the resonance frequency is important because filters and resonators based on noncompensated dielectric materials need additional mechanical and electrical design to ensure satisfactory electrical performance of the device over its operating temperature. Nearly zero τ_ε is preferred for LTCC applications. However, τ_f of ±10 ppm ^{o}/C is commonly accepted for substrate application [74].

1.9.2.3 Thermal properties

The removal of heat generated by the device during operation is critical for the efficient functioning of the package. It is therefore necessary to maintain the temperature below 100 ^{o}C for efficient and reliable operation of the device. The heat removal has become even more critical in recent years because of the ever-growing need to fabricate high density and high power devices that can operate at high speed. One disadvantage of LTCC is its low thermal conductivity usually in the order of 2-5 W/mK, although, it is ten times more than that for organic laminates. A common method to improve thermal dissipation is to use a heat spreader, but a more advantageous alternative provided by LTCC technology is to place metallic via arrays under high power components. Another important material aspect is its coefficient of thermal expansion. A thermal expansion mismatch

would give rise to failure of area solder connections between the chip and the substrate. These affect the reliability of the designed components.

1.9.2.4 Chemical compatibility with electrode material

The LTCC should not react with the electrode material. The formation of additional phases in the ceramic should be minimised since the reaction of the composites with the conducting electrode, deteriorate the performance of the microwave modules. A critical issue in manufacturing LTCC microelectronics is the precise and reproductive control of shrinkage on sintering. Thus when developing LTCC materials, one has to take into account reactions not only with the conductive material like silver but also with other additives of the conductor paste [78].

In general, there are three methods to lower the sintering temperature of ceramics such as low melting glass addition, chemical processing, and using starting materials with small particle size [80, 81]. The first method has been commonly found effective to decrease the firing temperature in spite of degradation of microwave dielectric properties of ceramics. In practice, there are two approaches to exploit the glasses to obtain ceramic compositions sinterable below 1000 ^{o}C. The first approach is via the glass-ceramic route, which starts with a fully glassy system that devitrifies almost completely during high temperature processing. The starting materials used in the glass -ceramics approach are pure glass, such as cordierite glass which densifies first, followed by crystallisation. The physical properties of the resulting composites in the glass-ceramic approach are controlled by the degree of crystallisation. The amorphous glass phase is the main component, but it may contain a small amount of crystalline phase which acts as a nucleating agent during firing. During firing, the glass recrystallises to low loss phases and produces a low dielectric loss ceramic body. The second approach (glass + ceramics) consists of adding a low softening point glass to

the crystalline ceramic component. Densification of glass + ceramics can be described by three-stage liquid phase sintering, i.e., particle rearrangement, dissolution and precipitation and solid state sintering. Depending upon the reactivity between glass and ceramics, the densification of glass + ceramics can be classified as non-reactive, partially reactive and completely reactive systems [73]. Little dissolution of ceramic filler in glass during firing is observed for nonreactive systems, such as borosilicate glass (BSG) + cordierite [82] in which densification is mainly achieved by particle rearrangement. Addition of glass has been widely used to reduce the sintering temperature. However, when glass is used in microwave ceramics $Q_u$xf invariably degrades due to loss mechanism associated with the glass. Therefore, the selection of glass and amount of glass required to lower the sintering temperature of the low loss ceramics is very important. CuO, B_2O_3, V_2O_5 are well known liquid phase sintering promoters. However, reports show that single component low melting additives easily forms second phase with parent materials which may degrades the microwave dielectric properties [73, 83-85]. Earlier investigations on glass added ceramics reveals that multicomponent glasses are more effective in lowering the sintering temperature of the ceramics without degrading the microwave dielectric properties [5, 73]. Wu *et al*. and Navias *et al*. reported the microwave dielectric properties of various borosilicate glasses [86, 87]. The multi component glasses with SiO_4 and B_2O_3 configurations joined to form (-Si-O-B-O-) linkages, will have high electrical resistance and low dielectric loss. The physical and dielectric properties of all the borosilicate glasses in the present investigation are shown in Table 1.2.

Table 1.2 Physical and dielectric properties of various borosilicate glasses

Glass code	Composition (mole%)	Density (g/cc)	Softening Temperature (°C)	ε_r	Tan δ	Ref.
PBS	40:PbO,40:B_2O_3, 20:SiO_2	4.31	448	12.9	$7.1x10^{-3}$ (12 GHz)	[73, 87]
BBS	30:BaO,60:B_2O_3, 10:SiO_2	3.40	627	7.20	$4.4x10^{-3}$ (15 GHz)	[73, 87]
ZBS	60:ZnO,30:B_2O_3, 10:SiO_2	3.60	582	7.50	$1.07x10^{-2}$ (15 GHz)	[73, 87]
LBS	35.5:Li_2O, 31.66:B_2O_3, 33.2:SiO_2	2.34	513	6.44	$3x10^{-3}$ (1 MHz)	[73, 88]
BZBS	35:Bi_2O_3, 32:ZnO, 27:B_2O_3, 6:SiO_2	4.30	950	8.80	$1.3x10^{-3}$ (1 MHz)	[73, 89]
LMZBS	20:Li_2O, 20:MgO, 20: ZnO, 20:B_2O_3, 20:SiO_2	2.75	900	6.90	$1x10^{-3}$ (1 MHz)	[73, 90]

1.10 High Permittivity Composite for Capacitor applications

1.10.1 Introduction

With technological progress, natural materials become insufficient to meet increasing demands on product capabilities and functions. These lead scientists to invent many new ceramic materials to meet increasing requirements and demands in various application areas. High k materials have received increasing interest in recent years as they are attractive as potential material for various applications including gate dielectrics, capacitor dielectrics and electrostrictive materials [91-94]. In memory devices based on capacitor components, the permittivity of the material will ultimately decide the degree of miniaturization. It is well known that enhanced electrostriction is related to the enhanced relative permittivity. This suggests that the electrostriction can be enhanced by increasing the

relative permittivity of the composite, so that same electric field can induce higher polarization and thus higher electrostriction [95]. Hence the development of high k materials has become one of the major scientific and technological issues. Few strategies have been developed to increase the permittivity of the ceramic or polymer [96-100]. A common approach is the addition of high permittivity ceramic fillers in to the polymer matrix. A very high relative permittivity could not be achieved through this approach. Another strategy is the introduction of conducting phase in ceramic or polymers. The study of two phase composite consisting of one phase, which is strongly conducting and the other phase which is insulating has been reported in number of papers due to potential advantageous changes in dielectric properties [101]. As the volume fraction of metals or conducting phases in these composites increase, the permittivity and conductivity increases gradually and when the volume fraction of the conductive powder reaches a critical value, the conductivity as well as relative permittivity of the composite increases by several orders of magnitude. This critical value is referred to as percolation limit of the composite. The high permittivity is obtained when the volume fraction of the conductive phase is very close to but not exceeds the percolation threshold due to the existence of large number of conductive particles in very close proximity and blocked by very thin layer of dielectric material. It is believed that in the percolative systems, the ultra high permittivity of the composites does not result from the intrinsic permittivity value of the filler, but from giant interfacial polarization and effective increase of electrode surface area due to the formation of conductive particle clusters at the filler contents just below the percolation threshold [99, 100].

1.10.2 Percolation

The theory of percolation was initially developed by Broadbent and Hammersley in 1957 to describe several abrupt transitions commonly found

in transport phenomena [102]. In common language, this term refers to the ability of a fluid to pass through a filter. However, based on this model, a general theory was built that satisfactorily explains a large number of physical processes in which macroscopic magnitudes are strongly modified as a result of small microscopic changes in connectivity. This theory predicts the permittivity of the composite comprising conductive filler embedded in a dielectric matrix diverges at the percolation threshold, where the insulator-metal transition occurs. In recent years several researchers made extensive theoretical and experimental studies on the critical behaviour of metal-insulator composites near percolation threshold. In such networks there is either direct contact between adjacent particles or sufficiently small gaps between them, to enable a mechanism of quantum mechanical tunnelling or hopping. Among other factors, the percolation threshold is strongly influenced by the geometrical characteristics of the conductive fillers such as aspect ratio, particle size and its distribution, so that increase in their value may dramatically drop the filler concentration required to achieve the conduction in a given insulating matrix. Composite materials of an insulating matrix and randomly dispersed metal particles are considered as heterogeneous disordered systems. Interfacial polarization is the result of the heterogeneity of the system, such as mobile charges accumulated at the metal particles–insulating matrix interface, forming large dipoles. On the other hand, locally restricted or extended through the whole system, migration of charges gives rise to materials conductivity. The concentration of the conductive inclusions has been proved to be a crucial parameter, governing the electrical behavior of the composites. When the filler content is low, the mean distance between metal particles or clusters is sufficiently large and conductance is restricted by the presence of the dielectric matrix. However, by increasing the conductive phase content, the metal ''islands'' get closer and at a critical concentration of the filler, a physical path is

formed, through which the current can flow percolating the whole system. Percolation theory describes the transition from the state of limited and spatially restricted connections of conductive elements to the state of an infinite network of connections. In the vicinity of the transition, transport properties exhibit strongly non-linear behavior which, in the case of electrical conduction, is expressed via a power-law variation of conductivity. The electrical properties of the composites formed by loading a kind of conducting particle into the insulating host media can be predicted by the classical percolation theory. According to the well known percolation theory, the permittivity of a percolating composite is inversely proportional to the difference between the real filling fraction of the fillers and the threshold value of the percolation. The concentration dependence of the electrical properties is given by the following power law on the basis of percolation theory [103],

$$\varepsilon_{(v)} \propto (V_c - V)^{-q} \text{------(1.40)} \qquad \sigma_{(v)} \propto (V_c - V)^{-s} \text{------(1.41)}$$

where $\varepsilon_{(v)}$ and $\sigma_{(v)}$ is the permittivity and conductivity of insulating phase, V_c is the volume fraction of metal at percolation, V is the volume fraction of metal, '*q* ' and '*s* ' are the critical exponents.

1.10.3. Embedded capacitor technology

As part of the general effort to miniaturize electronic equipments, the electronics packaging industry is continuously seeking ways to increase the integration density of printed circuit boards (PCBs). Towards this goal the so called "embedded passive technology" has attracted considerable interest in recent years. Embedded capacitor technology is an important emerging technology that will enable significant improvement in the performance and functionality of future electronic devices [104]. Embedded capacitors are especially printed portions of printed circuit board laminates which perform

the charge storing function but do not require space on the surface of PCB. Integration of embedded passive components into printed circuit board offers a significant reduction in size, better electrical performance, reliability, lower costs and improved design options. Among embedded passive components, the embedded capacitor is particularly important because they are used in large number of various functions such as decoupling, bypassing, energy storage and filtering capacitors. One major technical challenge for implementing this technology is the development of appropriate dielectric materials with good electrical and mechanical properties because traditional ceramic dielectrics can not be applied by current PCB manufacturing methodologies. Particulate filled (0-3 connectivity) polymer based composites provide an ideal solution, processing enhanced electrical properties and retaining the mechanical properties of the matrix. Much research work has been done on the ceramic-polymer systems that adopt traditional ceramic fillers. Advantages of these composites include predictable permittivity, low dielectric loss and easy fabrication. Embedded passive component technology is being researched by Georgia Tech's Packaging Research Centre in conjunction with the novel concept of a system on package [97, 104, 105]. Fig. 1.19 shows the typical layout of embedded capacitor technology.

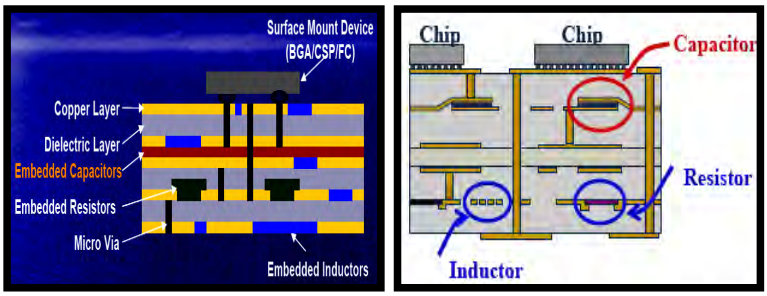

Fig. 1. 19 Typical Layout of Embedded passive Technology. (Ref: 104, 105)

Reference

1. D. Tse and P. Viswanath, "*Fundamentals of Wireless Communication*", Cambridge University press, Newyork, (2005).
2. A. Goldsmith, "*Design and Performance of 3G Wireless Networks and Wireless Lans*", Springer, US, (2005).
3. D. M. Pozar, "*Microwave engineering*", John Wiley & Sons, (1997).
4. M. Schwartz, "*Mobile Wireless Communications*", Cambridge University press, Newyork, (2005).
5. M. T. Sebastian, "*Dielectric materials for wireless communications*", Elseiver Publishers, Oxford, U. K, (2008).
6. W. Wersing, *Current Opinion In Solid State & Materials Science*, **1**, 715, (1996).
7. B. D. Hatton, K. Landskron, W. J. Hunks, M. R. Bennett, D. Shukaris, D. D. Perovic and G. A. Ozin, *Materials Today*, **9**, 22, (2006).
8. E. C. Jordan and K. G. Balmain, "*Electromagnetic waves and radiating systems*", Prentice-Hall, (1968).
9. C. A. Balanis, "*Antenna Theory, Analysis and Design* ", Wiley-Interscience, (1982).
10. J. M. Herbert, "*Ceramic Dielectrics and Capacitors*", Gordon and Breach Science Publishers, UK, (1992).
11. http://www.doitpoms.ac.uk/tlplib/dielectrics/.
12. http://www.microwaves101.com/.
13. H. Ohsato, *J. Ceram. Soc. Japan*, **113**, 703, (2005).
14. H. Ohsato, T. Tsunooka, A. Kan, Y. Ohishi, Y. Miyauchi, Y. Tohdo, T. Kawai, K. Kakimoto and H. Ogawa, *Electroceram. in Japan* ***Vii*****, 269**, 195, (2004).
15. H. Ohsato, T. Tsunooka, T. Sugiyama, K. Kakimoto and H. Ogawa, *J. Electroceram.*, **17**, 445, (2006).
16. K. P. Surendran, P. V. Bijumon, P. Mohanan and M. T. Sebastian, *Appl. Phys. A-Mater. Sci. Process.*, **81**, 823, (2005).
17. D. P. Button, B. A. Yost, R. H. French, W. Y. Hsu, J. D. Belt, M. A. Subrahmanian, H.-M. Zhang, R. E. Geidd, A. J. Whittacker and D. G. Onn, *Ceramic Substrates and Packages for Electronic Applications, Advances in Ceramics, American Ceramic Society, Westerville OH*, **26**, 353, (1989).
18. R. E. Newnham, D. P. Skinner and L. E. Cross, *Mater. Res. Bull.*, **13**, 525, (1978).

19. D. S. Malachlan, M. Blaszkiewicz and R. E. Newnham, *J. Am. Ceram. Soc.*, **73**, 2187, (1990).

20. C. J. Dias and D. K. Das Gupta, *IEEE Trans. Diele. Elect. Insu.*, **3**, 706, (1996).

21. R. W. Cahn, P. Haasen and E. J. Krawer, "*Materials Science and Technology a Comprehensive Study*", Structure and properties of composites VCH, Tokyo, (1993).

22. J. A. Bur, *Polymer*, **26**, 963, (1985).

23. S. K. Kaul, "*Millimeterwaves and Optical Dielectric Integrated Circuits*", Wiley, New York, (1997).

24. Y. Rao, J. M. Qu, T. Marinis and C. P. Wong, *IEEE Tran. Comp. Pack. Tech.*, **23**, 680, (2000).

25. R. Freer, *Silicate Industriels*, **9-10**, 191, (1993).

26. D. Kajfez and P. Guillon, "*Dielectric Resonators*", Noble Publishing Corporation, Atlanta, US, Atlanta, (1998).

27. R. D. Richtmyer, *J. Appl. Phys.*, **15**, 391, (1939).

28. H. M. Schlicke, *J. Appl. Phys.*, **24**, 187, (1953).

29. A. Okaya, *Proc. IRE, **48**, 1921,* (1960).

30. A. Okaya and L. F. Barash, *Proc. IRE,* **50**, 2081, (1962).

31. S. B. Cohn, *IEEE Trans. Microwave Theory Tech.*, **MTT-16**, 218, (1968).

32. D. J. Masse, R. A Purcel, D. W. Ready, E. A. Maguire and C. P. Hartwig, *Proc. IEEE.* **59**, 1628, (1971).

33. J. K. Plourde, D. F. Linn, H. M. J. O'Bryan and J. J. Thompson, *J. Am. Ceram. Soc.*, **58**, 418, (1975).

34. G. Wolfram and H. E. Goebel, *Mater. Res. Bull.*, **16**, 1455, (1981).

35. N. Michiura, T. Tatekawa, Y. Higuchi and H. Tamura, *J. Am. Ceram. Soc.*, **78**, 793, (1995).

36. C.-L. Huang and M.-H. Weng, *Mater. Res. Bull.*, **36**, 2741, (2001).

37. S. Nishigaki, S. Yano, H. Kato, T. Hirai and T. Nonomura, *J. Am. Ceram. Soc.*, **71**, C-11, (1988).

38. H. M. J. O'Bryan, J. J. Thomson and J. K. Plourde, *J. Am. Ceram. Soc.*, **57**, 450, (1974).

39. R. Roy, *J. Am. Ceram. Soc.*, **27**, 581, (1954).

40. S. Nishigaki, H. Kato, S. Yano and R. Kamimura, *Am. Ceram. Soc. Bull.*, **66**, 1405, (1987).

41. C.-L. Huang and M.-H. Weng, *Mater. Res. Bull.*, **37**, 1941, (2002).

42. B. Jancar, M. Valant and D. Suvorov, *Chem. Mater.*, **16**, 1075, (2004).

43. J. H. Moon, H. M. Jung, H. S. Park, J. Y. Shin and H. S. Kim, *Jpn. J. Appl. Phys.*, **38**, 6821, (1999).

44. P. Sun, T. Nakamura, Y. J. Shan, Y. Inaguma, M. Itoh and T. Kitamura, *Jpn. J. Appl. Phys*, **37**, 5625, (1998).

45. M. Sucher and J. Fox, "*Measurement of Q in Handbook of Microwave Measuremens*", 3rd Edition, Polytechnic Press, Brooklyn, (1963).

46. Y. Kobayashi and M. Miura, *IEEE MTT-S Int. Microwave Symp. Dig. San Fransico*, 184, (1984).

47. Y. Kobayashi and T. Tanaka, *IEEE Trans. Microwave Theory Tech*, **28**, 1077, (1980).

48. P. Vincent, *Appl. Phys. A*, **31**, 51, (1983).

49. H. Frohlics, "*Theory of Dielectrics*", Clarendon Press, Oxford, (1950).

50. R. D. Shannon, *J. Appl. Phys.*, **73**, 348, (1993).

51. I. J. Bahl and P. Bhartia, "*Microwave Solid State Circuit Design*", Wiley, New York,(1988).

52. R. Kudesia, PhD Thesis, (Alfred University), (1992).

53. K. Fukuda, R. Kotoh and I. Awai, *Jpn. J. Appl. Phys.*, **32**, 4584, (1993).

54. P. J. Harrop, *J. Mater. Sci.*, **4**, 370, (1969).

55. E. L. Colla, I. M. Reaney and N. Setter, *J. Appl. Phys.*, **74**, 3414, (1993).

56. A. Templeton, X. R. Wang, S. J. Penn, S. J. Webb, L. F. Cohen and N. M. Alford, *J. Am. Ceram. Soc.*, **83**, 95, (2000).

57. T. Negas, G. Yeager, S. Bell, N. Coats and I. Minis, *Am. Ceram. Soc. Bull.*, **72**, 80, (1993).

58. D. A. Sagala and S. Nambu, *J. Am. Ceram. Soc.*, **75**, 2573, (1992).

59. J. D. Breeze, J. M. Perkins, D. W. McComb and N. M. Alford, *J. Am. Ceram. Soc.*, **92**, 671, (2009).

60. A. K. Jonscher, "*Universal Relaxation Law*", Chelsea Dielectric, London, (1996).

61. S. J. Penn, N. M. Alford, A. Templeton, X. R. Wang, M. S. Xu, M. Reece and K. Schrapel, *J. Am. Ceram. Soc.*, **80**, 1885, (1997).

62. H. L. Curtis, *Bur. Stand. (US) Bull.*, **2**, 359, (1915).

63. R. F. Field, *J. Appl. Phys.*, **17**, 318, (1946).

64. W. R. Tinga, W. A. G. Voss and B. V. Blossey, *J. Appl. Phys*., **44**, 3897, (1973).

65. W. D. Kingery, H. K. Bowen and D. R. Uhlmann, "*Introduction to ceramics*", 2nd Ed., Wiley, New York, (1976).

66. J. W. R. Day, *IEEE MTT-S Int. Microwave Symp. Dig. San Fransico*, **24**, (1970).

67. K. Wakino, T. Nishikawa, S. Tamura and H. Tamura, *37th Annu. Freq. Contr. Symp, Japan*. (1983).

68. K. Wakino, T. Nishikawa, S. Tamura and Y. Ishikawa, *IEEE MTT-S Int. Microwave Symp. Dig.* (1975).

69. S. J. Fiedziuszko, I. C. Hunter, T. Itoh, Y. Kobayashi, T. Nishikawa, S. N. Stitzer and K. Wakino, *IEEE Trans. Microwave Theory and Tech.*, **50**, 706, (2002).

70. I. M Reaney, D. Iddles, *J. Am. Ceram. Soc*. **89**, 2063, (2007).

71. S. A. Long, M. W. Mac Allister and L. C. Shen, *IEEE Trans. Ant. Prop.*, **31**, 406, (1983).

72. K. M. Luk and K. W. Leung, "*Dielectric Resonator Antennas*", Research Studies Press, England, (2003).

73. M. T. Sebastian and H. Jantunen, *Int. Mater. Rev.*, **53**, 57, (2008).

74. Y. Imanaka, "*Multylayered Low Temperature Cofired Ceramics (LTCC) Technology*", Spinger, Japan, (2005).

75. L. Devlin, G. Pearson and J. Pittock, *Proc. of the 38th IMAPS Nordic Conference, Oslo, Norway*. (2001).

76. A. Sutono, D. Heo, Y. J. E. Chen and J. Laskar, *IEEE Trans. Microwave Theory and Tech.,* **MTT- 49**, (2001).

77. H. Jantunen, T. Kangasvieri, J. Vähäkangas and S. Leppävuori, *J. Eur.Ceram. Soc.*, **23**, 2541, (2003).

78. R. E. Mistler and E. R. Twiname, "*Tape Casting: Theory and Practice, 2.*" American Ceramic Society, Westerville, OH, (2000).

79. B. Schwartz, *Am. Ceram. Soc. Bull.*, **63**, 577, (1984).

80. K. P. Surendran, "PhD Thesis", University of Kerala, *Faculty of Science*, (2004),

81. K. P. Surendran, P. Mohanan and M. T. Sebastian, *J. Solid State Chem.*, **177**, 4031, (2004).

82. J.-H. Jean and T. K. Gupta, *J. Mater. Sci.*, **27**, 1575, (1992).

83. H. Jantunen, "PhD Thesis" *Faculty of Science*, (Finland, University of Oulu), (2001).

84. M. H. Kim, Y. H. Jepng, S. Nahm, H. T. Kim and H. J. Lee, *J. Eur. Ceram. Soc*, **26**, 2139, (2006).

85. M. H. Kim, S. Nahm, W. S. Lee, M. J. Yoo, N. K. Kang, H. T. Kim and H. J. Lee, *Jpn. J. Appl. Phys.*, **44**, 3091, (2005).

86. L. Navias and R. L. Green, *J. Am. Ceram. Soc.*, **29**, 267, (1946).

87. J. M. Wu and H. L. Huang, *J. Non-Cryst. Solids*, **260**, 116, (1999).

88. H. Jantunen, R. Rautioaho, A. Uusimaki and S. Leppavuori, *J. Eur. Ceram. Soc.*, **20**, 2331, (2000).

89. S. Thomas and M. T. Sebastian, *Mater. Res. Bull.*, **43**, 843, (2008).

90. S. Renjini, S. Thomas, M. T. Sebastian, S. R. Kiran and V. R. K. Murthy, *Int. J. Appl. Ceram. Tech.*, **6**, 286, (2009).

91. F. T. Chen, C. W. Chu, J. He, Y. Yang and J. L. Lin, *Appl. Phys. Lett.*, **85**, 3295, (2004).

92. C. Huang and Q. M. Zhang, *Adv. Funct. Mater.*, **14**, 501, (2004).

93. C. Huang, Q. M. Zhang, G. deBotton and K. Bhattacharya, *Appl. Phys. Lett.*, **84**, 4391, (2004).

94. Y. Rao, S. Ogitani, P. Kohl and C. P. Wong, *J. Appl. Poly. Sci.*, **83**, 1084, (2002).

95. S. George, J. James and M. T. Sebastian, *J. Am. Ceram. Soc.* **90**, 3522, (2007).

96. M. Arbatti, X. Shan and Z. Cheng, *Adv. Mater.*, **19**, 1369, (2007).

97. S. K. Bhattacharya and R. R. Tummala, *Microelectronics Journal*, **32**, 11, (2001).

98. Z. M. Dang, Y. H. Lin and C. W. Nan, *Adv. Mater.*, **15**, 1625, (2003).

99. C. Pecharroman, F. Esteban-Betegon, J. F. Bartolome, S. Lopez-Esteban and J. S. Moya, *Adv. Mater.*, **13**, 1541, (2001).

100. C. Pecharroman and J. S. Moya, *Adv. Mater.*, **12**, 294, (2000).

101. L. Qi, B. I. Lee, W. D. Samuels, G. J. Exarhos and S. G. Parler, *J. Appl. Poly. Sci.*, **102**, 967, (2006).

102. S. Kirkpatrick, *Rev. Mod. Phys*, **45**, 574, (1973).

103. G. C. Psarras, *Comp. Part A-Appl. Sci. Manuf.*, **37**, 1545, (2006).

104. J. X. Lu and C. P. Wong, *IEEE Trans. Diele. Elect. Insu.*, **15**, 1322, (2008).

105. S. K. Bhattacharya and R. R. Tummala, *J. Mater. Sci. Mater. Electr.*, **11**, 253, (2000).

Chapter 2

Synthesis and Characterization of Dielectric Substrates, Resonators and Composites

The sequential description of various steps involved in the synthesis of microwave dielectric ceramics and its composites is presented in this chapter. A brief description of the instrumentation techniques used for studying the structural, microstructural, dielectric and thermal characteristics of low loss microwave dielectric ceramics and polymer composites studied in the thesis is also presented.

2. 1 Synthesis of Dielectric Ceramics

2.1.1 Introduction

The term ceramics derived from the ancient Greek word "Keramos" which means fired clay. A ceramic is a polycrystalline non-metallic body made by forming a shape from a powder and heating the sample to impart mechanical strength [1]. Kingery, regarded as the father of modern ceramic engineering, suggested a new definition of ceramics: "art and science of making and using solid articles which have as their essential components, and are composed of inorganic and nonmetallic materials"[2]. The term ceramics is usually associated with pottery sculpture, sanitary ware, tiles etc. However, this view point is incomplete as it contains only the traditional or silicate based ceramics. Today the field of ceramics can be divided into traditional and advanced ceramics. Traditional ceramics are characterized by silicate based porous microstructures that are coarse, non uniform and multiphase. They are formed by mixing clays and feldspar followed by forming either by slip-casting or on potters wheel, then firing and finally glazing. Regarding the applications of traditional ceramics are quite common from sanitary ware to fine Chinas. Ceramics for today's engineering applications are synthesized using highly refined raw material, rigorously controlled composition, strictly regulated forming and sintering and are known as "Fine or Advanced Ceramics"[3]. Advanced ceramics possess properties which allow their use in a variety of defense and commercial applications. Advanced ceramics consist of oxides, carbides, perovskites and even completely synthetic materials which have no natural equivalents. The microstructure of the ceramics contains: fine crystalline grains, grain boundaries, impurities and crystal lattice defects in the grains and grain boundaries and pores in the grain as well as in grain boundaries [4, 5]. High technology advanced ceramics is an essential part of the

electronic and electrical equipment used for the consumer, industrial, and military applications. The electronic ceramics are integral components of the circuits used in computers, signal processing, telecommunications, power transmission, and power control technologies [2]. The electrical and electronic applications include, electrical insulators, ferroelectric and piezoelectric ceramics, semiconductors, superconductors, ionic conductors, thermistors, insulators in electronic applications, microwave dielectrics, magnetic materials etc. The telecommunication technology is the fastest growing technology in the world. Among electrical and electronic applications of ceramics, microwave dielectrics have extreme importance, since the dielectric materials play prominent role in microelectronic devices and satellite communications. Hence thorough investigations on dielectric ceramic materials are become increasingly important in our modern world.

Technical or engineering ceramic production is a demanding and complex procedure. Processing of ceramics into useful products requires transformation of powdered raw materials to a dense uniform body through the application of consolidation techniques and subsequent thermal processing. Ceramic fabrication techniques generally include various powder processing methods with powder synthesis, forming and sintering. The powder synthesis processes of ceramics include several techniques like (a) solid state reaction methods (b) mechanical methods and (c) chemical methods [6, 7]. The synthesis of specific powders and better control of chemical and physical characteristics of ceramic powders can deliver improved and reproducible properties. The physical and chemical characteristics of ceramic powders strongly influence their behavior during processing and thus impact the microstructure and performance of the ceramic component.

The most common method of preparing ceramic powders is by solid-state reaction method, because it is the simplest, easier and cost effective

method to make bulk amount of ceramics [8, 9]. The inhomogeneity of particle size distribution and high temperature of formation are the major drawbacks of solid state ceramic techniques. However, compared to chemical synthesis it is cost effective, less time consuming and hence it is more popular. In the mechanical methods, small particles are produced from larger ones by mechanical forces, a process referred to as comminution [10]. The process of comminution involves operations such as crushing, grinding and milling. Mechanical treatment of ceramic powders can reduce particle size and enables to obtain nano-structured powders, which are of the main interest in the current trend of miniaturization and integration of electronic components. However, this technique lacks the synthesis of phase pure ceramics, which is essential for the fabrication of microwave dielectric ceramics with optimum dielectric properties. The citrate gel, molten salt, co-precipitation, sol-gel, hydrothermal and polymer precursor methods are the well known chemical methods to prepare ceramics [11, 12]. But the sinterability of bulk ceramics prepared using chemically derived powders was found to be very poor and hence none of these techniques could give a higher quality factor for dielectric resonators compared to the dielectric resonators obtained through solid state technique. Moreover the stringent operation conditions involved in the reaction sequence as well as the high cost of chemicals limit the usage of chemical methods for the industrial fabrication of microwave dielectrics. Hence in the present study we have employed the conventional solid state synthesis of ceramics for the fabrication of microwave dielectrics, because this method is cost effective and can lead to better dielectric properties, which is the primary interest in the fabrication of devices employing microwave dielectrics.

2.1.2 Solid state synthesis of ceramics

The most realistic method of preparing ceramic powders is by solid-state reaction methods, because it is the simplest, easier and cost effective

method for producing bulk ceramics. Conventional solid state synthesis techniques involve heating mixtures of two or more solids to form a single solid phase product. High purity materials and precise methods of production must be employed to ensure that the desired properties of these advanced materials are achieved in the final product. On heating at high temperatures, a new material is formed (see Fig. 2.1) to reduce the free energy, at the points of contact through solid state diffusion. This new product layer (of a few Å) eventually acts as a potential barrier between the two grains and thus impeding further grain to grain material transport. This demands the need of new point of contacts to be introduced which is usually achieved through grinding or ball milling. This frequent grinding coupled with multiple calcination maximizes the product to reactant ratio [13]. The different stages for the solid state reaction method employed in the present work are shown in Fig.2.2.

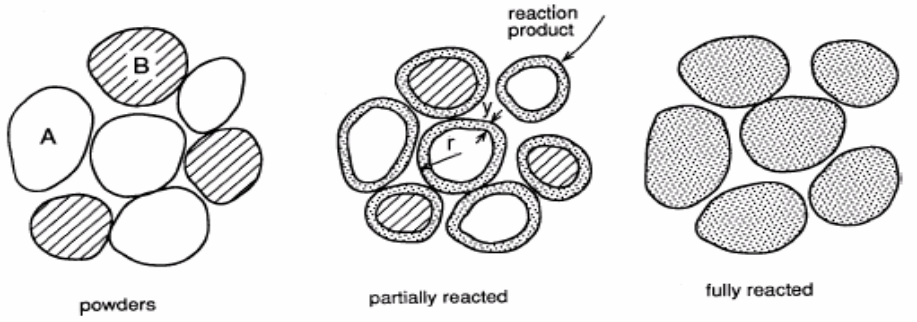

Fig. 2. 1 Reaction between two kinds of particles to form a product at the points of contact

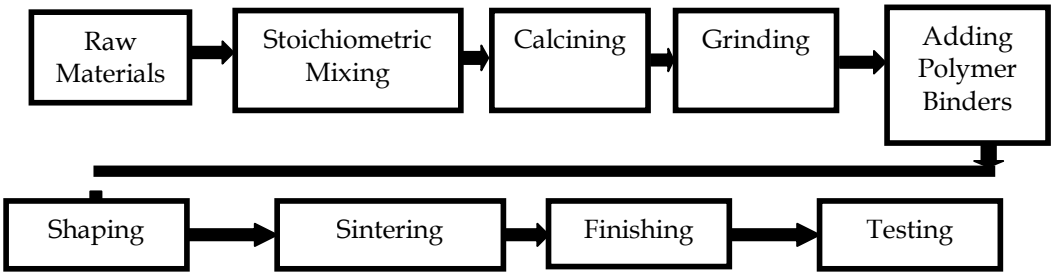

Fig. 2. 2 The different stages for the solid state reaction method employed in the present work

2.1.2.1 Weighing of raw materials

The first step to prepare the dielectric ceramic by the solid-state route is to weigh the different oxides or carbonates according to the stoichiometry of the product phase. The presence of impurities in the raw materials can affect reactivity as well as dielectric properties of the fired ceramics. Hence the raw material purity should be greater than 99.9 % for obtaining phase pure compounds. Electronic Balance is used to obtain accuracy up to four decimal places.

2.1.2.2 Mixing of raw materials

Solid state reaction of oxides involves the interdiffusion of the ions concerned to form a compound or solid solution which may be homogeneous in composition. The raw materials need to be intimately mixed to increase the point of contacts between reactant oxides, which in turn act as 'product layer formation centers'. The mixing and milling eliminates agglomerates and reduces particle size. If agglomerates are present, the densification may be more rapid resulting in pores. During the mixing process agglomerates are broken and defects are introduced into the grains that enhance diffusion mechanism. Therefore the mixture of powders is ground well and thoroughly mixed using liquid medium. The best dispersion of particles is obtained by milling in a liquid medium. Water is the most commonly used liquid, although alcohol or acetone is used where oxidation in water is undesirable. Ball mills using yittriya stabilized zirconia balls are used for the mixing purpose. In the milling process, the particles experience mechanical stresses at their contact points due to compression, impact or shear with the milling medium or with other particles [14]. The mechanical stress leads to elastic and inelastic deformation. If the stresses exceed ultimate strength of the particle, it will fracture the particles. The mechanical energy supplied to the particle is used not only to create new

surfaces but also to produce other physical changes in the particle [14, 15]. In the present investigation, the mixture of constituent powders taken in polythethylene bottles were ball milled for sufficient duration in ethanol medium using Yttria Stabilized Zirconia (YSZ) balls. The resultant slurry after stoichiometric mixing was dried using hot air oven.

2.1.2.3 Calcination

Calcination is the intermediate heat treatment process at a lower temperature prior to sintering [16]. Calcination reactions often play a vital role in the synthesis of multicomponent ceramic compounds. The purpose of calcination is to promote sufficient interaction between the constituents to form a material that will sinter to a dimensionally, mechanically and electrically satisfactory body. Calcination involves chemical decomposition reactions, in which a solid reactant is heated to produce a new solid product with the liberation of gas. The optimum calcination conditions are usually determined empirically to suit local manufacturing practice. The kinetics of solid state reactions occurring during calcination may be controlled by any one of three processes: (i) the reaction at the interface between the reactant and the solid product, (ii) heat transfer to the reaction surface or (iii) gas diffusion or permeation from the reaction surface through the porous product layer. The calcination conditions such as temperature, duration of heating and atmosphere are important factors controlling shrinkage during sintering. Though the final phases of interest may not be completely formed, the calcination yields a consistent product.

2.1.2.4 Grinding

Calcined powders are invariably agglomerated, often with a hierarchy of agglomerates. The largest agglomerates are usually porous. Grinding prepares the reacted material for ceramic forming. The grinding also helps to homogenize the compositional variations that may still exist or

that may arise during calcination. Generally, grinding to particles of about 1 to 10 μm is advisable. If the grinding is coarser, the ceramic can have larger intergranular voids and lower fired density. If grinding is too fine, the colloidal properties may interfere with subsequent forming operations. Generally, for grinding purpose ball mill or mortar with pestle is used. Ball-mills are commonly used for large scale operation [17]. The amount of balls and the liquid medium used in the mixing operation must be sufficient to allow free movement of the balls while the mills rotate. The process of ball milling for grinding is bound to introduce impurities coming from the surfaces getting into contact with the powder. Hence, grinding the ceramic powders using mortar and pestle is used in the present investigation

2.1.2.5 Addition of polymeric binder

The purposes of addition of binders are to impart sufficient strength and appropriate mechanical properties to ceramics for handling and shaping during the post forming stage. The constituents added to confer plasticity, strength prior to firing or to assist sintering must be carefully chosen such that it will not affect the properties of the ultimate product. Materials added to facilitate shaping in the green state are therefore usually organic, so that they will be completely burned off in the early stages of sintering. In modern ceramic technology, in die pressing, a narrow range of water-soluble organic binders, such as poly vinyl alcohol (PVA) is most often used to improve the rheological properties of the powder compact [18]. The polymeric dispersions and organic binders provide the pressed ceramic powders with optimal properties from the point of view of thickening abilities and mechanical strength of the pressed samples [19]. The commonly used polymers for ceramic binding purpose are poly vinyl alcohol (PVA), poly ethylene glycol (PEG), carboxymethylcellulose etc. most of which are water thinnable polymeric dispersions. The binder concentration for each process is about 3 % in dry process, 3-17 % in wet processing and 7-20 % in plastic

forming [20]. The recent research trends suggest that the PVA and PEG are ideal binder additives for fabrication of microwave dielectric ceramics [21]. The PVA will burn out on heating above 400^{o}C.

2.1.2.6 Forming

Forming or shaping is the process of making the powder in the desired form or shape. The primary processes for forming shaped compacts of a ceramic powder include dry pressing, slip casting, tape casting, extrusion, injection molding and green machining [3, 4]. The most common and widespread is uniaxial dry pressing. The aim of powder pressing is to form a net-shaped, homogeneously dense powder compact that is nominally free of defects. A typical pressing operation has three basic steps: (i) filling the mold or die with powder (ii) compacting the powder to a specific size and shape and (iii) ejecting the compact from the die. Die filling/uniformity influences compaction density, which ultimately determines the size, shape, microstructure and properties of the final sintered product. To optimize die filling and packing uniformity, free-flowing granulated powders are generally used. During powder pressing, the compaction pressure promotes consolidation by granule rearrangement and granule deformation. Particle coordination number, green density and compact strength all increase with increasing pressure, while volume and size of the porosity in the compact decrease [22, 23]. In the present study the fine powder is compacted into cylindrical and rectangular specimen by uniaxial dry-pressing. Compaction is done slowly to facilitate the escape of the entrapped air. Internal lubricants such as stearic acid dissolved in isopropyl alcohol, is used to reduce the friction between the powder and die wall. Pressure of 50-150 MPa is ideal for low loss ceramic forming.

2.1.2.7 Sintering

Sintering is a method for making objects from powder, by heating the material in a sintering furnace below its melting point where diffusional

mass transport is appreciable and which results in a dense polycrystalline solid [24, 25]. Thermodynamically, sintering is an irreversible process in which a free energy decrease is brought about by a decrease in surface area. The principal goal of sintering is the reduction of compact porosity. Atomic motion in sintering contributes to the formation of weld bonds between the particles and the elimination of pores. The development of microstructure and densification during sintering is a direct consequence of mass transport through several possible paths and one of these paths is usually predominant at any given stage of sintering. They are (i) evaporation/condensation (ii) solution/precipitation (ii) lattice diffusion and (iv) surface diffusion or grain boundary diffusion [26]. The normal sintering method is also termed as standard pressure sintering and is used in the present investigation. The pressed ceramic green sample is loaded over cleaned platinum plates and heated in high temperature furnaces. In this method at a certain temperature the ceramics begin to diffuse and shrinkage occurs resulting in densification. Usually the sintering temperature is a little below the melting point of the ceramics. Additive phases that improve diffusion rates during sintering are used in many ceramic materials. These phases can be used to stabilize desirable crystal structures or more typically to form a liquid phase to increase the rate of sintering. The sintering phenomena are of two types: Solid-state sintering, where all densification is achieved through changes in particle shape, without particle rearrangement or the presence of liquid and liquid-phase sintering, where some liquid that is present at sintering temperatures aids compaction.

2.1.2.7.1 Solid state sintering

Solid state sintering is the process in which fine particles, which are in contact with each other when heated to a suitable temperature, which results in the decrease in porosity [25]. During solid state sintering, the surface energy is reduced by transferring matter from the interior of grains to

adjacent pores. Grain boundaries serve as vacancy sinks. Grain growth also takes place in parallel with densification, which is favored by reduction in the area of grain boundaries. Rapid growth of discontinuous grains during sintering will trap porosity, which in turn will deteriorate the dielectric properties. Coble [26] described the sintering stage as an "interval of geometric change in which pore shape is totally defined or an interval of time during which the pore remains constant in shape while decreasing in size."

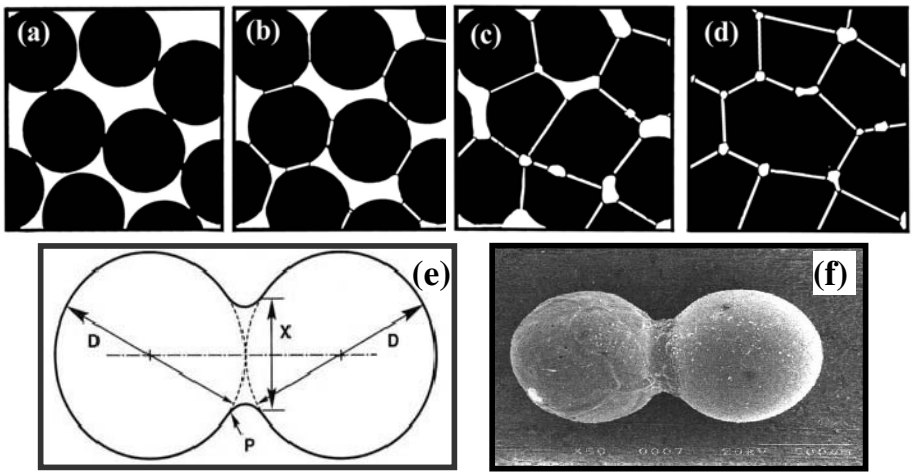

Fig. 2.3. Micrographs showing the perspectives of actual sintering behavior. (Ref. 4)

The micrographs provide the perspectives of actual sintering behavior (See Fig. 2.3). These photographs shows the change in density, grain size and pore structure that are characteristics of sintering. The initial stage of sintering generally corresponds to a microstructure with large curvature gradients. The neck size ratio and shrinkage are small and the grain size is no longer than the initial particle size [26]. In the intermediate stage, the pores are smoother and density is between 70 and 92% of the theoretical. Grain growth occurs late in the intermediate stage; thus grain size is larger than the initial particle size. By the final stages of sintering the pores are spherical and closed, and the grain growth is evident. Solid state

sintering involves movement of atoms that in turn is dependent on temperature and concentration of structural imperfections such as vacancies and interstitials. The process variables in sintering are (a) sintering temperature (b) sintering time (c) sintering atmosphere. The factors affecting solid state sintering are (a) particle size and particle size distribution (b) particle shape (c) uniformity of green microstructure (d) particle composition and (e) green density [27].

2.1.2.7.2 Liquid phase sintering (LPS)

Liquid Phase Sintering (LPS) is an important means of manufacturing dense ceramic components from powder compacts. LPS is a subclass of the sintering process involving particulate solid along with a coexisting liquid during some part of the thermal cycle [28, 29]. The major advantages of LPS over solid state sintering are the enhanced sintering kinetics and the tailorable properties. The disadvantages of LPS are that ceramics densified by LPS has a susceptibility to shape deformation and it may be difficult to control the sintering parameters due to additional complications from the liquid phase. The three general requirements for LPS are, (1) a liquid must be present at sintering temperature, (2) there must be a good wetting of a liquid on solid (3) there must be appreciable solubility of solid in liquid [29]. When the liquid coats each grain, the material can often be sintered to a higher density at a lower temperature. Less than 1 volume % of the liquid phase is sufficient to coat the grains if the liquid is distributed uniformly and the grain size is about 1 μm. The wetting liquid concentrates at the particle contacts and forms a meniscus; this exerts an effective compressive pressure on the compact. There is a rapid rearrangement of particles into a higher density configuration. The higher amount of liquid phases deteriorates the microwave properties. Upon melting, a wetting liquid will penetrate between grains and exert an attractive force, pulling them together. The combination of these forces and the lubricating effect of the liquid as it

penetrates between grains leads to the following mechanisms that operate in succession: [5, 29].

Rearrangement of particles: Initial densification results from particle rearrangement under the influence of capillary forces and the filling of pores by the liquid phase. The driving force for rearrangement arises because of an imbalance in capillary pressure as a result of particle size distribution, irregular particle shape, local density fluctuation in the powder compact and anisotropic material properties. Both solid and liquid are subjected to rearrangement because of unbalanced capillary forces around solid particles as dictated by particle contact and liquid meniscus geometries that result in shearing and rotational movements of particles. As density increases, particles experience increasing resistance to further rearrangement due to crowding by neighbouring particles until the formation of a closely packed dense structure.

Solution precipitation: In solution precipitation different solubilities of the solid in the liquid are responsible for the transport of the material from the points of solid-solid contacts to the free surfaces of the particles. When rearrangement becomes insignificant, additional densification can be achieved by dissolution of the solid at grain contacts thus resulting in the center-to-center approach of particles. The dissolved solute transfers to the uncompressed part of the grain structure by diffusion through a liquid phase followed by precipitation on uncompressed solid surface for a multicomponent system. There are two rate-limiting processes for solution-precipitation, diffusion controlled and interface reaction controlled material transport.

Pore removal: During intermediate stage of sintering the interconnected pore channels pinch off to form closed pores in the density range from 90 %

to 95 % depending upon the material. The final stage of LPS starts after pore closure.

2.2 Preparation of Borosilicate Glasses

The sintering temperature of the ceramics can be lowered by the addition of different borosilicate glasses. Following glasses such as lithium borosilicate (35.5:Li_2O, 31.66:B_2O_3, 33.2:SiO_2) (LBS), lead borosilicate (40:PbO, 40:B_2O_3, 20:SiO_2) (PBS), barium borosilicate (30:BaO, 60:B_2O_3, 10:SiO_2) (BBS), zinc borosilicate (60:ZnO, 30:B_2O_3, 10:SiO_2) (ZBS), bismuth zinc borosilicate (35:Bi_2O_3, 32:ZnO, 27:B_2O_3, 6:SiO_2) (BZBS) and lithium magnesium zinc borosilicate (20:Li_2O, 20:MgO, 20:ZnO 20:B_2O_3, 20:SiO_2) (LMZBS) have been selected in the present investigation. The above mentioned glass powders were synthesized from high purity oxide chemicals of B_2O_3, Li_2CO_3, SiO_2, ZnO, PbO, $BaCO_3$, Bi_2O_3 and $(MgCO_3)_4$ $Mg(OH)_2$ $5H_2O$ (99.9 % Aldrich chemical company, U.S.A). These oxides were weighed stoichiometrically and were mixed in an agate mortar for 2 hours using ethanol as medium. They were dried, melted in platinum crucible above their melting point, quenched and powdered.

2.3 Preparation of Ceramic-Polymer Composites

Composite materials are engineered materials made from two or more constituent materials with significantly different physical or chemical properties and which remain separate and distinct on a macroscopic level within the finished structure. Composite materials play a key role in the modern science and technology, especially in the area of electronics. Polymer based composite materials has a number of applications. Low dielectric loss ceramic loaded polymers can be used in electronic packaging and substrate applications. Mainly there are three preparation methods (i) Powder processing method (ii) Melt mixing and (iii) Molding or thermosetting. The powder processed polymer composites generally show

poor mechanical properties compared to other techniques and may limits their applications in electronic devices. Hence, melt mixing and thermosetting techniques have been used in the present investigation.

2.3.1 Melt mixing

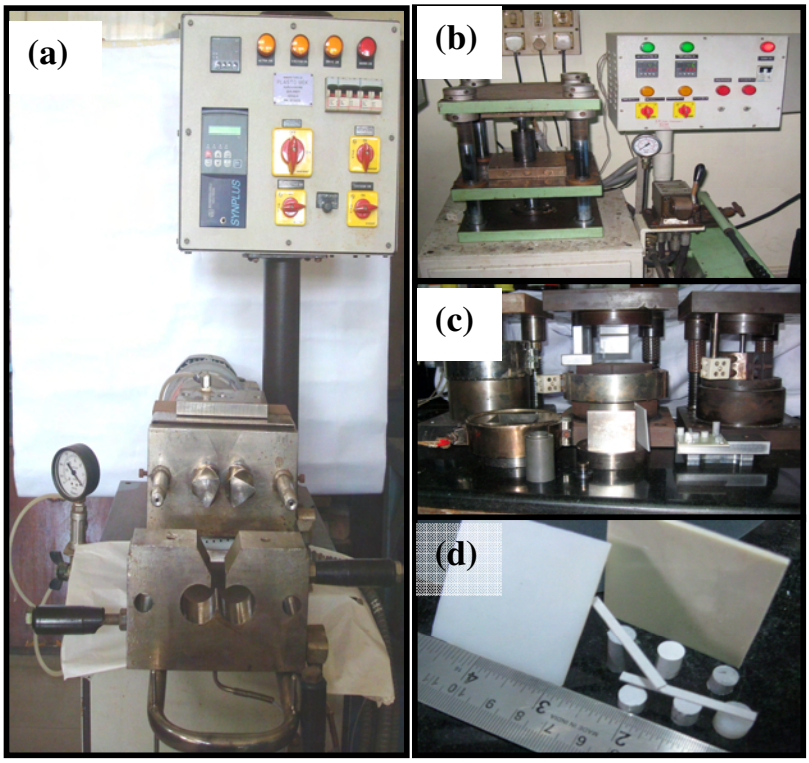

Fig. 2.4. Photographs of (a) Kneeding machine, (b) Hot press, (c) Die set used in hot press and (d) polymer-ceramic composite samples

Melt mixing technique can be employed to make composite if the polymers are thermoplastic with low viscosity during melting and low melting point (<300 ^{o}C). The melt mixing technique has been used to fabricate composite based on high density polyethylene (HDPE) and polystyrene (PS). A kneading machine was used to fabricate ceramic polymer composites. It consists of variable speed mixer having two counter rotating sigma blades and heating facility up to 300 ^{o}C. Fig. 2.4 shows the photograph of a) Kneading machine, (b) Hot press, (c) Die sets used in hot

press and (d) polymer-ceramic composite samples in the present investigation. Desired amount of polymer (normally 20 g) were taken in Kneading machine and slowly the temperature is increased. As the temperature is increased the polymer starts melting and viscous fluid is formed. Then the selected amount of ceramic was added in very small amount keeping the temperature constant and rotating the sigma blades. The preparation temperature is about 150 to 165 ^{o}C for HDPE and PS. The rotation of the sigma blades causes uniform mixing of polymer and ceramic. Thus obtained composite were hot pressed under a pressure of 50 MPa and 150 ^{o}C for 15 min.

2.3.2 Thermosetting or molding

Molding technique is used for making polymer composites involving thermosetting polymers like epoxy resin. This has an additional advantage of room temperature processing. The epoxy used in the present study was diglycidyl ether of bisphenol A (DGEBA). The curing agent used was polyamines. The epoxy to hardener ratio is 10:1. The starting materials, epoxy and ceramic powders were mixed separately using an agate and mortar for 45 minutes with an intermediate heat treatment of about 50 ^{o}C. The intermediate heat treatment lowers the viscosity of epoxy and thereby promotes the uniform dispersion of ceramic powders. The hardener was added to the epoxy-ceramic composite and mixed for 10 minutes. The presence of hardener also lowers the viscosity of the epoxy and fills up the gap between the ceramic fillers. The composite was then poured into corresponding die and kept in evacuated dessicator for 5 hours. The composite was then shaped for testing.

2.4 Structural and Microstructural Characterization of Dielectrics

2.4.1 X-Ray diffraction

X-ray diffraction is a tool for the investigation of crystal structure of matter. X-ray scattering techniques are a family of non-destructive analytical techniques which reveal information about the crystallographic structure, chemical composition, and physical properties of materials and thin films [30, 31]. X-ray diffraction techniques are based on the elastic scattering of X-rays from structures that have long range order. The crystal structures of the powdered ceramic specimens in this investigation were first analyzed by X-Ray diffraction (XRD) techniques. The X-Ray diffraction method is most useful for qualitative, rather than quantitative analysis. An X-Ray diffractometer utilizes a powdered sample, a goniometer, and a detector to measure the diffraction patterns of unknown samples. The powdered sample provides (theoretically) all possible orientations of the crystal lattice, the goniometer provides a variety of angles of incidence, and the detector measures the intensity of the diffracted beam. The resulting analysis is described graphically as a set of peaks with percentage intensity on the Y-axis and goniometer angle on the X-axis. The exact angle and intensity of a set of peaks is unique to the crystal structure being examined. A monochromator is used to ensure that a specific wavelength reaches the detector, eliminating fluorescent radiation. The resulting trace consists of recording of the intensity against counter angle (2θ). The trace can then be used to identify the phases present in the sample. Diffraction data from many materials have been recorded in a computer searchable Powder Diffraction File (PDF). Comparing the observed data with that in the PDF allows the phases in the sample to be identified [31]. In this investigation XRD spectra were recorded using CuKα radiations employing Philips X-ray Diffractometer (Model- Expert Pro, Netherlands).

2.4.2 Scanning electron microscopy

Scanning Electron Microscopic (SEM) methods were adopted in the present study to analyze the microstructure of sintered and thermally etched surface of ceramic samples [32, 33]. The scanning electron microscope (SEM) uses a focused beam of high-energy electrons to generate a variety of signals at the surface of solid specimens. The signals that derive from electron-sample interactions reveal information about the sample including external morphology (texture), chemical composition, and crystalline structure and orientation of materials making up the sample. In most applications, data are collected over a selected area of the surface of the sample, and a 2-dimensional image is generated that displays spatial variations in these properties. All metal samples are conductive and require no preparation before being used. However, all non-metals need to be made conductive by covering the sample with a thin layer of conductive material like gold. In this study we have used a JEOL-JSM 5600 LV, Tokyo, Japan for microstructural investigations.

2.4.3 Energy dispersive X-ray analyzer (EDXA)

Energy Dispersive X-Ray Spectroscopy (EDS or EDX) is a chemical microanalysis technique used in conjunction with scanning electron microscopy (SEM). The EDS is an analytical technique used for the elemental analysis or chemical characterization of a sample [34]. As a type of spectroscopy, it relies on the investigation of a sample through interactions between electromagnetic radiation and matter, analyzing x-rays emitted by the matter in response to being hit with charged particles. Its characterization capabilities are due in large part to the fundamental principle that each element has a unique atomic structure allowing x-rays that are characteristic of an element's atomic structure to be identified uniquely from each other. The electron beam in an SEM has energy typically

between 5,000 and 20,000 electron volts (eV). The energy holding electrons in atoms (the binding energy) ranges from a few eV up to many kilovolts. Many of these electrons are dislodged as the incident electrons pass through the specimen. Ejection of an atomic electron by an electron in the beam ionizes the atom, which is then quickly neutralized by other electrons. In the neutralization process an x-ray beam with an energy characteristic of the parent atom is emitted. By collecting and analyzing the energy of these x-rays, the constituent elements of the specimen can be determined. There are four primary components of the EDXA setup: the beam source; the X-ray detector; the pulse processor; and the analyzer. Electron microscopes are equipped with a cathode and magnetic lenses to create and focus a beam of electrons. A detector is used to convert X-ray energy into voltage signals; this information is sent to a pulse processor, which measures the signals and passes them onto an analyzer for data display and analysis.

2.5 Microwave Characterization

2.5.1 Introduction

Microwave materials have been widely used in a variety of applications ranging from communication devices to military satellite services, and the study of materials properties at microwave frequencies and the development of functional materials have always been among the most active area of materials science, electrical and electronic engineering. In recent years, the increasing requirements for the development of high speed, high frequency circuits and systems require complete understanding of the properties of materials functioning at microwave frequencies. All these aspects make the characterization of material properties an important field in microwave electronics. The microwave methods for materials characterization generally fall into non-resonant method and resonant methods [35, 36]. Non-resonant methods are often used to get a general

knowledge of electromagnetic properties over a frequency range while the resonant methods are used to get accurate knowledge of dielectric properties at a single frequency or several discrete frequencies.

2.5.2 Network analyzer

Network Analyzer is the major instrument used in this investigation for the characterization low loss microwave dielectric ceramics. A measurement of the reflection from and/or transmission through a material along with knowledge of its physical dimensions provides the information to characterize the permittivity and permeability of the material. Network Analyzer is a swept frequency measurement equipment to completely characterize the complex network parameters in comparatively less time, without any degradation in accuracy and precision. Two types of network analyzers are available, scalar and vector network analyzers. Scalar network analyzer measures only the magnitude of reflection and transmission coefficients while the vector network analyzer measures both the magnitude and phase. Both the magnitude and phase behavior of a component can be critical to the performance of a communications system. A vector network analyzer can provide information on a wide range of these devices, from active devices such as amplifiers and transistors, to passive devices such as capacitors and filters. A basic network analyzer is designed to show graphically, a plot of the voltage gain or loss of a network versus frequency. The network analyzer measures the magnitude, phase and group delay of two-port networks to characterize their linear behavior. A vector network analyzer consists of a signal source, a receiver and a display. The source launches a signal at a single frequency to the material under test. The receiver is tuned to that frequency to detect the reflected and transmitted signals from the material. The measured response produces the magnitude and phase data at that frequency. The source is then stepped to the next frequency and the measurement is repeated to display the reflection and

transmission measurement response as a function of frequency (Bode response plot). The analyzer can operate in ramp or in step mode. In the ramp mode the analyzer directs the source to sweep in a linear ramp over the frequency and in the step mode, it provides maximum precision.

2.5.3 Non-resonant method

In non-resonant methods, the properties of materials are fundamentally deduced from their impedance and wave velocities in the materials. When electromagnetic wave propagates from one material to another, both the characteristic wave impedance and velocity change, resulting in a partial reflection of the electromagnetic wave from the interface between the two materials. Measurements of the reflection from such an interface and the transmission through the interface can provide information for the deduction of permittivity and permeability relation between the materials. Non-resonant method mainly includes reflection methods and reflection/transmission methods [35].

Reflection methods: In reflection methods, the properties of a sample are obtained from the reflection due to the impedance discontinuity caused by the presence of sample in a transmission structure. When the permittivity becomes high, there occurs considerable error in the measurement of complex voltage reflection coefficient [37].

Transmission/reflection methods: In a transmission/reflection method, the material under test is inserted into a segment of transmission line and the properties of the materials are deduced on the basis of the reflection from the material and the transmission through the material.

Optical methods: Optical methods are applicable for wavelength below one centimeter. Since this method requires large amount of material it is not suitable for DRs [38].

Transmission line techniques: This technique has a serious disadvantage of the very small waveguide size used below 4 mm, which gives rise to practical difficulties [39]. Moreover imperfections in the sample dimensions produce errors in the measurement. It was reported that the accuracy of transmission mode measurements of the dielectric properties is more in weak coupling conditions [40].

2.5.4 Resonant method

Resonant methods usually have higher accuracy than non-resonant methods, and they are most suitable for low loss samples. Resonant methods generally include resonator method and resonant perturbation methods [35, 36].

Resonator method: Resonant methods are widely used because of their high accuracy and sensitivity. This method is often called dielectric resonator method. In this method the sample serves as a resonator or a key part of the resonator in the measurement circuit and the properties of the sample derived from the resonant properties of the resonator.

Resonant perturbation method: In a resonant perturbation method, the sample is inserted into a resonator, and the properties of the sample are calculated from the changes of the resonant frequency and the quality factor of the resonator caused by the sample. The perturbation methods are highly suitable for materials of small size since the material should not alter the field configuration considerably. These techniques are suitable for relative permittivity less than 10, although this range can be extended by an exact solution of the resonator containing the specimen. Hence this technique is not commonly used for DR characterization. However, this method is suitable for low loss, low permittivity substrate characterization.

The resonant method is the most accurate method as compared to the above-mentioned methods for the measurement of DRs and substrates. In

this method, the exact resonant frequency of the resonator is measured using different techniques. From the resonant characteristics, parameters like ε_r, Q_u etc are determined. This method is excellent for measuring the quality factor of microwave ceramics. Special techniques of exact resonance are used in the present study, which are described in detail in the following sections.

2.5.5 Measurement of relative permittivity (ε_r)

In this method developed by Hakki and Coleman [41] a circular disc of material whose ε_r to be measured is inserted between two mathematically infinite conducting plates, as shown in Fig 2.5.

If the dielectric material is isotropic then the characteristic equation for this resonant structure operating in the TE_{0ml} mode is written as

$$\alpha \frac{J_0(\alpha)}{J_1(\alpha)} = -\beta \frac{K_0(\beta)}{K_1(\beta)} \text{------(2.1)}$$

where $J_0(\alpha)$ and $J_1(\alpha)$ are Bessel functions of the first kind of orders zero and one respectively. The $K_0(\beta)$ and $K_1(\beta)$ are the modified Bessel functions of the second kind of order zero and one respectively. The parameters α and β depend on the geometry, the resonant wavelength inside and outside the DR respectively and dielectric properties. Thus

$$\alpha = \frac{\pi D}{\lambda_o} \left[\varepsilon_r - \left(\frac{l\lambda_o}{2L} \right)^2 \right]^{1/2} \text{------(2.2)}$$

$$\beta = \frac{\pi D}{\lambda_o} \left[\left(\frac{l\lambda_o}{2L} \right)^2 - 1 \right]^{1/2} \text{------(2.3)}$$

where l = the longitudinal variations of the field along the axis, L = Length of the DR, D = Diameter of the DR, λ_0 = free space resonant wave length.

The characteristic equation is a transcendental equation and hence a graphical solution is necessary. Corresponding to each value of β there are

infinite number of (α_n) that solves the characteristic equation. Hakki and Coleman [41, 42] obtained a mode chart showing the variation of α values as a function of β and are shown in Fig. 2.6.

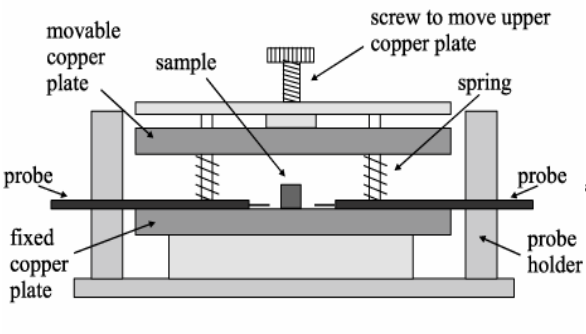

Fig. 2.5 Hakki-Coleman method for measuring ε_r by end shorted method Ref: 41, 42

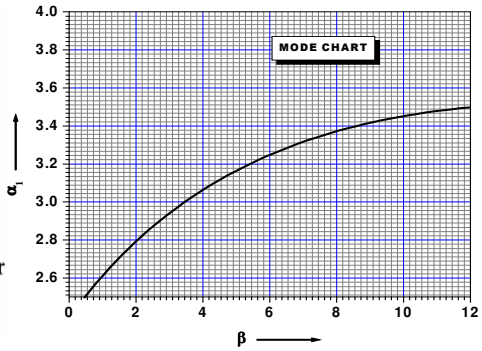

Fig. 2.6 Mode charts of Hakki –Coleman giving α_1 as functions of β. Ref: 36, 41, 42

The relative permittivity of the resonator can be calculated using the mode chart parameters (α_1 and β_1), the resonant frequency (f_r) and the dimensions of the dielectric puck using the equation

$$\varepsilon_r = 1 + \left[\frac{c}{\pi D f_r}\right]^2 \left(\alpha_1^{\,2} + \beta_1^{\,2}\right) \text{------(2.4)}$$

The horizontally oriented E-field probes for coupling microwaves to the DRs, was proposed by Courtney [42] which enabled to span a wide range of frequencies, since there is no cut-off frequency for coaxial lines. The TE_{011} mode is used for the measurements since this mode propagates inside the sample but is evanescent outside the geometry of DR. Therefore, a large amount of electrical energy can be stored in the high Q dielectric resonators [43]. However, in the open space post resonator setup, a part of electrical energy is radiated out as evanescent field and hence the axial mode number is usually expressed as δ since it is less than 1 (i.e. $TE_{01\delta}$). In the end shorted condition the E-field becomes zero close to the metal wall and electric energy vanishes in the air gap [44].

In the experimental setup, a Vector Network Analyzer, Agilent 8753 ET is used for taking measurements at microwave frequencies. The network analyzer was interfaced with computer for quick and accurate measurement. The specimen is placed approximately symmetrical with two *E*-probes. The resonant modes are visualized by giving a wide frequency range by adjusting the Network Analyzer. To select the TE_{011} resonance from the several modes having non zero E_z components, the upper metal plate is slightly tilted to introduce an air gap. As the plate is tilted the entire *TM* modes move rapidly to the higher frequencies while the TE_{011} mode remains almost stationary. It is well known that in exact resonance technique, TE_{011} is least perturbed by the surroundings. After identifying the TE_{011} resonant frequency or central frequency (f_r), the span around f_r is reduced as much as possible to get maximum resolution. The 3 dB bandwidth of the curve decreases and a stage of saturation is reached when the width will remain the least possible. The coupling loops are fixed at this position and the centre frequency can be noted corresponding to the maxima as f_r. By knowing the diameter '*D*' and length '*L*' of the sample β is calculated using equation 2.4. From the mode chart, the value of α_1 corresponding to β_1 value is noted. The permittivity ε_r is calculated using Eqn. 2.4.

2.5.6 Measurement of unloaded quality factor (Q_u)

Various methods [45-48] are available in literature for measurement of *Q*-factors of microwave resonators. However, all these methods failed to account for the practical effects such as noise, crosstalk, coupling losses, transmission line delay and impedance mismatch introduced by a real measurement system. Moreover the microwave loss factors of DRs are affected by many other intrinsic and extrinsic factors. Inadequate accounting of these effects may lead to significant uncertainty in the measured quality factor of the DRs. End-shorted method applied for the measurement of ε_r can

also be used for measuring the unloaded quality factor (Q_u). But the quality factor measured for the TE_{011} mode using the parallel plate rod resonator is very low since there occurs losses due to conducting plates, radiation etc.

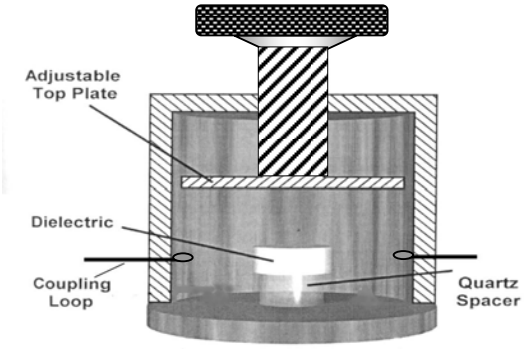

Fig. 2.7 The cavity set up for the measurement of Q factor, Ref: 36

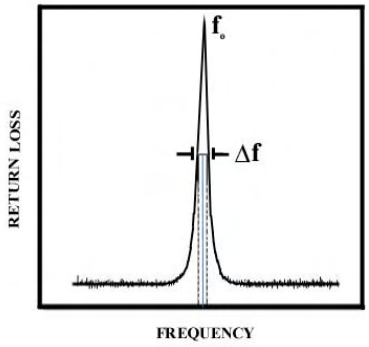

Fig. 2.8 The method of calculating *Q* from resonant mode using Eqn. 2.5, Ref: 36

In the present study the Q_u of the DR samples are measured by using a method proposed by Krupka et al.[46] (See Fig. 2.7). In this method, the DR specimen to be characterized is placed inside a cylindrical copper/invar cavity whose inner surface is silver coated to reduce radiation loss. The diameter of the cavity is designed almost four times of the sample diameter to reduce the effect of cavity shielding. Samples with diameter/length (D/L) ratio of 1.8 - 2.2 is preferable to get maximum mode separation and to avoid interference from other modes. The DR specimen is kept over a quartz spacer placed at the inner bottom surface, which enables to avoid the conduction loss. The cavity is provided with a tunable upper lid.

This enables to tune the height of air layer in the metallic cavity and hence more accuracy in the determination of the resonant mode and Q_u can be attained and also allows to measure samples with various dimensions. Microwaves are fed into the sample using two loop coaxial antennas which provides a magnetic coupling to excite the transmission mode resonance

spectrum of dielectric cylinder. The coupling is adjusted to be optimum (weak coupling for high Q_u and strong coupling for lossy samples). Observe S_{21} versus frequency spectrum. In principle the cavity has infinite number of modes, when excited with microwave spectrum of frequencies. $TE_{01\delta}$ mode is identified as the fundamental mode with least perturbation when the tunable top lid is adjusted properly. After identifying the desired mode, the lid is fine tuned to get maximum separation between $TE_{01\delta}$ and any nearby cavity modes, to attain maximum possible accuracy in the Q_u measurement. Measure $TE_{01\delta}$ mode frequency (f_0) and the 3 dB bandwidth (Δf) from the resonance spectrum (See Fig. 2.8) to calculate the Q factor as

$$Q = \frac{f_o}{\Delta f} \text{------(2.5)}$$

One can assume that for low loss dielectrics, the unloaded Q factor is equal to loaded Q factor if coupling is weak. In the microwave frequency range the dielectric loss increases with frequency and hence there exists an inverse relationship between quality factor and resonant frequency. Hence the quality factor of dielectric resonators are conventionally represented in units of Q_u *x f*, rather than Q_u.

2.5.7 Measurement of temperature coefficient of resonant frequency (τ_f)

Stability of resonant frequency with temperature is an important property of a DR to operate in microwave devices. τ_f is defined as

$$\tau_f = \frac{1}{f}\frac{\Delta f}{\Delta T} \times 10^6 (ppm/^o C) \text{------(2.6)}$$

The unit of τ_f is parts per million per degree Celsius. In order to measure τ_f, DR is kept in a cavity, same as that used for quality factor measurement. Then the entire set up is heated in the temperature range of 25 to 75 ^{o}C. The probe of the thermocouple is kept just inside the isothermal enclosure so that it does not disturb the resonant frequency. Shift in the

resonant frequency of $TE_{01\delta}$ is noted at every 2 ^{o}C increment in temperature. The variation of resonant frequency is noted using an interfaced computer and τ_f is calculated.

2.5.8 Split Post Dielectric Resonator (SPDR)

The SPDR provides another accurate method for measuring the complex permittivity and loss tangent of substrates and thin films at a single frequency point in the frequency range of 1 to 20 GHz [36]. In the split post dielectric resonator (SPDR) method, [49-53] the sample should be in the form of a flat rectangular piece or a sheet. The SPDR uses a particular resonant mode which has a specific resonant frequency depending on the resonator dimensions and the relative permittivity. This method does not have flexibility in the measurement frequency and dimensions as the samples need to be prepared in the form of thin sheets. In this method flat samples of the test material are inserted through one of the open sides of the fixture. The laminar dielectric under test is placed between two low loss dielectric rods or resonators kept in a metallic enclosure as shown in Fig. 2.9 (a).

The electric field in the resonator sample is parallel to the surface of the sample. Hence the test sample should have strictly parallel faces and the thickness of the sample should be less than the fixture air gap and the sample should have enough area to cover inside of the fixture. The air gap between the sample and the dielectric resonator does not affect the accuracy of the measurement. The required thickness of the sample also depends on the ε_r of the material. Materials with high ε_r must have less thickness. Fig 2.9 schematically shows the SPDR. Although, different modes of the resonator can be identified and used for the microwave characterization, $TE_{01\delta}$ mode is preferable since this mode is insensitive to the presence of air gaps perpendicular to z-axis of the fixture. The thickness of the sample needs to be measured and is provided as a parameter to the software. The real part

of the complex permittivity can be computed from the measured resonant frequencies and thickness of the sample as an iterative solution of the following equation.

$$\varepsilon_r = 1 + \frac{f_0 - f_s}{h f_0 \; K_\varepsilon(\varepsilon'_r, h)} \text{------(2.7)}$$

where h is the thickness of the test sample, f_0 is the resonant frequency of the empty SPDR, f_s is the resonant frequency of the SPDR with the dielectric sample. K_ε is a function of ε_r and has to be evaluated for a number of ε_r and using Rayleigh-Ritz technique. The loss tangent of the test sample is calculated from the measured unloaded Q factors of the SPDR with and without the dielectric sample based on

$$\tan\delta = \left(\frac{1}{Q_u} - \frac{1}{Q_{DR}} - \frac{1}{Q_c}\right) / P_e \text{------(2.8)}$$

where Q_{DR}^{-1} and Q_c^{-1} denote losses of the metallic and dielectric parts of the resonator respectively and P_e is the electric energy filling factor of the sample.

SPDR has superior accuracy as compared to the reflection-transmission methods. In terms of sample geometry, the only requirements are that the sample must extend beyond the diameter of the two cavity sections and the sample must be flat. This provides the accuracy of a resonator technique without having to machine the sample. Typical uncertainty of the permittivity measurements of a sample of thickness h can be estimated as $\Delta\varepsilon/\varepsilon = \pm(0.0015+\Delta h/h)$ and uncertainty in loss tangent measurements $\Delta \tan\delta = 2 \times 10^{-5}$. The method is convenient, fast to measure low loss laminar dielectrics such as substrates or LTCC, printed circuit boards and even thin films but not suitable for dielectric resonators.

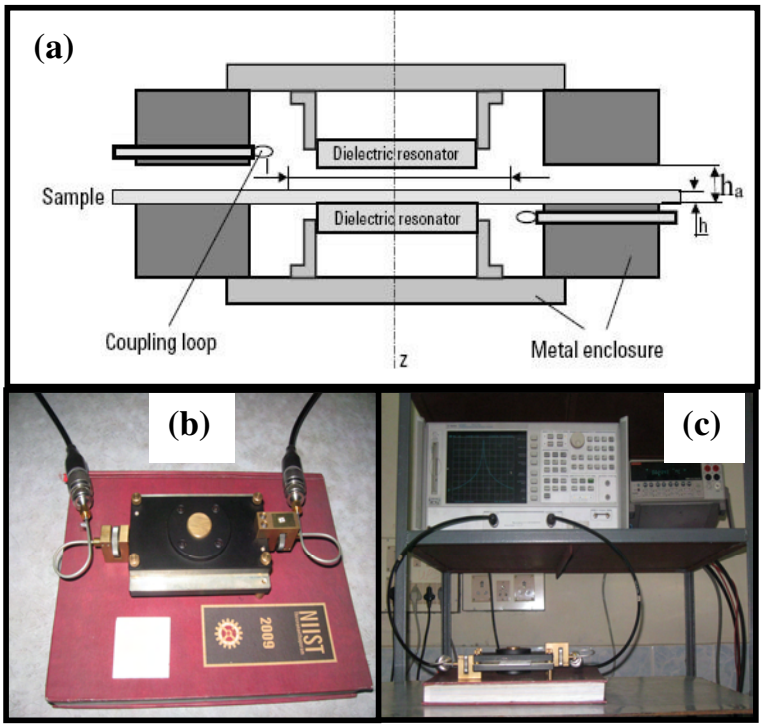

Fig. 2.9 Schematic representation of SPDR.

2.5.9 Cavity Perturbation Technique

Cavity perturbation methods are widely used in the study of electromagnetic properties of dielectrics, semiconductors, magnetic materials and composites materials [35, 36, 54]. This is a good technique for the low and medium dielectric loss materials. However, extremely low dielectric loss samples can not be characterized using the cavity perturbation technique. In this technique the sample is introduced to the antinode of electric field or magnetic field in a cavity, as shown in Fig. 2.10. The resonant frequency and quality factor of the cavity now changes. The dielectric permittivity and loss tangent can be calculated from the changes in the resonant frequency and quality factor of the cavity modes. The following equations were used for the measurement of permittivity and loss tangent.

$$\varepsilon_r' = 1 + \left(\frac{V_c (f_o - f_s)}{2 V_s f_s} \right) \text{------(2.9)}$$

$$\varepsilon_r'' = \left(\frac{V_c (Q_o - Q_s)}{4 V_s Q_s Q_0} \right) \text{------(2.10)}$$

$$\tan \delta = \frac{\varepsilon_r''}{\varepsilon_r'} \text{------(2.11)}$$

where f_o = resonant frequency of the cavity, f_s= resonant frequency of the samples, V_c= Volume of the cavity, V_s= Volume of the sample, Q_0 = Quality factor of the empty cavity, Q_s= Quality factor of the sample loaded cavity.

The microwave dielectric properties of the low relative permittivity substrates and composites in this thesis were measured using the cavity perturbation technique using HP 8510 C Network Analyzer (Agilent Technologies) in the X band (8 -12 GHz). The experimental error was found to be less than 2% in case of relative permittivity and 1.3% in the case dielectric loss.

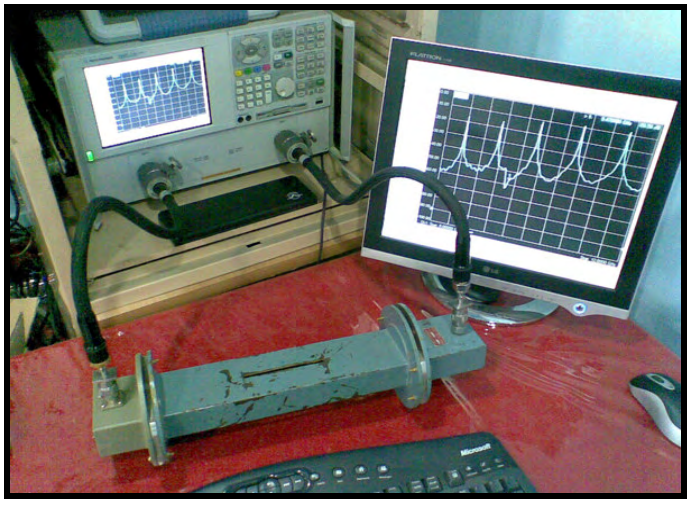

Fig. 2.10 Schematic representation of Cavity perturbation technique.

2.5.10 Radio frequency dielectric measurements

LCR meters are generally used for measurement of the capacitance conductance, impedance, and dissipation factor of dielectric ceramics in the radio frequency region by the well-known parallel plate capacitor method. The parallel plate capacitor method involves sandwiching a thin sheet of the material between two electrodes to form a capacitor. The capacitance of a parallel-plate capacitor in vacuum is compared with one in the presence of the material for which the dielectric properties are to be measured. Then relative permittivity is calculated using the equation

$$C = \frac{\varepsilon_r \varepsilon_o A}{d} \text{------(2.12)}$$

where C is the capacitance of material, ε_r and ε_0 are the relative permittivities of material and free space respectively.

In the present study, the dielectric properties at radio frequency were measured using LCR meter (HIOKI 3532-50 LCR Hi TESTER, Japan) (parallel plate capacitor method).

2.5.11 Error calculations in dielectric property measurements

The measurement of microwave dielectric properties was done with two decimal point accuracy. Usually three samples were prepared in a batch corresponding to a particular composition and the measurements were made at least twice per each specimen. The error in ε_r is calculated using the root sum of squares (RSS) method. The accuracy of ε_r measurement is restricted to the accuracy in measurement of resonant frequency and dimensions of the sample. Hence the possible errors in the measured value of permittivity of a sample of height (L), radius (r) and resonant frequency (f_r) given by

$$\Delta\varepsilon_r = \left[\left(\frac{\partial \varepsilon_r}{\partial L}\ \Delta L\right)^2 + \left(\frac{\partial \varepsilon_r}{\partial r}\ \Delta r\right)^2 + \left(\frac{\partial \varepsilon_r}{\partial f_r}\ \Delta f_r\right)^2\right]^{1/2} \text{------(2.13)}$$

If the independent sources of error corresponds to one standard deviation, then the error in ε_r will also corresponds to one standard deviation [55]. The errors in unloaded quality factor (Q_u) and temperature coefficient of resonant frequency (τ_f) were calculated using RSS method by taking partial derivative of these parameters with respect to independent variables. The low frequency relative permittivity was measured using LCR meter. The error in the measurement of relative permittivity depends on the error in the evaluation of sample dimensions. Since a digital vernier is used for the determination of the dimensions, the maximum error in the measurement is only 0.01mm. Hence the maximum error in the relative permittivity is less than 2%.

2.6 Calculation of Relative Density of Composites

The relative density of the specimen was measured by the Archimedes method. The theoretical density (D) of the composite can be calculated using the equation [56]

$$D = \frac{W_1 + W_2}{W_1/D_1 + W_2/D_2} \text{------(2.14)}$$

where W_1 and W_2 are the weight percentage of the two phases with densities D_1 and D_2 respectively.

2.7 Thermal Characterization

The determination of reaction during firing can best be accomplished by using techniques that measure chemical and physical changes as the sample being tested. Thermal analysis is defined as a group of methods by which the physical or chemical properties of a substance, a mixture and/or a

reactant are measured as a function of temperature or time while the sample is subjected to a controlled temperature program.

2.7.1 Thermo Gravimetric Analysis (TGA)

Thermo gravimetric analysis is a technique in which the weight of a sample is continuously measured as the sample is subjected to a selected firing profile that is usually linear [57]. In a thermo gravimetric analysis the mass of a sample in a controlled atmosphere is recorded continuously as a function of temperature or time as the temperature of the sample is increased. Thermo gravimetric methods are largely limited to decomposition and oxidation reactions and also to physical processes such as vaporization, sublimation and desorption.

2.7.2 Differential Thermal Analysis (DTA)

Differential thermal analysis (DTA) [57] employs two thermocouples connected differentially so that their electromotive force outputs are in opposition. DTA is a technique in which the difference in temperature between a substance and a reference material is measured as a function of temperature while the substance and reference material are subjected to a controlled temperature program. Information on the inorganic compounds such as dehydration, oxidation, reduction and solid-state reactions is provided by DTA.

2.7.3 Thermo Mechanical Analysis (TMA)

Dilatometry [57, 58] is the continuous measurement of the length of the sample as the specimen is subjected to a controlled linear heating rate. In this technique (TMA), dimensional changes in a sample are the primarily measured, with negligible force acting on it, while the sample is heated, cooled, or studied at a fixed temperature. The data obtained includes the shrinkage of a composition and more importantly the onset and completion

of the sintering cycle. TMA is also used to confirm the softening and melting temperature of glass-ceramic composites used for low temperature cofired ceramic applications. In the present study, TMA (TMA- 60 H, Shimadzu, Kyoto, Japan) is used to determine the shrinkage characteristics.

The sequential description of various steps involved in the synthesis of dielectric ceramics and composites is presented in this chapter. Next chapter discusses the synthesis, characterization and microwave dielectric properties of low loss and low permittivity ceramics for LTCC substrate applications.

References

1. J. M. Herbert, "*Ceramic Dielectrics and Capacitors*", Gorden and Breach Science Publishers, USA, (1985).
2. W. D. Kingery, "*Introduction to Ceramics*", John Wiley and Sons, New York, (1960).
3. N. Ichinose, "*Introduction to Fine Ceramics, Applications in Engineering*", John Wiley and Sons, New York, (1987).
4. D. W. Richerson, "*Modern Ceramic Engineering Properties Processing and Use in Design*", Taylor and Francis, CRC Press, London, (2006).
5. M. W. Bersaum, "*Fundamentals of Ceramics*", Magraw Hill, New York, (1997).
6. Y. Arai, "*Chemistry of powder production*", Chapman & Hall, London, (1996).
7. D. Seagal, "*Chemical Synthesis of Advanced Ceramic materials*", Cambridge University Press, Cambridge, (1991).
8. H. Schmalzried, "*Sold State Reactions*", Academic Press, New York, (1974).
9. P. Nanni, M. Viviani and V. Buscaglia, "*Synthesis of Dielectric Ceramic Materials, Handbook of Low and High Dielectric Constant and their Applications", Ed. H.S. Nalwa*, Materials and Processing, Academic Press, New York, (1999).
10. S. G. Malghan, "*Comminution, Engineering Materials Handbook, Ceramics and Glasses*", ASM Internationals, The Materials Information Society, SC, (1991).
11. M. Thirumal, P. Jain and A. K. Ganguli, *Mater. Chem. Phys.*, **70**, 7, (2001).
12. J. D. W. Johnson, *Am. Ceram. Soc. Bull*, **64**, 1597, (1985).
13. S. F. Hubert, *Br. Ceram. Soc. J.*, **6**, 11, (1967).
14. C. C. Harris, Trans. AIME, **238**, 17 (1967).
15. B. Beke, "*Principles of Comminution*", Akademi Kiado, Budapest, (1964).
16. J. W. Halloran, "*Calcination, Engineering Materials Handbook, Ceramics and Glasses*", ASM Internationals, The Materials Information Society, SC. (1991).
17. L. M. Sheppard, *Ceram. Int.*, **149**, 51, (1999).
18. G. Y. Onoda and L. L. Hench, "*Ceramic Processing before Firing*", Wiley Interscience, New York, (1973).
19. P. Winiewski, M. Szafran and G. Rokicki, *Key Engg. Mater.*, **264**, 428, (2000).
20. A. E. McHale, "*Processing Additives, Engineering Materials Handbook, Ceramics and Glasses*", ASM Internationals, The Materials Information Society, S C, (1991).

21. N. M. Alford, X. Wang, S. J. Penn, M. Poole and A. Jones, *Br. Ceram. Trans*, **99**, 212, (2000).

22. A. B. V. Groenou and R. C. D. Lissenburg, *J. Am. Ceram. Soc.*, **66**, 156, (1983).

23. E. Artz, *Acta Metall.*, **30**, 1883, (1982).

24. S.-J. L. Kang, "*Sintering, Densification, Grain Growth and Microstructure*", Elsevier, Amsterdam, (2002).

25. R. M. German, "*Fundamentals of sintering, Engineered Materials Hand book, Ceramics and Glasses*", ASM Internationals, Materials Information Society, S C, (1991).

26. R. L. Coble, *J. Appl. Phys.*, **32**, 789, (1961).

27. W. D. Kingery and M. Berg, *J. Appl. Phys.*, **26**, 1205, (1955).

28. R. German, P. Suri and S. Park, *J. Mater. Sci.*, **44**, 1, (2009).

29. O. H. Kwon, "*Liquid Phase Sintering, Engineering Materials Handbook, Ceramics and Glasses*", ASM international, The Materials Information Society, S C, (1991).

30. B. D. Cullity, "*Elements of X-ray Diffraction*", Printice Hall, New Delhi, (2001)

31. D. L. Bish and J. E. Post, "Modern Powder Diffraction. Reviews in Mineralogy, **20**, Mineralogical Association of America, Boston, (1989).

32. http://mse.iastate.edu/microscopy/whatsem.html,

33. I. M. Watt, "*The Principles and Practice of Electron Microscopy" 2nd Edn*., Cambridge University Press, Cambridge, (1997).

34. http://www.cranfield.ac.uk/cds/cfi/eds.jsp,

35. L. F. Chen, C. K. Ong, C. P. NeO, V. V. Varadan and V. K. Varadan, "*Microwave electronics: measurement and materials characterization*", John Wiley & Sons, page 256 England, (2004).

36. M. T. Sebastian, "*Dielectric materials for wireless communications*", Elseiver Publishers, Oxford, U. K, (2008).

37. D. Kajfez, "*Q Factor*, Vector Fields", Massachusetts, (1994).

38. J. Mussil and F. Zacek, "*Microwave Measurement of Complex Permittivity by Free Space Methods and Applications*", Elsevier, New York, (1986).

39. K. Leong "*Precise Measurements of Surface Resistance of HTS Thin Films using A Novel Method of Q-Factor Computations for Sapphire Dielectric Resonators in the Transmission Mode*", (James Cook University, Australia), (2000).

40. K. Leong and J. Mazierska, *J. Supercond.*, **14**, 93, (2001).

41. B. W. Hakki and P. D. Coleman, *IRE Trans. Microwave Theory Tech.,* ***MTT,*** **8**, 402 (1960).

42. W. E. Courtney, *IEEE Trans. Microwave Theory Tech*, **18**, 476, (1970).

43. Y. Kobayashi, *IEEE Trans. Microwave Theory Tech.*, **28**, 1077, (1980).

44. S. B. Cohn and K. C. Kelly, *IEEE Trans. Microwave Theory Tech.*, **14**, 406, (1966).

45. E. L. Ginzton, "*Microwave Measurements*", McGraw Hill Book Co., Boston, (1957).

46. J. Krupka, K. D. Derzakowski, B. Riddle and J. B. Jarvis, *Meas. Sci. Technol.*, **9**, 1751, (1998).

47. T. Miura, T. Takahashi and M. Kobayashi, *IEICE Trans. Elect.,* ***E7 7-C****, 900*, (1994).

48. E. J. Vanzura and J. E. Rogers, *Proc. IEEE Instr. Meas. Tech., May 14-16, Atlanta*, (1991).

49. J. Krupka, R. G. Geyer, J. B. Jarvis and J. Ceremurga, *Seventh Int. conference on dielectric materials, measurements and applications"*, **430**, 21, (1996).

50. J. Krupka, A. P. Gregonry, O. C. Kochard, R. N. Clarke, B. Riddle and J. B. Jarvis, *J. Eur. Ceram. Soc.*, **21**, 2673, (2001).

51. J. Krupka, S. Gabelich, K. Derzakowski and B. M. Pierce, *Meas. Sci. Tech.*, **10**, 1004, (1999).

52. G. Kent, *IEEE Micro.Theory and Tech.*, **36**, 1451, (1988).

53. J. Krupka, *Mater. Chem. Phys.*, **79**, 195, (2003).

54. A. Prakash, J. K. Vaid and A. Mansingh, *IEEE Trans. Micro Theo. Tech.*, **27**, 791, (1979).

55. J. B. Jarvis, R. G. Gayer, J. H. Grosvenor Jr, M. D. Janezic, C. A. Jones, B. Riddle, C. M. Weil and J. Krupka, *IEEE Trans. Diele. Elect. Insul.,* **5**, 571, (1998).

56. T. Takada, S. F. Wang, S. Yoshikawa, S. J. Jang and R. E. Newnham, *J. Am. Ceram. Soc.*, **77**, 1909, (1994).

57. L. Pennisi, "*The Firing Process, Engineered Materials Hand book, Ceramics and Glasses*", ASM International, The Materials Information Society, S C, (1991).

58. K. P. Menard, "*Dynamic Mechanical Analysis; A Practical Introduction*", CRC Press, Boca Raton, (1999).

Chapter 3

Low temperature sintering and microwave dielectric properties of Li_2ASiO_4 (A = Mg and Ca) ceramics for LTCC Substrate Applications.

This chapter discusses the synthesis, characterization and microwave dielectric properties of novel low loss low permittivity Li_2ASiO_4 (A=Mg and Ca) ceramics for microwave substrate applications. The effect of different borosilicate glasses on the sinterability, densification, structure, microstructure and the microwave dielectric properties of the Li_2ASiO_4 (A = Mg and Ca) dielectric ceramics are discussed. The present work aims to explore the adaptability of this ceramics and ceramic-glass composite for the possible applications in microelectronic industry as substrate and packaging materials.

3.1 Introduction

Recently, the utilizable region for the frequency has been expanding to the millimeter wave region because of the shortage of conventional frequency regions [1, 2]. The growing work frequency of microwave components make it essential to researching the low-permittivity and low loss ceramics used at higher frequency [3, 4]. Several microwave ceramics with excellent microwave dielectric properties have been developed for resonator filter and duplexer applications [5]. However, these ceramic systems show relatively higher relative permittivity (>15). In the case of substrate, packaging and antenna applications, the relative permittivity should be less than 10 and are ideal for integrated circuits. Reducing the permittivity, especially on large area high-speed chip will reduce cross talk, propagation delay time, noise, power dissipation and increase the signal speed [6-8]. The typical characteristics required for substrate applications [3, 5, 9-11] are described in chapter 1, section 1.4. At microwave frequencies, ionic polarization is dominant and is responsible for the relatively higher permittivity. The only way to avoid this type of polarization is the use of predominantly covalent bonded materials. In the context of low permittivity materials, several forsterite, willemite, and aluminate ceramics for millimeter wave applications have been developed and modified, according to the needs of the specific applications [3, 12-24]. In the commercial applications such as high frequency systems, silicates have been reported as the attractive candidate for practical use [3, 4]. Silicates are formed by SiO_4 tetrahedral framework with about 45% ionic bond and about 55% covalent bond. The covalent bond lowers ε_r because of higher bond strength and the atoms cannot rattle around. Most of the aluminates and silicate ceramics are having high processing temperature and limits its applications in Low Temperature Co-fired Ceramic (LTCC) based devices. A detailed description and requirements for LTCC technology is described in chapter 1, section 1.9.

Among the various methods, liquid phase sintering using glass addition is known to be the most effective and least expensive way of achieving high density sintered ceramics at low sintering temperature [25-28]. Generally, addition of glass degrades the microwave dielectric properties of ceramics. Hence the development of low loss and low permittivity LTCC ceramics is one of the major challenges in today's microelectronic industry. In this perspective, the development of alternative low loss ceramic substrate always attracts attention as a substitute for the existing conventional ceramic insulators that are used in microelectronics.

The aim of the present investigation is to develop novel low loss, low permittivity dielectric ceramics for substrate applications. In 1973, Gard et al. [29] reported the crystal structure of Li_2CaSiO_4. Luminescent and spectroscopic properties of rare earth doped Li_2CaSiO_4 has been extensively investigated [30-32]. However, low temperature sintering and the microwave dielectric properties of Li_2CaSiO_4 have not been reported in the literature. Mori et al. reported the Li_2MgSiO_4 crystal phase while developing new glass-ceramics consist of $MgAl_2O_4$ crystal and highly crystallized Li-Mg-Zn-B-Si-O glass [33]. However, a detailed investigation on the low temperature sintering and microwave dielectric properties of Li_2MgSiO_4 dielectric ceramics has not been investigated so far. This chapter reports the synthesis characterization and microwave dielectric properties of Li_2ASiO_4 (A=Mg, Ca) dielectric ceramics. The aim of the present work is also to develop low temperature sinterable low loss, low permittivity ceramics. Earlier investigations on glass added ceramics reveals that multicomponent glasses are more effective in lowering the sintering temperature of the ceramics without degrading the microwave dielectric properties [27, 34]. Hence the effect of different borosilicate glass (see table 1.2, chapter 1 section 1.9.3) additions on the sinterability and microwave dielectric properties of Li_2ASiO_4 (A=Mg, Ca) dielectric ceramics is investigated in this chapter. The

low temperature sintering and microwave dielectric properties of Li_2ASiO_4 (A=Mg, Ca) dielectric ceramics for LTCC application are also being reported for the first time.

3.2 Experimental

3.2.1 Preparation of Li_2ASiO_4 (A=Mg, Ca) ceramics

The Li_2ASiO_4 (A=Mg, Ca) ceramics were prepared by the conventional solid state ceramic route. High purity Li_2CO_3, $(MgCO_3)_4$ $Mg(OH)_2$ $5H_2O$, $CaCO_3$ and SiO_2 (99.9+%, Aldrich chemical company, Inc, Milwaukee, WI, USA) were used as the starting materials. Stoichiometric amounts of the powder samples were mixed and ball milled using zirconia balls in ethanol medium for 24 hours. The resultant slurry was then dried and calcined at 800 to 900 ^oC/4hrs for Li_2MgSiO_4 ceramics and 700 to 850 ^oC/4hrs for Li_2CaSiO_4 ceramics. Polyvinyl alcohol (PVA) (Molecular Weight 22000, BDH Lab Suppliers, England) solution was then added to the powder, mixed, dried and ground well and pressed into cylindrical disks of about 11 mm diameter and 2 mm thickness, by applying a pressure of about 100 MPa for low frequency measurements. These compacts were muffled by powder of the same composition and sintered at different temperatures in the range 1200 to 1300 ^oC/2hrs for Li_2MgSiO_4 ceramics and 900 to 1025 ^oC/2hrs for Li_2CaSiO_4 ceramics in air to optimize the sintering temperature. To study the dielectric properties in the microwave frequency range, rectangular sheets of dimensions (40x2x1 mm^3) were made and sintered at the optimized sintering temperature of 1250 ^oC/2hrs for Li_2MgSiO_4 ceramics and 1000 ^oC/2hrs for Li_2CaSiO_4 ceramics. The preparation of different borosilicate glasses is discussed in the chapter 2 section 2.2. Different weight percentage of various borosilicate glasses was added to the fine powder of calcined LMS and LCS ceramic. Polyvinyl alcohol (PVA) (4 wt%) solution was then added to the powder, mixed, dried and ground well and pressed

to form pellets as described earlier. These compacts were muffled by powders of the same composition and sintered at different temperatures in the range 800 ^{o}C to 975 ^{o}C/2hrs in air.

3.2.2 Characterization

The crystal structure and phase purity of the powdered samples were studied by X- ray diffraction technique using Ni-filtered Cu-Kα radiation using Rigaku Dmax-I, Japan, diffractometer. The microstructures of the thermally etched sintered samples were studied using scanning electron microscope (*JEOL-JSM* 5600 LV, Tokyo, Japan). The sintered density of the specimen was measured by the dimensional method. Electrodes were connected to both sides of the sintered and polished compacts using silver paste and these samples were used for measuring the dielectric properties. The dielectric properties were measured using a LCR meter (HIOKI 3532-50 LCR Hi TESTER, Japan). The microwave dielectric properties of the pure Li_2ASiO_4 (A=Mg, Ca) ceramics and its glass composites were measured by cavity perturbation technique using an HP 8510 C Vector Network Analyzer [5, 35, 36]. Detailed description of cavity perturbation technique is discussed in chapter 2.

3.3 Results and Discussion

3.3.1 Optimization of calcination and sintering temperature of Li_2ASiO_4 (A=Mg, Ca) ceramics

Figure 3.1 shows the optimization of calcination temperature of LMS and LCS ceramics. The calcination temperature is optimized for the best density and dielectric properties. The LMS ceramics is calcined in the temperature range 800 ^{o}C to 900 ^{o}C/4hrs and sintered at 1250 ^{o}C/2hrs and the LCS ceramics is calcined in the range 700 ^{o}C to 850 ^{o}C/4hrs and sintered at 1000 ^{o}C/2hrs. It is found that, the relative density and relative permittivity increases gradually with calcination temperature up to 850 ^{o}C

and further increase in the calcination temperature decreases the density and relative permittivity of LMS ceramics. However, for LCS ceramics the relative density and relative permittivity increases gradually with calcination temperature up to 800 ^{o}C and further increase in the calcination temperature decreases the density and relative permittivity. The dielectric loss is also found to be minimum at a calcination temperature of 850 ^{o}C for LMS and 800 ^{o}C for LCS ceramics. The best dielectric properties and densification is observed for LMS calcined at 850 ^{o}C/4hrs and that of LCS calcined at 800 ^{o}C/4hrs.

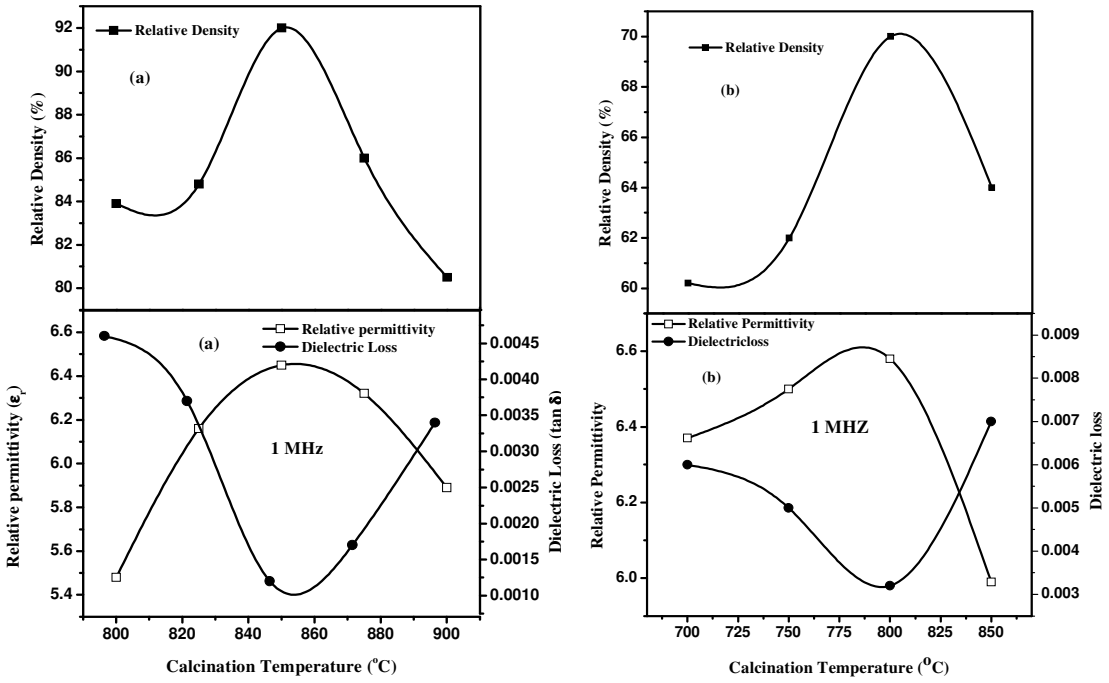

Fig. 3.1 Optimization of Calcination temperature of (a) Li_2MgSiO_4 and (b) Li_2CaSiO_4 ceramics

The Fig. 3.2 shows the optimization of sintering temperature of LMS and LCS ceramics calcined at 850 ^{o}C/4hrs and 800 ^{o}C/4hrs respectively. The best dielectric properties and densification are observed for LMS sintered at 1250 ^{o}C/2hrs and that of LCS sintered at 1000 ^{o}C/2hrs. Earlier investigations on lithium based ceramics showed that the lithium is volatile and evaporates

at higher sintering temperatures [37]. Hence the decreased density and dielectric properties of LMS and LCS at higher sintering temperature could be due to the escape of lithium. A maximum relative permittivity and minimum dielectric loss are observed for the best density. The LCS ceramics is difficult to densify by increasing the sintering temperature and a maximum densification of 70% of the theoretical density (2.93 g/cc) (ICDD File No: 27-0290) is observed at its optimum sintering temperature of 1000 ^{o}C/2hrs. Further increase in the sintering temperature decreases the density of LCS ceramics and starts to melt. The dielectric properties of LMS sintered at 1250 ^{o}C/2hrs are ε_r = 6.45 and tan δ = 3x10^{-4} at 1 MHz. The Li_2CaSiO_4 sintered at 1000 ^{o}C/2hrs has ε_r = 6.58 and tan δ = 3. 3x10^{-3} at 1 MHz. The relatively higher loss for LCS ceramics attributes to the high porosity.

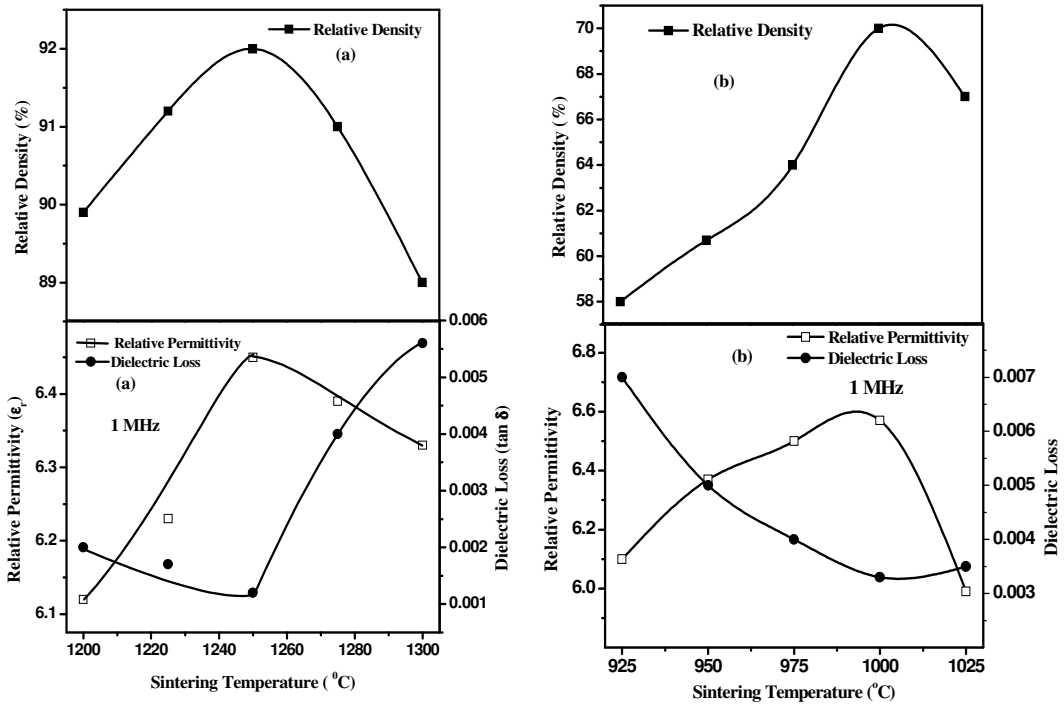

Fig. 3.2 Optimization of sintering temperature of (a) Li_2MgSiO_4 and (b) Li_2CaSiO_4 ceramics

3.3.2 Phase and microstructural analysis

Figure 3.3 (a) shows the XRD pattern of Li_2MgSiO_4 sintered at 1250 ^oC/2hrs. All the peaks are indexed based on orthorhombic crystal symmetry which is consistent with standard ICDD file No: 24-0636. Fig. 3.3 (b) shows the X-ray diffraction pattern of Li_2CaSiO_4 sintered at 1000 ^oC/2hrs. The peaks are indexed based on tetragonal symmetry (ICDD File No: 27-0290). Fig. 3.4 (a) and (b) shows the microstructure of pure LMS sintered at 1250 ^oC/2hrs and LCS sintered at 1000 ^oC/2hrs. The LMS are 2 – 10 µm grain size. However, it is evident from the microstructure (Fig. 3.4 (b)) that the LCS has less than 1 µm grain size with a porous structure. The microstructures are good in agreement with the percentage density value 92% for LMS and 70% for LCS ceramics at its optimum sintering temperature.

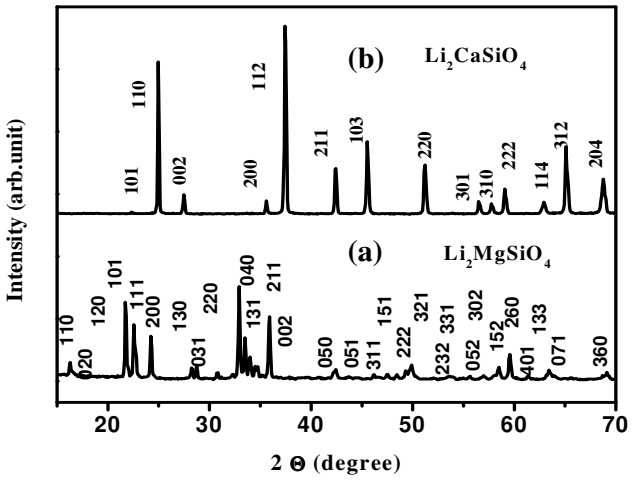

Fig. 3.3 The XRD pattern of Li_2MgSiO_4 and Li_2CaSiO_4 ceramics sintered at 1250 ^oC/2hrs and 1000 ^oC/2hrs respectively.

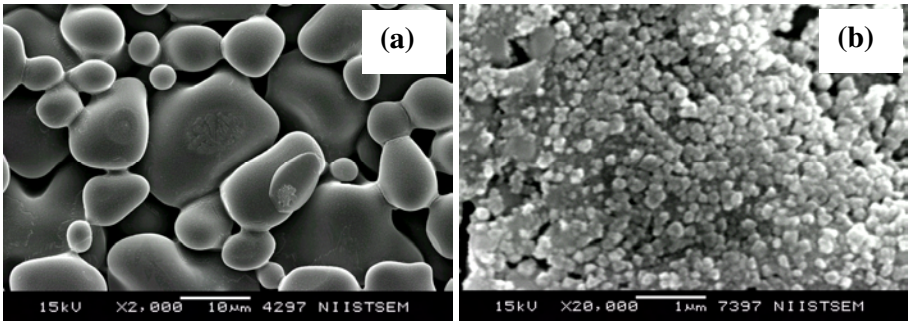

Fig. 3.4 The SEM images of thermally etched (a) Li_2MgSiO_4 and (b) Li_2CaSiO_4 ceramics sintered at 1250 ^oC/2hrs and 1000 ^oC/2hrs respectively

Table 3.1 shows the microwave dielectric properties of LMS and LCS sintered at its optimum sintering temperature. Both the silicates are found to have low densification. Hence, the porosity corrected relative permittivity is calculated using the equation (3.1) and is shown in the table 3.1.

$$\varepsilon_r = \varepsilon_r'\left(1-\frac{3P(\varepsilon_r'-1)}{2\varepsilon_r'+1}\right)-------(3.1)$$

where ε_r' is the permittivity of the material corrected for porosity, ε_r is the experimentally obtained permittivity and P is the fractional porosity.

Table 3.1 The microwave dielectric properties of LMS and LCS sintered at its optimum sintering temperature.

Material	Sintering Temperature	% Density	ε_r (9 GHz)	Porosity corrected ε_r'	Tan δ (9 GHz)	$\tau_{\varepsilon r}$ (1MHz)
Li_2MgSiO_4	1250 °C/2hrs	92	5.1	5.8	0.0005	0.11%
Li_2CaSiO_4	1000 °C/2hrs	70	4.4	7.1	0.0060	0.03%

The LMS and LCS ceramics shows excellent microwave dielectric properties, however the sintering temperature is slightly higher than melting point of silver for the possible application in the LTCC based devices. Hence it is necessary to reduce the sintering temperature and improve the densification for the useful LTCC applications. The next section discusses the effect of various borosilicate glass additions on the sinterability, structure, microstructure and microwave dielectric properties of both LMS and LCS ceramics.

3.3.3 Effect of borosilicate glass additions on the sinterability and microwave dielectric properties of Li_2ASiO_4 (A=Mg, Ca) ceramics

3.3.3.1 Shrinkage characteristics

Literature shows that the onset of sintering can be lowered well below the melting point of silver by the addition of low melting glasses [26, 27]. Based on this aspect, the dilatometry study provides insight to the densification process of the ceramic-glass system. The linear shrinkage of the as pressed pellets of ceramic-glass composite as a function of temperature is to be measured initially to check whether the glass additive would be effective on the low temperature firing of LMS and LCS ceramics.

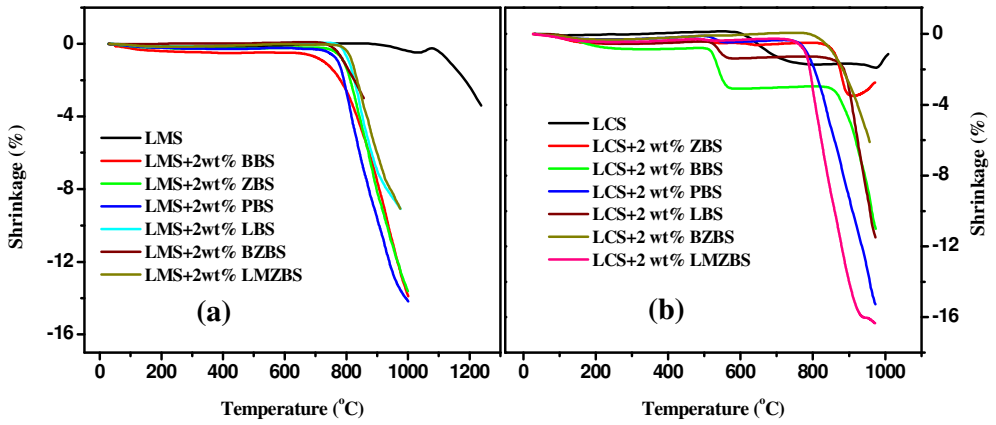

Fig. 3.5 The shrinkage characteristics of LMS and LCS ceramics with 2 wt% of various borosilicate glasses

Figure 3.5 shows the shrinkage characteristics of LMS and LCS ceramics with 2 wt% of various borosilicate glasses. It is found that less than 2 % of linear shrinkage takes place for pure LCS in the temperature range of 600-1000 °C which strongly supports the low densification of LCS ceramics at its optimum sintering temperature. However, the onset of sintering for LMS ceramics starts around 1000 °C. It is found that less than 4% of linear shrinkage for pure LMS in the temperature range of 1000-1250 °C. Addition of 2 wt% BZBS, LBS, BBS, LMZBS and PBS glass in LCS has a linear

shrinkage of 6%, 11%, 11% 16 % and 16% respectively in the temperature range 800-975^{o}C. However, nearly 4 % of linear shrinkage is observed for 2 wt% ZBS glass added LCS ceramics. For LMS-glass composites, the onset of sintering starts around 900 ^{o}C and nearly 14% of linear shrinkage is observed for 2 wt % PBS, ZBS and BBS glasses in LMS ceramics. Around 10 % of linear shrinkage is observed for 2 wt% of LMZBS and LBS glass added LMS ceramics.

3.3.3.2 Densification

From the previous section, it can be inferred that the onset of sintering starts early with the addition of borosilicate glasses in both the LMS and LCS ceramics. This indicates that the sintering temperature can be lowered with the addition of glasses in LMS and LCS ceramics. Figure 3.6 shows the variation of sintering temperature and relative density of Li_2MgSiO_4 (LMS) and Li_2CaSiO_4 (LCS) ceramics mixed with different wt% of various borosilicate glasses. The sintering temperature is optimized for best density and dielectric properties. In the case of LMS-glass system, all the borosilicate glasses except BZBS glass lower the sintering temperature below the melting point of silver suitable for LTCC application. It can be observed that small amount of glass addition in LMS ceramic itself lowers the sintering temperature below the melting point of silver and subsequent addition of glasses does not decrease the sintering temperature further. For example, 3 wt% of LBS decreases the sintering temperature of LMS from 1250^{o}C/2hrs to 850^{o}C/2hrs. However, higher wt% of glass addition (5 wt%) doesn't decrease the sintering temperature further. This trend has been observed in other borosilicate glasses in LMS ceramics. For LCS-glass composite, the addition of all the borosilicate glasses effectively lowers the sintering temperature from 1000 ^{o}C to below 900 ^{o}C. Apart from the LMS-glass systems, the sintering temperatures of the LCS-glass composite decreases gradually with increase in the glass addition.

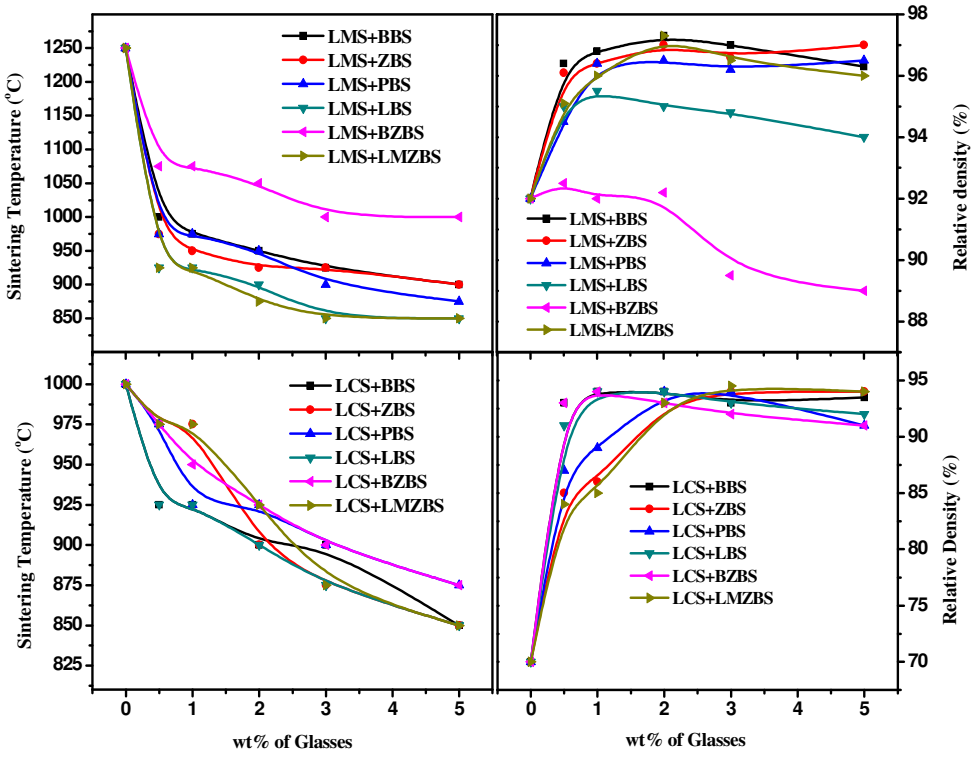

Fig. 3.6 Variation of sintering temperature and relative density of LMS-glass and LCS-glass composite as a function of glass content

Silicate based ceramics are generally found to have poor densification. The maximum densification of 92% and 70% is observed for LMS and LCS ceramics respectively which are in agreement with SEM results (see Fig. 3.4). Fig. 3.6 also shows the variation of relative density of both LMS-glass and LCS-glass composite as a function of the amount of borosilicate glasses. It can be observed that all the borosilicate glass except BZBS glass additions in LMS ceramics increases the relative density. As the amount of glass increases, the relative density increases to a maximum value and further addition of glasses decreases the relative density slightly. For example, the relative density of LMS increases from 92% to 96% with the addition of 1 wt% of LBS glass and decreases to 94% with the addition of 5wt% of LBS glass. A sharp increase in the relative density can be observed for the LCS-glass composites. It is worth to note that, a maximum

densification of 70% can only be achieved for pure LCS sintered at 1000 ^{o}C/2hrs. All the borosilicate glass additions in LCS increase the relative density which is well above 93%. The glassy liquid phase at the grain boundary effectively eliminates pores and thereby increases the relative density [26, 27, 38]. Trapped porosity associated with grain growth and formations of pores by the evaporation of excess glass components are the reasons for the decrease in the density for higher wt% of glass fluxing [25, 28]. In general, addition of small amount of glass improves densification and it degrades with higher wt% of glass. This trend has been observed in almost all the ceramic-glass systems [25, 27, 28]. However, it may be noted that the relative density for all the sintered LMS-glass and LCS-glass composite is slightly higher than that of pure LMS or LCS sintered at its optimum sintering temperature. It is worth to note that the addition of 5 wt% of all the borosilicate glasses except BZBS glass in LMS ceramics shows a relative density greater than 94%. The relative density greater than 90% is observed for all the LCS-glass composites. The bulk density of all the borosilicate glasses is comparable or greater than that of LMS and LCS ceramics. The physical and dielectric properties of all the borosilicate glasses in the present investigation are shown in Table 1.2 (see chapter 1, section 9.2.3). The eutectic glassy phase at the grain boundary effectively eliminates the pores and enhances the densification. The low densification of the LMS (92 %) and LCS (70 %) ceramics and the liquid phase sintering are the reasons for the increased density for the entire wt% of LBS glass addition in LMS.

3.3.3.3 Phase analysis

Low sintering temperature along with the non reactivity of electrode materials such as silver with the ceramic is essential for LTCC applications. Fig. 3.7 and 3.8 shows the XRD pattern of 20 wt% of silver added LMS-glass and LCS-glass composites respectively. All the peaks in Fig 3.7 are indexed based on orthorhombic crystal symmetry which is consistent with standard

ICDD file No: 24-0636. The peaks in Fig. 3.8 are indexed based on tetragonal symmetry (ICDD File No: 27-0290). It is worth to note from the X-ray diffraction pattern (Fig. 3.7 and Fig. 3.8) that, there are no additional phases are present other than silver (ICDD file No: 03-0921) and Li_2MgSiO_4 or Li_2CaSiO_4 ceramics. Hence, it can be concluded that silver can be used as an electrode material for both LMS-glass and LCS-glass composites for LTCC applications.

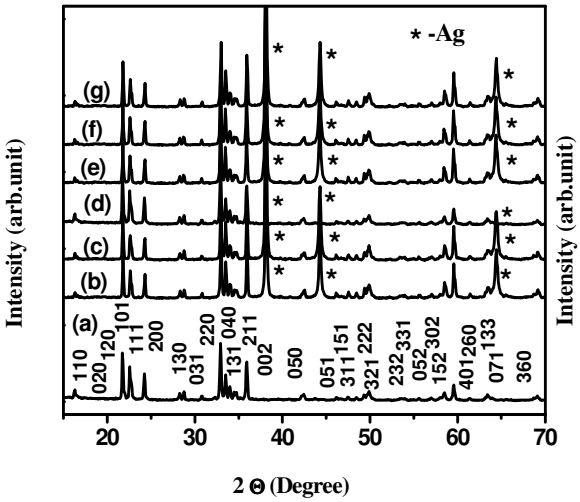

Fig. 3.7. X-ray diffraction pattern of (a) LMS, 20 wt% of silver added LMS and 2wt% of (b) ZBS, (c) BBS, (d) PBS, (e) LBS, (f) BZBS, (g) LMZBS glasses sintered at its optimum sintering temperature.

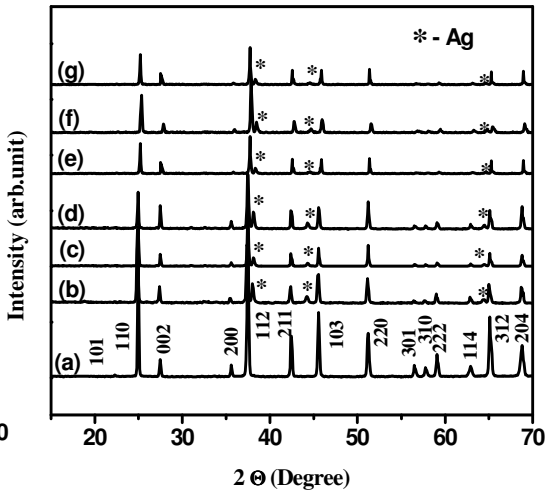

Fig. 3.8. X-ray diffraction pattern of (a) LCS, 20 wt% of silver added LCS and 2wt% of (b) ZBS, (c) BBS, (d) PBS, (e) LBS, (f) BZBS, (g) LMZBS glasses sintered at its optimum sintering temperature.

3.3.3.4 Microstructural analysis

Figure 3.9 shows the microstructure of thermally etched (a) LMS+1 wt% LBS, (b) LMS+2 wt% LMZBS, (c) LMS+2 wt% ZBS and (d) LMS+2 wt% PBS ceramic glass composites sintered at its optimum sintering temperature. It can be observed that the glass melts and wets the grains and enhances the densification. Fig. 3.9 (a) is an example of liquid phase sintering in which the LBS glass melts and flows through the grain boundaries. The glass added ceramics shows relatively dense microstructure with grain size in the range of 5-10 μm and is in agreement with the results of improved densification

with glass addition in LMS ceramics. Fig. 3.9 (e) and (f) shows the SEM images of 20 wt% of silver added LMS with 1 wt% of LBS and 2 wt% of LMZBS glasses sintered at 925 ^{o}C/2hrs and 875 ^{o}C/2hrs respectively. It is observed that the silver does not react with glass-ceramic composite and is distributed randomly which supports the results from the X-ray diffraction pattern (see Fig. 3.7 and Fig. 3.8).

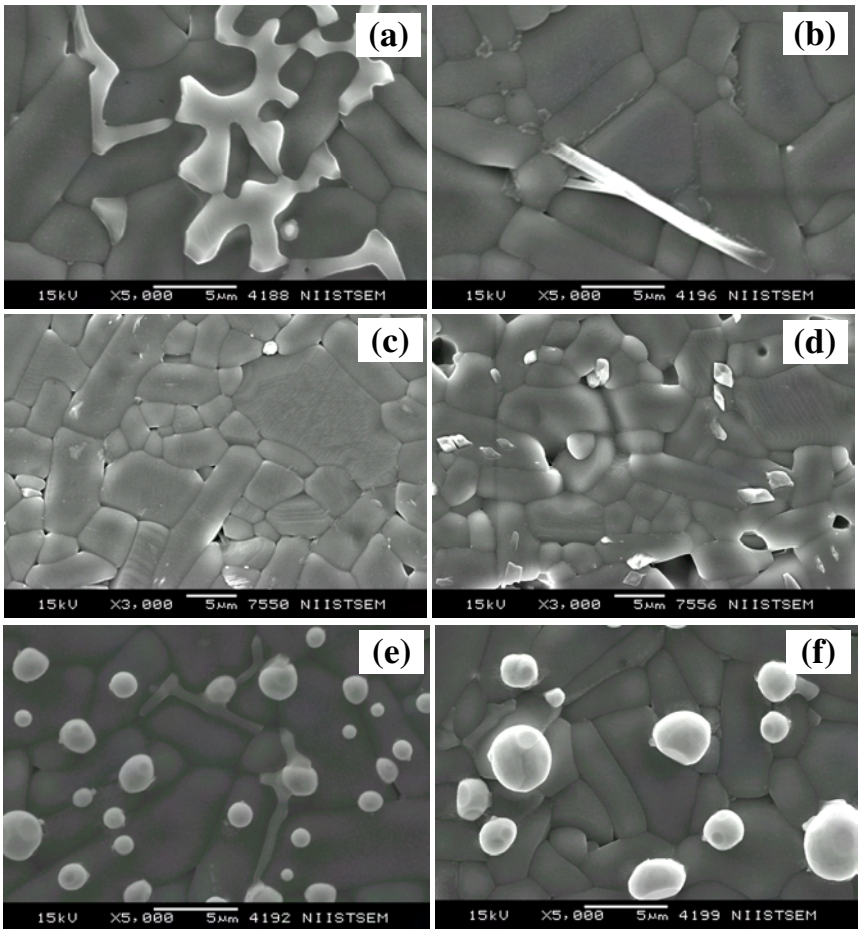

Fig. 3.9. The SEM images of thermally etched (a) LMS+1 wt% LBS, (b) LMS+2 wt% LMZBS, (c) LMS+2 wt% ZBS, (d) LMS+2 wt% PBS, (e) 20 wt% of silver added LMS with 1 wt% of LBS and (f) 20 wt% of silver added LMS with 1 wt% of LMZBS glass at its optimum sintering temperature.

Fig. 3.10 shows the microstructure of thermally etched (a) LCS+3 wt% ZBS, (b) LCS+2 wt% LBS and (c) LCS+2 wt% BBS ceramic glass composites sintered at its optimum sintering temperature. It can also be observed that

the glasses melt and lie at the grain boundaries and thereby enhance the densification. By comparing Fig 3.4 (b) and Fig. 3.10, it can be observed that the addition of glasses increases the grain growth and enhances the densification. Pure LCS sintered at 1000 ^{o}C has the grains of less than 1 μm size and the glass added LCS has the grains of about 10 μm size. It can be observed from Fig. 3.10 (d) that, the silver does not react with the LCS-glass composite and are distributed randomly.

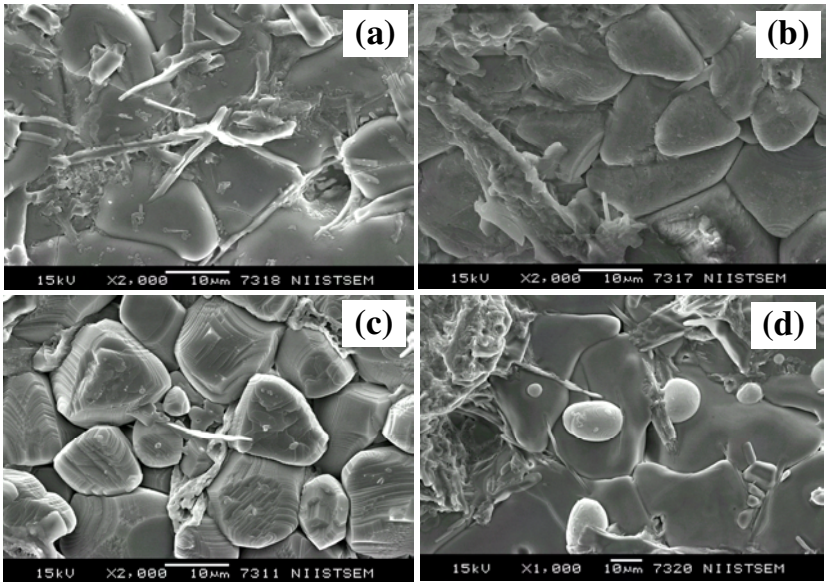

Fig. 3.10 The SEM images of thermally etched (a) LCS+3 wt% ZBS, (b) LCS+2 wt% LBS and (c) LCS+2 wt% BBS and (d) 20 wt% of silver added LCS with 2 wt% of LBS glass at its optimum sintering temperature.

3.3.3.5 Dielectric properties of various borosilicate glass added Li_2ASiO_4 (A=Mg and Ca) Ceramics.

It is well known that the relative density and dielectric properties are inter-related. Fig. 3.11 shows the dielectric properties of different wt% of various borosilicate glasses mixed with LMS and LCS ceramics at 1 MHz. It is found that the dielectric properties vary in a manner similar to that of density. As the amount of glass increases the relative permittivity increases to a maximum value and further increase in glass addition decreases the

permittivity slightly. This trend has been observed in both the LMS-glass and LCS-glass composites. For example, the relative permittivity increases from 6.45 to 6.82 with the addition of 1 wt% of LBS glass in LMS. However, subsequent glass addition (5 wt %) decreased the relative permittivity to 6.7. In the case of LCS-glass composites, the addition of 1 wt% of LBS glass increases the permittivity from 6.58 to 9.2 and subsequent addition of glass (5 wt%) decreases the permittivity slightly to 8.9. The improved relative permittivity can be attributed to the increased densification of ceramic-glass composite.

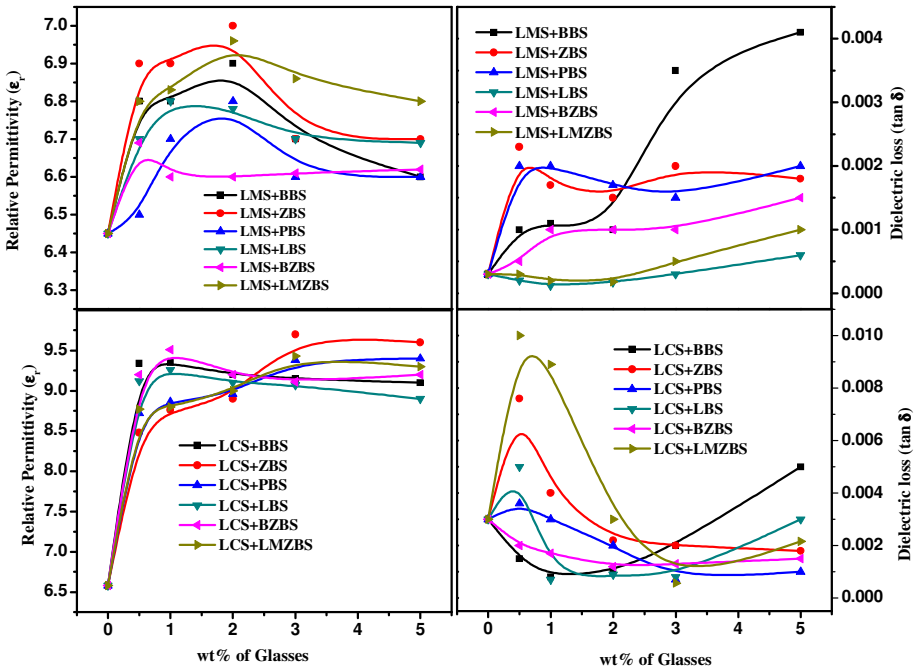

Fig. 3.11 Variation of relative permittivity and dielectric loss of LMS-glass and LCS-glass composite as a function of glass content

Generally, higher wt% of glass addition decreases the relative permittivity of ceramic glass composites [5, 25, 26, 28, 39-41]. This is due to the low relative permittivity of glass compared to that of high permittivity ceramics. However, the relative permittivity of entire LMS-glass and LCS-

glass composites are slightly higher than that of pure LMS and LCS at its optimized sintering temperature. This could be due to the nearly same relative permittivity of glasses compared to that of LMS and LCS. In addition, it is worth to note that the glass added ceramics in the present investigation has higher densification compared to glass free LMS and LCS ceramics. It is well known that the densification of dielectric ceramics has strong effect on the permittivity value. The relative permittivity increases with increase in the densification of ceramics. The high densification of LMS-glass and LCS-glass composites may also be the reason for the increase in the permittivity with glass addition. A slight decrease in the permittivity for higher wt% of glass addition may be due to the slightly lower densification by the evaporation of excess glass from the grain boundaries. Fig. 3.11 also shows the variation of dielectric loss of LMS-glass and LCS-glass as a function of glass content. As the amount of LBS and LMZBS glass increases in LMS-glass composites, the dielectric loss decreases initially and then increases with higher wt% of glass additions. For other borosilicate glass additions in the LMS ceramics, the dielectric loss increases gradually. However, all the LMS-glass composites in the present investigation have the dielectric loss less than 0.002 (except LMS-BZBS composite). Similar trend has been observed in the LCS-glass composites also. In the case of LCS-glass composites, addition of 1 wt% of BBS and BZBS glass decreases the dielectric loss slightly and increases with higher wt% of borosilicate glass additions.

The variation in the relative permittivity with temperature should be small for practical applications. Figs. 3.12 and 3.13 show the variation of the relative permittivity of LMS-glass and LCS-glass composite as a function of temperature. It is found that the relative permittivity of pure LMS, LCS and its composites with glass increases slightly with increase in temperature. Silicates are generally found to have positive temperature coefficient of permittivity *(τ_ε)* [13, 14, 23]. It has been reported that the glasses also have

positive temperature coefficient of permittivity [27]. Hence, the high τ_ε of glass could be the reason for the increase in the relative permittivity with temperature for all the ceramic-glass composites in the present investigation.

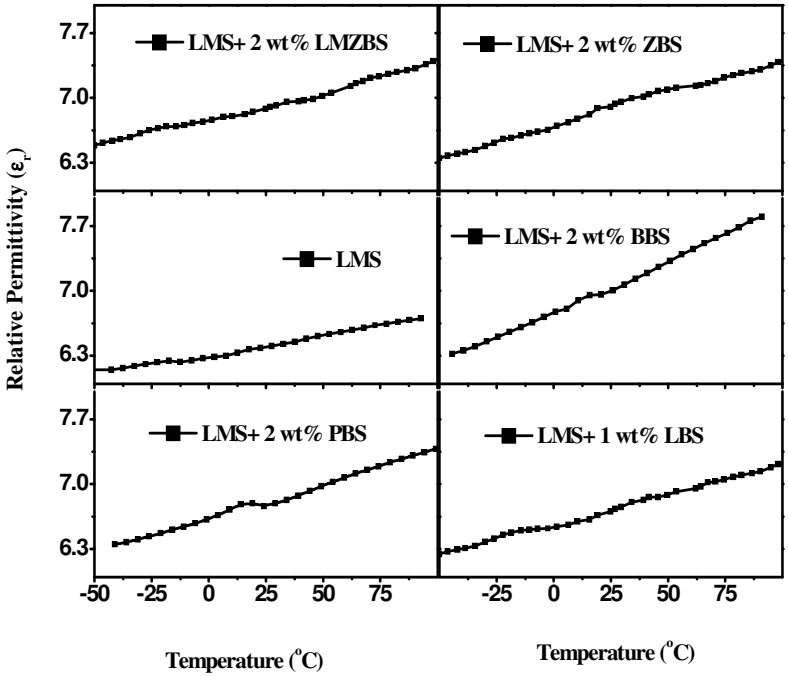

Fig. 3.12. The variation of the relative permittivity of LMS-glass composite as a function of temperature.

Fig. 3.13 shows a small peak in the temperature range of 15 to 25 °C for pure LCS sintered at 1000 °C/2hrs. As the temperature increases from 15 to 20 °C, the permittivity increases from 6.1 to 8.0 and further increase in the temperature decreases the permittivity to 6.2. The increase in relative permittivity in this range is around 33% and it is found that this anomalous behavior decreases with glass addition. For LBS, BZBS and PBS based glass ceramic composite, the deviation is less. Similar trend has been observed for $Ba_2P_2O_7$ ceramics [42]. This nonlinear behavior of pure LCS may be due to a change in symmetry or tilting of the tetrahedral or the reversible phase transitions and hence further work is needed to understand this.

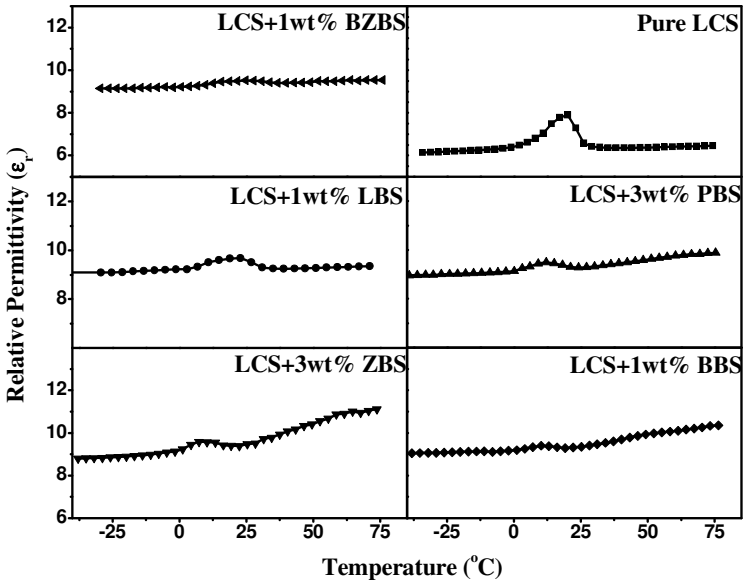

Fig. 3.13. The variation of the relative permittivity of LCS-glass composite as a function of temperature.

Tables. 3.2 and 3.3 show the microwave dielectric properties of LMS-glass and LCS-glass composites measured at 9 GHz for different wt% various borosilicate glasses. It is found that all the optimized ceramic-glass composites are sintered below the melting point of silver and shows excellent microwave dielectric properties. The microwave permittivity of all the LMS-glass composites varies in a manner similar to that of the variation of permittivity at low frequency (1 MHz) and the densification. Among all the borosilicate glass additions in the LMS ceramics, the addition of 1 wt% of LBS and 2 wt% of LMZBS glass in LMS shows excellent microwave dielectric properties. LMS sintered at 1250 ^{o}C/2hrs shows ε_r = 5.1 and tan δ = 5.2x10^{-4} at 9 GHz. LMS mixed with 2 wt% of LMZBS glass sintered at 875 ^{o}C/2hrs shows ε_r = 5.9 and tan δ = 7x10^{-5} at 9 GHz. Addition of 1 wt% LBS in LMS sintered at 925 ^{o}C/2hrs has ε_r = 5.5 and tan δ = 7x10^{-5} at 9 GHz. Similar trend has been observed in the LCS-glass composites also. LCS sintered at 1000 ^{o}C/2hrs has relative permittivity of 4.4 and dielectric loss of 0.006 at 9 GHz.

Addition of 2 wt % of LBS glass in LCS sintered at 925 ^{o} C/2hrs has ε_r = 7.4 and tan δ = 0.005 at 9 GHz. The LMS-glass composite shows excellent physical and microwave dielectric properties compared to LCS-glass composites. The excellent microwave dielectric properties of LMS-glass and LCS-glass composites offer the perspectives for LTCC substrate applications.

Table 3.2 Microwave dielectric properties of LMS-glass composites

Material	**wt % of glasses**	**Sintering Temperature (^{o}C)**	**ε_r (9 GHz)**	**tan δ (9 GHz)**
LMS		1250	5.1	0.00050
LMS+BBS	0.5	1000	5.5	0.00180
	1	975	5.7	0.00200
	2	950	6.3	0.00090
	3	925	6.1	0.00300
	5	900	5.9	0.00300
LMS+ZBS	0.5	1000	5.5	0.00180
	1	975	5.7	0.00200
	2	950	6.3	0.00090
	3	925	6.1	0.00300
	5	900	5.9	0.00300
LMS+PBS	0.5	975	5.5	0.00140
	1	975	5.6	0.00100
	2	950	5.6	0.00060
	3	900	5.5	0.00500
	5	875	5.3	0.00300

Table 3.2 continued…

Material	**wt % of glasses**	**Sintering Temperature (°C)**	**ε_r (9 GHz)**	**tan δ (9 GHz)**
LMS+LBS	0.5	925	5.4	0.00011
	1	925	5.5	0.00007
	2	875	5.2	0.00012
	3	850	5.1	0.00019
	5	850	5.2	0.00064
LMS+BZBS	0.5	1075	5.6	0.00050
	1	1075	5.8	0.00504
	2	1050	5.8	0.00456
	3	1000	5.9	0.00482
	5	1000	5.8	0.00176
LMS+LMZBS	0.5	925	5.5	0.00011
	1	925	5.6	0.00010
	2	875	5.9	0.00007
	3	850	5.0	0.00080
	5	850	4.9	0.00090

Table. 3.3. Microwave dielectric properties of LCS-glass composites

Material	wt % of glasses	Sintering Temperature (°C)	ε_r (9 GHz)	tan δ (9 GHz)
LCS	0	1000	4.4	0.006
LCS+BBS	0.5	925	6.5	0.006
	1	925	8.2	0.006
	2	900	8.2	0.007
	3	900	8.1	0.005
	5	850	8.0	0.008
LCS+ZBS	0.5	975	5.8	0.006
	1	975	6.0	0.004
	2	925	6.7	0.004
	3	875	7.1	0.006
	5	825	6.8	0.008
LCS+PBS	0.5	975	6.5	0.006
	1	925	6.8	0.007
	2	900	7.6	0.007
	3	900	7.8	0.005
	5	875	7.5	0.006
LCS+LBS	0.5	925	7.1	0.005
	1	925	7.2	0.004
	2	900	7.4	0.005
	3	875	7.0	0.005
	5	850	6.8	0.006

Table 3.3 continued…

Material	wt % of glasses	Sintering Temperature (°C)	ε_r (9 GHz)	tan δ (9 GHz)
LCS+BZBS	0.5	975	5.9	0.006
	1	950	6.0	0.006
	2	925	7.5	0.007
	3	900	7.3	0.007
	5	875	6.9	0.007
LCS+LMZBS	0.5	975	6.8	0.007
	1	975	7.3	0.008
	2	925	8.5	0.008
	3	875	7.6	0.009
	5	850	6.5	0.010

3.4. Conclusions

- The Li_2ASiO_4 (A=Mg, Ca) dielectric ceramics are prepared by solid state ceramic route and its structure, microstructure and microwave dielectric properties for substrate applications are investigated.
- The Li_2MgSiO_4 ceramics sintered at 1250 °C/2hrs has ε_r = 5.1 and tan δ = $5x10^{-4}$ at 9 GHz. The Li_2CaSiO_4 ceramics sintered at 1000 °C/2hrs has ε_r = 4.4 and tan δ = 0.006 at 9 GHz.
- The effect of various borosilicate glass additions on the sinterability densification structure and microstructure and microwave dielectric

properties of Li_2ASiO_4 (A=Mg, Ca) dielectric ceramics have been investigated for the possible applications in LTCC based devices.

- The SEM and XRD studies indicate that the low temperature sintered LMS-glass and LCS-glass system does not react with the silver electrode material.
- Addition of 1 wt% LBS in LMS sintered at 925^{o}C/2hrs has ε_r = 5.5 and tan δ = 7x10^{-5} at 9 GHz. LMS mixed with 2 wt% of LMZBS glass sintered at 875^{o}C/2hrs shows ε_r = 5.9 and tan δ = 7x10^{-5} at 9 GHz.
- Addition of 2 wt % of LBS glass in LCS sintered at 925 ^{o}C/2hrs has ε_r = 7.4 and tan δ = 0.005 at 9 GHz
- Compared to LCS-glass composites, the LMS-glass composites show excellent microwave dielectric properties at a low sintering temperature and can be a promising candidate for substrate and LTCC based devices.

This chapter discusses the synthesis, characterization and microwave dielectric properties of novel low loss low permittivity Li_2ASiO_4 (A=Mg and Ca) ceramics for LTCC substrate applications. Next chapter discusses microwave dielectric properties of novel temperature stable high Q dielectric ceramics for dielectric resonator applications.

References

1. http://ieeexplore.ieee.org/xpl/RecentIssue.jsp?punumber=6668,
2. http://www.sciencedirect.com/science/book/9780750697071,
3. H. Ohsato, *J. Ceram. Soc. Jpn.*, **113**, 703, (2005).
4. H. Ohsato, T. Tsunooka, A. Kan, Y. Ohishi, Y. Miyauchi, Y. Tohdo, T. Kawai, K. Kakimoto and H. Ogawa, *Electroceramics in Jpn. Vii*, **269**, 195, (2004).
5. M. T. Sebastian, "*Dielectric materials for wireless communications*", Elsevier Publishers, Oxford U. K, (2008).
6. K. Kata, Y. Shimada and H. Takamizawa, *IEEE Tran. Comp. Hybrids Mfg. Tech.*, **13**, 448, (1990).
7. Y. Shimada, Y. Yamashita and H. Takamizawa, *IEEE Tran. Comp. Hybrids Mfg. Tech.*, **11**, 163, (1988).
8. A. Sasaki and Y. Shimada, *Proc. 41st Elect. Comp. & Tech. Conf.*, 719, (1991).
9. D. D. L. Chung, "*Materials for Electronic Packaging*", Butterworth-Heinemann, Boston, (1995).
10. R. R. Tummala, *J. Am. Ceram. Soc.*, **74**, 895, (1991).
11. R. R. Tummala and R. B. Shaw, *Ceram. Int.*, **13**, 1, (1987).
12. M. Terada, K. Kawamura, I. Kagomiya, K. Kakimoto and H. Ohsato, *J. Eur. Ceram. Soc.*, **27**, 3045, (2007).
13. H. Ohsato, T. Tsunooka, T. Sugiyama, K. Kakimoto and H. Ogawa, *J. Electroceram.*, **17**, 445, (2006).
14. T. Tsunooka, M. Androu, Y. Higashida, H. Sugiura and H. Ohsato, *J. Eur. Ceram. Soc.*, **23**, 2573, (2003).
15. K. P. Surendran, P. V. Bijumon, P. Mohanan and M. T. Sebastian, *Appl. Phys. A-Mater. Sci. Process.*, **81**, 823, (2005).
16. K. P. Surendran, N. Santha, P. Mohanan and M. T. Sebastian, *Eur. Phys. J. B*, **41**, 301, (2004).
17. K. P. Surendran, M. T. Sebastian, M. V. Manjusha and J. Philip, *J. Appl. Phys.*, **98**, 044101, (2005).
18. S. Y. Cho, I. T. Kim and K. S. Hong, *J. Mater. Res.*, **14**, 114, (1999).
19. T. Okamura and T. Kishino, *Jpn. J. Appl. Phys.*, **37**, 5364, (1998).
20. H. P. Sun, Q. L. Zhang, H. Yang and J. L. Zou, *Mater. Sci. Engg. B.*, **138**, 46, (2007).

21. Y. P. Guo, H. Ohsato and K. I. Kakimoto, *J. Eur. Ceram. Soc.*, **26**, 1827, (2006).

22. K. X. Song and X. M. Chen, *Mater. Lett.*, **62**, 520, (2008).

23. K. X. Song, X. M. Chen and C. W. Zheng, *Ceram. Int.*, **34**, 917, (2008).

24. N. H. Nguyen, J. B. Lim, S. Nahm, J. H. Paik and J. H. Kim, *J. Am. Ceram. Soc.*, **90**, 3127, (2007).

25. P. V. Bijumon and M. T. Sebastian, *Mater. Sci. Engg. B.*, **123**, 31, (2005).

26. H. Jantunen, R. Rautioaho, A. Uusimaki and S. Leppavuori, *J. Eur. Ceram. Soc.*, **20**, 2331, (2000).

27. M. T. Sebastian and H. Jantunen, *Int. Mater.Rev.*, **53**, 57, (2008).

28. K. P. Surendran, P. Mohanan and M. T. Sebastian, *J. Solid State Chem.*, **177**, 4031, (2004).

29. J. A. Gard and A. R. West, *J. Sold state Chem.*, **7**, 422, (1973).

30. J. Liu, H. Y. Sun and C. S. Shi, *Mater. Lett.*, **60**, 2830, (2006).

31. M. Y. Sharonov, A. B. Bykov, V. Petricevic and R. R. Alfano, *Optics Communications*, **231**, 273, (2004).

32. M. G. Brik and K. Ogasawara, *Opt. Mater.*, **30**, 399, (2007).

33. N. Mori, Y. Sugimoto, J. Harada and Y. Higuchi, *J. Eur. Ceram. Soc.*, **26**, 1925, (2006).

34. H. Jantunen, "*PhD. Thesis*", (Finland, University of Oulu), *Faculty of Science*, (2001).

35. A. Prakash, J. K. Vaid and A. Mansingh, *IEEE Trans. Microwave Theory. Tech.*, **MTT 27**, 791, (1979).

36. L. F. Chen, C. K. Ong, C. P. NeO, V. V. Varadan and V. K. Varadan, "*Microwave electronics: measurement and materials characterization*", John Wiley & Sons, page 256 England, (2004).

37. J. W. Choi, C. Y. Kang, S. J. Yoon, H. J. Kim, H. J. Jung and K. H. Yeon, *J. Mater. Res.*, **14**, 3567, (1999).

38. C. L. Huang, C. L. Pan and S. J. Shium, *Mater. Chem. Phys.*, **78**, 111, (2003).

39. P. Liu, E. S. Kim, S. G. Kang and H. S. Jang, *Mater. Chem. Phys.*, **79**, 270, (2003).

40. P. Liu, E. S. Kim and K. H. Yoon, *Jpn. J. Appl. Phys. Part 1-Regular Papers Short Notes & Review Papers*, **40**, 5769, (2001).

41. J. X. Tong, Q. L. Zhang, H. Yang and J. L. Zou, *J. Am. Ceram. Soc.*, **90**, 845, (2007).

42. J. I. Bian, D. W. Kim and K. S. Hong, *Jpn. J. Appl. Phys.*, **43**, 3521, (2004).

Chapter 4

Microwave Dielectric Properties of Novel Temperature Stable High Q $Li_2Mg_{1-X}Zn_xTi_3O_8$ and $Li_2A_{1-X}Ca_xTi_3O_8$ (A=Mg, Zn) Ceramics

The technological advances always necessitate the discovery of new materials with innovative properties. This chapter discusses the synthesis, characterization and microwave dielectric properties of novel temperature stable high Q dielectric ceramics ($Li_2Mg_{1-x}Zn_xTi_3O_8$ (x=0 to 1) and $Li_2A_{1-x}Ca_xTi_3O_8$ (A=Mg, Zn, and x= 0 to 0.2)) which can be sintered at a low sintering temperature of 1075 ^oC/4hrs. Attempt has also been made to lower the sintering of $Li_2MgTi_3O_8$ and $Li_2ZnTi_3O_8$ ceramics for possible application in LTCC based devices. The microwave dielectric materials presented in this chapter are superior in terms of cost of raw materials, sintering temperature and microwave dielectric properties as compared to the existing microwave dielectric ceramics. The discovery of excellent properties of these materials may lead to a major milestone in microwave dielectric resonator research.

4.1 Introduction

In pace with the advances in microwave telecommunication and satellite broadcasting, a variety of microwave devices have been developed using dielectric resonator and the resonator has become indispensable component in microwave communication systems [1-4]. The microwave dielectric materials are advantageous in terms of compactness, light weight, temperature stability and low cost in the production of high frequency devices [5, 6]. A variety of microwave devices have been developed using dielectric resonators as the frequency determining components. Due to the constraints of size, frequency of operation, frequency stability and selectivity, only those materials with high relative permittivity (ε_r), low dielectric loss and nearly zero temperature coefficient of resonant frequency (τ_f) can meet the requirements for DR applications [1, 3, 4, 7, 8]. These requirements put constraints on the number of materials available for DR applications. The family of commercially available low loss dielectric materials and the materials which are the real breakthrough in the dielectric resonator research is shown in Table 4.1. The current trend and the state of the art of microwave dielectric materials for telecommunication applications are discussed in the book "Dielectric materials for wireless communications" [4]. The complex perovskite structure such as $Ba(Zn_{1/3}Ta_{2/3})O_3$ (BZT) and $Ba(Mg_{1/3}Ta_{2/3})O_3$ (BMT) shows the relative permittivity in the range 25-40 with high quality factor (Qxf > 200000) and low τ_f [9-11]. However, they are usually made up of expensive chemicals such as niobates and tantalates. Titanates occupy prominent position in advanced materials and the titanate based ceramics have low cost compared to tantalate and niobate based ceramics. The $(Zr_{1-x}Sn_x)TiO_4$, $BaTi_9O_{20}$, $BaTi_4O_9$ are the other low cost materials which shows excellent microwave dielectric properties [12-14]. However, high sintering temperature together with a long annealing time is necessary for obtaining excellent microwave dielectric properties. Hence,

these high Q dielectric ceramics are not cost effective either in terms of its cost of raw materials or its high processing temperature. Another constraint in making light weight electronic modules is the high density (≈5 g/cm^3) of dielectric ceramics. Several dielectric materials with excellent dielectric properties have been reported in the literature [4, 15-23]. Most of the ceramics developed cannot meet their requirements simultaneously and hence their properties need to be tuned. Much attention has been paid to tailor the sinterability and dielectric properties of ceramics by dopant addition, substitution, and the formation of solid solutions [24-32]. However, most of such system forms a second phase and which may degrade the dielectric properties. The developed dielectric materials reported so far have failed either atleast one of its important properties such as cost of the raw materials, sintering temperature, permittivity, quality factor, temperature coefficient of resonant frequency, or bulk density.

From the device design point of view, a good combination of high relative permittivity (for miniaturization), high quality factor (for selectivity), nearly zero temperature coefficient of resonant frequency (for stability), low processing temperature (for low cost), low cost of raw materials (for low cost of the device) and low density (for light weight of the electronic module) are required in a microwave dielectric material. In addition it is desirable that the temperature coefficient of resonant frequency be able to be tuned by small variations in the composition. Achieving all these requirements in one material is a formidable task and optimal balance of these properties is one of the major challenges in the electronic industry. If a material which can satisfies all the above mentioned requirements, then that material become the next major breakthrough in the dielectric resonator research after $(Zr_{1-x}Sn_x)TiO_4$ developed [14] by Murata manufacturing company, Japan. The physical and dielectric properties of $(Zr_{1-x}Sn_x)TiO_4$ ceramics is shown in Table 4.1. This chapter reports a family microwave

dielectric material which satisfies all the above mentioned requirements and can be the real landmark in the microwave dielectric resonator research. Design of dielectric resonator oscillator requires the accurate knowledge of electric parameters of the resonators such as resonant frequency, unloaded quality factor and the effect with temperature. This chapter discusses the synthesis, characterization and dielectric properties of novel low loss dielectric materials ($Li_2Mg_{1-x}Zn_xTi_3O_8$ (x=0 to 1) and $Li_2A_{1-x}Ca_xTi_3O_8$ (A=Mg, Zn, and x= 0 to 0.2)) having spinel structure and it's composite with glass, which can address the growing demand of microelectronic industry.

Table 4.1 The physical and dielectric properties of commercially available low loss microwave dielectric materials.

Material	ε_r	Qxf (GHz)	τ_f (ppm/^{o}C)	Sintering Temperature (^{o}C)	Ref.
$MgTiO_3 - CaTiO_3$	20	55000	0	1400	[33]
$BaTi_4O_9$	37	22700	15	1300	[12, 34]
$Ba_2Ti_9O_{20}$	39	32000	2	1350	[13]
$(Zr_{1-x}Sn_x)TiO_4$	39	51500	0.7	1600	[14]
$Ba(Zn_{1/3}Ta_{2/3})O_3$	28	168000	0.5	1500	[9]
$Ba(Mg_{1/3}Ta_{2/3})O_3$	24	430000	8	1640	[10, 35]
$BaO\text{-}Sm_2O_3\text{-}TiO_2$	77.5	11200	-3.4	1360	[36]
$CaTiO_3$ - $NdAlO_3$	41	33000	-17	1450	[37]
$SrTiO_3$ - $LaAlO_3$	39	32000	2	1450	[38]

4.2. Spinels

Dielectric ceramics having spinel structure shows high quality factor after complex perovskite structure. Hence much attention has been paid on the development of microwave dielectric ceramics having spinel structure.

Ideal spinel structure consist of a cubic close packed array of anions, with one eighth of the tetrahedral and one half of the octahedral intersticies occupied by cations, having general formula $A[B_2]O_4$, where A is tetrahedrally surrounded cations, B an octahedrally surrounded one and X an anion. Their cubic cell contain close packed array of 32 oxygen atoms with cations in the tetrahedral and octrahedral interstices. Fig. 4.1 shows the crystal structure of spinel. Complex spinel phases allow either tetrahedral or octahedral sites to be occupied by more than one kind of cation. The distributions over both sets of interstices tend to be random at high temperatures, while they are often ordered at low temperatures with lowering of the symmetry. The ternary spinels such as $Li_2MgTi_3O_8$ and $Li_2ZnTi_3O_8$ ceramics have been selected in the present investigation. Table 4.2 shows the structure data of lithium based spinel in the present investigation [39, 40].

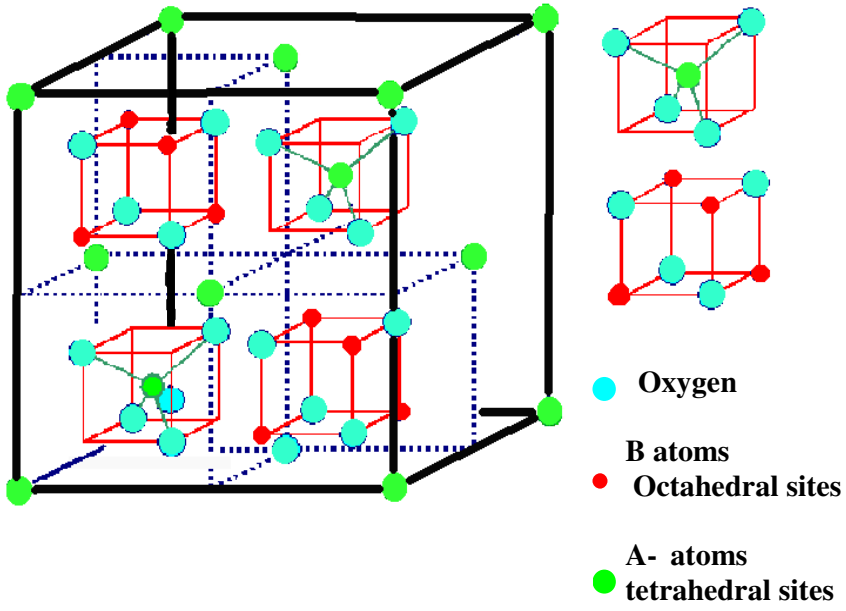

Fig. 4.1 Crystal structure of Spinel

Table 4.2 The structure data of lithium based spinel in the present investigation [ref: 39, 40].

Composition	Symmetry	Lattice parameter	Cation distribution
$Li_2MgTi_3O_8$	Cubic (p4332)	8.377(9)	$Li_{0.55}Mg_{0.45}[(Li_{0.45}Mg_{0.05})Ti_{1.5}]O_4$
$Li_2ZnTi_3O_8$	Cubic (p4332)	8.371(2)	$Li_{0.5}Zn_{0.5}[Li_{0.5}Ti_{1.5}]O_4$

4.3. Experimental

The $Li_2Mg_{1-x}Zn_xTi_3O_8$ (x=0 to 1) and $Li_2A_{1-x}Ca_xTi_3O_8$ (A=Mg, Zn, and x= 0 to 0.2) ceramic samples were prepared by the conventional solid state ceramic route. High purity Li_2CO_3, ZnO, $(MgCO_3)_4$ $Mg(OH)_2$ $5H_2O$, $CaCO_3$ and TiO_2 (99.9+%, Aldrich chemical company, Inc, Milwaukee, WI, USA) were used as the starting materials. Stoichiometric amounts of the powder samples were mixed and ball milled using zirconia balls in ethanol medium for 24 hours to prevent the dissolution of Li_2CO_3 in water. The resultant slurry was then dried. The thermal analysis were carried out on a simultaneous thermogravimetry differential thermal analysis (TG-DTA) instrument (Pyris Diamond TG/DTA, Perkin Elmer, US). The phase formation temperature was found to be 900 ^oC. The $Li_2Mg_{1-x}Zn_xTi_3O_8$ (x=0 to 1) and $Li_2A_{1-x}Ca_xTi_3O_8$ (A=Mg, Zn, and x= 0 to 0.1) ceramic powders were calcined at 900 ^oC for four hours. The calcined powders were ground to form fine powders and polyvinyl alcohol (PVA) (Molecular Weight 22000, BDH Lab Suppliers, England) solution was then added to the powder, mixed, dried and ground well and pressed into cylindrical disks of about 14 mm diameter and 7mm thickness, by applying a pressure of about 100 MPa. These compacts were muffled by powder of the same composition and sintered at different temperatures in the range 1000 ^oC – 1125 ^oC for 4 hours. The sintering temperature was optimized for the best density and dielectric

properties. The muffling was done to prevent the escape of volatile lithium at elevated sintering temperatures. The sintering temperature of the $Li_2MgTi_3O_8$ and $Li_2ZnTi_3O_8$ ceramics were lowered by the addition of lithium magnesium zinc borosilicate (20:Li_2O, 20:MgO, 20:ZnO, 20:B_2O_3, 20:SiO_2) (LMZBS) glass. This glass was chosen since the elements in the glass was lithium, magnesium, and zinc which was also present in the parent material. This may avoid the formation of second phase in the final product. The preparation of glass is discussed in chapter 2, section 2.2. Different weight percentage of LMZBS glass was added to the fine powder of calcined $Li_2MgTi_3O_8$ and $Li_2ZnTi_3O_8$ ceramics. Polyvinyl alcohol (PVA) (Molecular Weight 22000, BDH Lab Suppliers, England) solution (4 wt%) was then added to the powder, mixed, dried and ground well and pressed into cylindrical disks of about 14 mm diameter and 7mm thickness, by applying a pressure of about 100 MPa. These compacts were muffled by calcined powder of the same composition and sintered at different temperatures in the range 850 ^oC – 1075 ^oC for 4 hours. The sintering temperature of the ceramic glass composite was optimized for the best density and dielectric properties. The crystal structure and phase purity of the powdered samples were studied by X- ray diffraction technique using Ni-filtered Cu-Kα radiation using Rigaku Dmax-I, Japan, diffractometer. The microstructures of the sintered samples were studied using scanning electron microscope (JEOL-JSM 5600 LV, Tokyo, Japan). The sintered density of the specimen was measured by the Archimedes method. The theoretical density of the ceramic glass composite was calculated using the equation 2.14 (see chapter 2, section 2.6). The microwave dielectric properties were measured in the frequency range 4 to 6 GHz by a Vector Network Analyzer (8753 ET, Agilent Technologies). The dielectric constant and unloaded quality factor of the samples were measured by Hakki and Coleman and cavity methods

respectively [4, 41, 42] (discussed in chapter 2). Shrinkage characteristics were investigated using Dilatometer (TMA-60 H, Shimadzu, Kyoto, japan).

4.4 Results and discussion

4.4.1 TG/DTA analysis

The thermal characterization (TG/DTA) curve of (a) $Li_2MgTi_3O_8$ (LMT) and (b) $Li_2ZnTi_3O_8$ (LZT) ceramics are shown in Fig. 4.2. Large weight loss usually occurs when heat treating the precursor due to the decomposition of the oxides or carbonates of the raw materials used in the solid state ceramic route. The TG curve of as prepared LMT ceramics indicate that the mass loss occurs in three distinct stages. The first stage mainly occurring at 200 ^oC is due to the evaporation of absorbed moisture and the release of molecular water. The weight loss at this temperature is around 5%. The second stage, occurring in the range 300 to 400 ^oC, may correspond to the partial decomposition of $Li_2MgTi_3O_8$ to yield oxycarbonate intermediates [43, 44]. The weight loss at even higher temperature (third stage) is due to the further decomposition of oxycarbonate to yield oxides. The three distinct stages of decomposition is not observed in the TG/DTA curve of $Li_2ZnTi_3O_8$ ceramics. The $(MgCO_3)_4$ $Mg(OH)_2$ $5H_2O$ is used as the starting raw material for the preparation of $Li_2MgTi_3O_8$ ceramics and ZnO is used for the $Li_2ZnTi_3O_8$ ceramics. The evaporation of water in the hydrated magnesium carbonate is responsible for the three distinct stages of decomposition of LMT. The TG/DTA curve for LMT and LZT ceramics indicate that the decomposition has taken place in the temperature range 200 to 650 ^oC and there is only a minor weight loss between 650 to 950 ^oC. It can be observed that the complete decomposition and the X-ray crystalline phase of LMT and LZT is formed around 900 ^oC. Thus the calcination temperature is optimized for 900 ^oC.

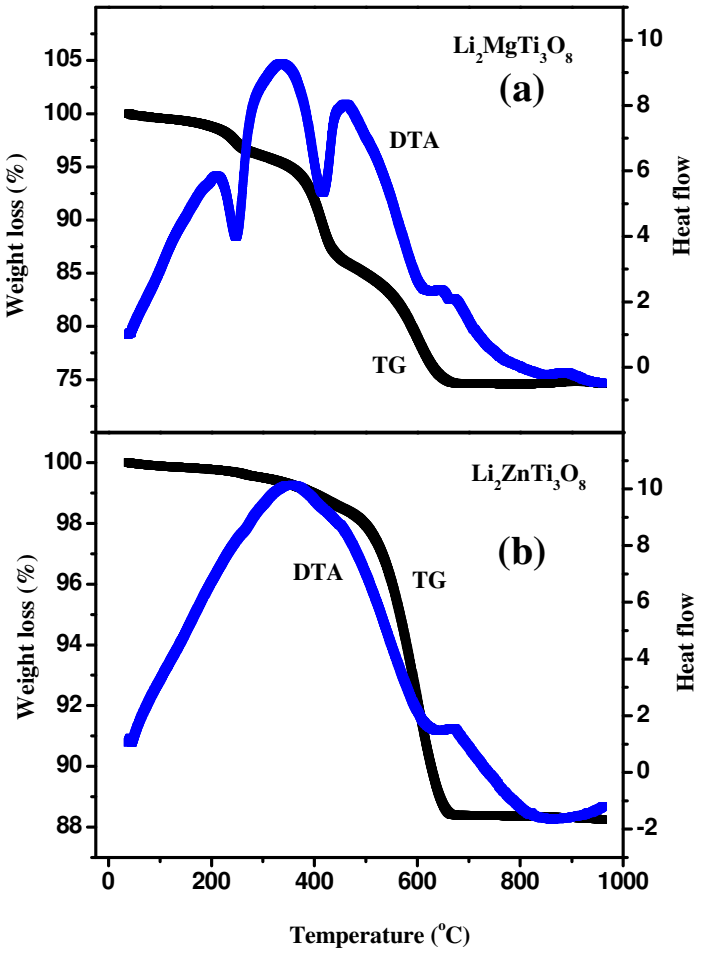

Fig. 4.2 TG/DTA curve of dried (a) $Li_2MgTi_3O_8$ and (b) $Li_2ZnTi_3O_8$ ceramics.

4.4.2 Densification of $Li_2MgTi_3O_8$ and $Li_2ZnTi_3O_8$ ceramics

Figure 4.3 shows the variation of the relative density of $Li_2MgTi_3O_8$ (LMT) and $Li_2ZnTi_3O_8$ (LZT) ceramics calcined at 900 °C/4hrs as a function of sintering temperature. As the sintering temperature is increased to 1075 °C the relative density increases to a maximum value and further increase in sintering temperature decreases the density. The increased densification could be due the elimination of pores in the ceramics. A maximum densification of 95.5 % and 95 % is observed for LMT and LZT ceramics

respectively at a sintering temperature of 1075 ^{o}C/4hrs. It is reported that lithium is volatile and evaporates at higher sintering temperatures [45]. The decreased densification at higher sintering temperature could be due to the trapped porosity by the evaporation of lithium and also due to the abnormal grain growth.

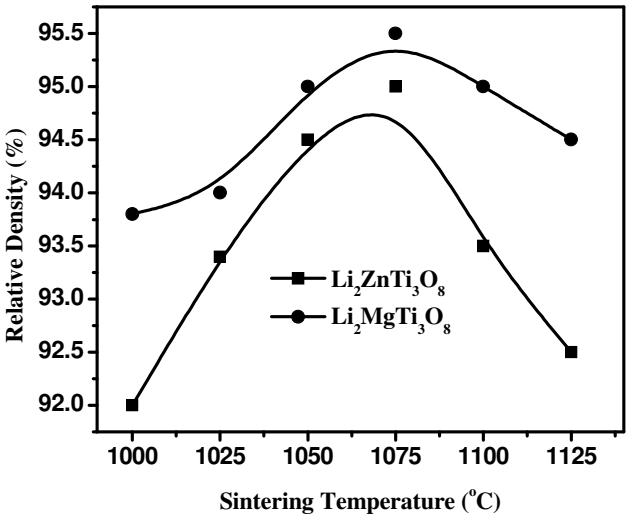

Fig. 4.3 Variation of Relative density of (a) $Li_2MgTi_3O_8$ and (b) $Li_2ZnTi_3O_8$ ceramics as a function of sintering temperature.

4.4.3 Crystalline phase and micro structural analysis

Figure 4.4 shows the X-ray diffraction pattern of $Li_2Mg_{1-x}Zn_xTi_3O_8$ (x = 0, 0.1, 0.2, 0.3, 0.4, 0.6, 0.8, 1) ceramics sintered at its optimized sintering temperature of 1075 ^{o}C/4hrs. All the peaks are indexed based on JCPDS file number 48-0263 for $Li_2MgTi_3O_8$ and 86-1512 for $Li_2ZnTi_3O_8$ with cubic crystal symmetry. The strongest peak is observed at 2θ of 18.2995 (d=4.8442) for $Li_2MgTi_3O_8$ and 2θ of 35.526 (d=2.52488) for $Li_2ZnTi_3O_8$ respectively. As the x increases in $Li_2Mg_{1-x}Zn_xTi_3O_8$ ceramics, a sudden shift of strongest intensity peak from 2θ =18.2995 to 2θ = 35.526 is observed. This transition is observed near x=0.1. Figure 4.5 shows the variation of lattice parameter and the cell volume as a function of composition. As x increases, the cell parameter and the cell volume of $Li_2Mg_{1-x}Zn_xTi_3O_8$ decreases. The lattice parameter is a = 8.381(4) Å for $Li_2MgTi_3O_8$ and a = 8.372(2) Å for $Li_2ZnTi_3O_8$

which is consistent with corresponding reported JCPDS files. Since the $Li_2Mg_{1-x}Zn_xTi_3O_8$ ceramics is cubic symmetry, the lattice parameters are calculated by plotting lattice parameter 'a' versus $Sin^2(\theta)$ [46]. A straight line will be formed and extrapolating this line to $Sin^2(\theta) = 1$ will give the value of lattice parameter 'a'. Inset of Fig 4.5 shows the extrapolation of the lattice parameter.

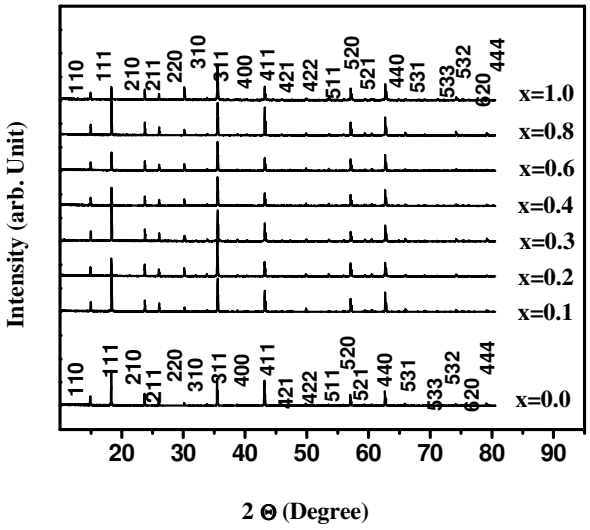

Fig. 4.4 X-ray diffraction patterns of $Li_2Mg_{1-x}Zn_xTi_3O_8$ (x = 0, 0.1, 0.2, 0.3, 0.4, 0.6, 0.8, 1) ceramics sintered at 1075 °C/4hrs.

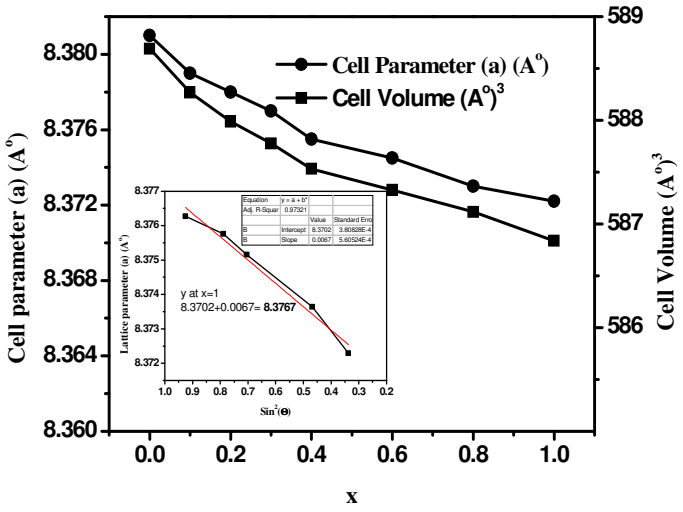

Fig. 4.5 The variation of lattice parameter and the cell volume of $Li_2Mg_{1-x}Zn_xTi_3O_8$ (x = 0, 0.1, 0.2, 0.3, 0.4, 0.6, 0.8, 1) ceramics sintered at 1075 °C/4hrs as a function of x. Inset shows the extrapolation of the lattice parameter

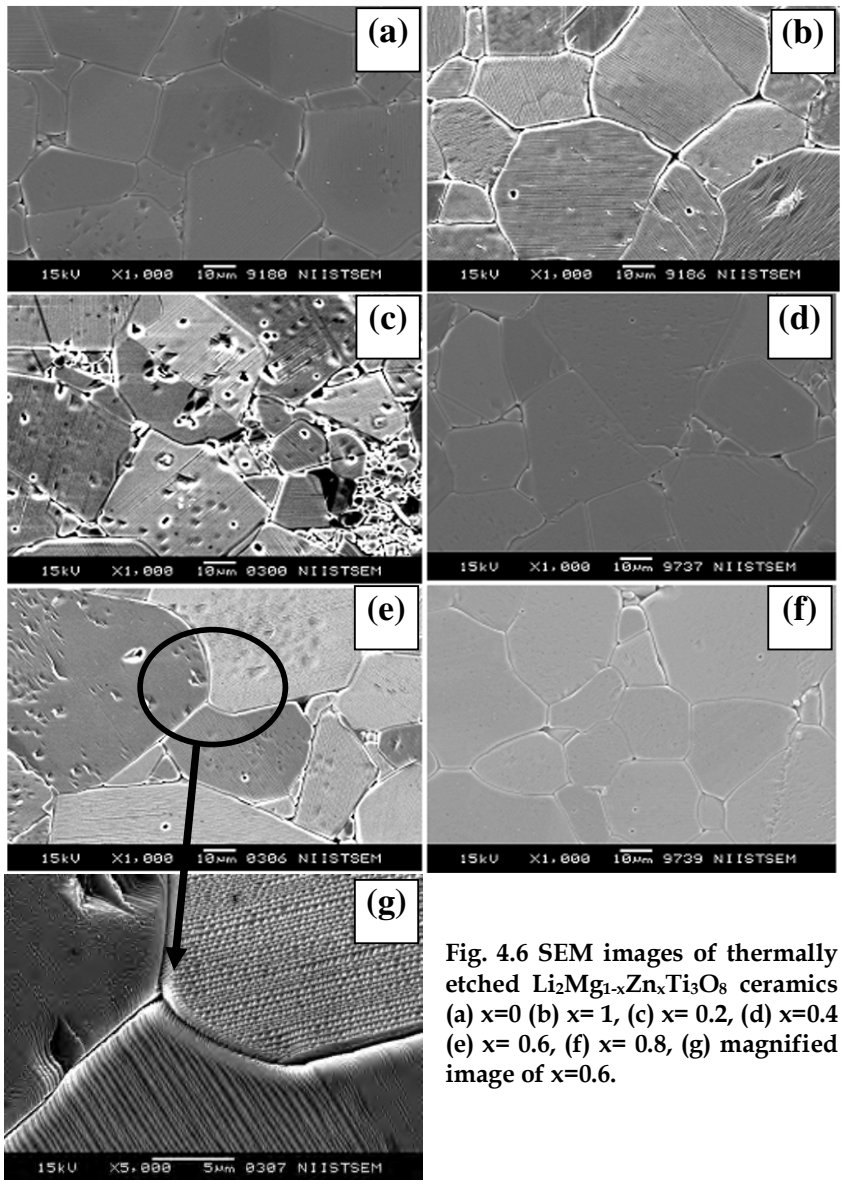

Fig. 4.6 SEM images of thermally etched $Li_2Mg_{1-x}Zn_xTi_3O_8$ ceramics (a) x=0 (b) x= 1, (c) x= 0.2, (d) x=0.4 (e) x= 0.6, (f) x= 0.8, (g) magnified image of x=0.6.

Figure 4.6 shows the SEM images of thermally etched (25 ^oC below the optimized sintering temperature) (a) $Li_2MgTi_3O_8$ and (b) $Li_2ZnTi_3O_8$ ceramics sintered at 1075 ^oC/4hrs. The grains are closely packed and small amount of porosity can be observed. The majority of the grains are having an average size of 30-40 μm. However, smaller grains are also observed for both the ceramics. Fig 4.6 also shows the SEM micrograph of the thermally

etched $Li_2Mg_{1-x}Zn_xTi_3O_8$ (c) x=0.2, (d) 0.4 (e) 0.6 and (f) 0.8. All the SEM images except Fig. 4.6 (c) (x=0.2) shows similar microstructure and the Fig. 4.6 (c) shows a porous microstructure. Two types of grains having different contrast are observed in the Fig 4.6 (e). Fig. 4.6 (g) is the magnified image of Fig 4.6 (e) which confirms the phase purity.

4.4.4 Microwave dielectric properties of $Li_2MgTi_3O_8$ and $Li_2ZnTi_3O_8$ ceramics with sintering temperature

Figure 4.7 shows the (a) relative permittivity (b) Quality factor and (c) temperature coefficient of resonant frequency of $Li_2MgTi_3O_8$ (LMT) and $Li_2ZnTi_3O_8$ (LZT) ceramics as a function of sintering temperature. It can be observed that the variation of microwave dielectric properties of LMT and LZT ceramics with sintering temperature is similar to that of densification. The best dielectric properties are observed for the best densification. As the sintering temperature increases to 1075 ^oC, the relative permittivity and quality factor reaches a maximum value and the temperature coefficient of resonant frequency is found to be minimum. However, subsequent increase in sintering temperature degrades the microwave dielectric properties. The improvements in microwave dielectric properties are attributed due to the improvement in densification. On the other hand, the dielectric properties are degraded due to the decreased densification by the evaporation of volatile element like lithium at elevated temperature [45]. The $Li_2MgTi_3O_8$ ceramics sintered at 1075 ^oC has ε_r = 27.2 and $Q_u$xf = 42000 GHz and τ_f = (+) 3.2 ppm/^oC at 5 GHz. The $Li_2ZnTi_3O_8$ ceramics sintered at 1075 ^oC shows ε_r = 25.6 and $Q_u$xf = 72000 GHz and τ_f = (-) 11.2 ppm/^oC at 5 GHz. Most of the titanium based ceramics have high processing temperature (>1400 ^oC). The high sintering temperature results coring effect in titanium based ceramics (oxygen deficient interior of the sintered pellet). This phenomenon has been observed in zirconium tin titanate ($Zr_{0.8}Sn_{0.2}TiO_4$), $BaTi_4O_9$ and $Ba_2Ti_9O_{20}$ ceramics [47]. The coring effect is due to the oxygen deficiency and this led

to the reduction of Ti^{4+} to Ti^{3+}. This causes the degradation of quality factor of microwave dielectric ceramics. In the present case the sintering temperature is relatively low for the titanium reduction.

The well known microwave dielectric materials with high quality factor in general need high sintering temperature together with long soaking time. However, the $Li_2MgTi_3O_8$ and $Li_2ZnTi_3O_8$ dielectric ceramics in the present investigation shows excellent dielectric properties at a low sintering temperature of 1075 ^oC/4hrs. The microwave dielectric losses in bulk ceramics fall into two categories, intrinsic and extrinsic [48, 49]. Intrinsic losses are dependent on the crystal structure and can be described by the interaction of phonon systems with ac electric field. The ac electric field alters the equilibrium of the phonon system and the subsequent relaxation associated with energy dissipation [48, 49]. Extrinsic losses are associated with the imperfections in the crystal structure like porosity, grain boundaries, microstructural defects etc [4]. Recently, Alford et al. [50] tried to answer the question of "Do grain boundary affect the microwave dielectric loss in oxides?". The interplay of other parameters such as porosity, liquid phase and cation ordering makes it difficult to make definitive remark on the relationship between grain size and dielectric loss. However, in sintered alumina, it has been reported that the dielectric loss is found to depend strongly on pore size, pore volume, and grain size [51]. The grain boundaries in the polycrystalline microwave dielectric ceramics have long been suspected for the dielectric loss. Report shows that the impurities even in minor amount will cause an increase in the dielectric loss of ceramics [52]. The sintering process sweeps the impurities to the grain boundaries so that the impurities and grain boundaries are inextricably linked. For small grains, there is a possibility of accumulation of impurities at the grain boundaries which is less for larger grains and that markedly affect the quality factor. Hence, it is reasonable to assume that if the grain boundaries

are a source of dielectric loss, then reducing their number might be expected to reduce the dielectric loss. It is generally accepted that ceramics having larger grains shows relatively better microwave dielectric properties in addition to the inherent properties. From the SEM image it is worth to note that both the ceramics are having the grain size of about 30-40 μm. The large grain size of the $Li_2MgTi_3O_8$ and $Li_2ZnTi_3O_8$ ceramics could be reason for the high quality factor when sintered at 1075 ^oC/4hrs.

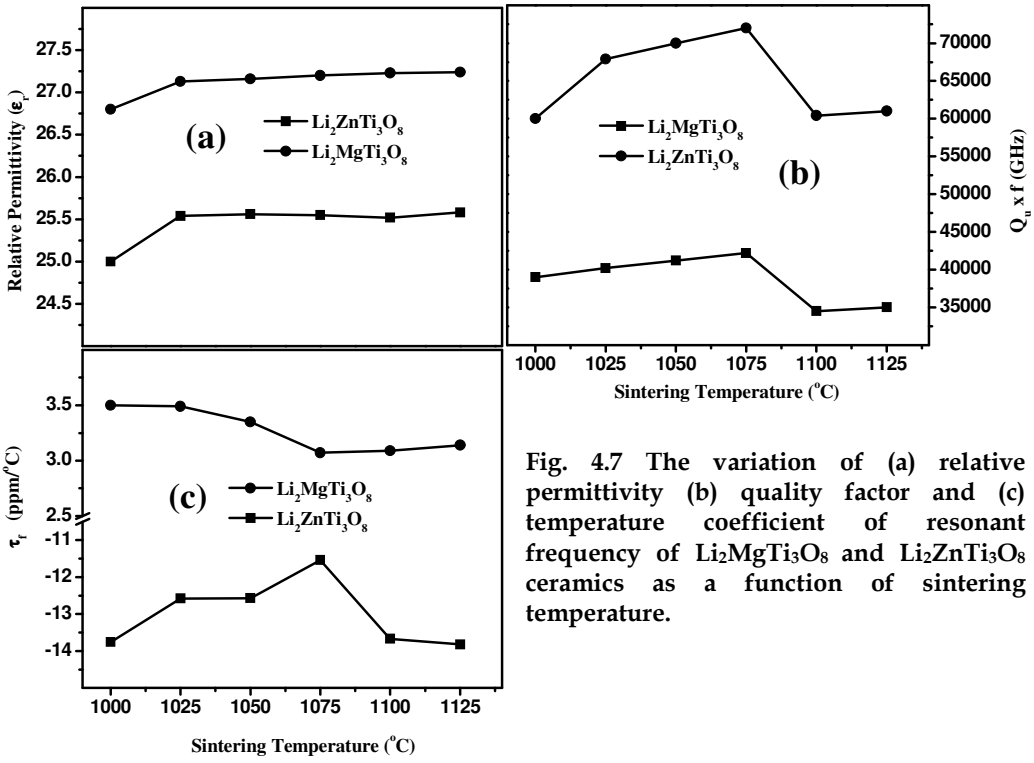

Fig. 4.7 The variation of (a) relative permittivity (b) quality factor and (c) temperature coefficient of resonant frequency of $Li_2MgTi_3O_8$ and $Li_2ZnTi_3O_8$ ceramics as a function of sintering temperature.

4.4.5 Densification and microwave dielectric properties of $Li_2Mg_{1-x}Zn_xTi_3O_8$ ceramics

It has been observed that the $Li_2MgTi_3O_8$ and $Li_2ZnTi_3O_8$ ceramics show excellent microwave dielectric properties with temperature coefficient of resonant frequency of +3.3 ppm/^oC and -11.3 ppm/^oC respectively. In order to tune the dielectric properties many attempts such A/B site modified

ceramics, layered system, solid solutions, dopant addition etc. have been proposed [24, 26, 29, 30, 53-55]. However, many of the system may result in multiphase with degradation in dielectric properties. Using two or compounds with positive and negative temperature coefficients to form a solid solution or mixed phase is the most promising method of obtaining zero τ_f. It is clear from the previous sections that the $Li_2MgTi_3O_8$ and $Li_2ZnTi_3O_8$ ceramics has τ_f of (+) 3.2 ppm/^oC and (-) 11.2 ppm/^oC respectively. The present section discusses the densification and microwave dielectric properties of $Li_2Mg_{1-x}Zn_xTi_3O_8$ ceramics.

Figure 4.8 shows the densification and the relative permittivity of $Li_2Mg_{1-x}Zn_xTi_3O_8$ ceramic as a function of x. A maximum densification of 95.5% and 95% is observed for $Li_2MgTi_3O_8$ and $Li_2ZnTi_3O_8$ ceramics respectively. The densification of $Li_2Mg_{1-x}Zn_xTi_3O_8$ ceramics is expected to be in between the densities of extreme composition. However, a sharp decrease in the densification (90% of theoretical density) is observed in the vicinity of x=0.2. This composition is very difficult to sinter and increasing the sintering temperature decreases the density of the samples further. From the SEM picture (see Fig 4.6 (c) (x = 0.2) it can be observed that the microstructure shows poor densification. Figure 4.8 shows relative permittivity curve of $Li_2Mg_{1-x}Zn_xTi_3O_8$ as a function of x. As the x increases from 0 to 1, the relative permittivity of $Li_2Mg_{1-x}Zn_xTi_3O_8$ ceramics decreases from 27 to 25.5. All the compositions of $Li_2Mg_{1-x}Zn_xTi_3O_8$ ceramics have the densification of about 93 to 95.5%. The porosity corrected permittivity of $Li_2Mg_{1-x}Zn_xTi_3O_8$ ceramics is calculated using the equation 3.1 (see chapter 3 section 3.3) [51] and shown in Fig 4.8. The porosity corrected relative permittivity of $Li_2Mg_{1-x}Zn_xTi_3O_8$ ceramics shows a decrease with an increase in x. As the x increases from 0 to 1, the porosity corrected relative permittivity of $Li_2Mg_{1-x}Zn_xTi_3O_8$ ceramics decreases from 29.5 to 27.8.

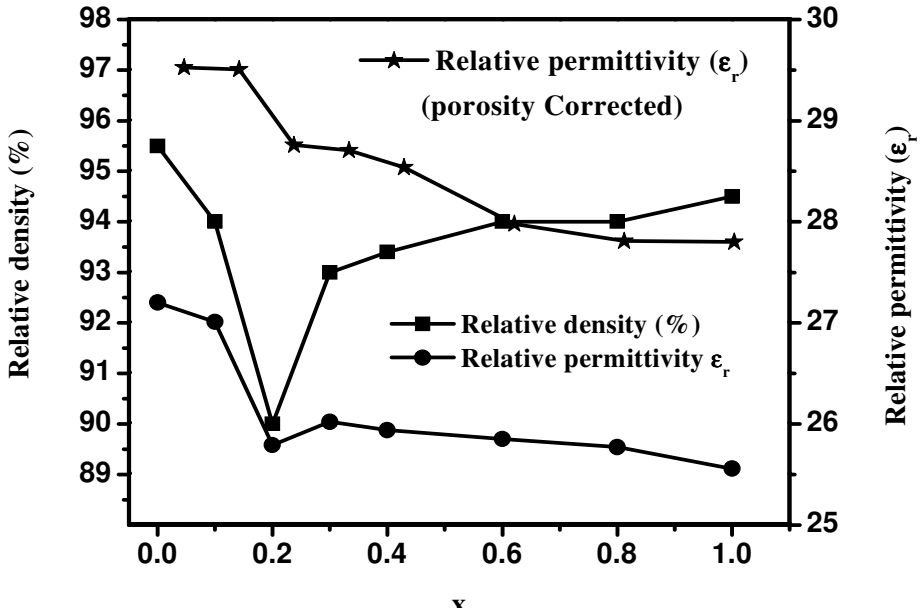

Fig. 4.8 The variation of densification and the relative permittivity of $Li_2Mg_{1-x}Zn_xTi_3O_8$ ceramic as a function of x.

Figure 4.9 shows the quality factor and the temperature coefficient of resonant frequency (τ_f) of $Li_2Mg_{1-x}Zn_xTi_3O_8$ ceramics sintered at 1075 ^oC/4hrs as a function of x. The quality factor of $Li_2MgTi_3O_8$ and $Li_2ZnTi_3O_8$ ceramics are 42000 GHz and 72000 GHz respectively. Hence the quality factor of $Li_2Mg_{1-x}Zn_xTi_3O_8$ ceramics sintered at 1075 ^oC/4hrs is expected to be in between the quality factor of the end compositions. As the x increases from 0 to 0.1, the quality factor of $Li_2Mg_{1-x}Zn_xTi_3O_8$ ceramics increases from 42000 GHz to 62000 GHz. However, subsequent increases in x (x = 0.2), the $Li_2Mg_{1-x}Zn_xTi_3O_8$ ceramics shows poor resonance (Q_u x f of about 10000 GHz). It is worth to note that this is the composition where the densification decreases rapidly. The extrinsic factors such as poor densification and the associated moisture may be the reason for high loss factor at x = 0.2. However, from Fig. 4.9 that further increase in the x value increases the quality factor of $Li_2Mg_{1-x}Zn_xTi_3O_8$ ceramics. The variation of temperature coefficient of resonant frequency of $Li_2Mg_{1-x}Zn_xTi_3O_8$ ceramics sintered at 1075 ^oC/4hrs as a function of x is also shown in Fig. 4.9. It can be observed

that, as the x increases from 0 to 1, the τ_f of $Li_2Mg_{1-x}Zn_xTi_3O_8$ ceramics varies from (+) 3.1 to (-) 11.2 ppm/^oC. Figure 4.9 clearly shows that as x=0.2 is the composition where the τ_f approaches the zero value with poor resonance.

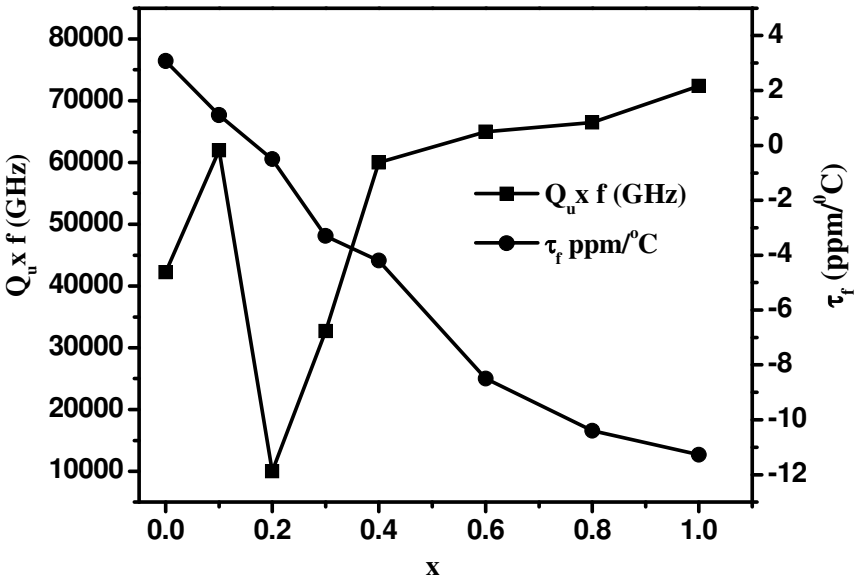

Fig. 4.9 The variation of quality factor and the temperature coefficient of resonant frequency of $Li_2Mg_{1-x}Zn_xTi_3O_8$ ceramics sintered at 1075 ^oC/4hrs as a function of x

4.4.6 Effect of calcium substitution on the structure and microwave dielectric properties of $Li_2(A_{1-x}Ca_x)Ti_3O_8$ ceramics (A=Mg, Zn, and x=0, 0.05, 0.1, 0.15, 0.20)

Extensive investigation has been paid for tailoring the microwave dielectric properties of several low loss dielectric ceramics by possible substitution, dopant addition, solid solution formation and layered dielectrics [4, 16, 30, 53, 56-58]. It has been reported that, substitutions always improve or degrade the dielectric properties depending on the chemical reactivity, solid solubility and the formation of the second phase of substituting element with the parent composition [57]. If the substituting element is having larger or smaller size compared to host element, then it is very difficult to be substituted at the respective site obeying vegard's law [59, 60] and may form second phase easily. This second phase may in

general degrade the microwave dielectric properties. However, if the second phase formed is low loss, then the properties may not be affected considerably. In the previous section we have see that the zinc act as good substitutant for magnesium in the composition $Li_2(Mg_{1-x}Zn_x)Ti_3O_8$ and improved the quality factor. The ionic radii of zinc (0.74 Å) and magnesium (0.72 Å) are comparable. The calcium is having slightly higher ionic radii (1.0 Å) compared to zinc and magnesium (CN=6). The present section discuss the effect of substitution element having higher ionic radii (calcium) on the microwave dielectric properties of $Li_2(A_{1-x}Ca_x)Ti_3O_8$ ceramics (A=Mg, Zn, and x=0, 0.05, 0.1, 0.15, 0.20) ceramics.

4.4.6.1 Crystalline phase and micro structural analysis

Figure 4.10 and 4.11 show the X-ray diffraction pattern of $Li_2(A_{1-x}Ca_x)Ti_3O_8$ ceramics (A=Mg, Zn, and x=0, 0.05, 0.1, 0.15, 0.20) ceramics sintered at 1075 ^oC/4hrs. All the peaks in Fig. 4.10 is indexed based on JCPDS file number 48-0263 for $Li_2MgTi_3O_8$ ceramics and Fig. 4.11 is indexed based on JCPDS file number 86-1512 for Ca substituted $Li_2ZnTi_3O_8$ ceramics with cubic crystal symmetry. A small amount of second phase ($CaTiO_3$) has been observed for the calcium substitution of $Li_2(A_{1-x}Ca_x)Ti_3O_8$ ceramics (A=Mg, Zn, and x=0, 0.05, 0.1, 0.15, 0.20) ceramics. The intensity of second phase is found to be increased with increase in the calcium substitution. The formation of the second phase could be due to the relatively higher ionic radius of calcium compared to that of magnesium and zinc. The second phase observed is $CaTiO_3$ and which can be indexed based on the JCPDS file 42-0423. In the case of Ca substitution for Mg, second phase is formed for x = 0.05 and the $CaTiO_3$ content increases with increase in x value. The intensity of XRD peak corresponding to $CaTiO_3$ increases with Ca substitution. In the case of Zn, the $CaTiO_3$ XRD peaks start appearing at x = 0.1 and the intensity of XRD peak corresponding to $CaTiO_3$ increases with increase in x.

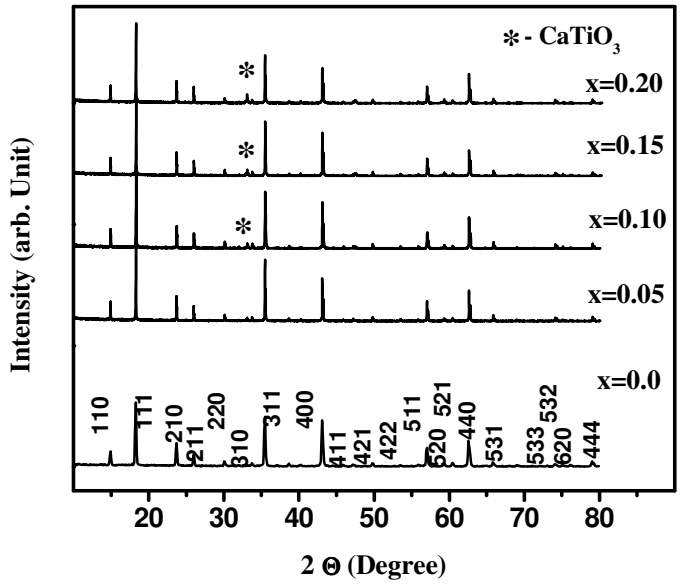

Fig. 4.10 X-ray diffraction patterns of $Li_2Mg_{1-x}Ca_xTi_3O_8$ (x = 0, 0.05, 0.10, 0.15, 0.20) ceramics sintered 1075 ^oC/4hrs.

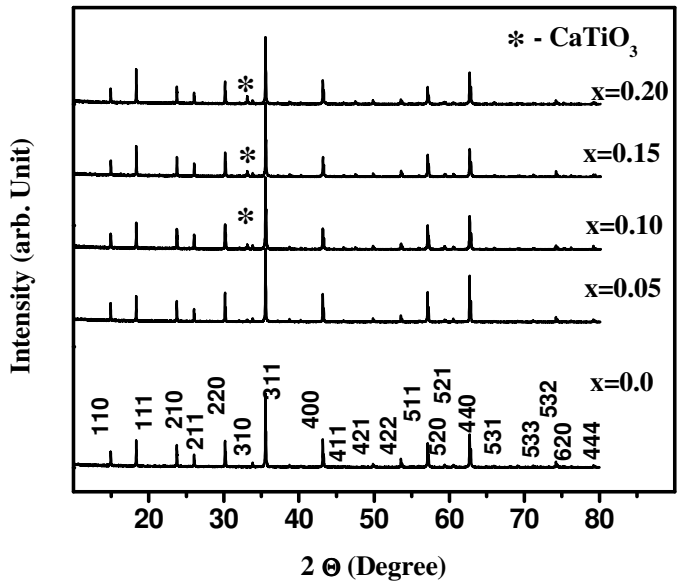

Fig. 4.11 X-ray diffraction patterns of $Li_2Zn_{1-x}Ca_xTi_3O_8$ (x = 0, 0.05, 0.10, 0.15, 0.20) ceramics sintered 1075 ^oC/4hrs.

Fig. 4.12 shows the microstructure of $Li_2(A_{1-x}Ca_x)Ti_3O_8$ (A=Mg, Zn) ceramics as a function of Ca concentration. The grains are having an average size of about 30-40 μm. By comparing the Figs. 4.6 and 4.12, it can be observed that the substitution of calcium does not change much the grain

morphology or grain size. However, small amount of second phase ($CaTiO_3$) which is randomly distributed on the grains and grain boundaries is observed. It is clear from the SEM image that, as the Ca concentration of $Li_2(A_{1-x}Ca_x)Ti_3O_8$ (A=Mg, Zn) ceramics increases, the amount of second phase ($CaTiO_3$) also increases. The mixture phase observed in the microstructure strongly support the secondary phase detected in the X-ray diffraction of $Li_2(A_{1-x}Ca_x)Ti_3O_8$ (A=Mg, Zn) ceramics. The second phase formed is marked in the inset of Fig. 4. 12(b).

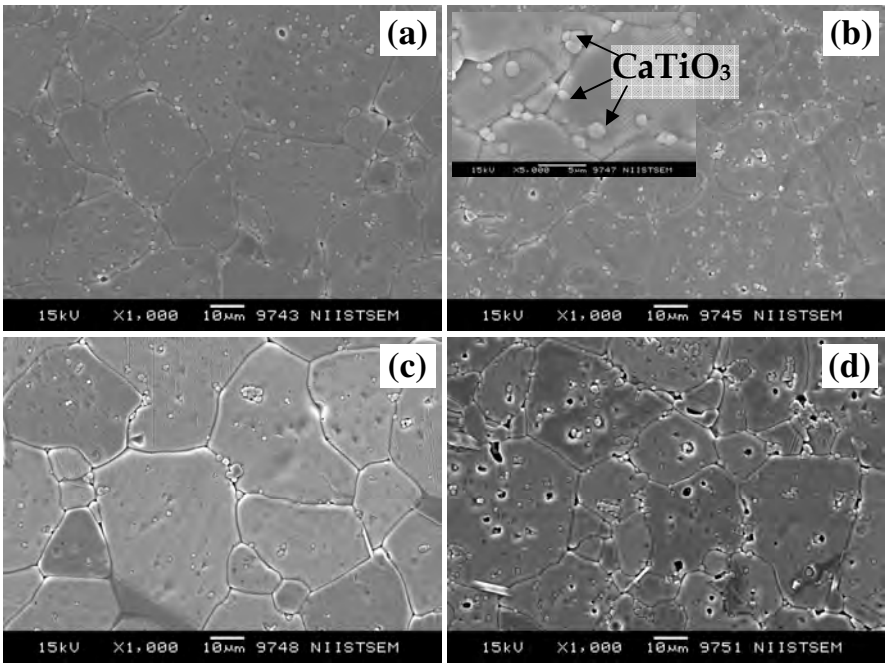

Fig. 4.12 SEM images of $Li_2(A_{1-x}Ca_x)Ti_3O_8$ (a) A=Mg and x=0.10, (b) A=Mg and x=0.20, (c) A=Zn and x=0.10, (b) A=Zn and x=0.20 ceramics sintered 1075 ^oC/4hrs. Inset of Fig. (b) is its magnified image.

4.4.6.2 Densification and microwave dielectric properties

Figure 4. 13 (a) shows the variation of density of $Li_2(A_{1-x}Ca_x)Ti_3O_8$ (A=Mg, Zn) ceramics as a function of x. It is clear from the SEM images that the increase in the Ca substitution increases the porosity. Hence it is expected to decrease the density of the $Li_2(Mg_{1-x}Ca_x)Ti_3O_8$ ceramics with Ca substitution. A slight decrease in the density is observed for the Ca

substitution (up to x = 0.05) for $Li_2(Mg_{1-x}Ca_x)Ti_3O_8$ ceramics. However, further increase in Ca substitution increases the density slightly. The second phase ($CaTiO_3$) has slightly higher density (4.036 g/cm^3) compared to that of LMT and LZT ceramics. The increase in the density of $Li_2(Mg_{1-x}Ca_x)Ti_3O_8$ with an increase in Ca substitution could be due to the $CaTiO_3$ second phase. The slight decrease in the density of $Li_2(Zn_{1-x}Ca_x)Ti_3O_8$ with an increase in Ca substitution could be due to the formation of pores which seems to be more for $Li_2(Zn_{1-x}Ca_x)Ti_3O_8$ compared to $Li_2(Mg_{1-x}Ca_x)Ti_3O_8$ (see Fig. 4.12). As the Ca substitution increases from 0 to 0.20 the density of $Li_2(Mg_{1-x}Ca_x)Ti_3O_8$ increases from 3.31 to 3.41g/cm^3 and that of $Li_2(Zn_{1-x}Ca_x)Ti_3O_8$ varies from 3.77 to 3.74g/cm^3. Fig. 4.13 (b) shows the variation of relative permittivity of $Li_2(A_{1-x}Ca_x)Ti_3O_8$ (A=Mg, Zn) ceramics as a function of calcium substitution. The relative permittivity is found to increase with an increase in the calcium substitution for both the $Li_2(Mg_{1-x}Ca_x)Ti_3O_8$ and $Li_2(Zn_{1-x}Ca_x)Ti_3O_8$ ceramics. It can be observed from the X-ray diffraction pattern and SEM micrograph that the amount of second phase ($CaTiO_3$) increases with calcium concentration in $Li_2(A_{1-x}Ca_x)Ti_3O_8$ (A=Mg, Zn) ceramics. The $CaTiO_3$ has permittivity of about 174 [4, 26, 29] which is much higher than that of $Li_2MgTi_3O_8$ and $Li_2ZnTi_3O_8$ ceramics. The higher permittivity of the second phase could be the reason for the increase in the permittivity of $Li_2(A_{1-x}Ca_x)Ti_3O_8$ (A=Mg, Zn) ceramics with calcium concentration. As the x increases from 0 to 0.2, the relative permittivity of $Li_2(Mg_{1-x}Ca_x)Ti_3O_8$ and $Li_2(Zn_{1-x}Ca_x)Ti_3O_8$ ceramics increases from 27.2 to 32.8 and 25.6 to 30.8 respectively. The variation of quality factor of $Li_2(A_{1-x}Ca_x)Ti_3O_8$ (A=Mg, Zn) ceramics as a function of calcium concentration is shown in Fig. 4.13 (c). The quality factor of both $Li_2(Mg_{1-x}Ca_x)Ti_3O_8$ and $Li_2(Zn_{1-x}Ca_x)Ti_3O_8$ ceramics is found to be decreased with increase in the calcium substitution. Compared to $Li_2MgTi_3O_8$ and $Li_2ZnTi_3O_8$ ceramics, the $CaTiO_3$ has a low quality factor of about 3600 GHz [4, 26, 29]. Hence the

increases in the amount of $CaTiO_3$ phase having lower quality factor with calcium concentration could be the reason for the decrease in the quality factor of $Li_2(A_{1-x}Ca_x)Ti_3O_8$ (A=Mg, Zn) ceramics.

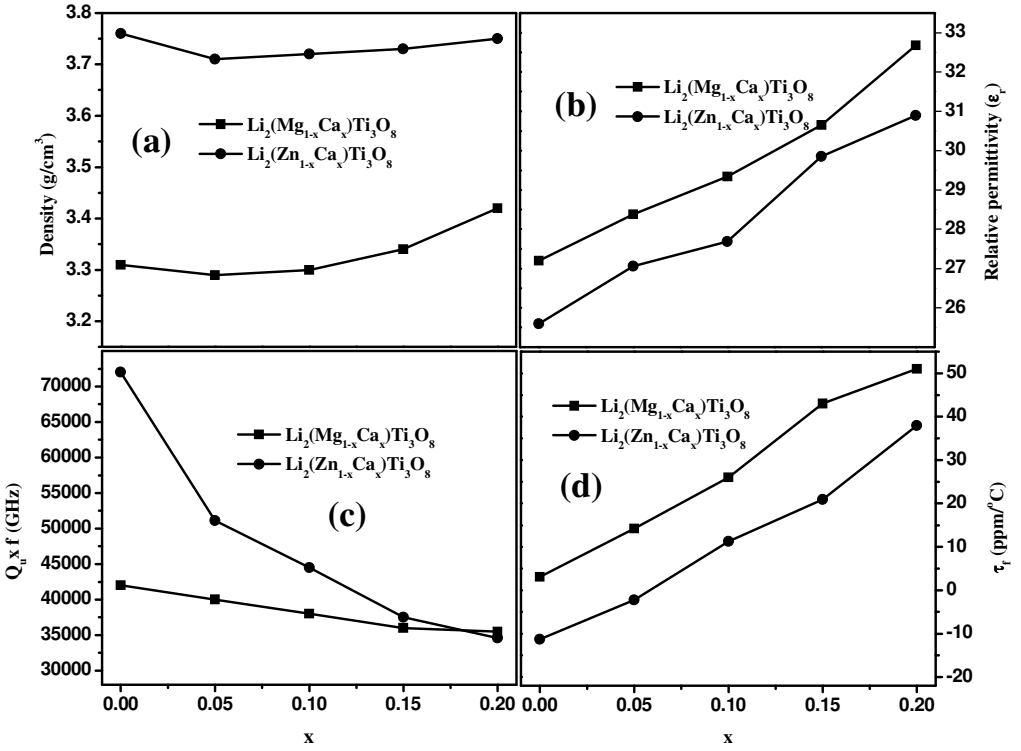

Fig. 4.13 Variation of (a) density, (b) relative permittivity, (c) quality factor, and (d) temperature coefficient of resonant frequency of $Li_2(A_{1-x}Ca_x)Ti_3O_8$ (A=Mg, Zn) ceramics as a function of x.

Fig. 4.13 (d) depicts the variation of the temperature coefficient of resonant frequency of $Li_2(A_{1-x}Ca_x)Ti_3O_8$ (A=Mg, Zn) ceramics as a function of calcium concentration. The τ_f of $Li_2(Mg_{1-x}Ca_x)Ti_3O_8$ increases from +3.1 to 51 ppm/^oC where as the τ_f of $Li_2(Zn_{1-x}Ca_x)Ti_3O_8$ shifts from -11.21 to +38 ppm/^oC. It is well known that the $CaTiO_3$ has a high positive τ_f of about (+800 ppm/^oC) and it is commonly used to tune the temperature coefficient of resonant frequency of microwave dielectric ceramics which are having a negative τ_f [37, 61, 62]. The high positive τ_f of the $CaTiO_3$ second phase could

be the reason for the increase in the temperature coefficient of resonant frequency of $Li_2(A_{1-x}Ca_x)Ti_3O_8$ (A=Mg, Zn) ceramics with calcium concentration.

4.4.7 Effect of glass addition on the sinterability and microwave dielectric properties of $Li_2ATi_3O_8$ ceramics (A=Mg, Zn)

Recently, the development of dielectric materials for microwave applications have focused on the low temperature co-fired ceramics due to their functional advantages for the miniaturization of the dimensions of multilayer devices [63]. LTCC materials are required to have good sinterability below the melting point of commonly used electrodes such as copper and silver with good microwave dielectric properties. From the previous sections, we have seen that the $Li_2MgTi_3O_8$ and $Li_2ZnTi_3O_8$ ceramics shows excellent microwave dielectric properties when sintered at 1075 ^oC/4hrs. The low sintering temperature of this dielectric ceramics opens a wide window for the possible application in LTCC based devices. However, slightly higher sintering temperature of these materials as compared to the melting point of silver electrode material restricts its immediate application in LTCC technology. It is well known that the liquid phase sintering by glass addition is the best method to lower the sintering temperature of the ceramics with reasonably good microwave dielectric properties [64-71]. Earlier investigations on glass added ceramics reveals that multicomponent glasses are more effective to lower the sintering temperature of the ceramics without degrading the microwave dielectric properties [63, 72]. In the present study we have selected lithium magnesium zinc borosilicate (LMZBS) glass as the sintering aid. The physical and dielectric properties of the LMZBS glass are shown in Table 1.2 (see chapter 1, section 1.9). If the amount of glass frit is large, the network formers in the excess glass can profoundly absorb the microwave at higher frequencies and

thereby degrade the quality factor of the final products [73]. Hence the amount of glass frit for lowering the sintering temperature of each ceramics has to be optimized. The following section discusses the effect of glass addition on the sinterability, microstructure and microwave dielectric properties of $Li_2MgTi_3O_8$ and $Li_2ZnTi_3O_8$ ceramics.

4.4.7.1 Shrinkage characteristics

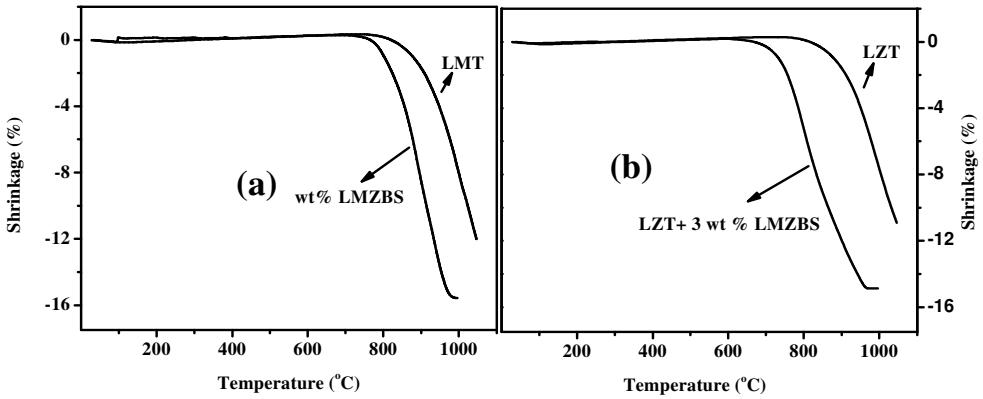

Fig. 4.14 Shrinkage characteristics of (a) $Li_2MgTi_3O_8$ and (b) $Li_2ZnTi_3O_8$ ceramics with and without 3 wt% of lithium magnesium zinc borosilicate (LMZBS) glass.

The dilatometry study provides an insight to the densification process for the ceramic glass systems. Fig. 4.14 shows the shrinkage characteristics of (a) $Li_2MgTi_3O_8$ and (b) $Li_2ZnTi_3O_8$ ceramics with and without 3 wt% of lithium magnesium zinc borosilicate (LMZBS) glass. It is found that the sintering of $Li_2MgTi_3O_8$ and $Li_2ZnTi_3O_8$ ceramics starts around 850 ^oC and 12 % of linear shrinkage is in the temperature range of 850-1050 ^oC. The low onset of sintering behavior of temperature stable high Q materials has not been reported so far. This offers the perspective of the application of these materials in LTCC based devices. It can be observed from Fig. 4.14 that the onset of sintering of both LMT + 3 wt% LMZBS and LMT + 3 wt% LMZBS ceramic glass composite starts around 750 ^oC and a linear shrinkage of about

15 % is observed in the temperature range of 750-950 ^{o}C. The eutectic liquid phase formation of the LMZBS glass could be the reason for the reduction of onset of sintering of both the microwave dielectric ceramics in the present investigation. This implies that the LMZBS glass acts as sintering aid to lower the sintering temperature of $Li_2MgTi_3O_8$ and $Li_2ZnTi_3O_8$ ceramics.

4.4.7.2 Crystalline phase and micro structural analysis

Generally addition of glass in ceramics degrades the microwave dielectric properties by the formation of secondary phases while sintering. Fig. 4.15 shows the X-ray diffraction pattern of (a) $Li_2MgTi_3O_8$ sintered at 1075 ^{o}C/4hrs, (b) $Li_2MgTi_3O_8$ + 3 wt% of LMZBS sintered at 925 ^{o}C/4hrs, (c) $Li_2MgTi_3O_8$ + 3 wt% of LMZBS + 20 wt% of Ag sintered at 925 ^{o}C/4hrs, (d) $Li_2ZnTi_3O_8$ sintered at 1075 ^{o}C/4hrs, (e) $Li_2ZnTi_3O_8$ + 3 wt% of LMZBS sintered at 900 ^{o}C/4hrs, and (f) $Li_2ZnTi_3O_8$ + 3 wt% of LMZBS + 20 wt% of Ag sintered at 900 ^{o}C/4hrs. It can be observed that the addition of LMZBS glass does not lead to formation of any secondary phase. All the peaks in the XRD pattern are indexed based on JCPDS file number 48-0263 for $Li_2MgTi_3O_8$+LMZBS system and JCPDS file number 86-1512 for $Li_2ZnTi_3O_8$+LMZBS system with cubic crystal symmetry. For LTCC applications the electrode material should not react with the ceramic material during co-firing. The X-ray diffraction pattern of dielectric ceramics and electrode material sintered at its optimized sintering temperature is an acceptable way to study the interface reaction. It can be observed from Figs. 4.15 (c) and (f) that, there is no additional phase other than metallic silver (JCPDS file number 03-0921) and $Li_2MgTi_3O_8$ (JCPDS file number 48-0263) or $Li_2ZnTi_3O_8$ (JCPDS file number 86-1512) phases. Since the formation of secondary phase is not observed in the pattern, it may be possible to use Ag as the electrode material for these ceramic glass composites.

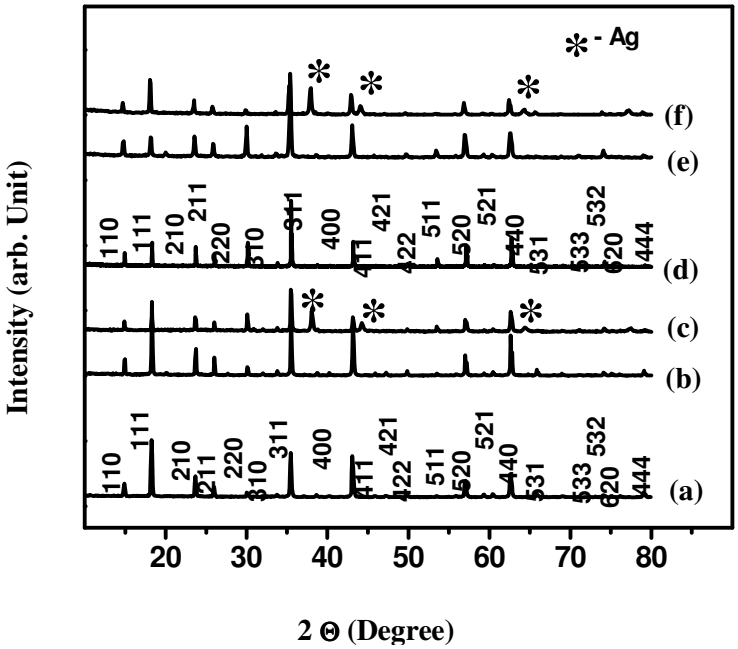

Fig. 4.15 The X-ray diffraction pattern of (a) $Li_2MgTi_3O_8$ sintered at 1075 °C/4hrs, (b) $Li_2MgTi_3O_8$ + 3 wt% of LMZBS sintered at 925 °C/4hrs, (c) $Li_2MgTi_3O_8$ + 3 wt% of LMZBS + 20 wt% of Ag sintered at 925 °C/4hrs, (d) $Li_2ZnTi_3O_8$ sintered at 1075 °C/4hrs, (e) $Li_2ZnTi_3O_8$ + 3 wt% of LMZBS sintered at 900 °C/4hrs, and (f) $Li_2ZnTi_3O_8$ + 3 wt% of LMZBS + 20 wt% of Ag sintered at 900 °C/4hrs.

Figure 4.16 shows the scanning electron micrograph of thermally etched 3 wt% of LMZBS glass added (a) $Li_2MgTi_3O_8$ ceramics sintered at 925 °C/4hrs and (b) $Li_2ZnTi_3O_8$ ceramics sintered at 900 °C/4hrs. The influence of glass addition in ceramics varies from material to material. Fig. 4.16 (a) is a typical example of liquid phase sintering in which the glass melts and wet the grains and flows between the grains of $Li_2MgTi_3O_8$ ceramics. It is well known that the liquid phase sintering decreases the grain size of dielectric ceramics [74]. The LMT ceramics sintered at 1075 °C/4hrs has a grain size of about 30-40 μm where as the 3 wt% of LMZBS glass added LMT ceramics sintered at 925 has a grain size of about 8 to 10 μm. The effect of LMZBS glass addition in $Li_2ZnTi_3O_8$ ceramics is different from that of $Li_2MgTi_3O_8$ ceramics. From Fig. 4.16 (b), it can be observed that the glass is concentrated mainly at the grain boundaries and there is no significant change in the grain

size compared to pure LZT sintered at 1075 ^{o}C/4hrs. This is clear from the low magnification image (see Fig. 4.17) of $Li_2ZnTi_3O_8$ + 3 wt% of LMZBS glass sintered at 900 ^{o}C/4hrs. Hence, it can be concluded that the LMZBS glass decreases the grain size of $Li_2MgTi_3O_8$ ceramics. This could be due to the liquid phase sintering and the decrease in the sintering temperature. However, no significant decrease in the grain size is observed for LMZBS glass added $Li_2ZnTi_3O_8$ ceramics.

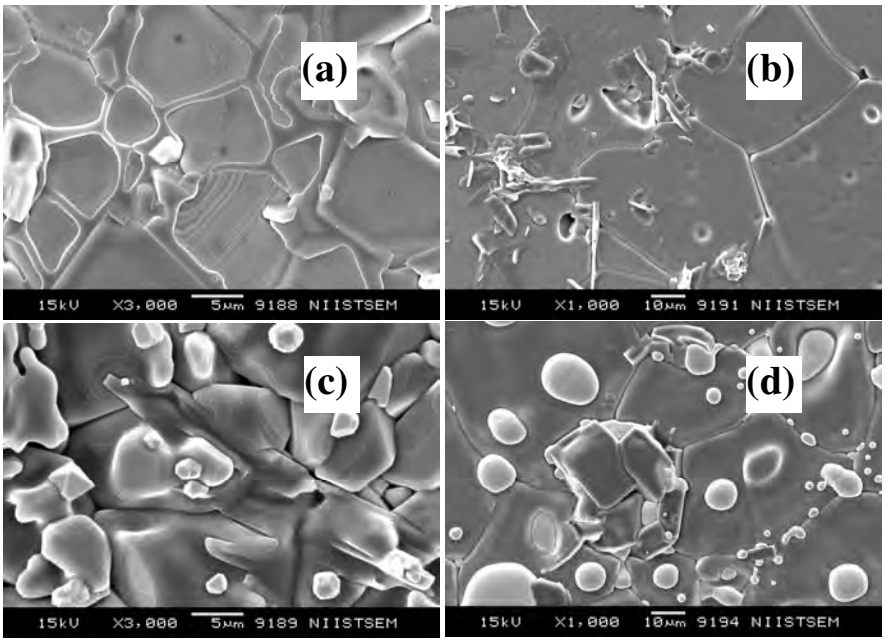

Fig. 4.16 SEM images thermally etched (a) 3 wt% of LMZBS glass added LMT ceramics sintered at 925 ^{o}C/4hrs and (b) 3 wt% of LMZBS glass added LZT ceramics sintered at 900 ^{o}C/4hrs, (c) LMT+3wt% of LMZBS+ 20 wt% of Ag sintered at 925 ^{o}C/4hrs, and (d) LZT+3 wt% of LMZBS + 20 wt% of Ag sintered at 900 ^{o}C/4hrs.

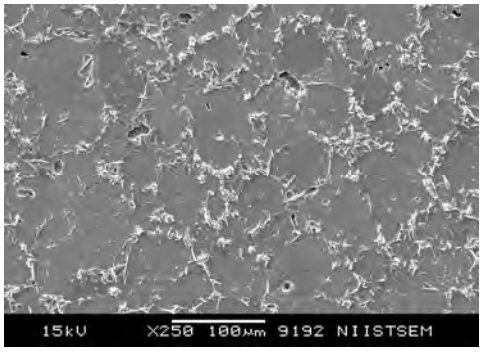

Fig 4.17 The Low magnification image of $Li_2ZnTi_3O_8$ + 3 wt% of LMZBS glass sintered at 900 ^{o}C/4hrs.

Fig. 4.16 shows the micrograph of (c) $Li_2MgTi_3O_8$ + 3 wt% of LMZBS + 20 wt% of Ag sintered at 925 ^oC/4hrs and (d) $Li_2ZnTi_3O_8$ + 3 wt% of LMZBS + 20 wt% of Ag sintered at 900 ^oC/4hrs. The silver did not react with the ceramic-glass composites and are distributed randomly. This micrograph strongly supports the results of non-reactivity of silver with ceramic glass system as evidenced from the X-ray diffraction pattern (see Fig. 4.15).

4.4.7.3 Densification and microwave dielectric properties

Addition of sintering aid not only lowers the sintering temperature but also affect the densification of the ceramics. Fig. 4.18 shows the variation of sintering temperature and relative density of (a) $Li_2MgTi_3O_8$ and (b) $Li_2ZnTi_3O_8$ ceramics as a function of LMZBS glass fluxing. The sintering temperature is optimized for best density and dielectric properties. As the amount of glass increases, a gradual decrease in the sintering temperature of both the $Li_2MgTi_3O_8$ + LMZBS and $Li_2ZnTi_3O_8$ + LMZBS ceramics glass composites are observed. Addition of 3 wt% of LMZBS decreases the sintering temperature of $Li_2MgTi_3O_8$ from 1075 ^oC/4hrs to 925 ^oC/4hrs and that of $Li_2ZnTi_3O_8$ ceramics from 1075 ^oC/4hrs to 900 ^oC/4hrs. However, higher wt% of glass fluxing does not decrease the sintering temperature further. The glassy liquid phase at the grain boundary effectively eliminates pores and thereby lowers the sintering temperature. Hence the decrease in the sintering temperature could be due to the liquid phase sintering as evident from SEM images (see Fig. 4 .16). The relative density of both $Li_2MgTi_3O_8$ and $Li_2ZnTi_3O_8$ ceramics is found to decrease with glass fluxing.

It is worth to note that the density of LMZBS glass (2.75 g/cm^3) (see Table 1.2, Chapter 1, Section 1.9) is slightly lower than the density of both LMT and LZT ceramics. It is strongly believed that the sintering characteristics are strongly correlated with the formation temperature of the eutectic liquid phase. The decrease in densification of glass added ceramics

could be due to the inhomogeneous evaporation of the liquid phase from the grain boundary causing incomplete wetting, formation of pores and suppressed grain growth [65]. Maximum densification of 93.5% is observed for 3 wt% of LMZBS glass added LMT ceramics and 93.5 % for 3 wt% of LMZBS glass added LZT ceramics. Trapped porosity associated with grain growth and formations of pores by the evaporation of excess glass components are the reasons for the reduction of density for higher wt% of glass fluxing.

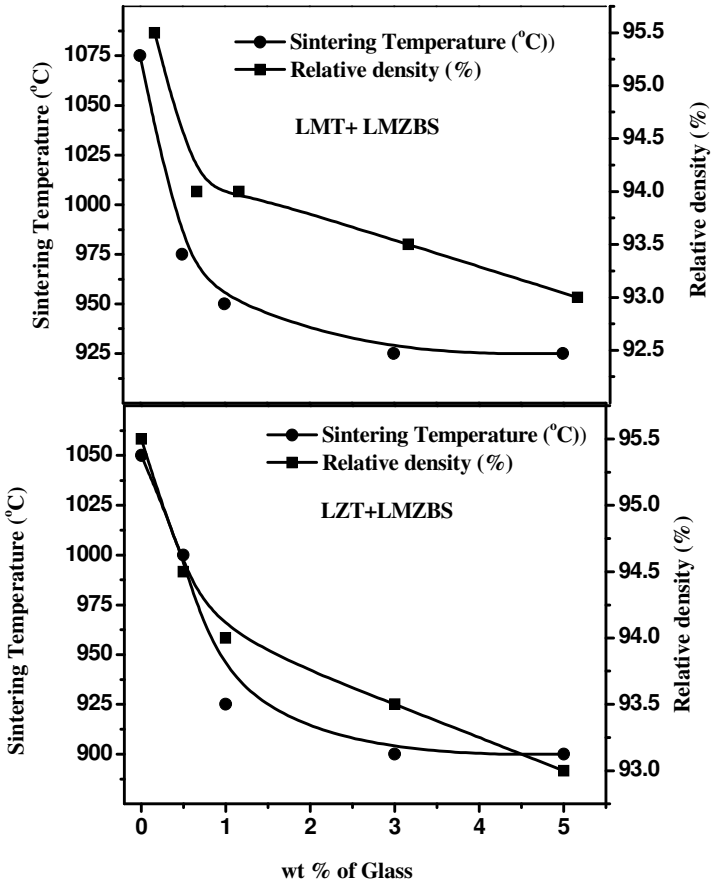

Figure 4.18 The variation of sintering temperature and relative density of (a) $Li_2MgTi_3O_8$ and (b) $Li_2ZnTi_3O_8$ ceramics as a function of LMZBS glass

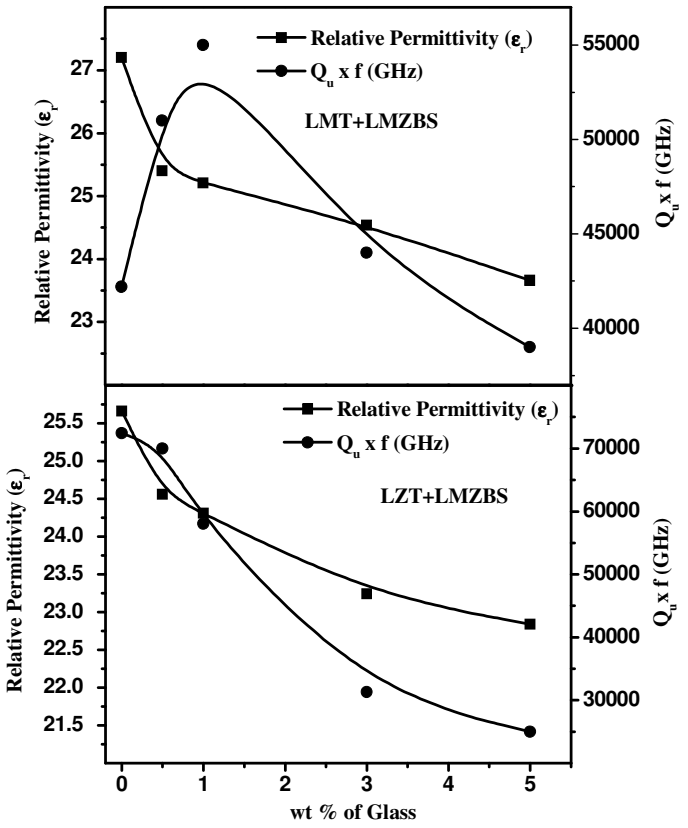

Figure 4.19 Variation of relative permittivity and quality factor of (a) LMT and (b) LZT ceramics as a function of LMZBS glass addition.

The eutectic liquid phase in the ceramic glass system will significantly change the microwave dielectric properties of the ceramics. The effect of glass addition on the microwave dielectric properties of dielectric ceramics depend strongly on the chemistry of glass, the chemical reaction, the phase change during sintering and the final density [65, 68]. Generally, the Q value of the ceramic glass composite decreased with increasing the glass content despite the increase in the density. Fig. 4.19 shows the relative permittivity and quality factor of (a) LMT and (b) LZT ceramics as a function of LMZBS glass addition. It is found that the dielectric properties changes in a manner similar to that of densification. As the LMZBS glass content increases from 0

to 5 wt%, the relative permittivity LMT decreases from 27.2 to 23.7 and that of LZT decreases from 25.7 to 22.8. The decrease in the permittivity of both the LMT + LMZBS and LZT + LMZBS ceramic glass composite is expected since the permittivity of LMZBS glass is (ε_r = 6.9) lower than that of LMT and LZT ceramics. It is also worth to note that the densification of glass added LMT and LZT ceramics decreases with increase in the amount of glass. The decrease in densification and the low relative permittivity of glass could be the reason for the decrease in the relative permittivity of the LMT + LMZBS and LZT + LMZBS ceramic glass composites. Fig. 4.19 also illustrates the variation of quality factor of (a) LMT and (b) LZT ceramics as a function of LMZBS glass fluxing. It can be observed that a small amount of glass (1 wt %) increases the quality factor of LMT ceramics from 42000 GHz to 52000 GHz and further addition of LMZBS glass (5 wt %) decreases the quality factor of LMT to 38000 GHz. For LZT + LMZBS ceramics glass composites, a gradual decrease in the quality factor is observed along with a decrease in sintering temperature. The quality factor of LZT ceramics decreases from 72000 GHz to 27000 GHz with the addition of 5 wt % of LMZBS glass. The added glasses not only acted as the sintering aid but also as an impurity phase with low quality factor and ε_r that can adversely affect the microwave dielectric properties. It has been reported that, the microwave dielectric loss is mainly caused not only by the lattice vibrations but also by the pores, the grain morphology and the second phase [3]. It can be evidenced by comparing the SEM image (see Fig 4.6, 4.16 and 4. 17) that the LMZBS glass addition in LMT and LZT ceramics increases porosity and the glasses are concentrated at the grain boundaries. It is reported that during sintering the impurities are concentrated at the grain boundary intersections and this accumulated impurities increases with an increase in the grain boundary intersections [63, 71]. In addition, the dielectric loss of glasses is much higher than that of LMT and LZT ceramics. The relatively higher dielectric loss of

the glass and the low densification could be the reason for the decrease in the quality factor of LMT + LMZBS and LZT + LMZBS ceramic glass composite with glass additions. Addition of 3 wt% of LMZBS glass in LMT and LZT shows the quality factor of 43000 GHz and 30000 GHz when sintered at 925 ^{o}C/4hrs and 900 ^{o}C/4hrs respectively.

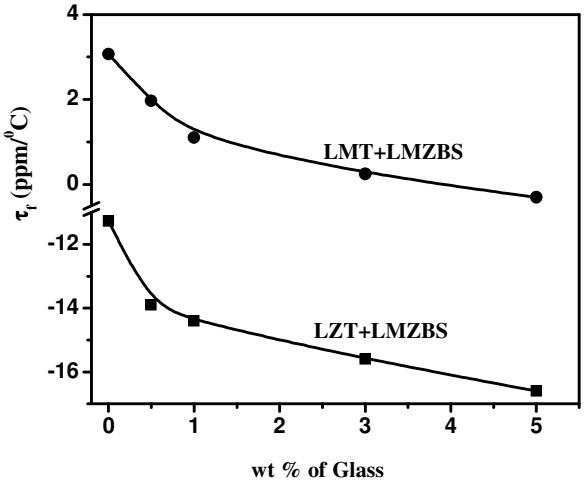

Fig. 4.20 The variation of temperature coefficient of resonant frequency of LMT and LZT ceramics as a function of LMZBS glass fluxing.

The stability of resonant frequency of resonator or filter with ambient temperature is important as far as the design and performance of the microelectronic devices are concerned. Fig. 4.20 shows the variation of temperature coefficient of resonant frequency of LMT and LZT ceramics with different wt% of LMZBS glass. It can be observed that the addition of 5 wt % LMZBS glass in LMT decreases the τ_f from (+) 3.1 to (+) 0.5 ppm/^{o}C and that of LZT varies from (-) 11.2 to (-) 16.5 ppm/^{o}C. The decrease in the τ_f of the present ceramic glass system could be due to the relatively high negative τ_f of LMZBS glass compared to LMT and LZT ceramics. The excellent sinterability and microwave dielectric properties of this new family of LTCC materials can address the growing demand of electronic manufacturers to reduce packaging size.

Table 4.3. The sintering temperature, permittivity, quality factor, τ_f and density of microwave dielectric ceramics developed in the present investigation

Material	Sintering Temperature (°C)	ε_r	$Q_u$xf (GHz)	τ_f (ppm/°C)	Density (g/cm³)
$Li_2MgTi_3O_8$ (LMT)	1075	27.20	42000	(+) 3.2	3.31
$Li_2(Mg_{0.9}Zn_{0.1})Ti_3O_8$	1075	27.01	62000	(+) 1.2	3.33
$Li_2(Mg_{0.8}Zn_{0.2})Ti_3O_8$	1075	25.79	10000	(-) 0.2	3.26
$Li_2(Mg_{0.7}Zn_{0.3})Ti_3O_8$	1075	26.02	32700	(-) 3.3	3.37
$Li_2(Mg_{0.6}Zn_{0.4})Ti_3O_8$	1075	25.94	60000	(-) 4.2	3.48
$Li_2(Mg_{0.4}Zn_{0.6})Ti_3O_8$	1075	25.85	65000	(-) 8.2	3.52
$Li_2(Mg_{0.2}Zn_{0.8})Ti_3O_8$	1075	25.77	66500	(-) 10.5	3.64
$Li_2ZnTi_3O_8$ (LZT)	1075	25.56	72000	(-) 11.2	3.77
$Li_2(Mg_{0.95}Ca_{0.05})Ti_3O_8$	1075	28.38	40000	(+)14.2	3.29
$Li_2(Mg_{0.9}Ca_{0.1})Ti_3O_8$	1075	29.34	38000	(+)26	3.30
$Li_2(Mg_{0.85}Ca_{0.15})Ti_3O_8$	1075	30.65	36000	(+)43	3.34
$Li_2(Mg_{0.80}Ca_{0.20})Ti_3O_8$	1075	32.7	35500	(+) 51	3.41
$Li_2(Zn_{0.95}Ca_{0.05})Ti_3O_8$	1075	27.06	51100	(-)2.24	3.71
$Li_2(Zn_{0.9}Ca_{0.1})Ti_3O_8$	1075	27.69	44500	(+) 11.3	3.72
$Li_2(Zn_{0.85}Ca_{0.1})Ti_3O_8$	1075	29.85	37500	(+) 20.9	3.73
$Li_2(Zn_{0.8}Ca_{0.2})Ti_3O_8$	1075	30.9	34600	(+) 38.0	3.74
LMT + 0.5 LMZBS	975	25.40	51000	(+)1.97	3.20
LMT + 1 LMZBS	950	25.21	55000	(+)1.1	3.17
LMT + 3 LMZBS	925	24.54	44000	(+)0.25	3.16
LMT + 5 LMZBS	925	23.70	38000	(-) 0.3	3.15
LZT + 0.5 LMZBS	1000	24.56	70000	(-)13.5	3.64
LZT + 1 LMZBS	925	24.31	58000	(-)14.4	3.62
LZT + 3 LMZBS	900	23.24	31300	(-)15.6	3.58
LZT + 5 LMZBS	900	22.8	25000	(-) 16.6	3.59

The major results such as sintering temperature, density, relative permittivity, quality factor and τ_f of $Li_2(Mg_{1-x}Zn_x)Ti_3O_8$ (x=0 to 1), $Li_2(A_{1-x}Ca_x)Ti_3O_8$ (A=Mg, Zn) ceramics and the effect of LMZBS glass addition on $Li_2MgTi_3O_8$ and $Li_2ZnTi_3O_8$ ceramics are given in Table 4.3. Materials with excellent physical (low sintering temperature and low bulk density) and microwave dielectric properties (high Q_u x f, high ε_r and low τ_f) have not been reported so far. The materials developed in the present investigation (see Table 4.3) are superior in terms of dielectric properties, sintering temperature and cost of raw materials as compared to commercially available high Q dielectric resonators (see Table 4.1). Hence the introduction of $Li_2(Mg_{1-x}Zn_x)Ti_3O_8$ ceramics and its glass composites can move the technology forward in wireless communication industry.

4.5 Conclusions

- The $Li_2Mg_{1-x}Zn_xTi_3O_8$ (x=0 to 1) and $Li_2A_{1-x}Ca_xTi_3O_8$ (A=Mg, Zn, and x= 0 to 0.2) ceramic samples are prepared by the conventional solid state ceramic route and the phase purity, microstructure and microwave dielectric properties are investigated.
- The $Li_2MgTi_3O_8$ and $Li_2ZnTi_3O_8$ ceramics shows ε_r = 27.2, Q_u x f = 42000 GHz, and τ_f = (+) 3.2 and ε_r = 25.56, Q_u x f = 72000 GHz, and τ_f = (-) 11.2 ppm/^oC respectively when sintered at 1075 ^oC/4hrs.
- Among all the compositions of $Li_2Mg_{1-x}Zn_xTi_3O_8$ ceramics, the $Li_2Mg_{0.9}Zn_{0.1}Ti_3O_8$ dielectric ceramic composition shows the best dielectric properties such as ε_r = 27, Q_u x f = 62000 GHz, and τ_f = (+) 1.2 ppm/^oC when sintered at 1075 ^oC/4hrs.
- The second phase ($CaTiO_3$) has been found with the Ca substitution in $Li_2A_{1-x}Ca_xTi_3O_8$ (A=Mg, Zn, and x= 0 to 0.2) ceramics and which degrades the microwave dielectric properties slightly.

- Effect of LMZBS glass addition on the sinterability and microwave dielectric properties of $Li_2MgZnTi_3O_8$ and $Li_2MgZnTi_3O_8$ dielectric ceramics has been investigated for LTCC applications.
- The LMT + 3 wt% of LMZBS glass sintered at 925 ^oC/4hrs has ε_r = 24.5, Q_u x f = 44000 GHz, and τ_f = (+) 0.25 ppm/^oC. Addition of LZT ceramics with 3 wt% of LMZBS glass sintered at 900 ^oC/4hrs has ε_r = 23.24, Q_u x f = 31300 GHz, and τ_f = (-) 15.6 ppm/^oC.
- The non reactivity of ceramic glass composite with silver evidenced from X-ray diffraction and SEM analysis reveals the silver can be used an electrode material for LMT+LMZBS and LMT+LMZBS ceramic glass composite for LTCC applications.
- The major results of $Li_2(Mg_{1-x}Zn_x)Ti_3O_8$ (x=0 to 1), $Li_2(A_{1-x}Ca_x)Ti_3O_8$ (A=Mg, Zn) ceramics and the effect of LMZBS glass addition on $Li_2MgTi_3O_8$ and $Li_2ZnTi_3O_8$ ceramics is shown in Table 4.3.
- The discovery of low cost and the excellent physical and microwave dielectric properties of $Li_2Mg_{1-x}Zn_xTi_3O_8$ (x=0 to 1), $Li_2A_{1-x}Ca_xTi_3O_8$ (A=Mg, Zn, and x= 0 to 0.2) dielectric ceramics and its glass composites will be the remarkable milestone in the microwave dielectric resonator research.

In this chapter we have introduced new temperature stable high Q high permittivity, $Li_2Mg_{1-x}Zn_xTi_3O_8$ (x=0 to 1) dielectric ceramics for dielectric resonator applications. The influence of various borosilicate glass additives on the sinterability, and microwave dielectric properties of the $Ca[(Li_{1/3}A_{2/3})_{1-x}Ti_x]O_{3-\delta}$ (A=Nb,Ta) complex perovskite ceramics is discussed in the next chapter.

References

1. M. Makimoto and S. Yamashita, "*Microwave Resonators and Filters for Wireless Communication: Theory, Design and Application*", Springer, Berlin Heidelberg, (2001).
2. K. Wakino, T. Nishikawa, S. Tamura and Y. Ishikawa, *IEEE MTT-S Int. Microwave Symp. Dig.* (1975).
3. W. Wersing, *Current Opinion in Solid State & Materials Science*, **1**, 715, (1996).
4. M. T. Sebastian, "*Dielectric materials for wireless communications*", Elseiver Publishers, Oxford, U. K , (2008).
5. R. Freer, *Silicate Industriels*, **9-10**, 191, (1993).
6. J. C. Sethares and S. J. Naumann, *Trans. on microwave theory and Tech.*, **MTT-14**, 2, (1966).
7. K. Wakino, *Ferroelectrics, Review*, **22**, 1, (2000).
8. S. J. Fiedziuszko, I. C. Hunter, T. Itoh, Y. Kobayashi, T. Nishikawa, S. N. Stitzer and K. Wakino, *IEEE Trans. Microwave Theory and Tech.*, **50**, 706, (2002).
9. S. Kawashima, M. Nishida, I. Ueda and H. Ouchi, *J. Am. Ceram. Soc.*, **66**, 421, (1983).
10. S. Nomura, K. Toyama and K. Tanaka, *Jpn. J. Appl. Phys.*, **21**, L624, (1982).
11. K. P. Surendran "Ph.D Thesis", (University of Kerala), *Faculty of Science*, (2004),
12. H. M. J. O'Bryan, J. J. Thomson and J. K. Plourde, *J. Am. Ceram. Soc.*, **57**, 450, (1974).
13. J. K. Plourde, D. F. Linn, H. M. J. O'Bryan and J. J. Thompson, *J. Am. Ceram. Soc.*, **58**, 418, (1975).
14. H. Tamura, *Am. Ceram. Soc. Bull.*, **73**, 92, (1994).
15. A. Borisevich and P. K. Davies, *J. Am. Ceram. Soc.*, **85**, 573, (2002).
16. A. Borisevich and P. K. Davies, *J. Am. Ceram. Soc.*, **85**, 2487, (2002).
17. J. W. Choi, C. Y. Kang, S. J. Yoon, H. J. Kim, H. J. Jung and K. H. Yeon, *J. Mater. Res.*, **14**, 3567, (1999).
18. K. Fukuda, R. Kitoh and I. Awai, *Jpn. J. Appl. Phys. Part 1*, **32**, 4584, (1993).
19. H. Sreemoolanadhan, J. Isaac, S. Solomon, M. T. Sebastian, K. A. Jose and P. Mohanan, *Phys. Stat. Solidi A-Appl. Res.*, **143**, K45, (1994).
20. H. Sreemoolanadhan, R. Ratheesh, M. T. Sebastian and P. Mohanan, *Mater. Lett.*, **33**, 161, (1997).
21. G. Subodh and M. T. Sebastian, *Mater. Sci. Engg. B-Solid State Mater. Adv. Tech.*, **136**, 50, (2007).

22. K. P. Surendran, P. V. Bijumon, P. Mohanan and M. T. Sebastian, *Appl. Phys. A-Mater. Sci. Process.*, **81**, 823, (2005).

23. K. P. Surendran and M. T. Sebastian, *J. Mater. Res.*, **20**, 2919, (2005).

24. Y. B. Chen, C. L. Huang and C. W. Lo, *Mater. Sci. Engg. B-Solid State Mater. Adv. Tech.*, **128**, 98, (2006).

25. C. L. Huang and J. Y. Chen, *J. Am. Ceram. Soc.*, **92**, 379, (2009).

26. L. Li, X. M. Chen and X. C. Fan, *J. Am. Ceram. Soc.*, **89**, 557, (2006).

27. L. Li, X. M. Chen and X. C. Fan, *J. Eur. Ceram. Soc.*, **26**, 3265, (2006).

28. L. Li, X. M. Chen and X. C. Fan, *J. Eur. Ceram. Soc.*, **26**, 2817, (2006).

29. T. Liu, X. Z. Zhao and W. Chen, *J. Am. Ceram. Soc.*, **89**, 1153, (2006).

30. R. C. Pullar, J. D. Breeze and N. M. Alford, *J. Am. Ceram. Soc.*, **88**, 2466, (2005).

31. A. N. Salak and V. M. Ferreira, *J. Eur. Ceram. Soc.*, **27**, 2887, (2007).

32. A. N. Salak, D. D. Khalyavin, P. Q. Mantas, A. M. R. Senos and V. M. Ferreira, *J. Appl. Phys.*, **98**, 034101, (2005).

33. C.-L. Huang and M.-H. Weng, *Mater. Res. Bull.*, **36**, 2741, (2001).

34. S. Nishigaki, S. Yano, H. Kato, T. Hirai and T. Nonomura, *J. Am. Ceram. Soc.*, **71**, C11, (1988).

35. K. P. Surendran, P. Mohanan and M. T. Sebastian, *Mater. Res. Bull.*, **41**, 784, (2006).

36. S. Nishigaki, H. Kato, S. Yano and R. Kamimura, *J. Am. Ceram. Soc. Bull.*, **66**, 1405, (1987).

37. B. Jancar, M. Valant and D. Suvorov, *Chem. Mater.*, **16**, 1075, (2004).

38. P. Sun, T. Nakamura, Y. J. Shan, Y. Inaguma, M. Itoh and T. Kitamura, *Jpn. J. Appl. Phys*, **37**, 5625, (1998).

39. V. S. Hernandez, L. M. T. Martinez, G. C. Mather and A. R. West, *J. Mater. Chem.*, **6**, 1533, (1996).

40. H. Kawai, M. Tabuchi, M. Nagata, H. Tukamoto and A. R. West, *J. Mater. Chem.*, **8**, 1273, (1998).

41. B. W. Hakki and P. D. Coleman, *IRE Trans. Microwave Theory Tech.*, ***MTT.*, 8**, 402, (1960).

42. J. Krupka, K. D. Derzakowski, B. Riddle and J. B. Jarvis, *Meas. Sci. Technol.*, **9**, 1751, (1998).

43. Y. R. Wang, T. Mori, J. G. Li, Y. Yajima and J. Drennan, *J. Eur. Ceram. Soc.*, **26**, 417, (2006).

44. S. Jayanthi and T. R. N. Kutty, *Mater. Lett.*, **60**, 796, (2006).

45. P. Liu, E. S. Kim, S. G. Kang and H. S. Jang, *Mater. Chem. Phys.*, **79**, 270, (2003).

46. B. D. Cullity, "*Elements of X-ray Diffraction*", Printice Hall, New Delhi, (2001).

47. T. Negas, G. Yeager, S. Bell, N. Coats and I. Minis, *Am. Ceram. Soc. Bull.*, **72**, 80, (1993).

48. V. B. Braginsky, V. S. Ilchenko and K. S. Bagdassarov, *Phys. Lett. A*, **120**, 300, (1987).

49. V. L. Gurevich and A. K. Tagantsev, *Adv. in Phys.*, **40**, 719, (1991).

50. J. D. Breeze, J. M. Perkins, D. W. McComb and N. M. Alford, *J. Am. Ceram. Soc.*, **92**, 671, (2009).

51. S. J. Penn, N. M. Alford, A. Templeton, X. R. Wang, M. S. Xu, M. Reece and K. Schrapel, *J. Am. Ceram. Soc.*, **80**, 1885, (1997).

52. N. M. Alford and S. J. Penn, *J. Appl. Phys.*, **80**, 5895, (1996).

53. A. Borosevich and P. K. Davies, *J. Eur. Ceram. Soc.*, **21**, 1719, (2000).

54. Y. B. Chen, *J. Alloys and Comp.*, **478**, 657, (2009).

55. Y. B. Chen, C. L. Huang and S. H. Lin, *Mater. Lett.*, **60**, 3591, (2006).

56. P. V. Bijumon and M. T. Sebastian, *Int. J. Appl. Ceram. Techn.*, **4**, 60, (2007).

57. R. Roy, *J. Am. Ceram. Soc.*, **27**, 581, (1954).

58. H. Shimoda, N. Ishitobi, K. Kawamura and M. Kobayashi, *Jpn. J. Appl. Phys. Part 1-Regular Papers Short Notes & Review Papers*, **31**, 3160, (1992).

59. L. Vegard, *Z. Krist.*, **67**, 148, (1928).

60. C. Castellanos and A. R. West, *J.C.S Faraday*, **76**, 2159, (1980).

61. J. H. Moon, H. M. Jung, H. S. Park, J. Y. Shin and H. S. Kim, *Jpn. J. Appl. Phys.*, **38**, 6821, (1999).

62. S. O. Yoon, D. M. Kim, S. H. Shim, J. K. Park and K. S. Kang, *J. Eur. Ceram. Soc.*, **26**, 2023, (2006).

63. M. T. Sebastian and H. Jantunen, *Int. Mater. Rev.*, **53**, 57, (2008).

64. P. S. Anjana and M. T. Sebastian, *J. Am. Ceram. Soc.*, **92**, 96, (2009).

65. P. V. Bijumon and M. T. Sebastian, *Mater. Sci. Engg. B-Solid State Mater. Adv. Tech.*, **123**, 31, (2005).

66. C. L. Huang, C. L. Pan and S. J. Shium, *Mater. Chem. Phys.*, **78**, 111, (2003).

67. J. H. Park, Y. J. Choi, J. H. Park and J. G. Park, *Mater. Chem. Phys.*, **88**, 308, (2004).

68. K. P. Surendran, P. Mohanan and M. T. Sebastian, *J. Solid State Chem.*, **177**, 4031, (2004).

69. T. Takada, S. F. Wang, S. Yoshikawa, S. J. Jang and R. E. Newnham, *J. Am. Ceram. Soc.*, **77**, 1909, (1994).

70. J. X. Tong, Q. L. Zhang, H. Yang and J. L. Zou, *J. Am. Ceram. Soc.*, **90**, 845, (2007).

71. H. Jantunen, R. Rautioaho, A. Uusimaki and S. Leppavuori, *J. Eur. Ceram. Soc.*, **20**, 2331, (2000).

72. H. Jantunen "*Ph D Thesis*", (Finland, University of Oulu), *Faculty of Science*, (2001).

73. M. Valant and D. Suvorov, *Mater. Chem. Phys.*, **79**, 104, (2003).

74. D. L. Corker, R. W. Whatmore, E. Ringgaard and W. W. Wolny, *J. Eur. Ceram. Soc.*, **20**, 2039, (2000).

Chapter 5

Effect of Borosilicate Glass Fluxing in $Ca[(Li_{1/3}A_{2/3})_{1-x}Ti_x]O_{3-\delta}$ (A=Nb,Ta) Complex Perovskite Ceramics

The development of low temperature sintered low loss high permittivity microwave ceramics is one of the major challenges in electronic industry. The influence of various borosilicate glasses mentioned in chapter 1, on the sinterability, densification, structure, microstructure and the microwave dielectric properties of the $Ca[(Li_{1/3}A_{2/3})_{1-x}Ti_x]O_{3-\delta}$ *(A=Nb,Ta) dielectric ceramics is discussed in this chapter. The objective of the present work is to find out an ideal glass system which can lower the sintering temperature of the ceramics with reasonably good microwave dielectric properties for the possible application in Low Temperature Co-fired Ceramics (LTCC) based devices.*

5.1 Introduction

Telecommunication industry today requires high volume efficiency without degradation of electrical performance of the devices [1, 2]. In order to reduce the size of microwave devices in communication systems, the dielectric components must also be miniaturized. To achieve the volume efficiency, a multilayer device has been developed [3, 4]. In order to use a material for incorporation into multilayer type elements, the dielectric material should be capable of being sintered along with electrode, in addition to having dielectric properties suitable for desired applications. Low Temperature Co-fired Ceramic (LTCC) technology is one of the promising technology for advanced packaging and multilayered structures with buried passive components for fast digital applications [5, 6]. A detailed description of advantages of LTCC technology is mentioned in chapter 1, section 1.9. Liquid phase sintering using glass addition is known to be the most effective and least expensive way of achieving high density sintered ceramics at low sintering temperature. Efforts have been made to lower the sintering temperature of low loss dielectric resonator materials like $(Zr,Sn)TiO_4$, $Ba_2Ti_9O_{20}$, $Ba(Mg_{1/3}Ta_{2/3})O_3$, $Ca_5Nb_2TiO_{12}$, $BaTi_4O_9$, $0.83ZnAl_2O_4$-$0.17TiO_2$, $Mg_xCa_{1-x}TiO_3$, Mg_2SiO_4 etc. with glass additions [7-15]. Earlier investigations on glass added ceramics reveals that multicomponent glasses are more effective in lower the sintering temperature of the ceramics without degrading the microwave dielectric properties [2, 6]. In the present investigation we have selected different borosilicate glasses mentioned in chapter 1, section 1.9.

Commercially available dielectric resonator materials for wireless applications show high quality factor, and high permittivity. However, they need to be sintered at high temperature (>1300 ^oC) for long duration to attain better densification and thereby the improved performance [2]. In

most of the high temperature processed high quality factor complex perovskites, a drastic degradation in microwave dielectric properties is observed with the glass addition which lower the sintering temperature. Generally, the amount of glass required to lower the sintering temperature of ceramics also depend on the sintering temperature of ceramics. Hence, large amount of glass is necessary to lower the sintering temperature for ceramics having high processing temperatures. As the amount of glass increases, generally the quality factor decreases. Hence the selection of the low loss ceramics having low processing temperature is important for glass addition. Earlier studies [16, 17] show that $Ca[(Li_{1/3}A_{2/3})_{1-x}Ti_x]O_{3-\delta}$ [A=Nb, Ta] ceramics have excellent dielectric properties and are promising candidate for low temperature sintering because they can be sintered at 1150 ^oC without sintering aid. However, the sintering temperature of this material is still too high to use silver or copper as an internal electrode in multilayered structures.

In the present work, we have carried out investigations on the liquid phase sintering and the microwave dielectric properties of $Ca[(Li_{1/3}A_{2/3})_{1-x}Ti_x]O_{3-\delta}$ [A=Nb, Ta] ceramics with different borosilicate glasses.

5.2 Milestones in the research of $Ca[(Li_{1/3}A_{2/3})_{1-x}Ti_x]O_{3-\delta}$ [A=Nb,Ta] complex perovskite ceramics

The perovskite family is of considerable technological importance for its excellent microwave dielectric properties. The first material reported in this family was $CaTiO_3$ and later named as mineral perovskite by Gustave Rose and named it after the memory of famous Russian mineralogist Count Lev Aleksevich von Perovski [18]. Ideal perovskites have general formula ABX_3, where A site cations are typically larger than the B site cations and similar in size to the X site anions [19]. Fig. 5.1 shows the ideal perovskite structure where the A cations are surrounded by 12 anions in the cubo-

octahedral coordination and B cations are surrounded by 6 anions in the octahedral coordination. The X anions are coordinated by two B site cations and 4 A site cations. Ideal perovskites structure adopts cubic symmetry $Pm\bar{3}m$ as in the case of $CaTiO_3$. However, the deviations from the ideal structure with orthorhombic, rhombohedral, tetragonal, triclinic, and monoclinic are known. These deviations from cubic perovskite structure may proceed from a simple distortion of the cubic cell, or the enlargement of cubic unit cell.

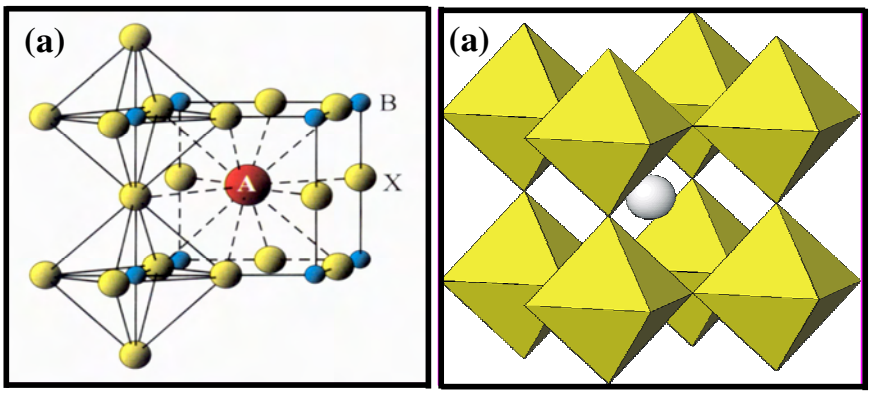

Fig. 5.1 (a) Ideal Perovskite (ABX_3) structure showing 6-fold and 12-fold co-ordinations of B and A site cations respectively (b) Unit cell of ABX_3 perovskite showing eight BX_6 octahedron enclosing the A-site. (Ref. [19])

Complex perovskites are formed when either or both of the A and B site cations are replaced by combination of other cations located at specific crystallographic sites. Hence perovskites with general formula $A(BB')O_3$, $(AA')BO_3$ and $(AA')(BB')O_3$ are possible [19, 20]. The perovskite structure can tolerate a wide range of elements of differing size and charge which results in a large number of possible permutations of the cations. The tolerance factor (t) to account for the limits of the size of the cations to form a perovskite structure is

$$t = \frac{R_A + R_O}{\sqrt{2}(R_B + R_O)} \text{------(5.1)}$$

For complex perovskites of the type $A(B'_{1/3}B''_{2/3})O_3$, the above equation can be modified as

$$t = \frac{R_A + R_O}{\sqrt{2}[0.33R_B' + 0.67R_B'' + R_O]} \text{------(5.2)}$$

Tolerance factor might be a guide as to whether a given assemblage of ions will adopt the perovskite structure at a particular temperature and pressure. For ideal perovskites the tolerance factor is unity. Majority of the ordered perovskite studied to date are oxide perovskite which exhibit B site ordering due to their application potential as dielectric resonators.

The $Ca[(Li_{1/3}Nb_{2/3})]O_3$ ceramics is a 1:2 complex perovskite structure with A site occupied by Ca and the B site by Li and Nb. Recently, Choi *et al*. and Liu *et al*. reported the microwave dielectric characteristics of $Ca[(Li_{1/3}A_{2/3})_{1-x}B_x]O_{3-\delta}$ ceramics (A=Nb, Ta, B=Ti, Zr, Sn) complex perovskite ceramics [16, 17, 21]. The X ray diffraction pattern of $Ca(Li_{1/3}A_{2/3})O_{3-\delta}$ [A=Nb,Ta] can be indexed based on $CaTiO_3$ orthorhombic perovskite structure with a small amount of second phase. However, the stability of $Ca[(Li_{1/3}Nb_{2/3})_{1-x}B_x]O_{3-\delta}$ increases with increase in concentration of B (Ti, Zr, and Sn) and the single phase was obtained in the range of $0.2 \leq x \leq 0.3$. In $Ca[(Li_{1/3}A_{2/3})_{1-x}B_x]O_{3-\delta}$ (A=Nb, Ta, B=Ti, Zr, Sn) complex perovskites, the relative permittivity increases with increasing amount of Ti and Zr, but decreases with Sn concentration. The temperature coefficient of resonant frequency increases from negative value to positive value for increase in Ti concentration but remains negative value for increase in both Zr and Sn concentration. $Ca[(Li_{1/3}Nb_{2/3})_{1-x}Ti_x]O_{3-\delta}$ (CLNT) ceramics with x=0.2 sintered at 1150 ^oC/4hrs has ε_r = 38.6 and $Q_u$xf =26100 GHz and nearly zero temperature coefficient of resonant frequency [16]. Table 5.1 shows the microwave dielectric properties of $Ca[(Li_{1/3}Nb_{2/3})_{1-x}B_x]O_{3-\delta}$ (B=Ti, Zr, Sn) complex perovskites with tolerance factor.

Table 5.1 Microwave dielectric properties of $Ca[(Li_{1/3}Nb_{2/3})_{1-x}B_x]O_{3-\delta}$ (B=Ti, Zr, Sn) complex perovskite ceramics..

Material	x	Tolerance factor	ε_r	$Q_u$xf (GHz)	τ_f (ppm/^{o}C
$Ca[(Li_{1/3}Nb_{2/3})_{1-x}Ti_x]O_{3-\delta}$	0.00	0.931656	29.6	40000	-21
	0.10	0.935010	34.6	27200	-2.3
	0.20	0.938388	38.6	26100	0
	0.30	0.941792	44.7	22500	20
	0.50	0.948672	55.2	18600	83
$Ca[(Li_{1/3}Nb_{2/3})_{1-x}Sn_x]O_{3-\delta}$	0.10	0.931191	25.2	48200	-14
	0.15	0.930958	24.8	49100	-25
	0.20	0.930725	23.3	50600	-30
	0.30	0.930261	22.6	46300	-39
$Ca[(Li_{1/3}Nb_{2/3})_{1-x}Zr_x]O_{3-\delta}$	0.05	0.930750	29.9	41800	-20
	0.10	0.929850	30.1	36000	-5
	0.20	0.928051	30.5	33000	-12
	0.30	0.926258	31.1	27100	-15

For $Ca[(Li_{1/3}Ta_{2/3})_{1-x}Ti_x]O_{3-\delta}$ (CLTT) ceramics, the single phase was obtained in the range of $0.3 \leq x \leq 0.4$. The microwave dielectric properties of CLTT ceramics sintered at 1200 ^{o}C/4hrs has ε_r = 36.2 and $Q_u$xf = 29500 GHz and the temperature coefficient of resonant frequency was nearly zero ppm/^{o}C at x = 0.30 [17]. Both the CLNT and CLTT ceramics shows excellent dielectric properties and is a promising candidate for low temperature sintering because they can be sintered near 1200 ^{o}C without sintering aid. Several authors tried to control the escape of volatile lithium by lowering the sintering temperature of CLNT ceramics by the addition of low melting additives such as B_2O_3, Bi_2O_3, glass frit and LiF [17, 22-28]. However, a

detailed investigation on the sinterability and microwave dielectric properties of CLNT and CLTT ceramics with different borosilicate glass has not been done so far. Among the $Ca[(Li_{1/3}A_{2/3})_{1-x}M_x]O_{3-\delta}$ [A=Nb, Ta and M=Ti, Zr, Sn] complex perovskites, the Ti^{4+} substitution has a wide range of τ_f extending from -21 to +83 ppm/^oC with reasonably good quality factor [16]. A single phase perovskites with zero τ_f were observed in the vicinity of x=0.2 for $Ca[(Li_{1/3}Nb_{2/3})_{1-x}Ti_x]O_{3-\delta}$ (CLNT) and x=0.3 for $Ca[(Li_{1/3}Ta_{2/3})_{1-x}Ti_x]O_{3-\delta}$ (CLTT). Hence we have selected CLNT and CLTT ceramics as the host dielectric ceramic materials for the present investigation.

The present study focused on (i) the effect of various borosilicate glass additions on the sinterability, densification, structure and microstructure and the microwave dielectric properties of the CLNT and CLTT dielectric ceramics, and (ii) to find out an ideal glass system which can lower the sintering temperature of the ceramics with reasonably good microwave dielectric properties.

5.3. Experimental

The $Ca[(Li_{1/3}Nb_{2/3})_{1-x}Ti_x]O_{3-\delta}$ (x=0.2 and 0.25) and $Ca[(Li_{1/3}Ta_{2/3})_{1-x}Ti_x]O_{3-\delta}$ (x=0.3 and 0.4) ceramic samples were prepared by the conventional solid state ceramic route. High purity $CaCO_3$, Li_2CO_3, TiO_2 (99.9+%, Aldrich chemical company, Inc, Milwaukee, WI, USA) Ta_2O_5 and Nb_2O_5 (99.9+%, NFC Hyderabad, India) were used as the starting materials. Stoichiometric amounts of the powder samples were ball milled using zirconia balls in ethanol medium for 24 hours. The resultant slurry was then dried and calcined. The calcinations were carried out at temperature in the range 900 to 1050 ^oC for four hours. The preparation of different borosilicate glasses were explained in the chapter 2, section 2.2. Different weight percentages of various glasses were added to the fine powder of calcined CLNT and CLTT ceramics. Polyvinyl alcohol (PVA) (Molecular Weight 22000, BDH Lab

Suppliers, England) solution was then added to the powder, mixed, dried, ground well and pressed into cylindrical disks of about 14 mm diameter and 7mm thickness, by applying a pressure of about 100 MPa. These compacts were muffled by CLNT or CLTT powder of the same composition and sintered at different temperatures in the range 875 ^{o}C – 1200 ^{o}C for 4 hours. The sintering temperature was optimized for the best density and dielectric properties. The muffling was done to prevent the escape of volatile lithium at elevated sintering temperatures. The crystal structure and phase purity of the powdered samples were studied by X- ray diffraction technique using Ni-filtered Cu-Kα radiation using Rigaku Dmax-I, Japan, diffractometer. The microstructures of the sintered samples were studied using scanning electron microscope (*JEOL-JSM* 5600 LV, Tokyo, Japan). The sintered density of the specimens was measured by the Archimedes method. The microwave dielectric properties were measured in frequency range 4 to 6 GHz by a Vector Network Analyzer (8753 ET, Agilent Technologies). The relative permittivity and unloaded quality factor of the samples were measured by Hakki and Coleman [29] and cavity method [30] respectively as explained in chapter 2. Shrinkage characteristics were done using Dilatometer (TMA-60 H, Shimadzu, Kyoto, Japan).

5.4. Results and Discussion

5.4.1 Optimization of sintering condition

It is well known that lithium is volatile and escape during sintering at elevated temperature [16, 25, 31-33]. Muffling of the samples with same composition or keeping the pellets in closed box is the best method to avoid the volatilization of lithium. It is also possible to control the escape of lithium by the addition of extra lithium in the parent composition. We compare the microwave dielectric properties of the $Ca[(Li_{1/3}Nb_{2/3})_{0.8}Ti_{0.2}]O_{3-\delta}$ ceramics with different sintering condition such as open sintering (without

muffling), with muffling and different wt% of extra lithium addition to the parent material. Fig. 5.2 shows the densification and the microwave dielectric properties of $Ca[(Li_{1/3}Nb_{2/3})_{0.8}Ti_{0.2}]O_{3-\delta}$ ceramics with different sintering condition such as muffling, without muffling, and addition of extra Li_2CO_3 to the parent material. It is found that the sample sintered without muffling has inferior dielectric properties as compared to other sintering conditions. Different wt% of extra lithium addition in parent material shows dielectric properties comparable to that of muffling. However, there is a possibility of the formation of second phase with the addition of extra lithium. Hence muffling is the best method to avoid the volatilization of lithium.

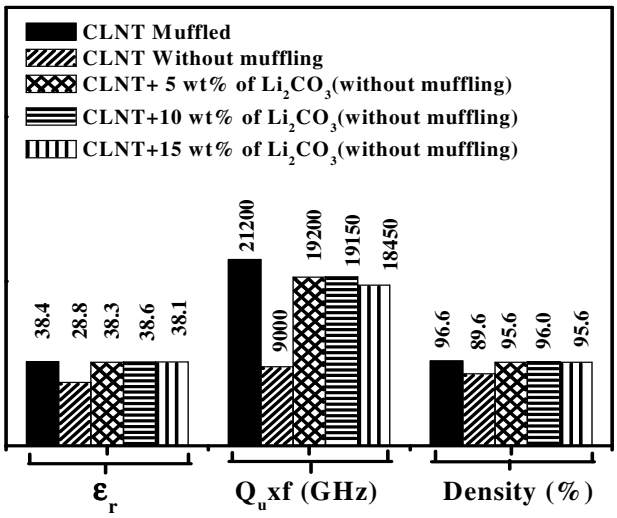

Fig 5.2 Relative density and dielectric properties of $Ca[(Li_{1/3}Nb_{2/3})_{0.8}Ti_{0.2}]O_{3-\delta}$ ceramics with different sintering condition.

5.4.2 Optimization of Calcination and Sintering temperatures

The microwave dielectric properties not only depend on the chemical composition but also on the calcination and sintering temperatures. Figs. 5.3 and 5.4 show the optimization of calcination and sintering temperatures of $Ca[(Li_{1/3}Nb_{2/3})_{0.8}Ti_{0.2}]O_{3-\delta}$ and $Ca[(Li_{1/3}Ta_{2/3})_{0.7}Ti_{0.3}]O_{3-\delta}$ ceramics respectively. These compositions have been taken for its phase purity and excellent temperature stable microwave dielectric properties. The calcination

and sintering temperature are optimized for best density and dielectric properties. It can be observed that an increase in calcination temperature increased the densification and dielectric properties. The best physical and dielectric properties are observed for the compounds calcined at 975 ^{o}C/4hrs. Further increase in the calcination temperature decreased the densification and dielectric properties. Unreacted materials in the under-calcined powder acted as an inhibitor during sintering. It is reported that high calcination temperature lowered the reactivity of ceramic powders resulting in the increase in the number of pores [34]. These could be the reason for poor densification and the degradation of dielectric properties below and above the optimum calcination temperatures.

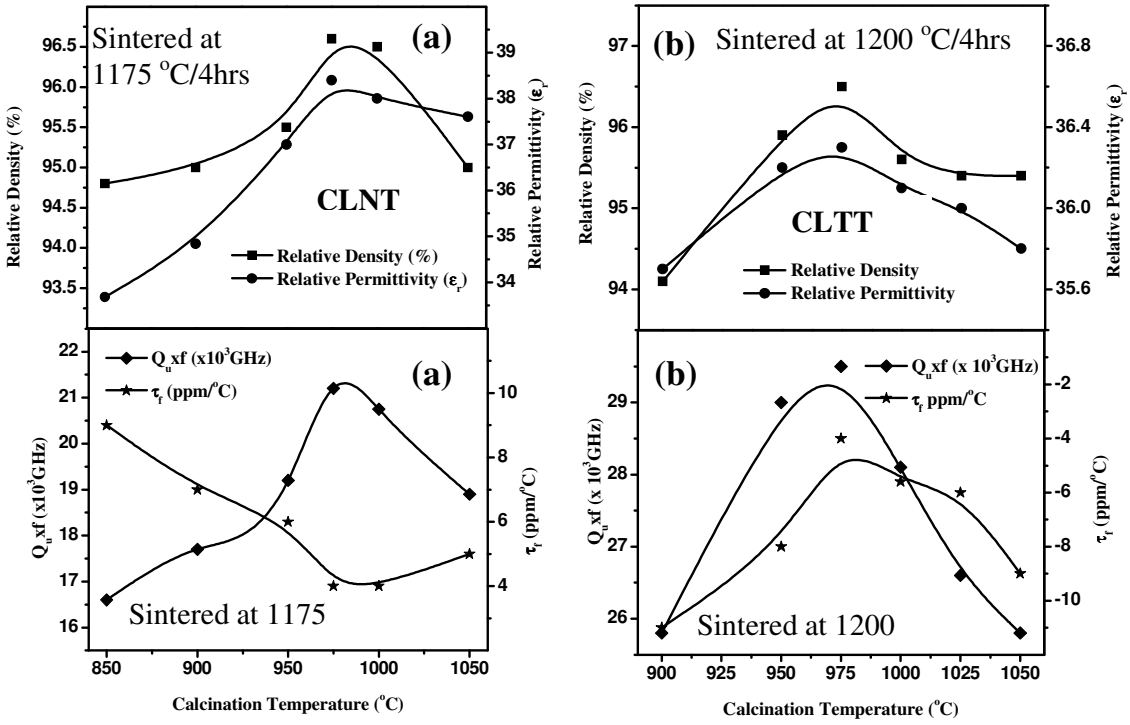

Fig. 5.3 Variation of densification and microwave dielectric properties of (a) CLNT and (b) CLTT ceramics as a function of calcination temperature for 4 hours.

Figure 5.4 shows the optimization of sintering temperature of $Ca[(Li_{1/3}Nb_{2/3})_{0.8}Ti_{0.2}]O_{3-\delta}$ and $Ca[(Li_{1/3}Ta_{2/3})_{0.7}Ti_{0.3}]O_{3-\delta}$ ceramics. It is found that the density and dielectric properties increase with increase in the

sintering temperature. The increase in the permittivity and quality factor with sintering temperature is attributed to the improvement in densification. On the other hand the dielectric properties are degraded due to the formation of pores and evaporation of volatile lithium at higher sintering temperature. The optimized sintering temperature of $Ca[(Li_{1/3}Nb_{2/3})_{0.8}Ti_{0.2}]O_{3-\delta}$ (CLNT) and $Ca[(Li_{1/3}Ta_{2/3})_{0.7}Ti_{0.3}]O_{3-\delta}$ (CLTT) ceramics are 1175 ^{o}C/4hrs and 1200 ^{o}C/4hrs respectively for the best density and dielectric properties.

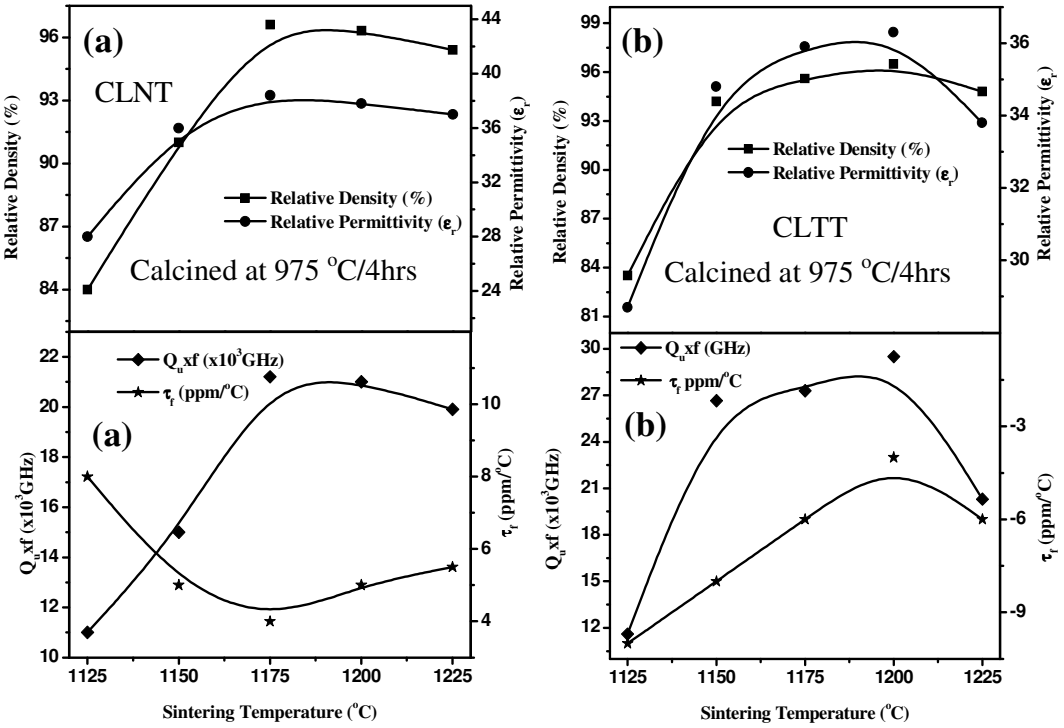

Fig. 5.4. Variation of densification and microwave dielectric properties of (a) CLNT and (b) CLTT ceramics as a function of sintering temperature for 4 hrs.

5.4.3 Shrinkage Characteristics

To identify whether the glass additive would be effective on the low temperature firing of CLNT / CLTT ceramics, the linear shrinkage of as pressed pellets as a function of temperature is to be measured initially. The dilatometry study provides insight to the densification process for the glass

ceramic systems. Figure 5.5 (a) and (b) show the shrinkage characteristics of CLNT / CLTT ceramics and with 12 wt% of various borosilicate glasses. It is found that no linear shrinkage take place for pure CLNT and CLTT in the temperature range of 800-1100 ^{o}C. This indicates that sintering does not start even at 1100 ^{o}C for both the ceramics. However, a linear shrinkage is observed for all the glass added ceramics which implies that all the borosilicate glasses act as sintering aid. Among the various borosilicate glasses, LBS, LMZBS, and ZBS glasses in CLNT and BZBS, ZBS and LMZBS glasses in CLTT ceramics shows a linear shrinkage of more than 12 % in the temperature range 800-1000 ^{o}C.

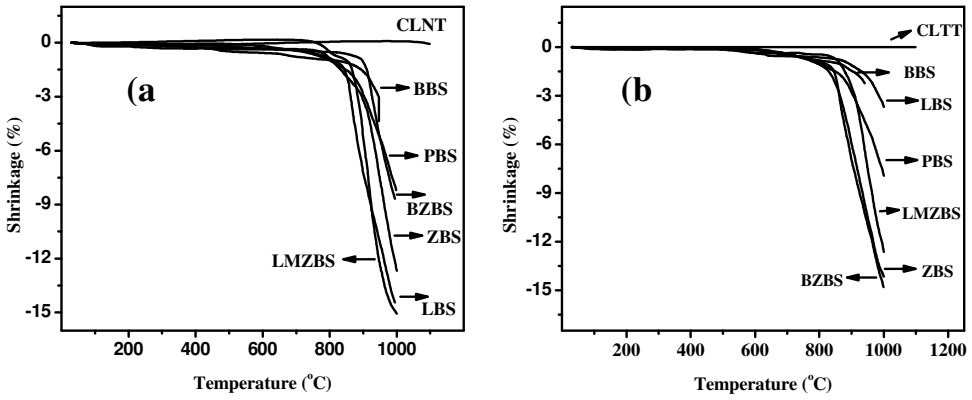

Fig. 5.5. Shrinkage characteristics of (a) CLNT and (b) CLTT ceramics with various borosilicate glass additions

5.4.4 Densification

Figure 5.6 shows the variation of sintering temperature, and the relative density of CLNT / CLTT ceramics mixed with different wt% of various borosilicate glasses. It is found that addition of all the glasses decrease the sintering temperature. However, among the six borosilicate glasses, LBS, LMZBS and ZBS glass could reduce the sintering temperature of CLNT ceramics and ZBS and BZBS glass reduce the sintering temperature of CLTT ceramics below the melting point of silver. Fig. 5.6 also shows the

variation of relative density as a function of glass content. The relative density of ceramic glass composite is calculated using the equation 2. 14 (see chapter 2, section 2.6). The relative density decreases with increase of glass content in CLTT ceramics. For CLNT-glass composite, the relative density increases slightly with a slight increase in the glass content. However, higher wt% of glass addition decreases the densification of CLNT-glass composite. The relative density and the densification temperatures are different for different glasses in both the CLNT and CLTT ceramics.

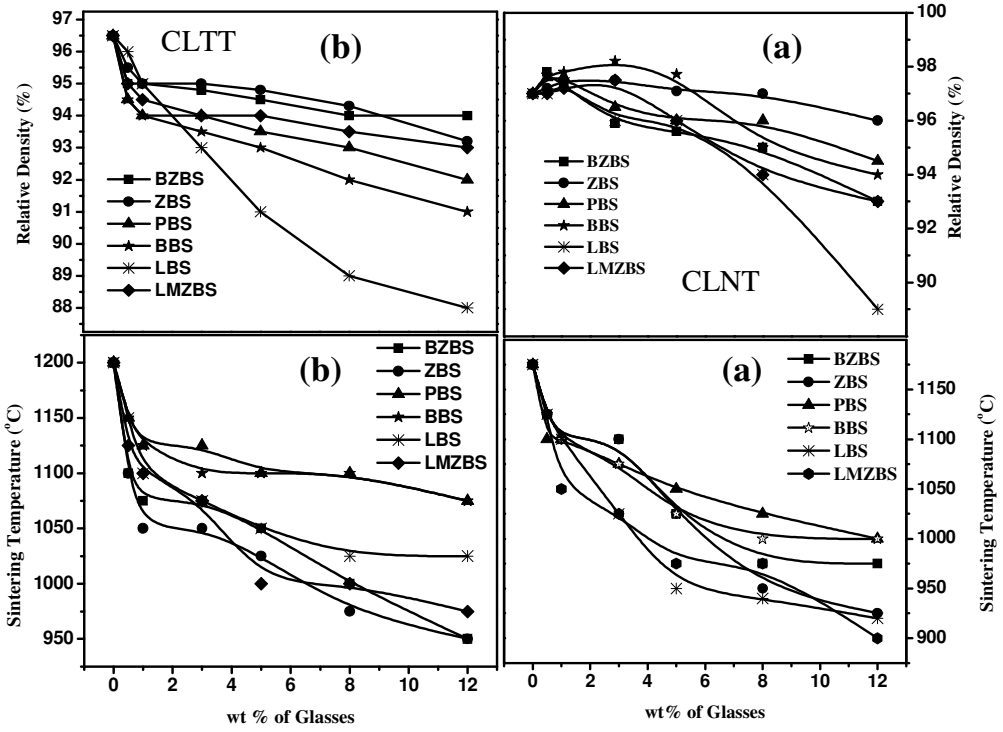

Fig. 5.6 Variation of sintering temperature for 4 hours and relative density of (a) CLNT and (b) CLTT ceramics with different wt% of various borosilicate glasses.

The effectiveness of sintering aid depends on several factors such as sintering temperature, viscosity, solubility, and glass wettability. The densification of ceramic-glass systems is due the formation of liquid phase. The glassy liquid phase at the grain boundary effectively eliminates pores

and this could be the reason for the increase in the relative density of CLNT-glass system. Trapped porosity associated with grain growth and formation of pores by the evaporation of excess glass components are the reasons for the reduction in the density for higher wt% of glass fluxing [35]. In addition to that, the glasses have lower density compared to CLNT / CLTT ceramics. The required densification for practical application could be obtained by the addition of glasses. However, undesirable decomposition of host dielectric material and the formation of second phase may occur which may degrade the microwave dielectric properties. Hence the best glass and the amount of glass frit have to be optimized to get the best dielectric properties. The best glass for CLNT ceramics are LBS, LMZBS, and ZBS glass and that for CLTT ceramics are BZBS and ZBS glasses.

5.4.5 Phase analysis

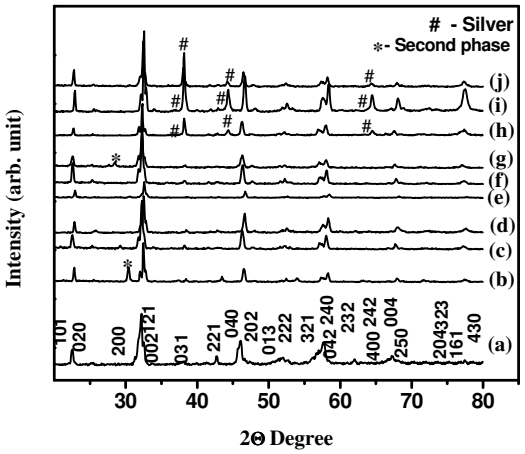

Fig. 5.7 The X-ray powder diffraction patterns of sintered (a) CLNT ceramics, CLNT ceramics with (b) 12 wt% of BBS, (c) 12 wt% of PBS, (d) 5 wt% of LBS, (e) 12 wt% of LMZBS, (f) 8 wt% of ZBS, (g) 12 wt% of BZBS glasses, (h) 5 wt% of LBS glass and 20 wt% of silver and (i) 8 wt% of ZBS glass and 20 wt% of silver and (j) 12 wt% of LMZBS glass and 20 wt% of silver using Ni-filtered Cu-Kα radiation.

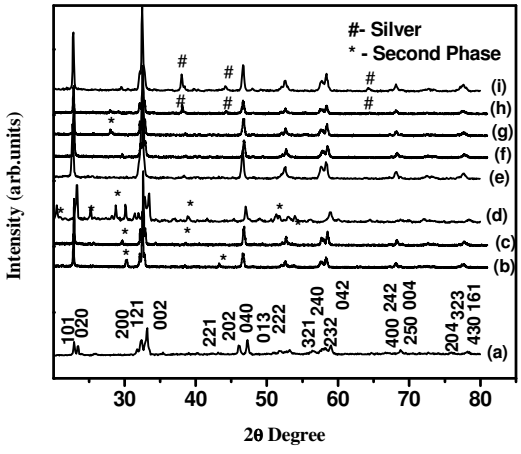

Fig. 5.8 The X-ray powder diffraction patterns of sintered (a) CLTT ceramics, CLTT ceramics with 12 wt% of (b) BBS, (c) PBS, (d) LBS, (e) LMZBS, (f) ZBS, (g) BZBS glasses, (h) CLTT ceramics with 12 wt% of ZBS glass and 20 wt% of silver and (i) CLTT ceramics with 12 wt% of BZBS glass and 20 wt% of silver using Ni-filtered Cu-Kα radiation.

Figure 5.7 and 5.8 shows X-ray powder diffraction patterns of sintered CLNT / CLTT ceramics and the various borosilicate glass added CLNT / CLTT ceramics at the respective optimized sintering temperature. The optimized sintering temperature is different for different wt% of various borosilicate glasses added ceramics (see Fig 5.6). The XRD patterns are indexed based on the $CaTiO_3$ type orthorhombic perovskite structure with four formula units per cell. It is found from Fig 5.7 that, no secondary phases are observed with the addition of LBS glass up to 5 wt%, ZBS up to 8 wt% and LMZBS glass up to 12 wt%. However, addition of higher wt% of other borosilicate glasses in CLNT ceramics results in small amount of secondary phases. Higher wt% glasses resulted in a small amount of second phase which is prominent for LBS glass addition in CLTT ceramics.

For co-firing applications, the glass ceramic composite should not react with silver. The X-ray powder diffraction patterns of heat treated mixture of dielectric ceramic and electrode material is an acceptable way to study the reaction between them. Fig. 5.7 (h), (i) and (j) shows the X-ray diffraction pattern of sintered CLNT ceramics with 20 wt% of silver and 5 wt% of LBS, 12 wt% of LMZBS, and 8 wt% of ZBS glasses respectively. Similarly Fig. 5.8 (h) and (i) shows the X-ray diffraction pattern of 20 wt% of silver added CLTT ceramics with 12 wt% of ZBS and BZBS glasses sintered at its optimum sintering temperature. It is evident from the X-ray diffraction patterns that there is no additional phases other than orthorhombic CLNT / CLTT ceramics and metallic silver (ICDD File No: 03-0921), which is one of the stringent requirement for LTCC based devices.

5.4.6 Microstructure analysis

Figures 5.9 (a) and 5.10 (a) shows the scanning electron micrographs of thermally etched CLNT and CLTT at its optimized sintering temperature (see Fig 5.6). The etching temperature is 25 ^oC below the optimized sintering

temperature for each sample. The CLNT and CLTT ceramics sintered at 1175 ^{o}C/4hrs and 1200 ^{o}C/4hrs gives an average grain size of 2-4 μm.

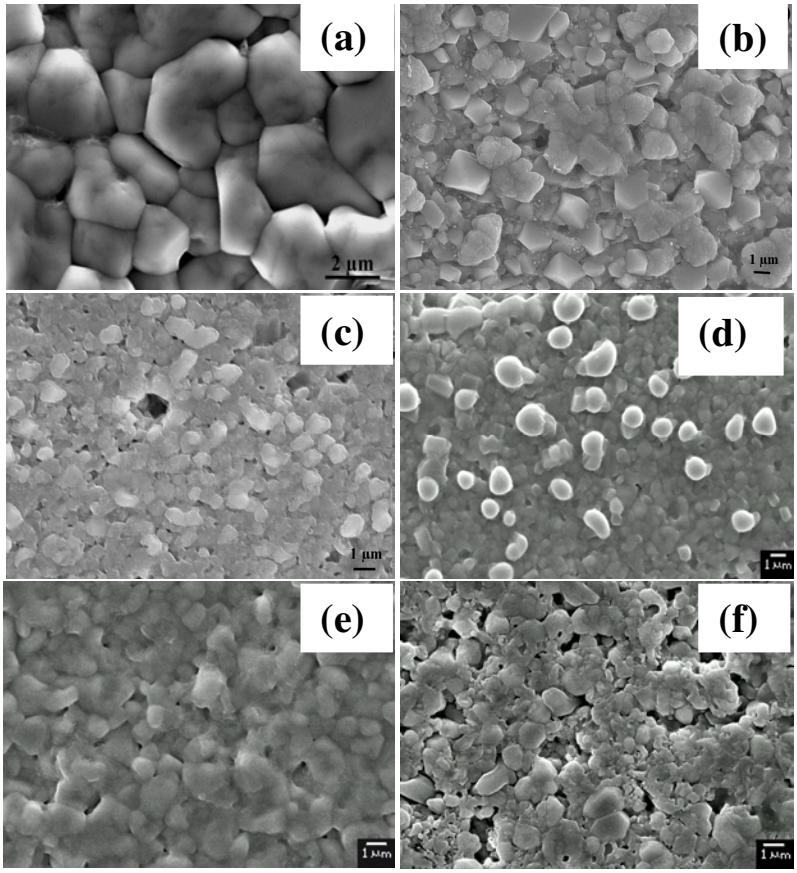

Fig.5.9 The microstructure of sintered $Ca[(Li_{1/3}Nb_{2/3})_{0.8}Ti_{0.2}]O_{3-\delta}$ ceramics with (a) 0wt%, (b) 1 wt% LBS (c) 5 wt% LBS, (d) 5 wt% of LBS + 20 wt% Ag, (e) 8 wt % ZBS and (f) 12 wt% LMZBS glass.

It is evident from the micrograph that lower wt% glass addition helps the densification of CLNT ceramics by liquid phase sintering. The density increases initially up to 1 wt% of LBS glass and further addition of glass increases the porosity which can be clearly seen from Fig 5.9 (c). Figs 5.9 (e), and (f) show the SEM images of 8 and 12 wt% of ZBS and LMZBS glass added CLNT ceramics sintered at 950 ^{o}C/4hrs and 900 ^{o}C/4hrs respectively. It is also evident from the micrographs (see Fig 5.9 and 5.10) that the glass addition decreases the grain size which is in agreement with previous

reports [25]. At higher sintering temperature the glasses melts and may evaporate and generate porosity which can be seen in Fig. 5.10 (b) and (c). Figs. 5.9 (d) and 5.10 (d) show the scanning electron micrographs of CLNT + 5 wt% of LBS + 20 wt% of Ag and CLTT + 12 wt% of BZBS + 20 wt% of Ag respectively. It is observed that the silver does not react with ceramic-glass composite and hence silver can be used as the electrode material for the LTCC materials developed in the present investigation.

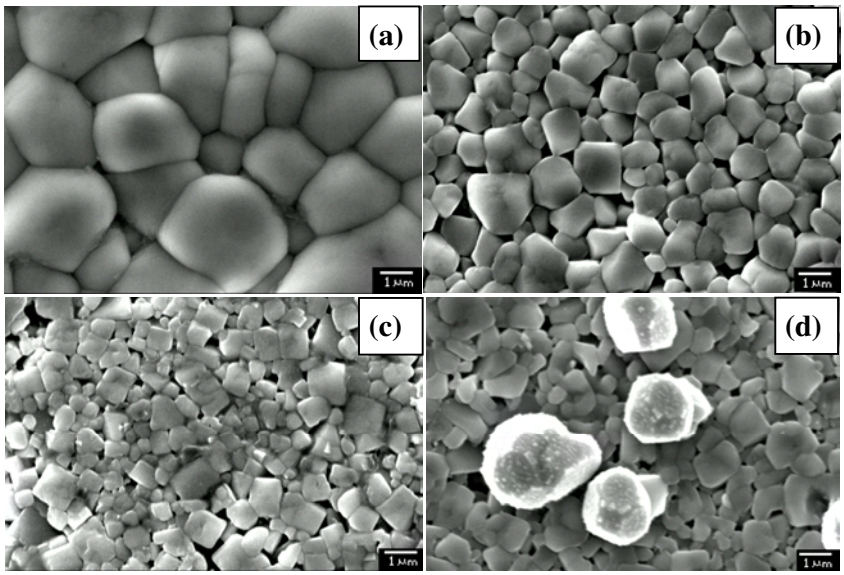

Fig. 5.10 The microstructure of sintered $Ca[(Li_{1/3}Ta_{2/3})_{0.7}Ti_{0.3}]O_{3-\delta}$ ceramics with (a) 0 wt %, (b) 12 wt% BZBS (c) 12 wt% ZBS, and (d) 12 wt% of BZBS + 20 wt% Ag.

5.4.7 Microwave Dielectric Properties

Addition of glass not only promotes the sinterability but also affect the microwave dielectric properties. It is well known that relative density and dielectric properties are interrelated. Fig. 5.11 shows the microwave dielectric properties CLNT / CLTT ceramic as a function of different wt% of various borosilicate glasses. It is found that the relative permittivity of glass added CLNT / CLTT ceramics decreases with increase of glass content. It can be noted from Table 1.2 (chapter 1, section 1.9) that the relative

permittivity of all the borosilicate glasses is much lower than that of both the CLNT/CLTT ceramics. Moreover, the addition of higher wt% of glass increased the porosity and decreased the densification. The low permittivity of glass and the poor densification are the reasons for the decrease in the relative permittivity of CLNT/CLTT ceramics with higher wt% of glass addition.

Figure 5.11 (a) also shows the optimized quality factor for the addition of 0-12 wt% of different borosilicate glasses in CLNT ceramics. It can be concluded from Fig. 5.6 that, all the glasses could not act as good sintering aid to lower the sintering temperature below 950 ^{o}C/4hrs. Among six borosilicate glasses, only the LBS, LMZBS, and ZBS glass could reduce the sintering temperature of CLNT ceramics with reasonably good dielectric properties. It is observed that the addition of small amount of LBS, ZBS and LMZBS glass increased the quality factor slightly. Maximum $Q_u$xf value of 22900 GHz, 24500 GHz, and 23500 GHz (f = 4 to 5 GHz) is found with the addition of 1 wt% of LBS, 3 wt% of LMZBS, and 1 wt% of ZBS glass respectively at optimized sintering temperature (for optimized sintering temperature see fig 5.6). These could be due to the increased densification of CLNT ceramics by liquid phase sintering. These compositions have relative permittivity of 34.2, 34 and 38.3 respectively with a τ_f of around -10 ppm/ ^{o}C. Higher wt% of glass addition in CLNT ceramics lowered the sintering temperature with slightly inferior quality factor. The CLNT ceramics with 5 wt% of LBS glass sintered at 950 ^{o}C/4hrs has ε_r = 30.5, Q_u x f = 14700 GHz (f = 4.6 GHz) and τ_f = -18 ppm/ ^{o}C. A similar trend is also observed with the addition of ZBS and LMZBS glasses in CLNT ceramics. Addition of 12 wt% of ZBS glass in CLNT ceramics shows the relative permittivity of 33.5 with Q_ux f of about 13200 GHz and τ_f of -28 ppm/^{o}C when sintered at 950 ^{o}C/4hrs. Hence for CLNT ceramics, out of various six borosilicate glasses the LBS, LMZBS, and ZBS glass act as good sintering aid to lower the

sintering temperature with reasonably good microwave dielectric properties.

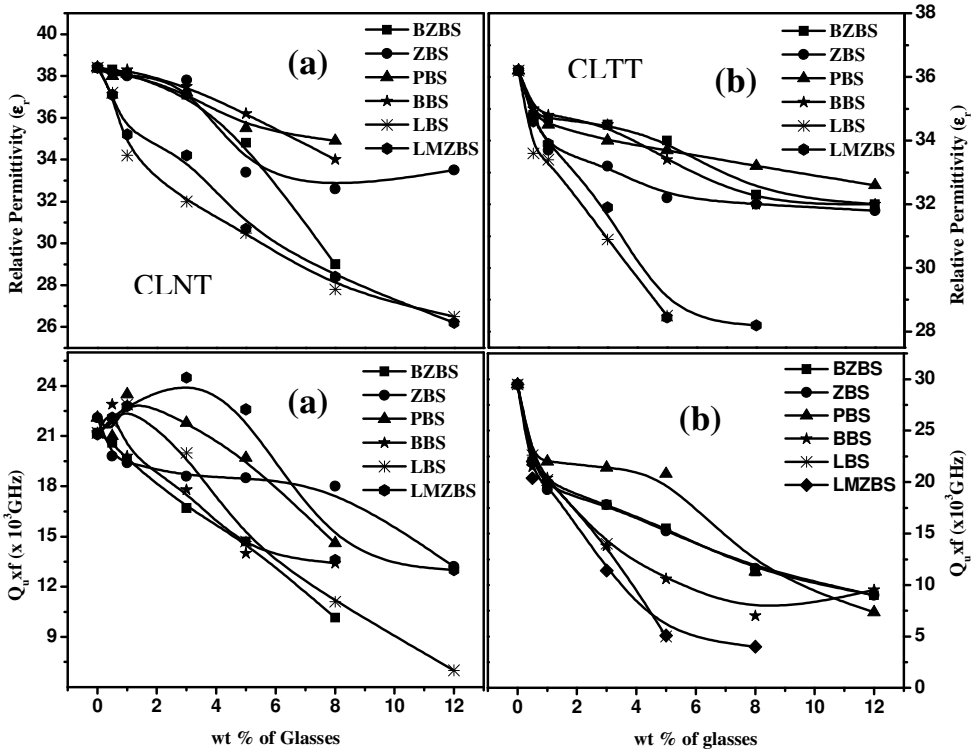

Fig. 5.11 Variation of relative permittivity and quality factor of (a) CLNT and (b) CLTT ceramics with different wt% of various borosilicate glasses.

It can be observed from Fig. 5.11 (b) that the quality factor of CLTT ceramics decreased with increase of all the borosilicate glass additions. For CLTT ceramics, the ZBS and BZBS glass act as a good sintering aid and the other glasses such as BBS, PBS, LBS, and LMZBS could not lower the sintering temperature below 950 ^{o}C with reasonably good dielectric properties. The CLTT ceramics with 12 wt% of ZBS glass sintered at 950 ^{o}C showed ε_r = 31.8, Q_u x f = 9000 GHz (f = 4.6 GHz). Addition of 12 wt% of BZBS glass in CLTT ceramics sintered at 950 ^{o}C showed ε_r = 32.0, Q_u x f = 9000 GHz (f = 4.7 GHz). The addition of 12 wt% of LBS and LMZBS glass in CLTT ceramics diminishes the resonance. The glass addition decreases the

grain size and increases the porosity. In addition, the dielectric loss of glasses is much higher than that of pure CLTT ceramics. The added glasses not only acted as the sintering aid but also as an impurity that can adversely affect the microwave dielectric properties. It is reported that the microwave dielectric loss was mainly caused not only by the lattice vibrations but also by the pores, the grain morphology and the second phase [6]. These could be the reason for the decrease in the quality factor of CLNT and CLTT ceramics with glass additions.

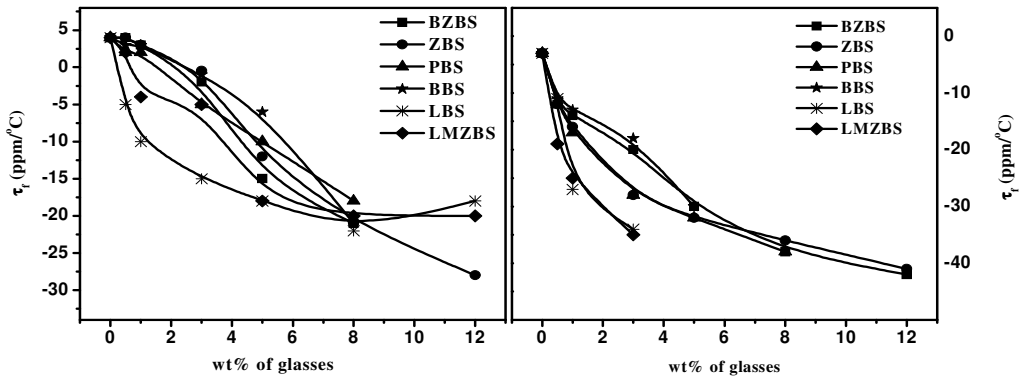

Fig. 5.12 Variation of temperature coefficient of resonant frequency of (a) CLNT and (b) CLTT ceramics with different wt% of various borosilicate

Figure 5.12 shows the variation of temperature coefficient of resonant frequency of CLNT / CLTT ceramics with different wt% of various borosilicate glasses. Addition of various borosilicate glasses decreased the temperature coefficient of resonant frequency (τ_f) of CLNT ceramics from +4 ppm/^{o}C to -22 ppm/^{o} C and that of CLTT ceramics from -3 ppm/^{o} C to -41 ppm/^{o} C. This is due to the high negative τ_f of all the borosilicate glasses compared to that of CLTT ceramics [2, 36]. The CLNT/CLTT ceramics sintered below 950 ^{o}C with borosilicate glasses show excellent dielectric properties. However, the temperature coefficient of resonant frequency is slightly higher (> -20 ppm/^{o} C). Hence, it is necessary to lower the τ_f close to zero for applications in LTCC based devices. It is well known that rutile has high positive τ_f and is widely used for tuning the temperature coefficient of

resonant frequency of dielectric resonators [37-40]. In order to lower the τ_f value, the $Ca[(Li_{1/3}Nb_{2/3})_{0.8}Ti_{0.2}]O_{3-\delta}$ ceramics is modified to $Ca[(Li_{1/3}Nb_{2/3})_{0.75}\ Ti_{0.25}]O_{3-\delta}$ and the $Ca[(Li_{1/3}Ta_{2/3})_{0.7}Ti_{0.3}]O_{3-\delta}$ ceramics is modified to $Ca[(Li_{1/3}Ta_{2/3})_{0.6}\ Ti_{0.4}]O_{3-\delta}$ by increasing the rutile content.

5.4.8 τ_f tuning

Table 5.2 Microwave dielectric properties of LBS and LMZBS glass added $Ca[(Li_{1/3}Nb_{2/3})_{0.75}Ti_{0.25}]O_{3-\delta}$ ceramics and the BZBS glass added $Ca[(Li_{1/3}Ta_{2/3})_{0.6}\ Ti_{0.4}]O_{3-\delta}$ ceramics.

Material	Sintering Temperature ^oC	ε_r	$Q_u$xf (GHz)	τ_f ppm/^{o} C
$Ca[(Li_{1/3}Nb_{2/3})_{0.75}\ Ti_{0.25}]O_{3-\delta}$	1175	41.9	17500	+23
$Ca[(Li_{1/3}Nb_{2/3})_{0.75}\ Ti_{0.25}]O_{3-\delta}$ + 5 wt% LBS	950	33.0	11500	-2
$Ca[(Li_{1/3}Nb_{2/3})_{0.75}\ Ti_{0.25}]O_{3-\delta}$ + 8 wt% LBS	940	30.5	9750	-5
$Ca[(Li_{1/3}Nb_{2/3})_{0.75}\ Ti_{0.25}]O_{3-\delta}$ + 12 wt% LMZBS	920	28.5	11000	-3
$Ca[(Li_{1/3}Nb_{2/3})_{0.75}\ Ti_{0.25}]O_{3-\delta}$ + 15 wt% LMZBS	900	27.4	11100	-8
$Ca[(Li_{1/3}Ta_{2/3})_{0.6}Ti_{0.4}]O_{3-\delta}$	1200	38.7	15000	+15
$Ca[(Li_{1/3}Ta_{2/3})_{0.6}Ti_{0.4}]O_{3-\delta}$ + 12 wt% of BZBS glass	950	34.90	6500	-6

Table 5.2 shows the microwave dielectric properties of LBS and LMZBS glass added $Ca[(Li_{1/3}Nb_{2/3})_{0.75}Ti_{0.25}]O_{3-\delta}$ ceramics and the BZBS glass added $Ca[(Li_{1/3}Ta_{2/3})_{0.6}\ Ti_{0.4}]O_{3-\delta}$ ceramics. The Ti substitution increased the relative permittivity of the CLNT / CLTT ceramics. This can be due to the incorporation of small Ti^{4+} ion (0.605 Å) to the B site $[Li_{1/3}\ Nb/Ta_{2/3}]^{3.67+}$ with slightly larger ionic radius (0.66 Å) and hence the atoms can not rattle around with the electric field. The $Ca[(Li_{1/3}Nb_{2/3})_{0.75}\ Ti_{0.25}]O_{3-\delta}$ ceramics with 12 wt% LMZBS glass sintered at 900^o C has ε_r =28.5, Q_u x f =11000 GHz (f =

4.7 GHz) and τ_f = -3 ppm/^oC and that of LBS glass addition of 5 wt% sintered at 950 ^oC has ε_r = 33, Q_u x f =11500 GHz (f = 4.6 GHz) and $\tau_f \approx$ -2 ppm/^oC. The $Ca[(Li_{1/3}Ta_{2/3})_{0.6}\ Ti_{0.4}]O_{3-\delta}$ ceramics with 12 wt% of BZBS glass sintered at 950 ^oC has ε_r = 34.9, Q_u x f =6500 GHz (f = 4.4 GHz) and $\tau_f \approx$ -6 ppm/^oC. The CLNT ceramics shows excellent dielectric properties at low sintering temperature compared to CLTT ceramics. Hence the $Ca[(Li_{1/3}Nb_{2/3})_{0.75}\ Ti_{0.25}]O_{3-\delta}$ ceramics with suitable amount of glass addition can find application in LTCC based devices.

5.5. Conclusions

- The $Ca[(Li_{1/3}Nb_{2/3})_{0.8}Ti_{0.2}]O_{3-\delta}$ ceramics and $Ca[(Li_{1/3}Ta_{2/3})_{0.7}Ti_{0.3}]O_{3-\delta}$ ceramics are single phase and have best temperature stable microwave dielectric properties. Hence, they are chosen for LTCC studies.
- The effect of various borosilicate glass additions on the sinterability, densification structure, microstructure and microwave dielectric properties of $Ca[(Li_{1/3}Nb_{2/3})_{1-x}Ti_x]O_{3-\delta}$ (x=0.2 and 0.25) and $Ca[(Li_{1/3}Ta_{2/3})_{1-x}Ti_x]O_{3-\delta}$ (x=0.3 and 0.4) ceramics have been investigated.
- The SEM and XRD studies indicate that the addition of glasses decrease the grain size and thereby increase the porosity and also reveals that the low temperature sintered CLNT-glass and CLTT-glass system does not react with the silver electrode material.
- The sintering temperature of $Ca[(Li_{1/3}Nb_{2/3})_{0.8}Ti_{0.2}]O_{3-\delta}$ (CLNT) ceramics lowered below the melting point of silver by the addition of LBS, LMZBS and ZBS glasses. Among these the CLNT ceramics with 5 wt% of LBS glass sintered at 950 ^oC/4hrs shows best dielectric properties such as ε_r = 30.5, Q_u x f = 14700 GHz (f = 4.6 GHz) and τ_f = -18 ppm/ ^oC.

- The sintering temperature of $Ca[(Li_{1/3}Ta_{2/3})_{0.7}Ti_{0.3}]O_{3-\delta}$ (CLTT) ceramics lowered by the addition of ZBS and BZBS glasses. Addition of 12 wt% of BZBS glass in CLTT ceramics sintered at 950 ^{o}C/4hrs shows ε_r = 32.0, Q_u x f = 9000 GHz (f = 4.7 GHz) and -41 ppm/^{o}C.
- The temperature coefficient of the CLNT-glass and CLTT-glass system are tuned in the range ± 10 ppm/^{o}C with reasonably good microwave dielectric properties by increasing the rutile content in the CLNT and CLTT ceramics.
- Compared to CLTT-glass system, the CLNT-glass system shows excellent temperature stable microwave dielectric properties at a low sintering temperature of 950 ^{o}C and can be a promising candidate for LTCC based devices.

The influence of various borosilicate glasses on the sinterability, densification, structure and microstructure and the microwave dielectric properties of the $Ca[(Li_{1/3}A_{2/3})_{1-x}Ti_x]O_{3-\delta}$ (A=Nb,Ta) complex perovskite dielectric ceramics is discussed in this chapter. Next chapter discusses the preparation and dielectric properties $Ca[(Li_{1/3}Nb_{2/3})_{0.8}Ti_{0.2}]O_{3-\delta}$ ceramic filled polymer composites for substrate applications.

References

1. W. Wersing, *Curr. Opin. Solid State Mater. Sci.*, **1**, 715, (1996).
2. M. T. Sebastian, *Dielectric materials for wireless communications*, Elseiver Publishers, Oxford U. K ,(2008).
3. Y. Wang, G. Zhang and J. Ma, *Mater. Sci. Eng. B*, **94**, 48, (2002).
4. Q. L. Zhang, H. Yang, J. L. Zou and H. P. Wang, *Mater. Lett.*, **59**, 880, (2005).
5. Y. Immanaka, "*Multylayered Low Temperature Cofired Ceramics (LTCC) Technology", Spinger, Japan,* (1999).
6. M. T. Sebastian and H. Jantunen, *Int. Mater. Rev.*, **53**, 57, (2008).
7. P. V. Bijumon and M. T. Sebastian, *Mater. Sci. Engg. B*, **123**, 31, (2005).
8. C.-L. Huang, M.-H. Weng, C.-T. Lion and C.-C. Wu, *Mater. Res. Bull.*, **35**, 2445, (2000).
9. G. Huang, D. Zhou, J. Xu, X. Chen, D. Zhang, W. Lu and B. Li, *Mater. Sci. Eng. B.*, **99**, 416, (2003).
10. H. Jantunen, R. Rautioaho, A. Uusimaki and S. Leppavuori, *J. Eur. Ceram. Soc.*, **20**, 2331, (2000).
11. D. W. Kim, D.-G. Lee and K. S. Hong, *Mater. Res. Bull.*, **36**, 585, (2001).
12. Y.-C. Lee, W.-H. Lee and F.-S. Shieu, *Jpn. J. Appl. Phys.*, **419**, 6049, (2002).
13. K. P. Surendran, P. Mohanan and M. T. Sebastian, *J. Sol. State Chem*, **177**, 4031, (2004).
14. S. Thomas and M. T. Sebastian, *Mater. Res. Bull.*, **43**, 843, (2008).
15. T. S. Sasikala, M. N. Suma, P. Mohanan, M. T. Sebastian, *J. Alloys Comp*. **461**, 555, (2008).
16. J.-W. Choi, C.-Y. Kang, S.-J. Yoon, H.-j. Kim and H.-J. Jung, *J. Mater. Res.*, **14**, 3567, (1999).
17. P. Liu, H. Ogawa, E. S. KIM and A. Kan, *J. Eur. Ceram. Soc.*, **23**, 2417, (2003).
18. W. Wong-Ng, T. Holesinger, G. Riley and R. Guo, "*Ceramic Transactions", 104, American Ceramic Society, Westerville*, (2000).
19. R. H. Mitchell, "*Perovskites Modern and Ancient*", Almaz Press Ontario, Canada, (2002).
20. L. A. Khalam, "Ph. D Thesis", (Kerala University), *Faculty of Science*, (2007).

21. J.-W. Choi, J. Y. Ha, S.-J. Yoon, H.-j. Kim and K. H. Yoon, *Jpn. J. Appl. Phys*, **43**, 223, (2004).

22. J.-Y. Ha, J.-W. Choi, C.-Y. Kang, S.-J. Yoon, D. J. Choi and H.-J. Kim, *Jpn. J. Appl. Phys.*, **44**, 1322, (2005).

23. J.-Y. Ha, J.-W. Choi, C.-Y. Kang, S.-J. Yoon, D. J. Choi and H.-J. Kim, *J. Electroceramics*, **17**, 399, (2006).

24. J.-Y. Ha, J.-W. Choi, S.-J. Yoon, D. J. Choi, K. H. Yoon and H.-J. Kim, *J. Eur. Ceram. Soc.*, **23**, 2413, (2003).

25. P. Liu, E. S. Kim and K. H. Yoon, *Jpn. J. Appl. Phys.*, **40**, 5769, (2001).

26. P. Liu, H. Ogawa, E. S. KIM and A. Kan, *J. Eur. Ceram. Soc.*, **24**, 1761, (2004).

27. J. X. Tong, Q. L. Zhang, H. Yang and J. L. Zou, *Mater. Lett.*, **59**, 3252, (2005).

28. J. X. Tong, Q. L. Zhang, H. Yang and J. L. Zou, *J. Am. Ceram. Soc.*, **90**, 845, (2007).

29. B. W. Hakki and P. D. Coleman, *IRE Trans. Microwave Theory Tech., **MTT.,** **8**, 402, (1960).

30. J. Krupka, K. D. Derzakowski, B. Riddle and J. B. Jarvis, *Meas. Sci. Technol.*, **9**, 1751, (1998).

31. A. Borisevich and P. K. Davies, *J. Am. Ceram. Soc.*, **85**, 2487, (2002).

32. A. Borisevich and P. K. Davies, *J. Am. Ceram. Soc.*, **85**, 573, (2002).

33. A. Borosevich and P. K. Davies, *J. Eur. Ceram. Soc.*, **21**, 1719, (2000).

34. S. O. Yoon, D. M. Kim, S. H. Shim, J. K. Park and K. S. Kang, *J. Eur. Ceram. Soc.*, **26**, 2023, (2006).

35. P. V. Bijumon, "Ph. D Thesis", (Cochin University of Science and Technology) *Faculty of Technology,* (2005).

36. K. P. Surendran, P. Mohanan and M. T. Sebastian, *J. Solid. State Chem.*, **177**, 4031, (2004).

37. S. X. Dai, R. F. Huang and D. L. Wilcos Sr, *J. Am. Ceram. Soc.*, **85**, 828, (2002).

38. K. Fukuda, R. Kitoh and I. Awai, *Jpn. J. Appl. Phys.*, **32**, 4584, (1993).

39. K. Haga, T. Ishi, J. Mashiyama and T. Ikeda, *Jpn. J. Appl. Phys.*, **31**, 3156, (1992).

40. H. Kagata, J. Kato, K. Nishimoto and T. Inoue, *Jpn. J. Appl. Phys.*, **32**, 4332, (1993).

Chapter 6

Dielectric Response of $Ca[(Li_{1/3}Nb_{2/3})_{0.8}Ti_{0.2}]O_{3-\delta}$ Ceramic Filled Polymer Composites

This chapter discusses the preparation and dielectric properties $Ca[(Li_{1/3}Nb_{2/3})_{0.8}Ti_{0.2}]O_{3-\delta}$ ceramic filled polymer composites for substrate applications. The dielectrics properties are investigated in terms of volume fraction of filler, frequency, and temperature. The prediction of the dielectric properties of polymer-ceramic composites using different theoretical models is also discussed. A Coplanar Waveguide Monopole Antenna is designed and fabricated using epoxy-CLNT polymer-ceramic composite and compared its response with standard FR-4 epoxy.

6.1 Introduction

The lower regions of microwave spectrum are increasingly getting overcrowded in the communication sector with the advent of modern communication systems. This has necessitated microwave dielectric materials with low dielectric loss, optimum relative permittivity, low coefficient of thermal expansion, moisture absorption resistance and good mechanical stability [1-4]. In the context of low permittivity materials, several ceramics such as silicates and aluminates with excellent microwave dielectric, thermal and mechanical properties have been developed for substrate and packaging applications [5-9]. However, they are brittle and have high processing temperature. This leads to difficulty in fabrication of complex shapes or machining the ceramic substrates during circuit fabrication. Moreover, expensive conductor layers have to be patterned over ceramic substrates for circuit realization. Polymer materials play a vital role in electronic packages as a result of their ease of processing, low cost, excellent microwave dielectric properties, and adhesive properties [10, 11]. However, they suffer from poor thermal, mechanical and dimensional stability and high coefficient of thermal expansion. Therefore the application of an individual polymer or ceramic is restricted in many aspects. Recently, Button et al. proposed a composite strategy of combining the advantages of ceramic and polymer to achieve a superior property balance [12]. Polymer-ceramic composite have shown a synergetic behavior between the polymer and inorganic materials. They offer an attractive combination of processibility and properties, which cannot be attained from individual components. Filled polymer substrates are generally classified as soft substrates, which are advantageous over ceramic substrates because of their ease of machinability, thermal shock resistance, low density and cheap conducting layer [13]. Significant amount of work has been done on Polytetrafluroethylene (PTFE) based polymer-ceramic composites [14-22].

However, high melt viscosity of PTFE (≈10^{10} Pa S) restricts the uniform distribution of filler materials in the polymer matrix while employing conventional powder processing route. In addition, these composites suffer from poor mechanical stability. It has been reported that polyethylene (PE) and polystyrene (PS) have low processing temperature (160^{o}C), good flexibility and excellent microwave dielectric properties compared to polyvinylidene fluoride, polymethyl methacrylate and polyanilene [10]. Epoxy resins (diglicidyl ether of bisphenol A) is considered as a common and successful polymer matrix for the fabrication of composite material due to its good adhesion with reinforcing element, enhanced chemical stability, enhanced thermal stability, resistance to degradation under the influence of corrosive environment [23]. Moreover, epoxy is thermosetting polymer so that it can be easily fabricated into different shapes. In the present investigation, we have taken polyethylene, polystyrene and epoxy as the polymer bases for polymer-ceramic composites. The microwave dielectric properties of the polyethylene, polystyrene and epoxy used in the present investigation are shown in Table 6.1.

Table 6.1 Microwave dielectric properties of the polymers used in the present investigation at 9 GHz.

Polymer	Relative Permittivity	Loss tangent
Epoxy	3.0	≈10^{-2}
Polyethylene (HDPE)	2.3	≈10^{-4}
Polystyrene	2.1	≈10^{-4}

The relative permittivity of the individual phases and the volume fraction of the filler are the most important factors influencing the dielectric properties of the composites. The permittivity of the polymer can be tailored to greater extent by using high permittivity low loss fillers. Generally, as the permittivity increases, the loss tangent also increases and the number of

temperature stable low loss materials with high permittivity is also limited [6]. Commonly used high relative permittivity ceramics for polymer-ceramic composites are $Pb(Mg_{1/3}\ Nb_{2/3})O_3$-$PbTiO_3$ (PMNT), $Pb(Zr\ Ti)O_3$ (PZT), $50Pb(Ni_{1/3}\ Nb_{2/3})O_3$ -$35PbTiO_3$ -$15PbZrO_3$ (PNN-PT-PZ), $BaTiO_3$ [24-27]. However, these ceramics are ferroelectrics with relatively high dielectric loss compared to low loss linear dielectrics. In addition, lead based ceramics are not environmentally friendly and have strong temperature and frequency dependence. Earlier studies show that $Ca[(Li_{1/3}Nb_{2/3})_{1-x}Ti_x]O_{3-\delta}$ (CLNT) ceramics have excellent temperature stable microwave dielectric properties (ε_r = 38, $Q_u$xf = 22000 GHz and τ_f = 0 ppm/^oC) [28]. It is reported that the micron size particle filled composites show excellent properties compared to nano sized filler loaded composites [19, 29]. Hence in the present study, we have selected micron size CLNT ceramic as the filler to improve the dielectric properties of the polymers.

The performance of the chip antenna and electronic circuits depends on the electrical properties of the encapsulating material. Hence it is necessary to investigate the properties of polymer ceramic composites for such applications. In the present work we report the physical and microwave dielectric properties of polyethylene-CLNT (PE-CLNT), polystyrene – CLNT (PS-CLNT) and Epoxy-CLNT polymer-ceramic composites for substrate applications. The experimentally observed results are compared with different theoretical models [23, 30-40]. In the present study, attempts also have been paid to explore the possibility of using CLNT filled epoxy as a substrate material for high frequency antenna applications. A Coplanar Waveguide Monopole Antenna is designed [41] and fabricated using epoxy-CLNT polymer-ceramic composite and compared its response with standard FR-4 epoxy.

6.2 Theoretical Modeling

6.2.1 Relative Permittivity

The composites are considered as heterogeneous disordered systems. Their performance depends up on many factors such as electrical properties of their constituents, geometric characteristics, volume fraction of the filler, spatial distribution, and the interactions between the phases. One of the attractive features of the composites is that their dielectric properties can be designed by varying the volume fraction of the filler. Hence the prediction of effective dielectric behavior of the composite is important as far as its application in electronic packaging is concerned. There have been several attempts to model and predict the effective properties of random filler distributed composites [23, 30-40].

Recently, Rao *et al*. [34] proposed an EMT model to predict the effective relative permittivity of the composite. In this model the composite is treated in terms of an effective medium whose effective ε_r can be obtained by averaging over the relative permittivity of the two constituents. The ceramic morphology factor '*n*' of the EMT model is related to ceramic particle and can be determined empirically.

$$\varepsilon_{eff} = \varepsilon_m \left[1 + \frac{V_f \left(\varepsilon_i - \varepsilon_m \right)}{\varepsilon_m + n\left(1 - V_f\right)\left(\varepsilon_i - \varepsilon_m\right)} \right] \quad \text{EMT model} \qquad (6.1)$$

where ε_{eff}, ε_i, and ε_m are the relative permittivities of the composites, ceramic and the polymer matrix respectively, V_f is the volume fraction of the ceramic and n is the correction factor (ceramic morphology factor) to compensate for the shape of the fillers used in polymer-ceramic composite. The schematic representation of the microstructure of polymer ceramic composites is shown in Fig. 6.1. In order to account for the major features of

a composite microstructure, a random unit cell is defined as core of ε_1 surrounded by a shell of host matrix ε_2 as shown in Fig. 6.1 (a) [where ε_i, ε_m and ε_{eff} are the permittivity of ceramics, matrix and composites respectively].

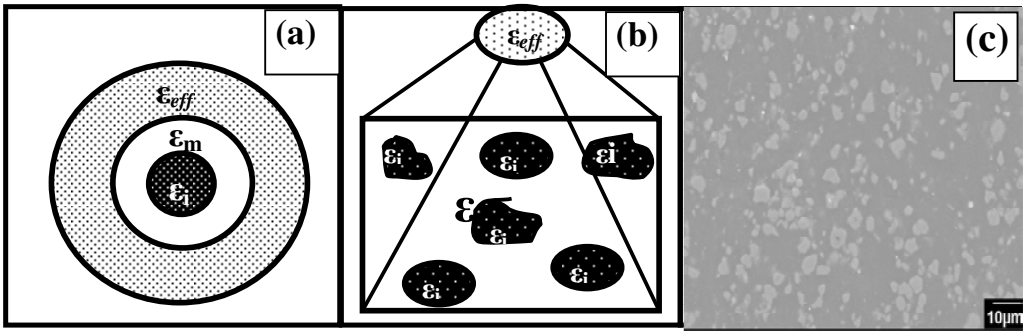

Fig. 6.1 Schematic diagram of random unit cell embedded in the effective medium, (b) aggregate of Random unit cell and (c) microstructure of composite materials.

The most commonly used equation is the logarithmic law of mixing as shown in equation 6.2. It considers the composite system as randomly oriented spheroids that are uniformly distributed in a continuous matrix [42].

$$\ln \varepsilon_{eff} = V_f \ln \varepsilon_i + (1 - V_f) \ln \varepsilon_m \qquad \text{Lichtenecker Eqn.} \qquad (6.2)$$

The Maxwell - Garnett mixing rule was initially used to calculate the effective permittivity of a system where metal particles are encapsulated in an insulating matrix. This mixing rule was modified for polymer-ceramic composites incorporating homogeneous distribution of spherical ceramic particles.

$$\frac{\varepsilon_{eff} - \varepsilon_m}{\varepsilon_{eff} + 2\varepsilon_m} = V_f \frac{\varepsilon_i - \varepsilon_m}{\varepsilon_i + 2\varepsilon_m} \qquad \text{Maxwell Garnett Eqn.} \qquad (6.3)$$

Jayasundere and Smith derived an equation which was modified from the well known Kerner equations by including interactions between neighboring spheres for the measurement of relative permittivity of binary composite [30].

$$\varepsilon_{eff} = \frac{\varepsilon_m(1-V_f)+\varepsilon_i V_f\left[\frac{3\varepsilon_m}{\varepsilon_i+2\varepsilon_m}\right]\left[1+\left(\frac{3V_f[\varepsilon_i-\varepsilon_m]}{\varepsilon_i+2\varepsilon_m}\right)\right]}{(1-V_f)+V_f\left[\frac{3\varepsilon_m}{\varepsilon_i+2\varepsilon_m}\right]\left[1+\left(\frac{3V_f[\varepsilon_i-\varepsilon_m]}{\varepsilon_i+2\varepsilon_m}\right)\right]}$$

Jayasundere.Eqn. (6.4)

6.2.2 Dielectric Loss

The number of theoretical models available for predicting loss tangent is relatively less, as it is more complicated. Literatures show that a composite of two low loss materials generally exhibits higher dielectric loss than the constituents. The trend of dielectric loss with different volume fraction of filler in the composite is entirely different from that of permittivity relation. The following relations are used to model the dielectric loss tangent of the composites [23, 39, 40].

$$(\tan\delta_c)^\alpha = \Sigma\phi_i(\tan\delta_i)^\alpha \quad \text{General mixing rule} \quad (6.5)$$

$$\varepsilon' = \frac{(\varepsilon'_i-\varepsilon')(\varepsilon'_i+2\varepsilon'_m)\varepsilon'}{(\varepsilon'_i-\varepsilon'_m)(\varepsilon'_i+2\varepsilon'_m)\varepsilon'_m}\varepsilon''_m + \frac{3(\varepsilon'-\varepsilon'_m)}{(\varepsilon'_i-\varepsilon'_m)(\varepsilon'_i+2\varepsilon'_m)}\varepsilon''_i$$

Bruggemen model (6.6)

where tan δ_c, tan δ_i, are the loss tangent of the composite and the i th material and φ_i is the volume fraction of the i th material. The constant α determines the mixing rule, if α = -1 serial mixing, and α = 1 parallel mixing rule. In Bruggemen model, ε_i', ε_m', ε', ε_i'', ε_m'', ε'' are the real and imaginary parts of the permittivity of the filler, matrix and the composite respectively.

6.3 Experimental

$Ca[(Li_{1/3}Nb_{2/3})_{0.8}Ti_{0.2}]O_{3-\delta}$ (CLNT) ceramics were prepared by conventional solid-state ceramic route. A detailed description of the experimental procedure is described in chapter 5, section 5.3. The sintered CLNT ceramics were ground well to form fine powders. Polystyrene-CLNT and polyethylene-CLNT polymer-ceramic composites were prepared by sigma blending technique (melt mixing technique) as described in chapter 2, section 2.3. The epoxy based polymer-ceramic composites were prepared by mechanical mixing and subsequent curing in vacuum as discussed in chapter 2, section 2.3. A maximum of 50 volume percentage of filler loading was made for polystyrene and polyethylene based composites and 40 volume percentage of filler loading for epoxy based composites. The density of the specimen was measured by the Archimedes method. The relative density was calculated using the equation 2.14 (see chapter2, section 2.6). The surface morphology of the composites was studied by scanning electron microscope (JEOL-JSM 5600 LV, Tokyo, Japan). Electrodes were made on both sides of the samples having the dimensions of 11 mm in diameter and 1 mm in thickness. The low frequency dielectric properties were measured by LCR meter (Hioki 3532-50 Japan). The coefficient of thermal expansion (CTE) of the composites was measured using a thermo mechanical analyzer (TMA – 60H, Shimadzu) in the range 25 – 100^{o}C. The micromechanical properties of PS/CLNT composites were measured using micro hardness tester (Clemex 4, Germany). Both the surfaces of the samples were polished to have optically flat surface for indentation. The specimen was subjected to a load of 50 g and dwell time of 10 s. For pure ceramic sample the load was increased to 500 g. A total of 5 readings were taken to get average hardness. The microwave dielectric properties (x-band) of the sample were measured by the cavity perturbation technique using HP 8510 C Network Analyzer

(Agilent Technologies). The detailed description of cavity perturbation technique is discussed in chapter 2.

6.4 Results and discussion

Typical microstructure (both planar and fractured surface) of polyethylene-CLNT (PE-CLNT), polystyrene-CLNT (PS-CLNT) and epoxy-CLNT polymer-ceramic composites for different volume fraction of ceramic loading is shown in Fig. 6.2. It can be observed that the CLNT ceramic particles are randomly distributed throughout the polymer and higher volume fraction of ceramic loading results connectivity of ceramics in some localized regions. Figs. 6.2 (e) and (f) show the fractured surface of both PE-CLNT and PS-CLNT polymer-ceramic composite for 0.50 volume fraction of ceramic loading. Figure 6.2 (g) and (h) shows the polished surface of epoxy-0.10 V_f of CLNT, and fractured surface of epoxy-0.30 V_f of CLNT. The fractured surface shows a dense microstructure and the polymer surrounds each ceramic particles. It is clear from the micrograph that the polymers act as good adhesives for combining ceramic particles.

The CLNT ceramics are prepared by solid state ceramic route and the particles may have different size. Fig. 6.3 shows the particle size distribution of CLNT ceramics in micrometer scale. It is clear from the figure that CLNT possess a very small particle size variation and have an average size of 3.7 μm which is in agreement with the SEM image (Fig. 6.2).

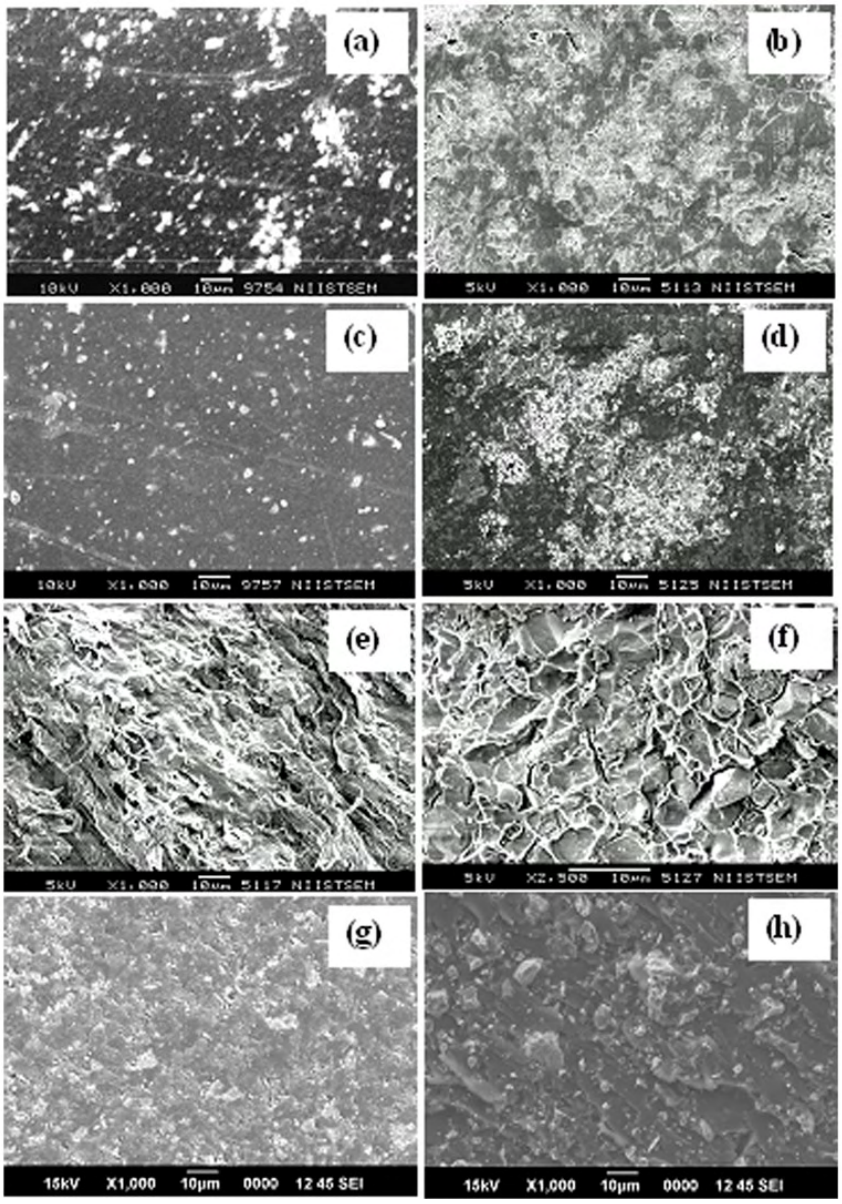

Fig. 6.2. SEM images of (a) Polyethylene-0.20 V_f of CLNT, (b) Polyethylene-0.40 V_f of CLNT, (c) Polystyrene-0.20 V_f of CLNT, (d) Polystyrene-0.40 V_f of CLNT, (e) fractured surface of polyethylene-0.40 V_f of CLNT, (f) fractured surface of polystyrene-0.40 Vf of CLNT, (g) polished surface of epoxy-0.10 V_f of CLNT, and (h) fractured surface of epoxy-0.30 V_f of CLNT.

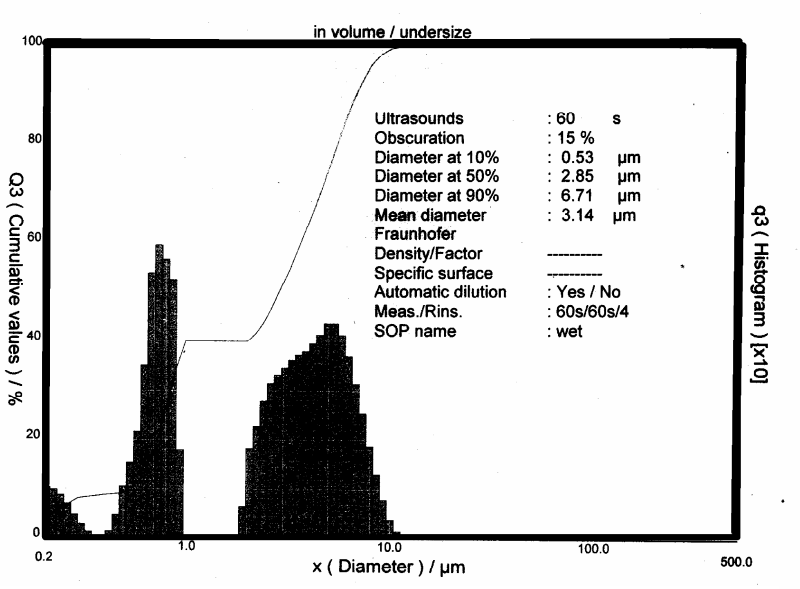

Fig. 6.3 Particle size distribution of CLNT powder in micrometers.

It can be observed from Fig. 6.4 (a) that, the coefficient of thermal expansion (CTE) of polymer-ceramic composite decreases with increase in the filler loading. This is due to the relatively low thermal expansion of ceramic compared to polymers. The addition of ceramic fillers hinders the expansion of polymers with temperature. As the volume fraction of ceramic increases from 0.0 to 0.40, the CTE of epoxy-CLNT composites decrease from 90 to 20 ppm/^{o}C. For 0.50 volume fraction of ceramic loading, the CTE of polyethylene and polystyrene are 65 ppm/^{o}C and 21 ppm/^{o}C respectively. Fig. 6.4 (b) shows the micromechanical properties of both the polymer-ceramic composites as a function of ceramic loading. The micro hardness increases with increase in the ceramic loading and around more than 100 percent of increase is observed for all the polymer-ceramic composite at higher volume fraction of ceramic loading. The microhardness of CLNT ceramics is (640 Kg/mm^2) much higher than polyethylene (10 Kg/mm^2), polystyrene (20 Kg/mm^2) and epoxy (30 Kg/mm^2). This is the reason for the

increase in the microhardness even though the densification decreases with ceramic loading.

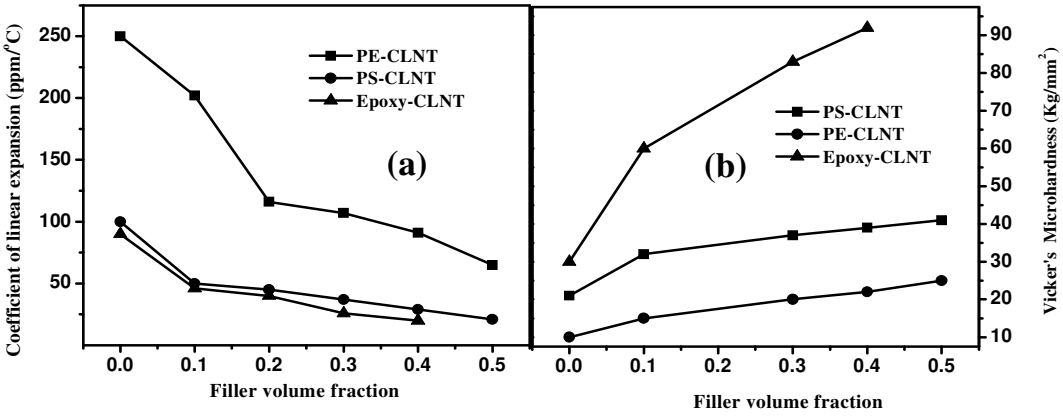

Fig. 6.4. Variation of (a) coefficient of linear expansion and (b) microhardness of polymer ceramic composite as a function of ceramic loading.

Table 6.2 shows the physical and electrical properties of PE-CLNT, PS-CLNT and Epoxy-CLNT polymer-ceramic composites for different volume fraction of filler content. It is found that the relative density decreases with increase in the ceramic loading. Recently, Doyle et al. [43] reported that clustering of particle in the composite may have significant effect on the effective composite properties. As the volume fraction of filler increases, the ceramic-ceramic connectivity increases and accordingly the polymer matrix slowly losses its 0-3 connectivity. This leads to the development of internal pores [17-19]. Hence it can be inferred that the reduction in densification is due to the void formation at higher filler loading. For 0.50 volume fraction of ceramic loading 95.8% of density is observed for PE-CLNT composite and 97.1% for PS-CLNT polymer-ceramic composite. More than 99% of densification is observed for epoxy-CLNT composite. Therefore the percentage of porosity is less than 5% for both the PE-CLNT and PS-CLNT composites and less than 1% for epoxy-CLNT composite. It can be observed from Table 6.2 that, the relative permittivity, dielectric loss and conductivity increases with increase in the filler content.

The overall properties of the composites mainly depend on the properties of constituent components. The increase in the relative permittivity of the entire composite under study is due to the relatively higher permittivity of CLNT ceramic (41 at 1 MHz) compared to polyethylene (2.62 at 1 MHz), polystyrene (3.2 at 1 MHz) and epoxy (4.2 at 1 MHz). In addition, the increase in the volume fraction of CLNT ceramic increases the interface between CLNT and polymer and hence the influence of interfacial polarization on the relative permittivity and dielectric loss tangent is significant. The Maxwell-Wagner-Sillars effect appears generally in heterogeneous media due to the accumulation of charges at the interface which leads to the formation of large dipoles [44]. As the filler loading increases, the connectivity among the filler particle increases and this leads to an increase in the dipole – dipole interaction [45]. Hence the relative permittivity increases with ceramic loading. The dielectric loss of CLNT ceramics and polymers are of the order of 10^{-4}. However, the dielectric loss of polymer-ceramic composites increases with increase of ceramic loading in PE-CLNT and PS-CLNT polymer-ceramic composite. The origin of dielectric loss in polymers are the dipolar impurities, end groups, chain fold and branch point [10]. The lower the concentration of the groups, the lower will be the dielectric loss [10]. It has been reported that, the dielectric loss of polymer-ceramic composite is affected by a number of factors such as porosity, water content and interface between two components in the composite [46]. The interfacial area and porosity increases with increase in the ceramic loading. As the interfacial area increases, the possibility of accumulation of space charges at interface of polymer-ceramic composite increases which in turn increases the dielectric loss.

Table 6.2 Physical and dielectric properties (1 MHz) of polyethylene-CLNT, polystyrene – CLNT and epoxy-CLNT polymer ceramic composites.

Composite Material	Filler Volume Fraction	Relative Density (%)	ε_r (1MHz)	tan δ (1 MHz)	Conductivity (S/cm)	Water absorption (%)
Polyethylene-CLNT	0.0	98.5	2.62	0.0006	2.40×10^{-9}	0.02
	0.10	97.2	3.36	0.0008	2.60×10^{-9}	0.06
	0.20	96.8	4.55	0.0020	5.70×10^{-9}	0.05
	0.30	96.5	5.96	0.0028	8.70×10^{-9}	0.05
	0.40	96.0	8.55	0.0050	1.10×10^{-8}	0.07
	0.50	95.8	11.60	0.0070	4.90×10^{-8}	0.16
Polystyrene-CLNT	0.0	99.2	3.20	0.0017	1.10×10^{-8}	0.02
	0.10	98.8	3.60	0.0014	1.86×10^{-8}	0.02
	0.20	98.2	4.70	0.0022	1.90×10^{-8}	0.03
	0.30	98.0	6.40	0.0028	2.30×10^{-8}	0.03
	0.40	97.5	8.02	0.0045	2.50×10^{-8}	0.04
	0.50	97.1	11.40	0.0054	3.30×10^{-8}	0.04
Epoxy-CLNT	0.00	100.0	4.27	0.020	2.43×10^{-8}	0.04
	0.10	99.7	5.10	0.017	4.56×10^{-8}	0.12
	0.20	99.8	6.60	0.013	4.96×10^{-8}	0.10
	0.30	99.0	8.00	0.009	5.03×10^{-8}	0.30
	0.40	99.3	10.30	0.011	4.55×10^{-8}	0.40

Generally, the dielectric loss of almost all the polymer ceramic composites increases with ceramic filler loading [15, 17-19, 21]. However, in the present epoxy based polymer-ceramic composites, a slight decrease in the dielectric loss is observed with higher ceramic loading. This could be due to the low dielectric loss of ceramics (tan $\delta = 10^{-4}$) compared to that of epoxy

(tan δ =10^{-2}). For 0.3 volume fraction of CLNT ceramic loading, the epoxy-CLNT composite shows ε_r = 8.0 with tan δ = 0.009 at 1 MHz. Subodh *et al.* also observed similar trend in $Sr_9Ce_2Ti_{12}O_{36}$ ceramic filled epoxy composites [23]. It can be observed that the conductivity of the composite increases with ceramic loading. This is due to the slightly higher conductivity of the CLNT ceramics compared to polymer and also due to the heterogeneity of the composites. Moisture absorption is an important parameter for materials used for packaging applications. Absorption of moisture from the working atmosphere will degrade especially the dielectric properties since the water is a polar molecule. It is evident from the Table 6.2 that as the filler content increases, the water absorption of both the composites increases. This is probably due to the void formation at higher ceramic loading. For 0.50 volume fraction of filler loading, a maximum value of 0.16 % and 0.04 % of water absorption is observed for PE-CLNT and PS-CLNT polymer ceramic composite respectively. A maximum value of 0.4 % of water absorption is observed for epoxy-CLNT polymer-ceramic composite. The relative density of epoxy-CLNT composite is much higher than PE-CLNT and PS-CLNT. However, the water absorption of the epoxy-CLNT composite is found to be much higher. This could be due to the open pores in the epoxy-CLNT compared to the other two composites.

The composite may be considered to be a homogeneous phase of composite particles. Each composite particle consists of a ceramic particle surrounded by a layer of polymer, although there can be distributions in the layer thickness. As the ceramic content increases with a corresponding decrease in the polymer ratio, the homogeneity of the composites decreases because the composite now consists of some ceramic particles which are not covered by the polymer layer (due to a reduction in the polymer content), thus leading to a heterogeneous mixture. As the ceramic increases, the

heterogeneity of composite increases and this lead to an increase in relative permittivity and dielectric loss of polymer ceramic composites.

Figure 6.5 shows the microwave dielectric properties of both PE-CLNT and PS-CLNT polymer-ceramic composite as a function of ceramic loading. It is found that, at 9 GHz both the relative permittivity and dielectric loss increase with increase in the ceramic loading in polymer-ceramic composite. The increase in the relative permittivity of polymer-ceramic composite is expected since; the particulate filler has much higher relative permittivity compared with that of the polymer matrix. The variation of relative permittivity of polymer-ceramic composite with respect to the filler concentration can be attributed to an increase in the total polarizability of the composite material. As the filler content increased from 0 to 0.50 volume fractions, the relative permittivity and dielectric loss increased from 2.3 to 9 and 0.0006 to 0.005 respectively for polyethylene-CLNT composite. The relative permittivity increases from 2.1 to 10.5 and dielectric loss increases from 0.0005 to 0.0032 with an increase of CLNT loading of 0.0 to 0.50 volume fraction in polystyrene. For 0.4 volume fraction of filler loading, the Polyethylene-CLNT composite shows ε_r = 7.7 and tan δ = 0.004 and for polystyrene-CLNT composite, the ε_r = 7.4 and tan δ = 0.003 at 9 GHz. As the filler content increases from 0 to 0.40 volume fractions, the relative permittivity of epoxy-CLNT increases from 3.02 to 9.60. The loss tangent initially shows an increasing trend up to a filler concentration of 0.10 volume fraction and with further filler addition, the loss tangent starts decreasing. Similar observations in loss tangent have been reported by Subodh *et al*. [23]. For 0.3 volume fraction of filler loading, the epoxy-CLNT composite shows an ε_r of 7.1 and tan δ of 0.026.

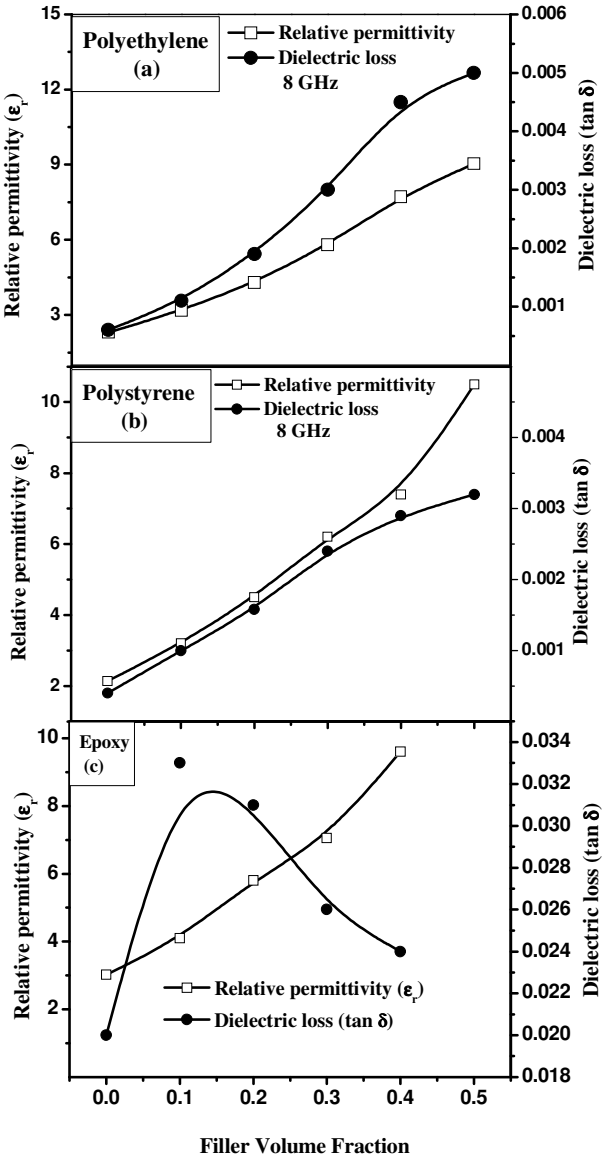

Fig. 6.5. Microwave dielectric properties of (a) polyethylene-CLNT, (b) Polystyrene-CLNT and (c) Epoxy-CLNT polymer ceramic composite as function of filler

Figure 6.6 shows the comparison of experimentally observed effective relative permittivity with the values predicted using the equations (6.1) to (6.4). The variation of effective permittivity of both the polymer-ceramic composites obtained using numerical equations shows the same trend as experimentally observed results. The morphology factor 'n' for EMT model is found to be 0.11, 0.07 and 0.10 for PE-CLNT, PS-CLNT and Epoxy-CLNT composites respectively. This is in agreement with previous reports [14, 21-

23, 47]. The composite morphology does not necessarily exhibit a homogeneous distribution of the dispersed component. Therefore, effective medium results are indeterminate for arbitrary composite architectures. It is found that the EMT, Jayasundere-Smith and Maxwell Garnet models are valid for low volume fraction of filler loading where as the Lichtenecker equation is found to match with experimental values for PE-CLNT and PS-CLNT polymer-ceramic composites. For epoxy-CLNT composites, the Maxwell Garnett models is valid for low volume fraction of filler loading where as the EMT, Jayasundere-Smith and Lichtenecker equations are found to match with experimental results. Generally, the theoretical predictions are valid for lower volume fraction of filler loading [14-20, 22, 23, 47]. This is due the imperfect dispersion of ceramic particle in polymer matrix. Many theoretical models suggest that the filler particles in a material should ideally be separated, non-interacting and roughly spherical [48]. Moreover, the ceramic filler should be sufficient concentric layers of polymer matrix. However, many composites of interest in practice deviate markedly from this ideal configuration. In PMN-PT- polymer composite, it has been reported that the failure of theoretical predictions at higher filler loading could be either due to increase in porosity or the clustering of filler particles [25]. Recent studies show that, the interface regions of polymer-ceramic composites have a relative permittivity significantly different from that of polymer or ceramic phases [49]. Hence the effective permittivity of the composite depends on the permittivity of each phase in the mixture, their volume fractions, shape, size, porosity, interface polarizabiliy and interface volume fractions. As a result, the effective permittivity has a nonlinear behaviour and consideration of all these parameters make the calculations tedious. Hence accurate prediction of dielectric properties of such composite is difficult. This is the reason for the deviation of experimental value of relative permittivity from the theoretical value for higher filler loading.

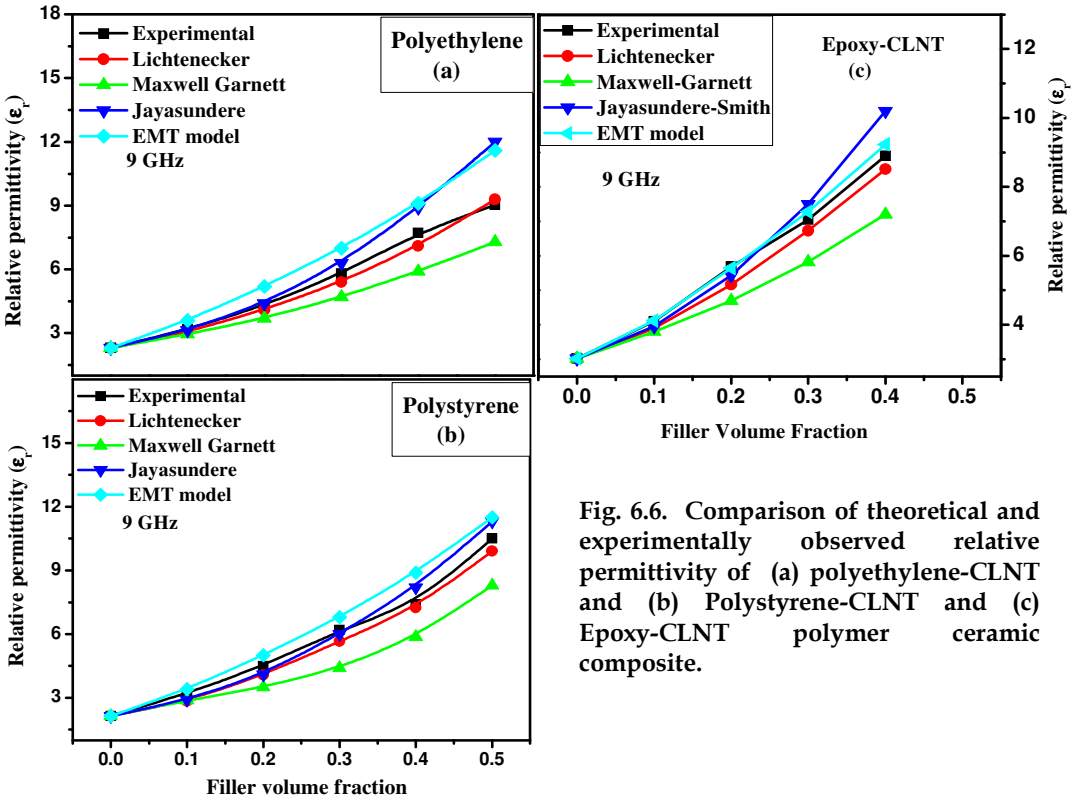

Fig. 6.6. Comparison of theoretical and experimentally observed relative permittivity of (a) polyethylene-CLNT and (b) Polystyrene-CLNT and (c) Epoxy-CLNT polymer ceramic composite.

The comparison of theoretical and experimentally observed dielectric loss of (a) polyethylene-CLNT and (b) Polystyrene-CLNT and Epoxy-CLNT polymer ceramic composite as function of ceramic loading is shown in Fig. 6.7. The dielectric loss of all the three composite using Bruggemen model, serial mixing model and the parallel mixing model is very low compared to experimentally observed results. All the calculated dielectric loss is nearly the same for the different models in the PE-CLNT and PS-CLNT system. However, in the epoxy-CLNT composite, Bruggemen model and the parallel mixing model shows the same trend as that of experimentally observed results. The dielectric loss depends on intrinsic and extrinsic factors. In heterogeneous materials such as composites, the intrinsic factor such as interaction of ac field with phonon is pronounced. Extrinsic factors such as defects, interfaces, size and shape of the fillers, moisture, impurities in the

interface of the composites, and pores can contribute to dielectric loss in the composites. A model which can consider all these parameters can predict the dielectric loss of the composites. Hence accurate prediction of dielectric loss of such composite is difficult and this is the reason for the deviation of experimental value of dielectric loss from the theoretical value.

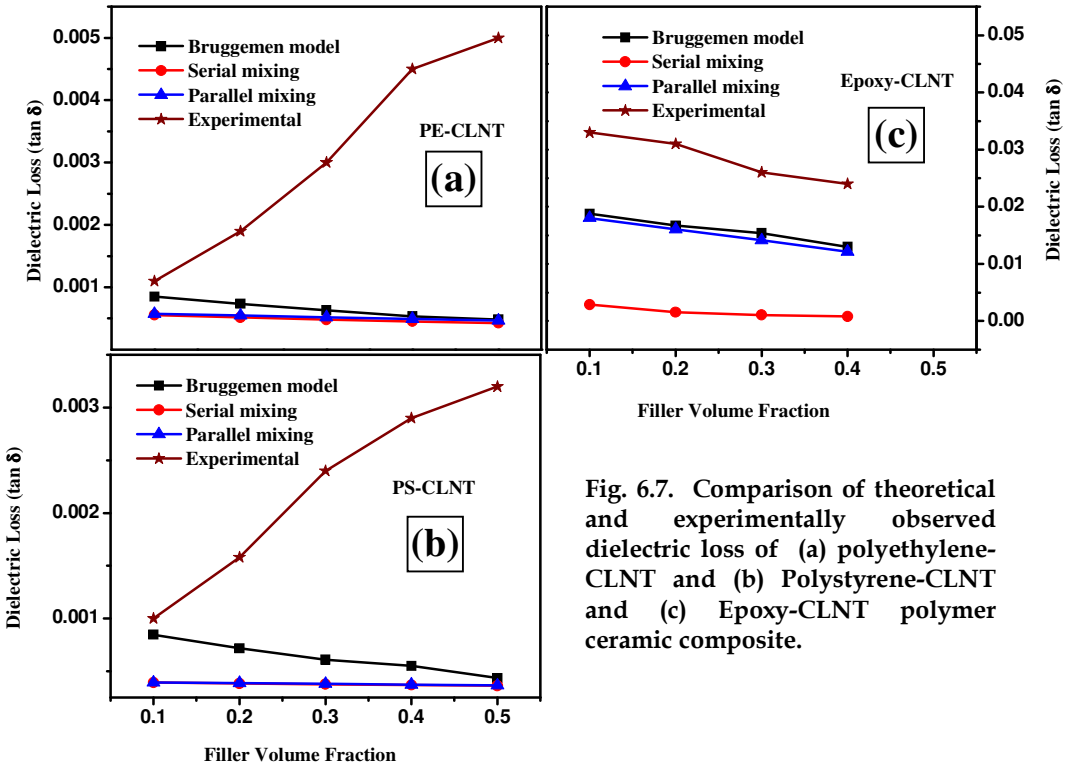

Fig. 6.7. Comparison of theoretical and experimentally observed dielectric loss of (a) polyethylene-CLNT and (b) Polystyrene-CLNT and (c) Epoxy-CLNT polymer ceramic composite.

Figure 6.8 shows the stability of relative permittivity with frequency for different volume fraction of filler in polyethylene and polystyrene. For all volume fractions of filler loading the relative permittivity is nearly constant in the range 1 kHz to 1 MHz. Such a frequency independent behavior is consistent with other polymer-ceramic composites [14, 17, 20-22]. Loading of fillers in polymers makes the system heterogeneous and the interfacial area increases with ceramic loading. In addition to the dipolar polarization, interfacial polarization is also present in the composites. A slight decrease in

relative permittivity is noted for both the composites at 170 kHz. This may be probably due to the dipolar relaxation process associated with the matrices. Subodh et al.[20, 21, 47] and Thomas et al. [22, 50] reported a similar broad relaxation peak at 170 kHz in the polymer-ceramic composites.

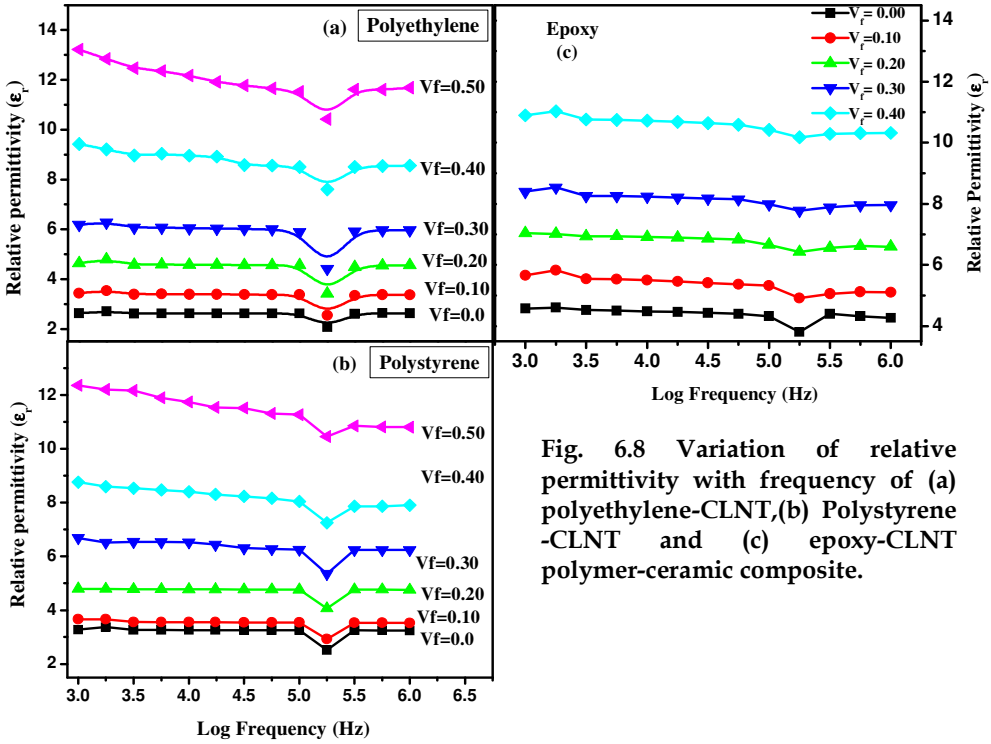

Fig. 6.8 Variation of relative permittivity with frequency of (a) polyethylene-CLNT,(b) Polystyrene -CLNT and (c) epoxy-CLNT polymer-ceramic composite.

Figure 6.9 shows the variation in relative permittivity of CLNT filled polyethylene, polystyrene and epoxy as a function of temperature. The drift in relative permittivity with temperature should be small for practical applications. The variations in the relative permittivity are less than 2% for the entire polymer-ceramic composite in the temperature range -20 to +70^{o}C. Literature shows that polyethylene, polystyrene based composite generally have a tendency of decrease in relative permittivity with temperature. It can be observed from Fig 6.9 (a) and (b) that the relative permittivity decreases slightly at higher temperature of around 70 ^{o}C. This is in agreement with previous reports. However, the relative permittivity increases slightly with

temperature for epoxy-CLNT composites. Earlier investigations on pure epoxy using thermally stimulated depolarizing current technique showed that the space charge density increases with increase in temperature of pure epoxy and controls the dielectric behavior above room temperature. It has been reported that space charge density increases inside the material with increase in the temperature of heterogeneous composites [23, 44, 51]. The thermally created charge carriers become more mobile at higher temperature and are responsible for the increase in the relative permittivity with temperature for epoxy-CLNT polymer-ceramic composites. The increase in relative permittivity with temperature of epoxy-CLNT is in agreement with several epoxy based composites [23, 51].

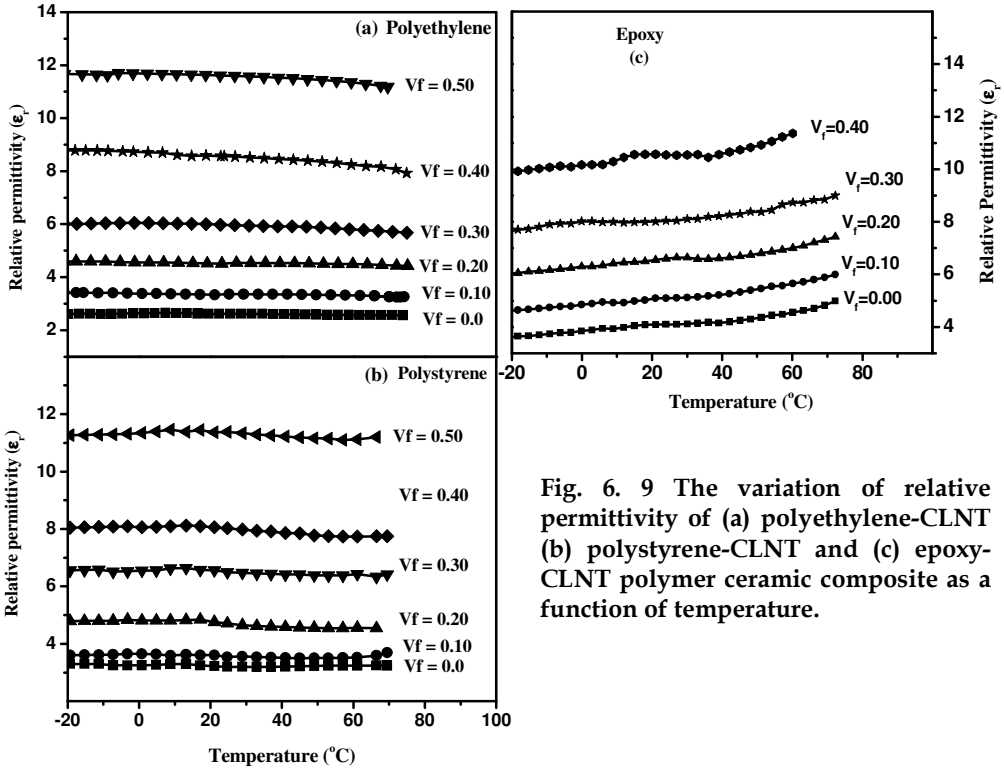

Fig. 6. 9 The variation of relative permittivity of (a) polyethylene-CLNT (b) polystyrene-CLNT and (c) epoxy-CLNT polymer ceramic composite as a function of temperature.

6.5 Coplanar Waveguide Monopole Antenna using Epoxy-CLNT substrate

The field of antenna engineering is the central to all wireless technologies. The advances in wireless communications technologies has promoted the development of chip antennas due to its advantages such as light weight, compact, relatively cheap, and easy to manufacture. With the development of microwave integrated circuits and high frequency semiconductor devices, microstrip has drawn the maximum attention of antenna community in recent years. One of the basic form of microstrip antenna comprised of a metallic radiating patch of any shape etched on low loss dielectric substrate with a ground plane. The dielectric properties of the substrate material are the one of the governing factor that controls the size and performance of the microstrip antenna. Using high permittivity substrate is a well known effective way to reduce the antenna size [52]. This chapter discusses the polymer ceramic composites for substrate applications. In the present work, attempts have been paid to explore the possibility of using CLNT filled epoxy as a substrate material for high frequency antenna applications.

Epoxy is a thermosetting polymer and hence, it can be easily fabricated with different shapes which are suitable for antenna applications. The epoxy-CLNT composite shows higher microhardness and low coefficient of thermal expansion compared to polyethylene and polystyrene based composites. Moreover, the polyethylene and polystyrene based composites cannot withstand higher temperature and hence we have selected epoxy-CLNT as the substrate for the fabrication of coplanar monopole antenna. The epoxy + 0.30 V_f of CLNT shows ε_r = 7.1 and tan δ = 10^{-2}. Fig. 6.10 shows the typical structure of coplanar wave guide monopole antenna. The epoxy + 0.30 V_f of CLNT polymer ceramic substrate having the dimensions of 40 x 40 x 2 mm^3 is fabricated and copper metal is coated using

electroplating method. The patterns are etched according to the standard design [41]. Ground plane is having 15 mm x 10 mm on both sides of the centre signal strip with 0.35mm gap. The dimension of the resonating element is 31 mm length and 3 mm width. The coplanar wave guide monopole antenna with same dimension has been made on standard FR-4 epoxy. The variation of the return loss characteristics of coplanar waveguide fed monopole antenna fabricated using CLNT-epoxy composite and the comparison with standard FR-4 epoxy substrate with same resonating length is shown in Fig 6.12. It is found that the resonant frequency (4.6GHz) is shifted to lower region (3.8 GHz) for Epoxy + 0.30 V_f of CLNT polymer ceramic composite compared to standard FR4 substrate. This is due to relatively high permittivity of epoxy-CLNT substrate compared to FR-4 substrate. Hence the radiating length and the size of the antenna can be reduced to make it more compact compared to standard FR-4. The radiation characteristic of the antenna on new substrate is found to be same as that of the standard antenna with an average gain of 2.7dBi.

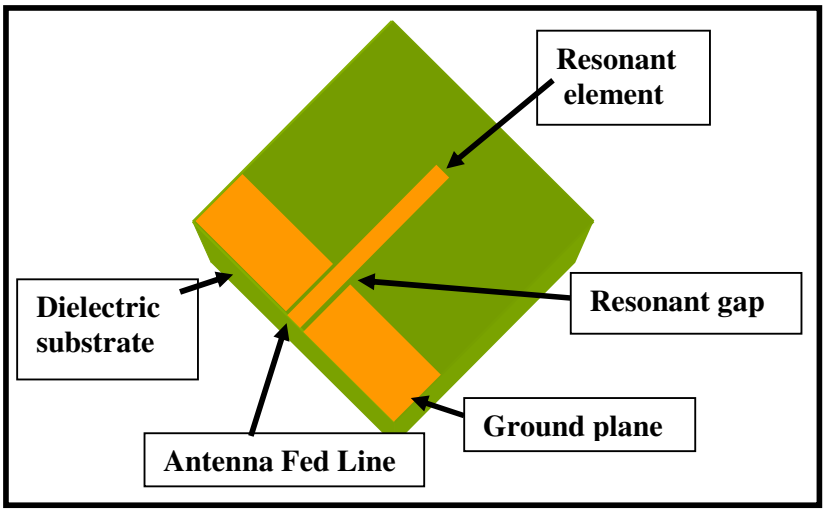

Fig. 6.10 Schematic image of coplanar wave guide monopole antenna

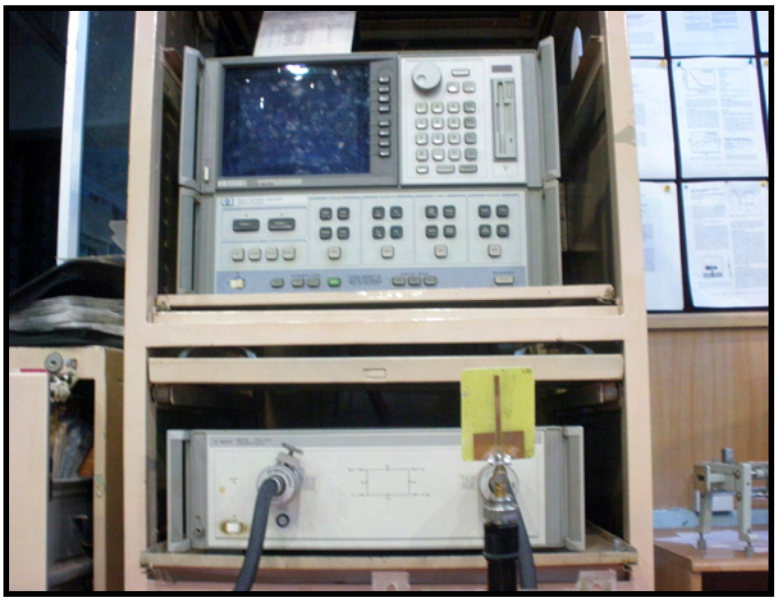

Fig. 6.11 Measurement setup for the coplanar wave guide monopole antenna

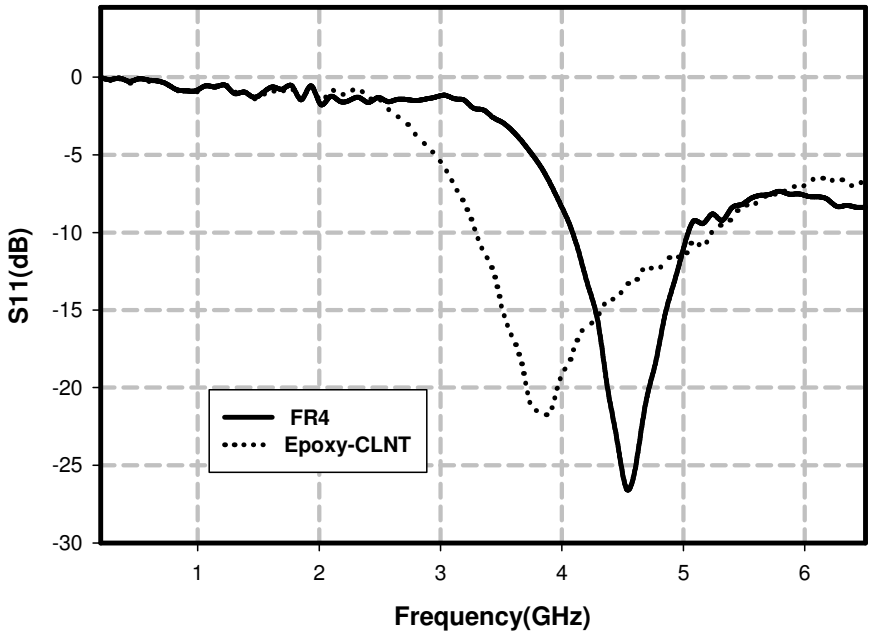

6.12 Return loss characteristics of coplanar waveguide fed monopole antenna fabricated using CLNT-epoxy composite and the comparison with standard FR4 epoxy substrate.

6.6 Conclusions

- The CLNT ceramic loaded polyethylene and polystyrene composites are prepared by melt mixing and hot molding techniques and the epoxy composites are prepared by mechanical mixing and thermosetting techniques.
- The physical and dielectric properties of the composites are investigated in terms of volume fraction of filler, frequency, and temperature.
- The experimentally observed relative permittivity and dielectric loss are compared with different theoretical models.
- As the volume fraction of filler in the polymer increases, the relative permittivity, dielectric loss and microhardness increases where as, the coefficient of linear thermal expansion decreases in CLNT ceramic reinforced polymer composites. For 0.4 volume fraction of filler loading, the Polyethylene-CLNT composite shows ε_r = 7.7 and tan δ = 0.004 and for polystyrene-CLNT composite, the ε_r = 7.4 and tan δ = 0.003 at 9 GHz. The predicted relative permittivity of this composites using Lichtenecker equation is in agreement with experimentally observed results.
- For 0.3 volume fraction of filler loading, the epoxy-CLNT composite shows an ε_r of 7.1 and tan δ = 0.026 at 9 GHz. The predicted relative permittivity of epoxy-CLNT composite using Lichtenecker and EMT model is in agreement with experimentally observed results.
- Coplanar Waveguide Fed monopole Antenna was designed and fabricated using epoxy-CLNT polymer-ceramic composite and compared the return loss characteristics with standard FR-4 epoxy.

References

1. D. D. L. Chung, "*Materials for Electronic Packaging*", *Butterworth Heinemann,* Washington, (1995).
2. T. Hu, J. Juuti, H. Jantunen and T. Vilkman, *J. Eur. Ceram. Soc.*, **27**, 3997, (2007).
3. M. G. Pecht, G. Agarwal, R., P. McCluskey, T. Dishongh, S. Javadpour and R. Mahajan, "*Electronic Packaging Materials and their Properties*", CRC Press, London, (1999).
4. R. R. Tummala, *J. Am. Ceram. Soc.*, **74**, 895, (1991).
5. H. Ohsato, T. Tsunooka, T. Sugiyama, K. Kakimoto and H. Ogawa, *J. Electroceramics*, **17**, 445, (2006).
6. M. T. Sebastian, "*Dielectric materials for wireless communications*", Elseiver Science and Technology Publishers, Oxford, U.K, (2008).
7. H. P. Sun, Q. L. Zhang, H. Yang and J. L. Zou, *Mater. Sci. Engg. B.*, **138**, 46, (2007).
8. K. P. Surendran, N. Santha, P. Mohanan and M. T. Sebastian, *Eur. Phys. J. B*, **41**, 301, (2004).
9. K. P. Surendran, M. T. Sebastian, M. V. Manjusha and J. Philip, *J. Appl. Phys.*, **98**, 044101, (2005).
10. J. A. Bur, *Polymer*, **26**, 963, (1985).
11. S. Rimdusit and H. Ishida, *Polymer*, **41**, 7941, (2000).
12. D. P. Button, B. A. Yost, R. H. French, W. Y. Hsu, J. D. Belt, M. A. Subrahmanian, H.-M. Zhang, R. E. Geidd, A. J. Whittacker and D. G. Onn, *Ceramic Substrates and Packages for Electronic Applications, Advances in Ceramics, American Ceramic Society, Westerville OH*, **26**, 353, (1989).
13. C. Brosseau, B. Sareni, L. Krahenbuhl and A. Beroual, *Proc. 5th Int. Conf. Properties and applications of dielectric materials,* **1- 2**, 892, (1997).
14. P. S. Anjana, M. T. Sebastian, M. N. Suma and P. Mohanan, *Int. J. Appl. Ceram. Techn.*, **5**, 325, (2008).
15. K. P. Murali, S. Rajesh, O. Prakash, A. R. Kulkarni and R. Ratheesh, *Comp. Part A-Appl. Sci. Manuf.*, (2009).
16. V. S. Nisa, S. Rajesh, K. P. Murali, V. Priyadarsini, S. N. Potty and R. Ratheesh, *Comp. Sci. Tech..*, **68**, 106, (2008).
17. S. Rajesh, K. P. Murali, V. Priyadarsini, S. N. Potty, R. Ratheesh and P. Mohanan, *Poly.-Plastics Tech. Engg.*, **47**, 242, (2008).

18. S. Rajesh, K. P. Murali and R. Ratheesh, *Poly. Comp.*, **30**, 1480, (2009).

19. S. Rajesh, V. S. Nisa, K. P. Murali and R. Ratheesh, *J. Alloys Comp.*, **477**, 677, (2009).

20. G. Subodh, M. Joseph, P. Mohanan and M. T. Sebastian, *J. Am. Ceram. Soc*, **90**, 3507, (2007).

21. G. Subodh, C. Pavithran, P. Mohanan and M. T. Sebastian, *J. Eur. Ceram. Soc.*, **27**, 3039, (2007).

22. S. Thomas, V. Deepu, P. Mohanan and M. T. Sebastian, *J. Am. Ceram. Soc.*, **91**, 1971, (2008).

23. G. Subodh, V. Deepu, P. Mohanan and M. T. Sebastian, *Appl. Phys. Lett.*, **95**, 062903, (2009).

24. M. Arbatti, X. Shan and Z. Cheng, *Adv. Mater.*, **19**, 1369, (2007).

25. Y. Bai, Z. Y. Cheng, V. Bharti, H. S. Xu and Q. M. Zhang, *Appl. Phys. Lett.*, **76**, 3804, (2000).

26. S. K. Bhattacharya and R. R. Tummala, *J. Mater. Sci. Mater. Electr.*, **11**, 253, (2000).

27. C. Huang, Q. M. Zhang, G. deBotton and K. Bhattacharya, *Appl. Phys. Lett.*, **84**, 4391, (2004).

28. J. W. Choi, C. Y. Kang, S. J. Yoon, H. J. Kim, H. J. Jung and K. H. Yeon, *J Mater. Res.*, **14**, 3567, (1999).

29. J. I. Hong, P. Winberg, L. S. Schadler and R. W. Siegel, *Mater. Lett.*, **59**, 473, (2005).

30. N. Jayasundere and B. V. Smith, *J. Appl. Phys.*, **73**, 2462, (1993).

31. L. Jylha, J. Honkamo, H. Jantunen and A. Sihvola, *J. Appl. Phys.*, **97**, 104104, (2005).

32. L. Jylha and A. H. Sihvola, *IEEE Trans. Geosci. Remote Sensing*, **43**, 59, (2005).

33. Y. M. Poon and F. G. Shin, *J. Mater. Sci.*, **39**, 1277, (2004).

34. Y. Rao, J. M. Qu, T. Marinis and C. P. Wong, *IEEE Trans. Comp. Pack. Techn.*, **23**, 680, (2000).

35. B. Sareni, L. Krahenbuhl, A. Beroual and C. Brosseau, *J. Appl. Phys.*, **81**, 2375, (1997).

36. B. Sareni, L. Krahenbuhl, A. Beroual, A. Nicolas and C. Brosseau, *IEEE Trans. Magnetics*, **33**, 1580, (1997).

37. A. H. Sihvola, *Surface Sensing Techn. Applications*, **1**, 393, (2000).

38. A. H. Sihvola and J. A. Kong, *IEEE Trans. Geosci. Remote Sensing*, **26**, 420, (1988).

39. K. Wakino, T. Okada, N. Yoshida and K. Tomono, *J. Am. Ceram. Soc.*, **76**, 2588, (1993).

40. R. Abraham, R. Guo and A. S. Bhalla, *Ferroelectrics*, **315**, 1, (2005).

41. R. Garg, P. Bhartia, I. Bahl and A. Ittipiboon, "*Microstrip Antenna Design Handbook*", Norwood, MA: Artech House, (2001).

42. F. Xiang, H. Wang and X. Yao, *J. Eur. Ceram. Soc.*, **26**, 1999, (2006).

43. W. T. Doyle and I. S. Jacobs, *Phys. Rev. B*, **42**, 9319, (1990).

44. H. Smaoui, L. E. L. Mir, H. Guermazi, S. Agnel and A. Toureille, *J. Alloys Comp.*, **477**, 316, (2009).

45. D. H. Kuo, C. C. Chang, T. Y. Su, W. K. Wang and B. Y. Lin, *Mater. Chem. Phys.*, **85**, 201, (2004).

46. N. G. Devaraju, E. S. Kim and B. I. Lee, *Microelectronic Engineering*, **82**, 71, (2005).

47. G. Subodh, V. Deepu, P. Mohanan and M. T. Sebastian, *Poly. Engg. Sci.*, **49**, 1218, (2009).

48. D. Stroud, *Phys. Rev. B.*, **19**, 1783, (1979).

49. M. G. Todd and F. G. Shi, *J. Appl. Phys.*, **94**, 4551, (2003).

50. S. Thomas, V. Deepu, S. Uma, P. Mohanan, J. Philip and M. T. Sebastian, *Mater. Sci. Engg. B-Adv. Funct. Solid-State Mater.*, **163**, 67, (2009).

51. C. F. Yang, C. C. Wu, C. C. Su and Y. C. Chen, *Appl. Phys. A*, **97**, 455, (2009).

52. K. C. Cheng, C. M. Lin, S. F. Wang, S. T. Lin and C. F. Yang, *Mater. Lett.*, **61**, 757, (2007).

Chapter 7

High Permittivity Composites for Embedded Passive Applications

The high permittivity ceramic-metal and polymer-ceramic-metal composites for embedded passive applications are discussed in this chapter. The effect of sintering temperature on the percolation threshold and the dielectric properties of $Ca[(Li_{1/3}Nb_{2/3})_{0.8}Ti_{0.2}]O_{3-\delta}$ *(CLNT)– Ag composite for LTCC based high permittivity application is discussed in the first section and the polymer based CLNT-epoxy-Ag three phase composite for printed wiring board compatible embedded capacitor application is discussed in the next section. The objective of the present work is to address the materials, processes and properties of high permittivity composites for LTCC based modules and printed wire board compatible high permittivity composite for embedded capacitor applications.*

7.1 Introduction

Recently, ever-increasing demand for high-density-circuits in electronics has greatly accelerated the miniaturization and integration of chip electronic components with high performance, multifunctionality, smaller size, high efficiency, and low cost [1, 2]. This has led to considerable attention towards the high permittivity materials for its technologically important applications in high k gate dielectrics, capacitor dielectrics and electrostrictive materials [1, 3-5]. Development of high permittivity materials has become one of the major scientific and technological issues. High relative permittivity, reasonably low loss, low temperature coefficient of permittivity and low processing temperature are the basic requirements of these materials for such applications. Commonly used high permittivity ceramics are ferroelectric with high processing temperature and are less stable with temperature and frequency [6-9]. Polymers have low processing temperature but it has low permittivity. Hence, monolithic polymers and dielectrics cannot be used as such in high permittivity based devices. Therefore, the concept of two component and three component composites which contain randomly distributed conductive fillers in an insulating matrix have been developed [10-14]. As the volume fraction of metals or conducting phases in these composites increase, the relative permittivity and conductivity increases gradually and when the volume fraction of the conductive powder reaches a critical value, the conductivity as well as relative permittivity of the composite increases by several orders of magnitude. This critical value is referred to as percolation limit of the composite [15-21]. The concentration of the conductive additives has been proved to be a crucial parameter, governing the electrical behavior of the composites. Percolation theory describes the transition from the state of limited and spatially restricted connections of conductive elements to the state of an infinite network of connections. The percolation threshold

represents the critical concentration or volume fraction of the conductive inclusions, which is necessary for the onset of conductive behavior [16, 22, 23]. In the context of high relative permittivity percolative materials, several polymer-ceramic [1, 5, 6, 24-27], polymer-metal composites [28-37] and ceramic-metal composites [12, 13, 23, 38-45] have been studied. Fig 7.1 shows the typical permittivity versus filler volume fraction curve of polymer-ceramic, polymer-metal, ceramic-metal and polymer-ceramic-metal composites.

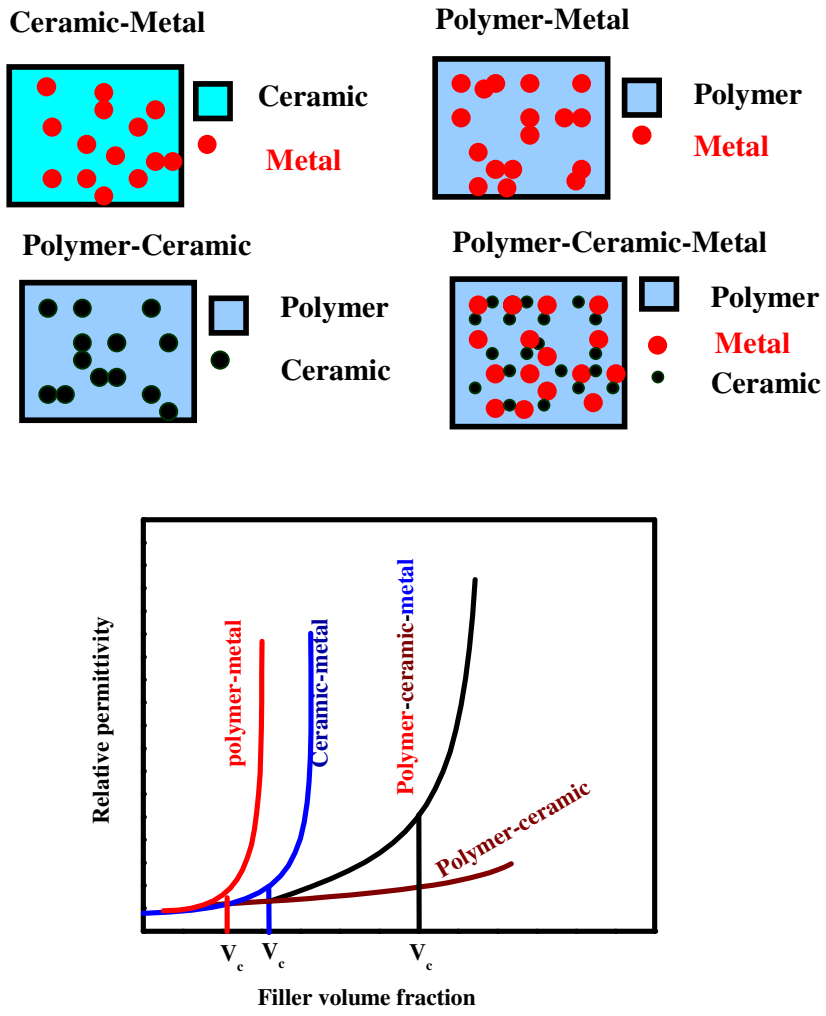

Fig. 7.1 Typical permittivity versus filler volume fraction curve of polymer-ceramic, polymer-metal, ceramic-metal and polymer-ceramic-metal composites.

In polymer-ceramic composite higher volume fraction of ceramics loading is needed to enhance the relative permittivity and the higher filler loading results processability issues and poor performance. But in polymer metal and ceramic metal composite small amount of filler loading is quite enough to raise the relative permittivity. The conductor-insulator percolative composite system has been recognized as the promising method to achieve high permittivity. In order to apply percolative system for manufacturing of capacitors, the conductive filler content and the distribution within the matrix have to be precisely controlled, because less than 1% variation of filler content exerts a dramatic effect on the permittivity, conductivity and dielectric loss. This problem can be alleviated by the concept of three phase composite where the insulating ceramic filler in polymer-ceramic-metal three phase composite extend the percolation threshold and improves the electrical performance of the devices [46-49]. This chapter consists of two sections; first section discuss the ceramic-metal composites for LTCC based embedded passive application and the second section discusses the polymer-ceramic-metal three phase composites for PCB compatible embedded capacitor applications.

7. 2 Giant permittivity Ceramic-metal composites

7.2.1 Introduction

Ceramic-metal composites have been extensively studied for its potential application in high permittivity based modules. The metallic powders used in ceramic metal composites are Pt, Pd, Ag, Al, Cu, Ni, etc. Among them Pt and Pd are too expensive and Al, Cu, Ni have the problem of oxidization while sintering at higher temperatures and require inert atmosphere. Hence these metal powders cannot be considered as possible candidates for practical applications. However, silver containing composites do not have such drawbacks and show excellent permittivity near the

percolation threshold [23, 38, 40-42]. In order to achieve high relative permittivity in cermets system below percolation, the relative permittivity of the ceramics must also be as high as possible. Commonly used high relative permittivity ceramics are $Pb(Mg_{1/3}\ Nb_{2/3})O_3$-$PbTiO_3$ (PMNT), $Pb(Zr\ Ti)O_3$ (PZT), $50Pb(Ni_{1/3}\ Nb_{2/3})O_3$ -$35PbTiO_3$ -$15PbZrO_3$ (PNN-PT-PZ), $BaTiO_3$ [1, 5, 6, 24, 50, 51]. However, these ceramics are ferroelectrics with relatively high dielectric loss compared to low loss dielectrics. In addition, lead based ceramics are not environmentally friendly and have strong frequency and temperature dependence. All the ceramic-silver composites reported so far were sintered at the sintering temperature of ceramics, which is much above the melting point of silver. Several previous reports show that silver can diffuse along open pores in the ceramics at higher temperatures and escape from the surface, since the melting point of silver (961^oC) is lower than the sintering temperature used for the ceramic-Ag composites [52-54]. This loss of silver during sintering of ceramic-Ag composites and its impact on the properties were ignored in the earlier studies [54, 55]. Thus, it is necessary to lower the sintering temperature of composite to prevent the loss of silver. Hence, the selection of ceramics is important in the context of high relative permittivity ceramic-metal composites.

Earlier studies show that, the $Ca[(Li_{1/3}Nb_{2/3})_{1-x}Ti_{\ x}]O_{3-\delta}$ (CLNT) with x=0.2 sintered at 1150^oC/2hrs shows the ε_r = 38, tanδ = 10^{-4} and nearly zero temperature coefficient of relative permittivity in microwave frequency range [56]. However, the sintering temperature of this material is still higher than the melting point of silver. In chapter 5 we have seen that the sintering temperature of the CLNT can be lowered from 1150 ^{o}C to 950 ^{o}C by addition of 5 wt % of lithium borosilicate glass without much degradation on the microwave dielectric properties. The dielectric and conducting properties of CLNT + LBS + Ag composites are systematically investigated in terms of frequency, volume fraction of silver and temperature. The effect of sintering

temperature on the percolation threshold of ceramic metal composite is also discussed.

7. 2. 2 Experimental

The $Ca[(Li_{1/3}Nb_{2/3})_{0.8}Ti_{0.2}]O_{3-\delta}$ (CLNT) ceramic samples were prepared by the conventional solid state ceramic route as described in chapter 5 (section 5.3). Preparation of lithium borosilicate ($35.1Li_2O$-$31.7B_2O_3$-$33.2SiO_2$) (LBS) glass and the detailed description of experimental procedure are discussed in chapter 2 (section 2.2). From chapter 5, it is evident that, the addition of 5 wt% of LBS glass lowers the sintering temperature of CLNT ceramics below 950 ^oC. The calcined CLNT powder with 5 wt% of LBS glass powder was prepared by mixing in ethanol medium followed by drying and grinding. Different volume fraction of silver (99.99%, -60 mesh, Aldrich chemical company, Inc, Milwaukee, WI, USA) were added to calcined CLNT powder and 5 wt% of LBS glass added CLNT powder separately and mixed again in ethanol medium. Polyvinyl alcohol (PVA) (Molecular Weight 22000, BDH Lab Suppliers, England) solution was then added to the powder, mixed, dried and ground well. This composite was pressed into cylindrical disks of about 11 mm diameter and 1mm thickness, by applying a pressure of 100 MPa. The CLNT+Ag composites were sintered at different temperatures from 1050 ^oC to 1175 ^oC/2hrs and that of CLNT+5 wt% LBS + Ag composites from 875 ^oC to 950 ^oC/2hrs. Electrodes were connected to both sides of the sintered and polished compacts using silver paste and these samples were used for measuring the dielectric properties. The dielectric properties were measured using a LCR meter (HIOKI 3532-50 LCR Hi TESTER, Japan). The sintered density of the specimen was measured by the Archimedes method. The crystal structure and phase purity of the powdered samples were studied by X- ray diffraction technique using Ni-filtered Cu-Kα radiation using Rigaku Dmax-I, Japan diffractometer. The surface morphology of the sintered

samples was studied using an optical microscope (Leica, DMRX, Germany). The variation in relative permittivity with temperature was also investigated for the composites in the temperature range 25-70 ^{o}C.

7.2.3 Results and Discussion

Figure 7.2 shows the X-ray diffraction patterns of (a) CLNT ceramics sintered at 1150 ^{o}C, (b) CLNT+5 wt% LBS sintered at 950 ^{o}C and (c) 0.20 volume fraction of silver added CLNT+5wt% of LBS glass sintered at 1150 ^{o}C/2hrs. The XRD patterns are indexed based on the $CaTiO_3$ type orthorhombic perovskite structure with four formula units per unit cell. Fig.7.2 (c) shows the XRD pattern of CLNT ceramics with 5 wt% of LBS glass and 0.20 volume fraction of silver sintered at 925 ^{o}C/2hrs. XRD analysis did not show any phase other than pure CLNT and metallic silver. This indicates that there is no chemical reaction between silver and CLNT+5 wt% of LBS glass.

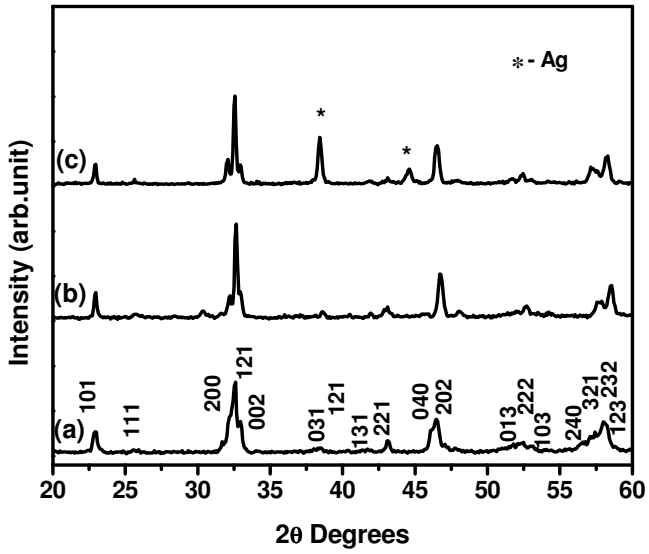

Fig. 7.2 X-ray diffraction patterns of sintered $Ca[(Li_{1/3}Nb_{2/3})_{0.8}Ti_{0.2}]O_{3-\delta}$ ceramics with; (a) 0 wt%, (b) 5 wt% of LBS and (c) 5 wt% of LBS + 0.20 Vf of Ag.

Figure 7.3 shows the variation of relative density of CLNT+Ag composite as a function of sintering temperature. It is found that all the CLNT+Ag composite shows maximum densification when sintered at 1150

°C/2hrs. Thus the optimized sintering temperature of CLNT+Ag composite is 1150 °C/2hrs. The decrease in the relative density could be due to the evaporation of silver at higher sintering temperature.

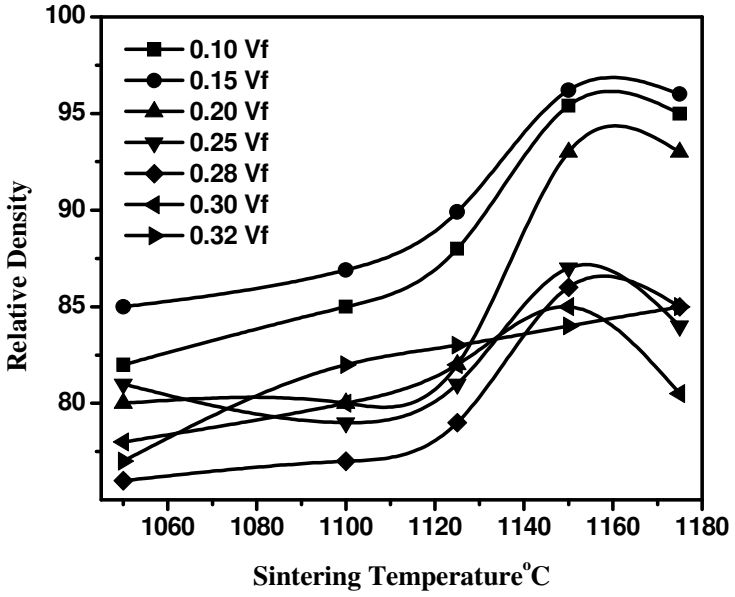

Fig. 7.3 Variation of relative density of CLNT-Ag composite as a function of sintering temperature of LBS + 0.15 Vf of Ag.

Figure 7.4 (a) shows the relative permittivity and dielectric loss of CLNT+Ag composite sintered at 1150 °C/2hrs as a function of silver loading. The relative permittivity and dielectric loss increases with increase in the volume fraction of silver. The increase in relative permittivity can be explained by the existence of large number of metal particles in parallel and in very close proximity but blocked by thin barriers of dielectric materials forming microcapacitiors [13, 23, 33, 35]. It has been reported that, above percolation threshold, the relative permittivity of the ceramic–silver composite increased to a very high value ($\approx 10^5$) accompanied by an increase in dielectric loss and conductivity [12, 13, 21, 35, 38, 44]. Generally the percolation threshold for ceramic–silver composite was around 0.16 volume fraction [12, 13, 54, 57]. However, in CLNT + Ag composite the percolation

threshold is not attained even at 0.28 volume fraction of silver. It is worth to note that all samples were sintered at 1150 ^{o}C/2hrs for maximum densification, and this is well above the melting point of silver.

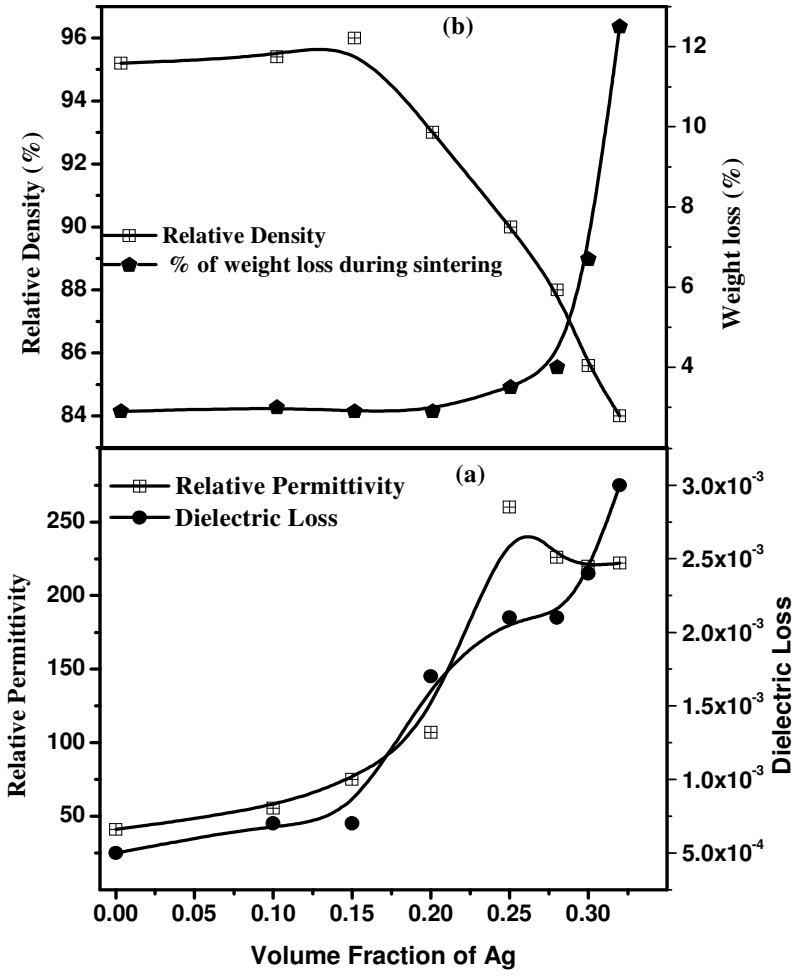

Fig. 7. 4 Variation of (a) Relative permittivity and Dielectric loss and (b) Relative density and percentage of weight loss after sintering of $Ca[(Li_{1/3}Nb_{2/3})_{0.8}Ti_{0.2}]O_{3-\delta}$ - Ag composite sintered at 1150^{o}C/ 2hrs as a function of silver loading.

Figure 7.4(b) shows the relative density and difference in weight percentage before and after sintering (weight loss in percentage) of the composites with different volume fraction of silver. It is observed that relative density of CLNT+Ag composite increased to a maximum value at 0.15 volume fraction of silver loading sintered at 1150 ^{o}C/2hrs. However,

further silver addition decreased the relative density. The composites having more than 0.25 volume fraction of silver loading shows the relative density less than 90% and this densification is attained only at 1150 ^{o}C/2hrs. In ceramic-silver composite, it is reported that above 960 ^{o}C, silver melts, diffuse along the open pores of ceramics and escape [54]. Hence the volume fraction of silver after sintering will be reduced from the starting value due to the escape of silver. The escape of silver could be quantitatively evaluated by comparing the weight before and after sintering. Fig. 7.4(b) suggest that volatilization of silver is more remarkable at high silver concentration. In CLNT + Ag composites, the silver melts at 960 ^{o}C and the density of ceramics is still low so that silver diffuse to external region and then escape. As a result the actual volume fraction of Ag in the composite becomes lower than the initial amount. This could be the reason for the decrease in density of CLNT + Ag composite at higher volume fraction of silver.

Figure 7.5 shows the optical micrograph of CLNT ceramics with 25 and 28 volume fraction of silver loading sintered at 1075 ^{o}C/2hrs. It is observed that at this sintering temperature, the relative density of CLNT+Ag composite is less than 80% and silver melts and comes to the surface as bubbles. It strongly supports the escape of silver at elevated temperatures. At higher sintering temperature, the silver particles melt and move along the grain boundary and accumulate at the boundary intersections [43]. Hence the particle size of the silver is increased. Thus in CLNT+Ag composite, the size of the silver particle increased and volume of silver decreased at its optimum sintering temperature. Thus the number of microcapacitor decreased and thereby decreased the relative permittivity. It is worth to note that the relative density of high volume fraction of silver loaded CLNT ceramics is less than 90% at its optimum sintering temperature of 1150 ^{o}C. Hence the high optimum sintering temperature of the CLNT+Ag composite

could be the reason for the percolation threshold not reaching even at 0.28 volume fraction of silver.

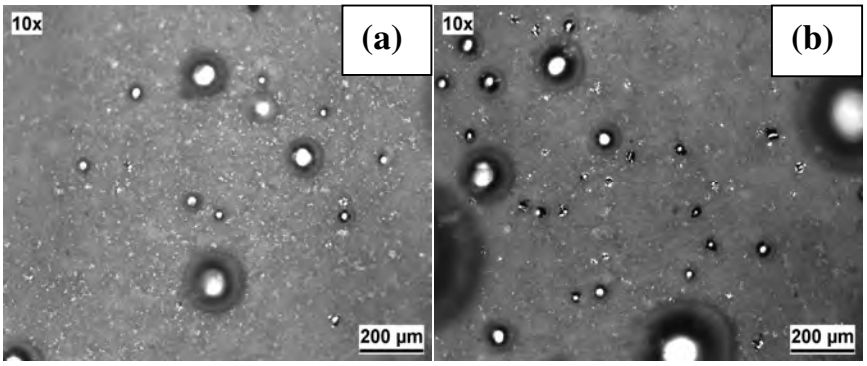

Fig. 7. 5 The optical micrograph of unpolished CLNT ceramics with (a) 25 and (b) 28 volume fraction of silver loading sintered at 1075°C/2hrs.

The escape of silver at higher sintering temperature is avoided by lowering the sintering temperature of ceramics below 950 °C by the addition of low melting glass. The sintering temperature of CLNT ceramics can be lowered below the melting point of silver with the addition of LBS glass which is explained in chapter 5. The sintering temperature of CLNT + LBS + Ag is optimized for best density and dielectric properties. The densification and relative permittivity of CLNT + 5 wt% LBS + Ag with different volume fraction of silver as a function of sintering temperature is shown in Fig. 7.6. It is observed that relative density increases first with increasing sintering temperature and then slightly decreases for all samples. The temperature at which maximum density attained varies with different volume fraction of silver loading in CLNT + 5 wt% LBS composites. The optimum sintering temperature of CLNT + 5 wt% LBS + Ag composite up to 0.15 volume fraction of silver loading was found to be 925 °C/2hrs and that of composites with higher volume fraction of silver (0.16 volume fraction onwards) is found to be 900 °C/2hrs. Addition of silver further reduces the sintering temperature. It is found that more than 90% of the relative density is attained at 900 °C, which is well below the melting point of silver. Hence,

the detailed study of the CLNT+5 wt% LBS +Ag composite is done at its corresponding optimum sintering temperature.

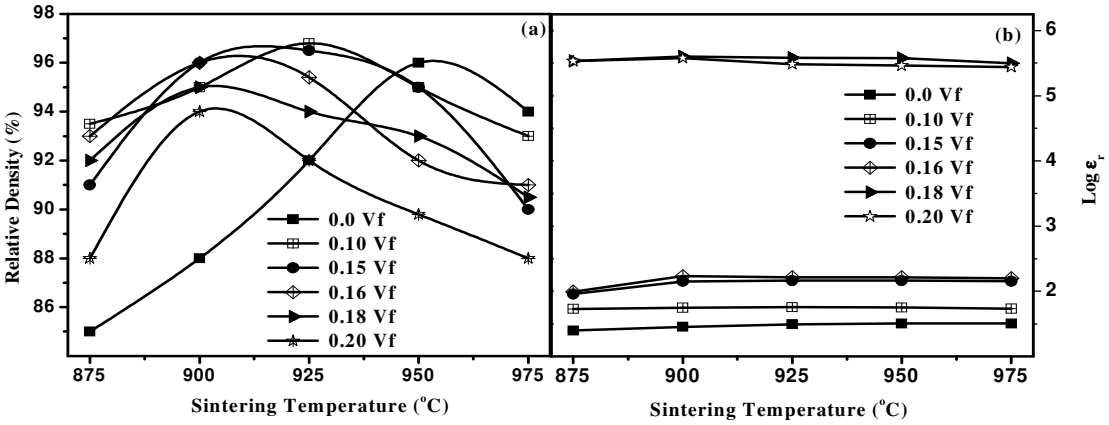

Fig. 7.6 The variation of (a) relative density and (b) relative permittivity of CLNT + 5 wt% LBS + Ag with different volume fraction of silver as a function of sintering temperature.

The variation of relative permittivity, dielectric loss and conductivity of CLNT + 5 wt% LBS + Ag composite with different volume fraction of silver at 100 KHz and 1 MHz are shown in Fig. 7.7. It is observed that 0.17 volume fraction silver loading increased the relative permittivity of the composite from 32 to 272 with dielectric loss of 10^{-3} and conductivity of 1.8×10^{-7} S/cm at 1 MHz. However, a maximum relative permittivity of $\varepsilon_r \approx 4 \times 10^5$ were observed for 0.18 volume fraction of silver loading. It is reported that silver particles are primarily located at grain boundaries when sintering is performed around 900 °C [41]. The sudden increase in relative permittivity is due to the interfacial polarization phenomenon which occurs at the interface of the dissimilar materials [58]. The charge carriers in the different phases of the composite are trapped at the interfaces within the dielectrics. These charges are unable to discharge freely and give rise to an over all field distortion, which results in an increase in capacitance and relative permittivity [10, 59]. Interfacial polarization is the result of the heterogeneity

of the system, such as mobile charges accumulated at the metal matrix interface, form large dipoles. Another reason for the enhancement of relative permittivity is the formation of micro capacitors. There are regions in the microstructure where the conductive clusters are separated by a thin insulating layer [13]. The silver particles in the composites act as internal electrodes of unit micro-capacitor. Such regions contribute to extremely large capacitance, which adds up macroscopically and result in a giant effective relative permittivity. It can be seen from Fig. 7.7(b) that the dielectric loss also increases sharply at percolation threshold. The addition of silver increases the defects and induces space charge. Therefore the increase in dielectric loss could be due to increase in metallic silver in the composite. It is well known that ceramic metal composite can have insulator-metal transition with increasing metal concentration. An abrupt change in conductivity at percolation in CLNT + 5wt% LBS + Ag composite with different volume fractions of silver is shown in Fig. 7.7(c). The concentration of the conductive inclusions has been proved to be a crucial parameter, governing the electrical behavior of the composites. When the filler content is low, the mean distance between metal particles or clusters is sufficiently large and conductance is restricted by the presence of the dielectric matrix. However, by increasing the conductive phase content, the metal ''islands'' get closer and at a critical concentration of the filler, a physical path is formed, through which the current can flow percolating the whole system. In such a network there is either direct contact between the adjacent conducting particles or sufficiently small gap between them to enable a mechanism of jump over the potential barrier and quantum mechanical tunnelling. The insulator-metal transitions are characterized by an abrupt change in conductivity [17, 18, 33, 60].

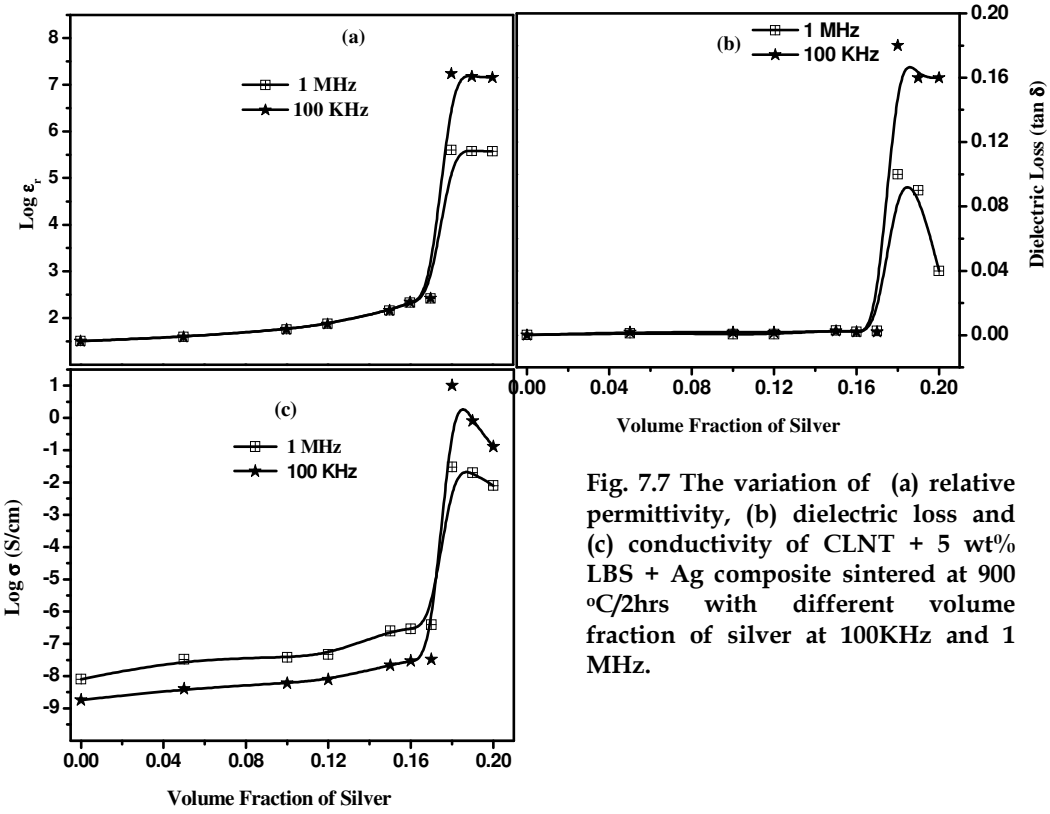

Fig. 7.7 The variation of (a) relative permittivity, (b) dielectric loss and (c) conductivity of CLNT + 5 wt% LBS + Ag composite sintered at 900 ^{o}C/2hrs with different volume fraction of silver at 100KHz and 1 MHz.

Figure 7.8 shows both experimental and theoretical values of relative permittivity of CLNT + 5wt% LBS + Ag composite with different volume fraction of silver at 1 MHz. It is observed that as the silver content increases from 0 to 0.16-volume fraction, the relative permittivity increases from 32 to 221 with dielectric loss of 10^{-3}. The concentration dependence of relative permittivity is given by the following power law on the basis of percolation theory [15, 22].

$$\varepsilon(v) = \varepsilon_o \left(\frac{V_c - V}{V_c} \right)^{-q} \text{------(7.1)}$$

where ε_o is the relative permittivity of pure silver free CLNT + 5wt% LBS, V_c is the volume fraction of silver at percolation, V is the volume fraction of

silver and q is a critical exponent. The experimental values of effective relative permittivity are in agreement with equation-7.1, with q=0.86 and V_c=0.17 as can be seen from Fig. 7.8.

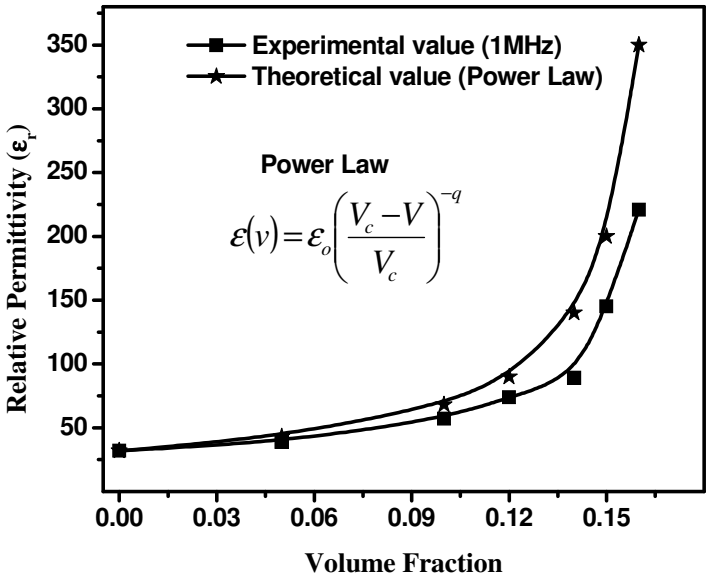

Fig. 7.8. Variation of relative permittivity of CLNT + 5wt% LBS + Ag composites with different volume fraction of silver below percolation threshold and the comparison with power law.

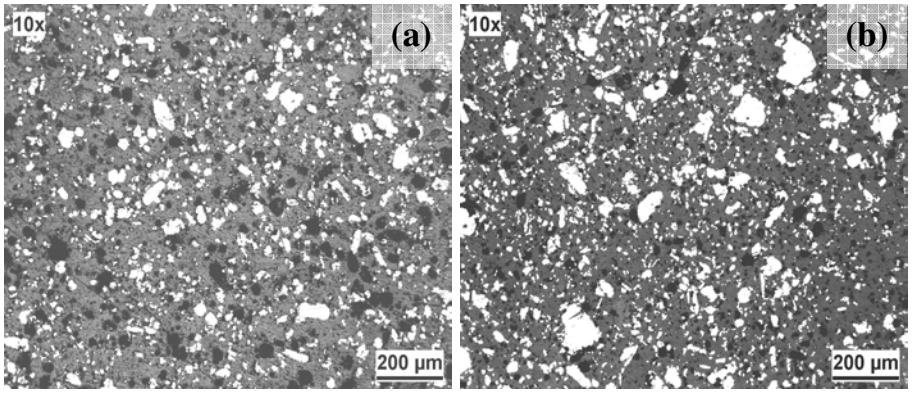

Fig. 7.9 The optical micrograph of polished CLNT + 5 wt% LBS + (a) 0.17 V_f and (b) 0.20 V_f of Ag composites sintered at 900° C /2hrs.

Figure 7.9 shows the optical micrograph of sintered CLNT + 5 w% LBS + Ag composite with 0.17 and 0.20 volume fraction of silver. It can be

noted that silver particles (white area) are distributed in CLNT matrix and some silver particles are lost during polishing (black area). It clearly reflects the dispersion of Ag particle in the CLNT matrix and there is no apparent interconnection among silver particles. However, above percolation threshold (0.17) the silver particles agglomerated to become larger size as shown in Fig. 7.9(b).

Figure 7.10 (a) shows the variation of relative permittivity of sintered CLNT + 5wt% LBS + Ag composites with frequency for different volume fraction of silver. As described earlier the relative permittivity increases gradually with silver content when the volume fraction is less than the percolation limit. When the silver content is beyond the percolation limit, the relative permittivity also increases by several orders of magnitude. It is found that relative permittivity decreases with increase in frequency above percolation threshold. It is well known that the polarization mechanism has strong dependence on the frequency. The direct relation to polarization, relative permittivity can have strong frequency variation as different polarization mechanisms become active. The variation of conductivity of sintered CLNT + 5wt% LBS + Ag composites with frequency for different volume fractions of silver are shown in Fig. 7.10 (b). It can be noticed that as the silver content in the composite increases the conductivity also increases. Composites containing silver less than the percolation limit, show gradual increase in conductivity while those with more silver than the percolation limit show conductivity values that are several orders higher. As the frequency increases, the conductivity increases to a maximum value for composites containing less silver than that of the percolation limit. However, subsequent increase in silver content in the composite beyond the percolation limit decreases the conductivity with increase in frequency. Below percolation threshold, as the frequency increases, the current passing through the each capacitor increases resulting in the increased conductivity

of the sample. To describe the frequency dependent conductivity, over a wide range of frequencies, in disordered solids at constant temperature Dyre [61, 62] proposed the random free-energy barrier model (also referred to as the symmetric hopping model). The conductivity values are increasing with frequency, since alternating current conductivity sums all dissipative effects including an actual ohmic conductivity, caused by migrating charge carriers on isolated metallic clusters, as well as a frequency dielectric dispersion [63]. According to percolation theory below percolation threshold, the conductivity is proportional to applied frequency ($\sigma = f^{x}$, where f is the frequency and x is the critical exponent) [64]. The frequency dependence of relative permittivity and conductivity of disordered solids generally results from the polarization between the clusters and anomalous diffusion within each cluster. The capacitive effect between clusters on the conductivity and relative permittivity becomes significant at high frequency.

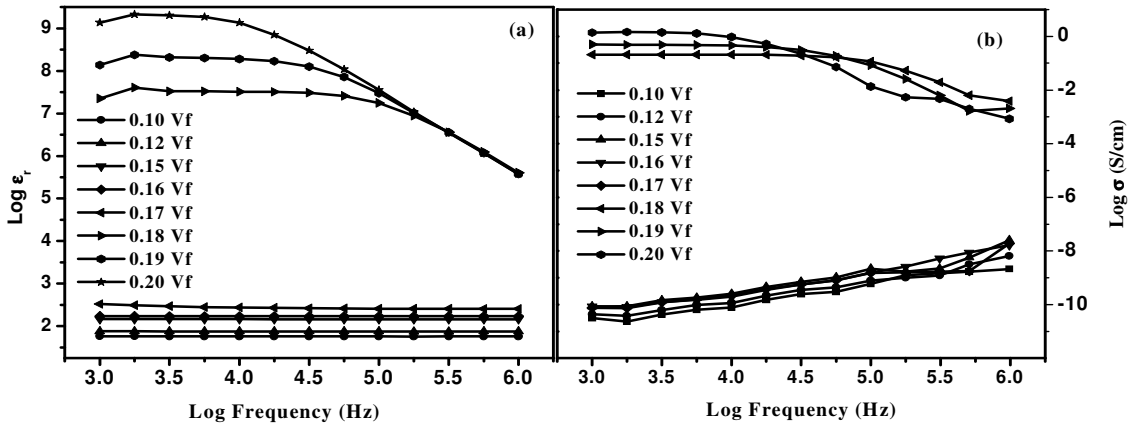

Fig. 7.10 The variation of (a) relative permittivity (b) conductivity of sintered CLNT + 5 wt% LBS + Ag composites with different volume fraction of silver as a function of frequency.

Figure 7.11 shows the temperature dependence of relative permittivity of CLNT +5 wt% LBS + Ag composites with different volume

fraction of silver measured at 1 MHz. It is clear that for all the volume fractions of silver, the relative permittivity is independent of temperature.

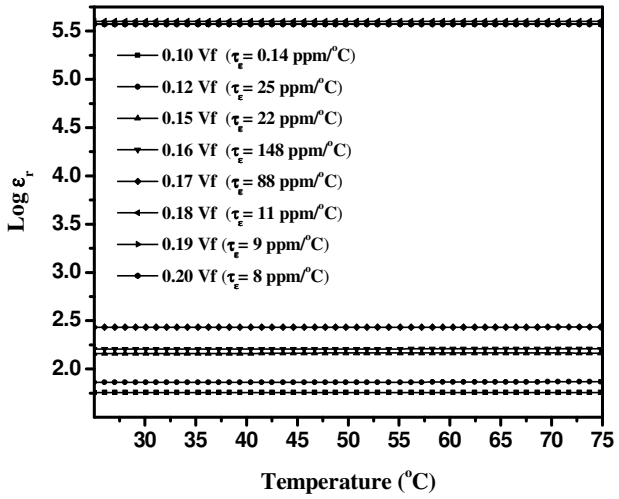

Fig. 7.11 The temperature dependence of relative permittivity of CLNT +5 wt% LBS + Ag composites with different volume fraction of silver measured at 1 MHz.

The percolative composites show an abrupt rise in the permittivity near percolation threshold and have a narrow smearing region [23, 25, 28, 29, 33]. The region at which percolation starts is called the smearing region. In these composites, it is very difficult to control the filler loading very close to the percolation threshold to achieve high relative permittivity. This can be alleviated by the introduction of third component (ceramic) in the polymer-metal composites. This polymer based three phase composite has an additional advantage of low processing temperature. The giant permittivity of polymer-ceramic-metal composite is discussed in the next section.

7.3 Polymer-Ceramic-Metal Three-Phase Composite for Embedded Capacitor Applications

7.3.1 Introduction

The fundamental building component of all electronic packaging system consists of active and passive components. Majority of the electronic component in microelectronic circuits are passive and occupy more than 80% of the printed wired surface area. Discrete passives have already become the major barrier for the miniaturization of the electronic system.

Integration of embedded passive components into printed circuit board offers a significant reduction in size, better electrical performance, reliability, lower costs and improved design options. Among embedded passive components, the embedded capacitor is particularly favorable because they are used in large numbers of various functions such as decoupling, bypassing, energy storage and filtering capacitors [1, 3, 50, 65]. One major challenge for implementing the embedded capacitor technology is the development of new dielectric material that possesses good dielectric and mechanical properties and processabilities. Recently significant efforts have been focused on developing percolative composites that are suitable for a dielectric material as capacitor in embedded passive devices. Ceramic metal composites show high relative permittivity but the processing temperature is too high hence it cannot be used for printed wired board compatible devices. Polymer-metal and ceramic-metal composites show an abrupt rise in the permittivity near percolation threshold and have a narrow smearing region [23, 28, 29, 33]. The narrow percolation transition region in the polymer metal and ceramic metal has limited their applications in embedded passive devices. In these composites, it is very difficult to control the filler loading very close to the percolation threshold to achieve high relative permittivity. Recently, Lim et. al [66] reported that the smearing region can be expanded by introducing a third component in the two phase composite. This three phase polymer based composite is advantageous in terms of its broad smearing region, good dielectric properties, low processing temperature, ease of fabrication in to various shapes and the compatibility with PWB.

The present section discusses the synthesis and dielectric properties of three-phase composite containing epoxy as the polymer base and silver and $Ca[(Li_{1/3}Nb_{2/3})_{0.8}Ti_{0.2}]O_{3-\delta}$ (CLNT) [56] ceramic as the filler. In this three-phase composite, temperature stable low loss CLNT ceramics is used as the

dielectric filler and silver as the conducting phase to improve the dielectric properties of the composites. Epoxy was taken as the polymer base because it is thermosetting and can be easily fabricated in to various shapes. This three phase composite can be treated as the adhesion of ceramic and metal using polymer to achieve high relative permittivity with low processing temperature. Such a three phase polymer matrix composite is flexible and can be easily fabricated in to various shapes with low processing temperature. It might be an attractive for applications in capacitors and electric energy storage devices.

7.3.2. Experimental

The epoxy-CLNT-Ag three-phase composites were prepared by two step mixing and thermosetting method. The low loss CLNT ceramics were prepared by solid state ceramic route. Different volume fractions of fine powders of sintered CLNT ceramics, epoxy and hardener were mechanically mixed for 30 minutes to have uniform distribution of ceramic powder in the matrix. The mixture was then poured into a cylindrical mold of 10 mm diameter and 2 mm thickness. These samples were cured at 70 ^{o}C for 2 hours. A series of CLNT/epoxy composite with CLNT volume varying from 0.0 to 0.40 volume fractions were fabricated. Epoxy with 0.30 volume fractions of CLNT was considered for further studies to visualize the effect of metallic inclusions on the dielectric properties of three-phase composites. The epoxy-CLNT-Ag composites in which the volume fraction of Ag is varying from 0.0 to 0.32 were prepared. Copper electrodes were connected to both sides of the polished compacts using silver paste and these samples were used for measuring the dielectric properties. The dielectric properties (1 KHz to 1 MHz) were measured using LCR meter (HIOKI 3532-50 LCR Hi TESTER, Japan). The surface morphology of the samples was studied using an optical microscope (Leica, DMRX, Germany). The variation in relative

permittivity with temperature was also investigated for the composites in the temperature range -50 to +100 ^{o}C.

7.3.3. Results and Discussion

Fig. 7.12 shows the variation of dielectric properties of epoxy-CLNT two phase composites with different volume fraction of the CLNT loading. A gradual increase in relative permittivity with CLNT loading is observed in the epoxy-CLNT polymer ceramic composite. The resultant properties of the composites mainly depend on the properties of constituent components. The increase in the relative permittivity of the epoxy-CLNT composite is due to the relatively high permittivity of CLNT ceramic (41 at 1 MHz) compared to epoxy. In addition, the increase of CLNT filler content in the composite increases the interface between CLNT and polymer and hence the significant influence of interfacial polarization on the relative permittivity [60]. Thus the relative permittivity increases with increase in ceramic loading. Generally, the dielectric loss of almost all the polymer ceramic composites increases with increase in ceramic filler loading. However, in the present epoxy-CLNT composite the dielectric loss decreases with ceramic loading. This could be due to the low dielectric loss of CLNT ceramic (tan $\delta = 10^{-4}$) compared to that of epoxy (tan $\delta = 10^{-2}$). For 0.3 volume fraction of CLNT ceramic loading, the epoxy-CLNT composite shows ε_r = 8.0 with tan δ = 0.009 at 1 MHz. As the volume fraction increases the agglomeration of ceramic particle also increases, which results in higher porosity and thereby decreases the densification. This could be the reason for the slight increase in the dielectric loss at higher volume fraction (V_f = 0.40) of CLNT loading in epoxy-CLNT composite. It is observed that the addition of 0.40 volume fraction of CLNT ceramics in the epoxy increases the relative permittivity from 4.3 to 10.2. It has been reported that higher ceramic loading is necessary to enhance the relative permittivity in the polymer ceramic composite for embedded capacitor applications [1]. However, higher ceramic loading dramatically

decreases the adhesion of the composite, which will degrade its processability and reliability of embedded capacitors. Therefore, a limitation of ceramic loading is existing for polymer-ceramic composite to improve its relative permittivity. The relative permittivity of the polymer-ceramic composites can be enhanced further by incorporating conducting phase in the two phase composites. Hence we have added metallic silver as a conducting phase in epoxy with 0.30 volume fraction of CLNT ceramics.

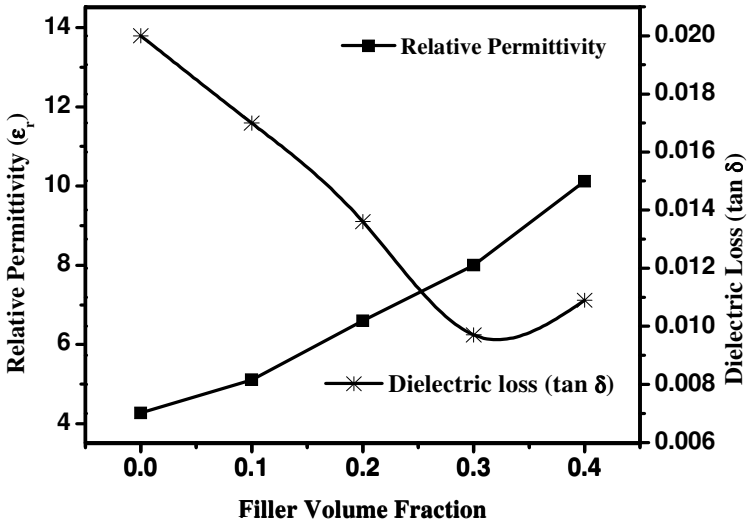

Fig. 7.12 Variation of relative permittivity and dielectric loss of epoxy-CLNT composites at 1 MHz as a function of filler loading.

Table 7.1 shows the dielectric properties and conductivity of epoxy-CLNT-Ag composite with different volume fraction of silver loading at 1 KHz and 1 MHz. The increase in relative permittivity with silver loading is a result of interfacial polarization associated with the entrapment of free charges generated in the interface of conducting and insulating phase of the composites. The dielectric response of the specimens is attributed to interfacial polarization or Maxwell–Wagner–Sillars (MWS) effect. The MWS effect arises in heterogeneous systems due to the accumulation of charges at the interface of the constituents. The charges can migrate under the influence of the applied field contributing to the electrical response of the system.

These charges are unable to discharge freely and give rise to an overall field distortion. This dielectric field developed around the conducting phase can result an increase of relative permittivity [10].

Table 7.1 The dielectric properties and conductivity of epoxy-CLNT-Ag composites at 1 kHz and 1 MHz

Volume fraction of Silver	ε_r (1 kHz)	Tan δ (1 kHz)	σ (S/cm) (1 kHz)	ε_r (1 MHz)	Tan δ (1 MHz)	σ (S/cm) (1 MHz)
0	8.4	0.013	6.26×10^{-11}	8.00	0.009	4.30×10^{-8}
0.05	11.5	0.011	6.45×10^{-11}	10.8	0.020	1.30×10^{-7}
0.08	14.6	0.030	2.67×10^{-10}	13.1	0.023	1.79×10^{-7}
0.10	16.8	0.019	6.15×10^{-10}	15.4	0.024	2.08×10^{-7}
0.12	18.4	0.026	8.75×10^{-10}	16.6	0.027	2.54×10^{-7}
0.14	22.1	0.030	7.53×10^{-10}	19.1	0.032	3.47×10^{-7}
0.16	23.0	0.026	9.31×10^{-10}	20.2	0.032	4.24×10^{-7}
0.18	24.1	0.025	1.06×10^{-9}	22.1	0.039	6.21×10^{-7}
0.20	30.4	0.025	1.44×10^{-9}	26.4	0.042	7.09×10^{-7}
0.22	34.8	0.031	1.93×10^{-9}	29.3	0.060	9.54×10^{-7}
0.24	65.0	0.065	2.41×10^{-9}	51.1	0.069	1.87×10^{-6}
0.26	95.0	0.090	6.7×10^{-9}	72.3	0.065	2.51×10^{-6}
0.28	550	0.870	5.9×10^{-7}	142	0.15	2.05×10^{-5}
0.30	9.73×10^{8}	4.400	2.9×10^{-2}	818000	2.6	2.80×10^{-2}
0.32	4.46×10^{6}	9.900	1.29	510000	9.9	1.31

The existence of large number of conducting particles in parallel and blocked by thin insulating layers can also increase the relative permittivity [13]. Each conducting phase in the composites acts as an internal electrode of tiny capacitors. Hence the Ag-CLNT-Ag forms a microcapacitor and these tiny microcapacitors are connected each other by epoxy. These tiny super

capacitor networks with large electrode area and small dielectric thickness macroscopically add up to result giant permittivity. The addition of silver increases not only the permittivity but also the dielectric loss. The conduction is the dominative mechanism near percolation threshold, so the dielectric loss increases as the content of conductive filler increases. The increase in dielectric loss in the present three phase composite could also be due to the increase in defects concentration and induced space charge with silver loading. It can also be useful for number of applications such as flash lamp and heart actuators working at low frequency for which large capacitance is more important than dielectric loss [49]. As the volume fraction of silver is increased, the conductive phase has a tendency to connect to form a conductive network. Above percolation limit, there is a continuous path of adjacent allowed sites across the system. This leads to a sudden increase in conductivity of the composite above percolation threshold.

Generally, percolation threshold of both the ceramic-metal and polymer-metal composites is around 0.16 volume fraction of metal and have a narrow smearing region. However, in the present three-phase composite, the ceramic particle effectively isolates the silver particles and extends the smearing region of present high permittivity composite. Addition of 0.28 volume fraction of silver in epoxy-CLNT composite increases the relative permittivity from 8.4 to 550 at 1 KHz and 8 to 142 at 1 MHz respectively with low dielectric loss and low conductivity. The increase in the capacitance and relative permittivity is not particular to a given composition of a particular dielectric material, but depends only on the microstructure of the aggregate and on the ratio between the conducting and insulating phase.

The present epoxy-CLNT-Ag three phase composite can be considered as the loading of conducting silver particle in the insulating epoxy-CLNT phase. Fig. 7.13 shows both experimental and theoretical

values of relative permittivity of epoxy-CLNT- Ag composite with different volume fraction of silver at 1 MHz. It is observed that as the silver content increases from 0 to 0.26-volume fraction, the relative permittivity of the epoxy-CLNT composite increases from 8 to 73. The concentration dependence of relative permittivity is given by the following power law on the basis of percolation theory (equation 7.1) [15, 22]. In this case ε_o is the relative permittivity of pure silver free epoxy-CLNT composite, V_c is the volume fraction of silver at percolation, V is the volume fraction of silver and q is a critical exponent. The experimental values of effective relative permittivity are in agreement with equation-7.1, with q=0.86 and V_c=0.28 as can be seen from Fig. 7.13.

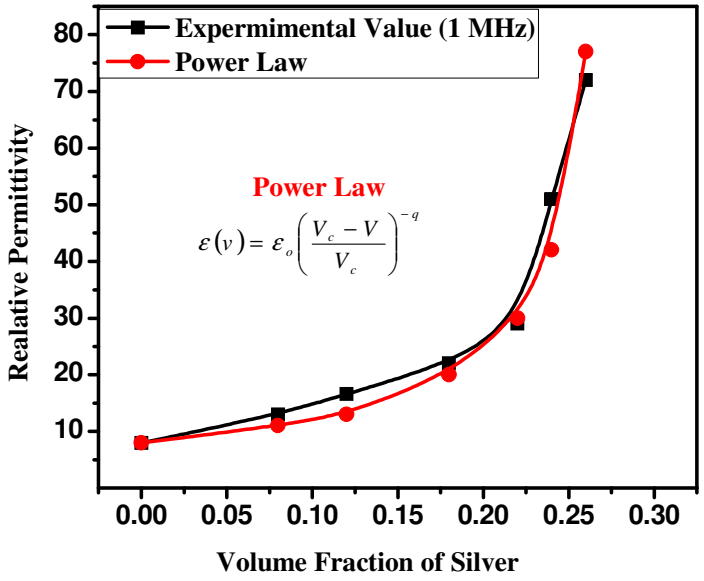

Fig. 7.13 Variation of relative permittivity of epoxy-CLNT-Ag composites with different volume fraction of silver below percolation threshold and the comparison with power law.

Figure 7.14 shows the optical micrograph of epoxy-CLNT-Ag composite with (a) 0.10 and (b) 0.20 volume fraction of Ag. The silver particles and CLNT ceramics are distributed randomly in the epoxy matrix and no apparent interconnection is observed among silver particles.

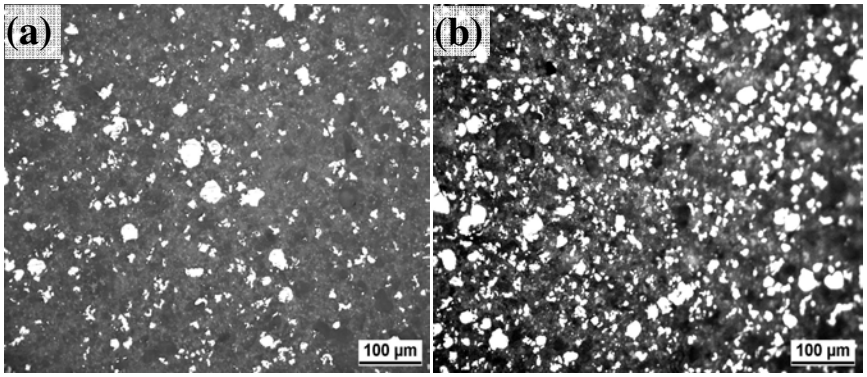

Fig. 7.14 Optical micrograph of epoxy-CLNT- Ag composite having (a) 0.10 and (b) 0.20 V_f of silver

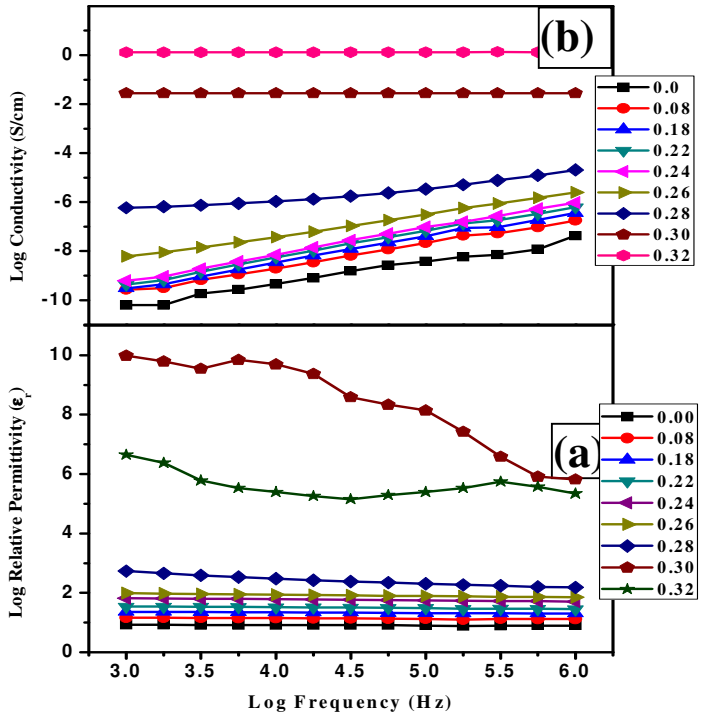

Fig. 7. 15 Variation of (a) relative permittivity and (b) conductivity of epoxy-CLNT-Ag composites as a function of frequency.

Figure 7.15 shows the frequency dependence of both relative permittivity and conductivity of epoxy-CLNT-Ag composite. A gradual decrease in the relative permittivity with frequency is observed for all the composites. This is expected since different polarization mechanisms are frequency dependent. It has been reported that the gradual decrease of permittivity with frequency was due to an interfacial polarization [30, 60, 67]. The interfacial polarization effect is a slow process and is predominant at low frequency region. It can be observed that the conductivity increases with increase in frequency for low volume fraction of silver loading. At low frequencies where the applied electric field, forces the charge carriers to drift over large distance [61]. As the frequency increases, the mean displacement of the charge carriers is reduced and the real part of conductivity increases, which follows the law $\sigma = f^{x}$, where f is the frequency and x is the critical exponent ($0 \leq x \leq 1$) [64]. The frequency dependence of relative permittivity and conductivity of disordered solids generally results from the polarization between the clusters and anomalous diffusion within each cluster.

The drift in relative permittivity with temperature should be small for practical applications. Fig. 7.16 shows the variation of relative permittivity in epoxy-CLNT-Ag composite as a function of temperature. The relative permittivity of the composite is found to be independent of temperature and it satisfies X7R EIA specifications. In ceramic-metal and polymer-metal composites, above percolation threshold the conductivity is also increased. This may lead to undesirable leakage current in the composite. However, the composite for 0.28 volume fraction of silver loading in epoxy-CLNT composite shows excellent dielectric properties such as high permittivity, low conductivity and low processing temperature and hence this composition is suitable for embedded capacitor applications.

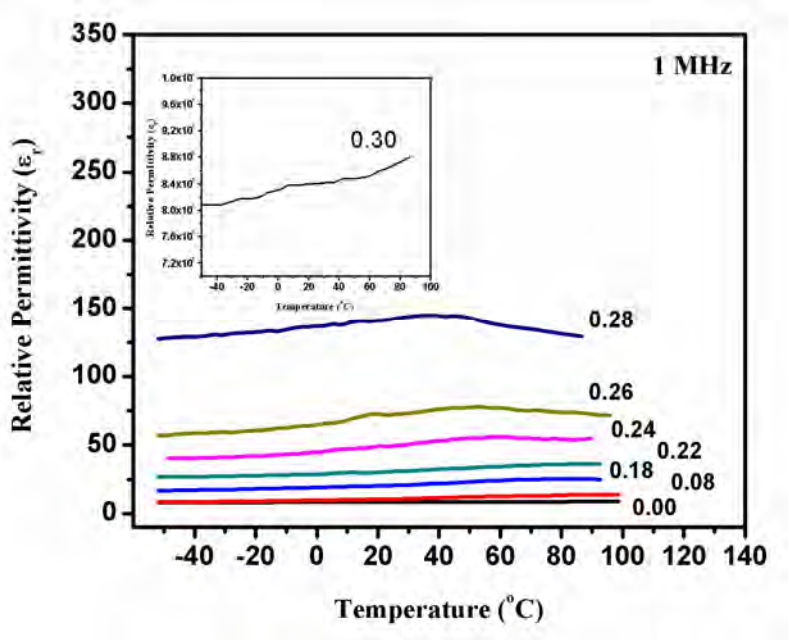

Fig. 7.16 Variation of relative permittivity of epoxy-CLNT-Ag composites with temperature and the inset shows the variation of relative permittivity for 0.30 volume fraction of silver loaded epoxy-CLNT-Ag composite.

7.4. Conclusions

- The high permittivity ceramic-metal and polymer-ceramic-metal composite for microelectronic application have been investigated.
- The sintering temperature of ceramic metal composite is found to have strong dependence on the percolation threshold.
- Addition of 0.17-volume fraction of silver increases the relative permittivity of CLNT + 5 wt% LBS from 32 to 272 with dielectric loss of 10^{-3} and conductivity of 1.8 x 10^{-7} S/cm at 1 MHz. 0.18-volume fraction of silver loading in CLNT + 5 wt% LBS composite shows a maximum relative permittivity ($\varepsilon_r \approx 4x10^5$) with low dielectric loss ($\tan\delta \approx 10^{-2}$) at 1 MHz.

- The high processing temperature of the ceramic metal composite have been overcome by the preparing polymer-ceramic-metal three phase composite.
- Near percolation threshold (0.28 volume fraction of Ag in epoxy+0.30 V_f of CLNT) the composite shows a relative permittivity of 142 with low dielectric loss (0.15) and low conductivity (10^{-5} S/cm) at 1 MHz.
- The experimentally observed relative permittivity of ceramic-metal and polymer-ceramic-metal composites is in agreement with power law.
- The relative permittivity of the composite is found to be independent of temperature.

References

1. S. K. Bhattacharya and R. R. Tummala, *J. Mater. Sci. Mater. Elect.*, **11**, 253, (2000).
2. S. K. Bhattacharya and R. R. Tummala, *Microelectronics Journal*, **32**, 11, (2001).
3. F. T. Chen, C. W. Chu, J. He, Y. Yang and J. L. Lin, *Appl. Phys. Lett.*, **85**, 3295, (2004).
4. C. Huang, Q. M. Zhang, G. deBotton and K. Bhattacharya, *Appl. Phys. Lett.*, **84**, 4391, (2004).
5. Y. Rao, S. Ogitani, P. Kohl and C. P. Wong, *J. Appl. Poly. Sci.*, **83**, 1084, (2002).
6. M. Arbatti, X. Shan and Z. Cheng, *Adv. Mater.*, **19**, 1369, (2007).
7. Z. Y. Cheng, R. S. Katiyar, X. Yao and A. Q. Guo, *Phys. Rev. B*, **55**, 8165, (1997).
8. N. Duan, J. E. Ten Elshof, H. Verweij, G. Greuel and O. Dannapple, *Appl. Phys. Lett.*, **77**, 3263, (2000).
9. J. F. Li, K. Takagi, N. Terakubo and R. Watanabe, *Appl. Phys. Lett.*, **79**, 2441, (2001).
10. P. Chylek and V. Srivastava, *Phys. Rev. B.*, **30**, 1008, (1984).
11. Z. M. Dang, Y. H. Lin and C. W. Nan, *Adv. Mater.*, **15**, 1625, (2003).
12. C. Pecharroman, F. Esteban-Betegon, J. F. Bartolome, S. Lopez-Esteban and J. S. Moya, *Adv. Mater.*, **13**, 1541, (2001).
13. C. Pecharroman and J. S. Moya, *Adv. Mater.*, **12**, 294, (2000).
14. J. W. Xu and C. P. Wong, *Appl. Phys. Lett.*, **87**, 082907, (2005).
15. D. M. Grannan, J. C. Garland and D. B. Tanner, *Phys. Rev. Lett.*, **46**, 375, (1981).
16. M. B. Heaney, *Phys. Rev., B*, **52**, 12477, (1995).
17. H. F. Hess and K. DeConde, *Phys Rev B*, **25**, 5578, (1982).
18. S. Kirkpatrick, *Rev. Mod. Phys*, **45**, 574, (1973).
19. A. K. Sarychev and F. Brouers, *Phys. Rev. Lett.*, **73**, 2895, (1994).
20. Y. Song, T. W. Noh, S. Lee and J. R. Gaines, *Phys. Rev. B.*, **33**, 904, (1986).
21. D. Wilkinson, J. S. Langer and P. N. Sen, *Phys Rev B*, **28**, 1081, (1983).
22. E. L. Efors and B. I. Shktovskii, *Phys. Stat. Solidi. B*, **76**, 475, (1976).
23. S. George, J. James and M. T. Sebastian, *J. Am. Ceram. Soc.*, **90**, 3522, (2007).
24. Y. Bai, Z. Y. Cheng, V. Bharti, H. S. Xu and Q. M. Zhang, *Appl. Phys. Lett.*, **76**, 3804, (2000).
25. K. S. Deepa, M. T. Sebastian and J. James, *Appl. Phys. Lett.*, **91**, 202904, (2007).

26. Y. Rao, S. Ogitani, P. Kohl and C. P. Wong, *Int. Symp. Adv. Pack. Mater.: Processes, Properties and Interfaces, Proceedings*, 32-37, (2000).

27. G. Subodh, V. Deepu, P. Mohanan and M. T. Sebastian, *Appl. Phys. Lett.*, **95**, 062903, (2009).

28. C. Huang and Q. M. Zhang, *Adv. Funct. Mater.*, **14**, 501, (2004).

29. C. Huang, Q. M. Zhang and J. Su, *Appl. Phys. Lett.*, **82**, 3502, (2003).

30. X. Y. Huang, P. K. Jiang and U. C. Kim, *J. Appl. Phys.*, **102**, 124103-1, (2007).

31. J. Y. Li, C. Huang and Q. M. Zhang, *Appl. Phys. Lett.*, **84**, 3124, (2004).

32. Y. Li, S. Pothukuchi and C. P. Wong, *9th Int. Symp. Adv. Pack. Mater.: Processes, Properties and Interfaces, Proceedings*, 175-181, (2004).

33. J. Lu, K. S. Moon and C. P. Wong, *J. Mater. Chem.*, **18**, 4821, (2008).

34. J. Lu, K. S. Moon, J. Xu and C. P. Wong, *J. Mater. Chem*, **16**, 1543, (2006).

35. L. Qi, B. I. Lee, S. Chen, W. D. Samuels and G. J. Exarhos, *Adv. Mater.*, **17**, 1777, (2005).

36. J. W. Xu, K. S. Moon, C. Tison and C. P. Wong, *IEEE Trans. Adv. Pack.*, **29**, 295, (2006).

37. K. S. Deepa, S. Nisha, P. Parameswaran, M. T. Sebastian and J. James, *Appl. Phys. Lett.*, **94**, 142902, (2009).

38. R. Z. Chen, X. H. Wang, Z. L. Gui and L. T. Li, *J. Am. Ceram. Soc.*, **86**, 1022, (2003).

39. W. W. Cho, I. Kagomiya, K. I. Kakimoto and H. Ohsato, *Appl. Phys. Lett.*, **89**, 152905-1, (2006).

40. N. Halder, A. Das Sharma, S. K. Khan, A. Sen and H. S. Maiti, *Mater. Res. Bull.*, **34**, 545, (1999).

41. H. J. Hwang, T. Nagai, T. Ohji, M. Sando, M. Toriyama and K. Niihara, *J. Am. Ceram. Soc.*, **81**, 709, (1998).

42. H. J. Hwang, K. Watari, M. Sando, M. Toriyama and K. Niihara, *J. Am. Ceram. Soc.*, **80**, 791, (1997).

43. H. J. Hwang, M. Yasuoka, M. Sando, M. Toriyama and K. Niihara, *J. Am. Ceram. Soc.*, **82**, 2417, (1999).

44. D. J. Lewis, D. Gupta, M. R. Notis and Y. Imanaka, *J. Am. Ceram. Soc.*, **84**, 1777, (2001).

45. P. H. Xiang, X. L. Dong, C. D. Feng, R. H. Liang and Y. L. Wang, *Mater. Chem. Phys.*, **97**, 410, (2006).

46. H. W. Choi, Y. W. Heo, J. H. Lee, J. J. Kim, H. Y. Lee, E. T. Park and Y. K. Chung, *Appl. Phys. Lett.*, **89**, 132910, (2006).

47. Z. M. Dang, Y. Shen and C. W. Nan, *Appl. Phys. Lett.*, **81**, 4814, (2002).

48. B. S. Prakash and K. B. R. Varma, *Comp. Sci. Tech.*, **67**, 2363, (2007).

49. L. Qi, B. I. Lee, W. D. Samuels, G. J. Exarhos and S. G. Parler, *J. Appl. Poly. Sci.*, **102**, 967, (2006).

50. Y. Rao, S. Ogitani, P. Kohl and C. P. Wong, *50th Electronic Components & Technology Conference - 2000 Proceedings*, 183-187, (2000).

51. J. W. Xu, S. Bhattacharya, P. Pramanik and C. P. Wong, *J. Electr. Mater.*, **35**, 2009, (2006).

52. C. Y. Chen and W. H. Tuan, *J. Am. Ceram. Soc.*, **83**, 1693, (2000).

53. S. Y. Cho, H. J. Youn, D. W. Kim, T. G. Kim and K. S. Hong, *J. Am. Ceram. Soc.*, **81**, 3038, (1998).

54. S. Panteny, C. R. Bowen and R. Stevens, *J. Mater. Sci.*, **41**, 3845, (2006).

55. S. Panteny, R. Stevens and C. R. Bowen, *Integrated Ferroelectrics*, **63**, 643, (2004).

56. J. W. Choi, C. Y. Kang, S. J. Yoon, H. J. Kim, H. J. Jung and K. H. Yeon, *J. Mater. Res.*, **14**, 3567, (1999).

57. S. Panteny, C. R. Bowen and R. Stevens, *J. Mater. Sci.*, **41**, 3837, (2006).

58. S. H. Foulger, *J. Poly. Sci. Part B-Poly. Phys.*, **37**, 1899, (1999).

59. W. J. Kaiser, E. M. Logothetis and L. E. Wenger, *J. Phys. C: Solid State Phys.*, **18**, L 837, (1985).

60. X. Huang, J. Jiang, C. Kim, Q. Ke and G. Wang, *Comp. Sci. Tech.*, **68**, 2134, (2008).

61. J. C. Dyre and T. B. Schrøder, *Rev. Mod. Phys*, **72**, 873, (2000).

62. J. C. Dyre and T. B. Schrøder, *phys. Stat. Sol. B*, **230**, 5, (2002).

63. G. C. Psarras, *Comp. Part A-Appl. Sci. Manuf.*, **37**, 1545, (2006).

64. C. W. Nan, *Progress in Mater. Sci.*, **37**, 1, (1993).

65. J. X. Lu and C. P. Wong, *IEEE Trans. Diele. Elect.l Insu.*, **15**, 1322, (2008).

66. E. S. Lim, J. C. Lee, J. J. Kim, E. T. Park, Y. K. Chung and H. Y. Lee, *Integrated Ferroelectrics*, **74**, 53, (2005).

67. R. Popielarz and C. K. Chiang, *Mater. Sci. Engg. B*, **139**, 48, (2007).

Chapter 8

Conclusions and Scope of Future Work

This chapter provides a brief summary of the thesis and future direction of the work. The major results in thesis is outlined as chapter wise and also highlighted in table.

In wireless communication industry, dielectric materials are being used as electronic packages, substrates, dielectric resonators, waveguides, dielectric resonator antenna and capacitor applications etc. The value of relative permittivity of the dielectric material mainly distinguishes its use in above mentioned application. The thesis entitled "**Investigations on Low Dielectric Loss Lithium Based Ceramics and Their Composites for Microwave and Embedded Passive Applications"** is divided into 8 chapters. It is the outcome of a detailed investigation carried out on the synthesis and characterization of several low loss ceramics and composites for substrate, LTCC, dielectric resonators and capacitor applications.

The first chapter of the thesis gives a general introduction to dielectric substrates, resonators and composites. Emerging technologies such as low temperature co-fired ceramic and embedded capacitor technology for miniaturization and its requirements and advantages are also discussed in this chapter. The preparation and characterization techniques used for the microwave dielectric ceramics and polymer ceramic composite are given in the chapter 2.

The chapter 3 discusses the synthesis, characterization and microwave dielectric properties of novel low loss low permittivity Li_2ASiO_4 (A=Mg and Ca) ceramics for microwave substrate applications. The effects of synthesis condition on the microwave dielectric properties of both the ceramics are discussed. The Li_2MgSiO_4 (LMS) ceramics sintered at 1250 ^oC/2hrs has ε_r = 5.1 and tan δ = $5x10^{-4}$ at 9 GHz. The Li_2CaSiO_4 ceramics sintered at 1000 ^oC/2hrs has ε_r = 4.4 and tan δ = 0.006 at 9 GHz. The influence of different borosilicate glass additions on the sinterability, densification, structure, microstructure and the microwave dielectric properties of the Li_2ASiO_4 (A=Mg and Ca) dielectric ceramics has been investigated. These ceramics show relative permittivity in the range 4-9 with low dielectric loss (tan $\delta \approx 10^{-4}$). Addition of 1 wt% LBS in LMS sintered at

925^{o}C/2hrs has ε_r = 5.5 and tan δ = 7x10^{-5} at 9 GHz. LMS mixed with 2 wt% of LMZBS glass sintered at 875^{o}C/2hrs shows ε_r = 5.9 and tan δ = 7x10^{-5} at 9 GHz. Addition of 2 wt % of LBS glass in LCS and sintered at 925 ^{o}C/2hrs has ε_r = 7.4 and tan δ = 0.005 at 9 GHz. Compared to LCS-glass composites, the LMS-glass composites show excellent microwave dielectric properties at a low sintering temperature and can be a promising candidate for substrate and LTCC based devices.

Fourth chapter discusses the synthesis, characterization and microwave dielectric properties of novel temperature stable high Q dielectric ceramics ($Li_2Mg_{1-x}Zn_xTi_3O_8$ (x=0 to 1) and $Li_2A_{1-x}Ca_xTi_3O_8$ (A=Mg, Zn, and x= 0 to 0.2)) which can be sintered at a low sintering temperature of 1075 ^{o}C/4hrs. An attempt has also been made to lower the sintering temperature of $Li_2MgTi_3O_8$ and $Li_2ZnTi_3O_8$ ceramics for the possible application in LTCC based devices. The $Li_2MgTi_3O_8$ and $Li_2ZnTi_3O_8$ ceramics shows ε_r = 27.2, Q_u x f = 42000 GHz, and τ_f = (+) 3.2 ppm/^{o}C and ε_r = 25.56, Q_u x f = 72000 GHz, and τ_f = (-) 11.2 ppm/^{o}C respectively when sintered at 1075 ^{o}C/4hrs. Among all the compositions of $Li_2Mg_{1-x}Zn_xTi_3O_8$ ceramics, the $Li_2Mg_{0.9}Zn_{0.1}Ti_3O_8$ dielectric ceramic composition shows the best dielectric properties such as ε_r = 27, Q_u x f = 62000 GHz, and τ_f = (+) 1.1 ppm/^{o}C when sintered at 1075 ^{o}C/4hrs. The effect of Ca substitution on the structure and microwave dielectric properties of $Li_2A_{1-x}Ca_xTi_3O_8$ (A=Mg, Zn, and x= 0 to 0.2 has been investigated and it is found that formation of second phase degrades the microwave dielectric properties slightly. Effect of LMZBS glass addition on the sinterability and microwave dielectric properties of $Li_2MgZnTi_3O_8$, $Li_2MgZnTi_3O_8$ dielectric ceramics has been investigated for LTCC applications. The LMT + 3 wt% of LMZBS glass sintered at 925 ^{o}C/4hrs has ε_r = 24.5, Q_u x f = 44000 GHz, and τ_f = (+) 0.25 ppm/^{o}C. Addition of LZT ceramics with 3 wt% of LMZBS glass sintered at 900 ^{o}C/4hrs has ε_r = 23.24, Q_u x f = 31300 GHz, and τ_f = (-) 15.6 ppm/^{o}C. The microwave dielectric

materials presented in this chapter are superior in terms of cost of raw materials, sintering temperature and microwave dielectric properties compared to the already developed microwave dielectric ceramics and these materials will be the major milestone in microwave dielectric resonator research.

The development of low temperature sintered low loss high permittivity microwave ceramics for resonator applications are discussed in the fifth chapter. The $Ca[(Li_{1/3}Nb_{2/3})_{0.8}Ti_{0.2}]O_{3-\delta}$ ceramics sintered at 1175 ^oC has ε_r = 38.6, $Q_u$xf = 21200 GHz and τ_f = +4 ppm/^oC. The $Ca[(Li_{1/3}Ta_{2/3})_{0.7}Ti_{0.3}]O_{3-\delta}$ ceramics sintered at 1200 ^oC has ε_r = 36.0, $Q_u$xf = 29500 GHz and τ_f = -3ppm/^oC. The influence of various borosilicate glasses on the sinterability, densification, structure and microstructure and the microwave dielectric properties of the $Ca[(Li_{1/3}A_{2/3})_{1-x}Ti_x]O_{3-\delta}$ (A=Nb,Ta) dielectric ceramics is investigated. The sintering temperature of $Ca[(Li_{1/3}Nb_{2/3})_{0.8}Ti_{0.2}]O_{3-\delta}$ (CLNT) ceramics is lowered below the melting point of silver by the addition of LBS, LMZBS and ZBS glasses. Among these the CLNT ceramics with 5 wt% of LBS glass sintered at 950 ^oC/4hrs shows best dielectric properties such as ε_r = 30.5, Q_u x f = 14700 GHz (f = 4.6 GHz) and τ_f = -18 ppm/ ^oC. The sintering temperature of $Ca[(Li_{1/3}Ta_{2/3})_{0.7}Ti_{0.3}]O_{3-\delta}$ (CLTT) ceramics is lowered by the addition of ZBS and BZBS glasses. Addition of 12 wt% of BZBS glass in CLTT ceramics sintered at 950 ^oC/4hrs shows ε_r = 32.0, Q_u x f = 9000 GHz (f = 4.7 GHz) and -41 ppm/^oC. The temperature coefficient of the CLNT-glass and CLTT-glass system are tuned in the range ± 10 ppm/^oC by increasing the rutile content in the CLNT and CLTT ceramics.The microwave dielectric properties of $Ca[(Li_{1/3}Nb_{2/3})_{0.75}\ Ti_{0.25}]O_{3-\delta}$ ceramics with 5 wt% LBS glass sintered at 950 ^oC/4hrs shows ε_r = 33, Q_u x f =11500 GHz (f = 4.6 GHz) and $\tau_f \approx$ -2 ppm/^oC. The $Ca[(Li_{1/3}Ta_{2/3})_{0.6}\ Ti_{0.4}]O_{3-\delta}$ ceramics with 12 wt% of BZBS glass sintered at 950 ^oC shows ε_r = 34.9, Q_u x f =6500 GHz (f = 4.6 GHz) and $\tau_f \approx$ -6 ppm/^oC. Compared to CLTT-glass system, the CLNT-glass system

shows excellent temperature stable microwave dielectric properties at a low sintering temperature of 950 ^{o}C and can be a promising candidate for LTCC based devices.

Sixth chapter discusses the preparation and dielectric properties $Ca[(Li_{1/3}Nb_{2/3})_{0.8}Ti_{0.2}]O_{3-\delta}$ ceramic filled polymer composites for substrate applications. The CLNT ceramic loaded polyethylene and polystyrene composites are prepared by melt mixing and hot molding techniques and the epoxy composites are prepared by mechanical mixing and thermosetting techniques. The physical and dielectric properties of the composites are investigated in terms of volume fraction of filler, frequency, and temperature. The experimentally observed relative permittivity and dielectric loss are compared with different theoretical models. As the volume fraction of filler in the polymer increases, the relative permittivity, dielectric loss and microhardness increases where as, the coefficient of linear thermal expansion decreases in CLNT ceramic reinforced polymer composites. For 0.4 volume fraction of filler loading, the Polyethylene-CLNT composite shows ε_r = 7.7 and tan δ = 0.004 and for polystyrene-CLNT composite, the ε_r = 7.4 and tan δ = 0.003 at 9 GHz. The predicted relative permittivity of this composites using Lichtenecker equation is in agreement with experimentally observed results. For 0.3 volume fraction of filler loading, the epoxy-CLNT composite shows an ε_r of 7.1 and tan δ = 0.026 at 9 GHz. The predicted relative permittivity of epoxy-CLNT composite using Lichtenecker and EMT model is in agreement with experimentally observed results. The relative permittivity of polymer-ceramic composite is almost stable with respect to temperature. Coplanar Waveguide Fed Monopole Antenna was designed and fabricated using epoxy-CLNT polymer-ceramic composite and compared the return loss characteristics with standard FR-4 epoxy.

The high permittivity ceramic-metal and polymer-ceramic-metal composites for capacitor applications are discussed in chapter seven. The effect of sintering temperature on the percolation threshold and the dielectric properties of $Ca[(Li_{1/3}Nb_{2/3})_{0.8}Ti_{0.2}]O_{3-\delta}$ (CLNT) – Ag composite for LTCC based high permittivity application is discussed in the first section and the polymer based CLNT-epoxy-Ag three phase composite for printed wiring board compatible embedded capacitor application is discussed in the next section. Addition of glass lowers the percolation threshold of CLNT – Ag composite. The sintering temperature of ceramic silver composite is found to have strong dependence on the percolation threshold. Addition of 0.17-volume fraction of silver increases the relative permittivity of CLNT + 5 wt% LBS from 32 to 272 with dielectric loss of 10^{-3} and conductivity of 1.8 x 10^{-7} S/cm at 1 MHz when sintered at 925 ^{o}C. The 0.18-volume fraction of silver loading in CLNT + 5 wt% LBS composite shows a maximum relative permittivity ($\varepsilon_r \approx 4x10^5$) with low dielectric loss ($\tan\delta \approx 10^{-2}$) at 1 MHz. The high processing temperature of the ceramic metal composite have been overcome by preparing the polymer-ceramic-metal three phase composite. Near percolation threshold (0.28 volume fraction of Ag in epoxy+0.30 V_f of CLNT) the composite shows a relative permittivity of 142 with low dielectric loss (0.15) and low conductivity (10^{-5} S/cm) at 1 MHz. The experimentally observed relative permittivity of ceramic-metal and polymer-ceramic-metal composites is in agreement with power law. These composites can be considered as promising candidate for capacitor applications.

The most important results from the thesis are summarized in Table 8.1, 8.2, 8.3 and 8.4. Table 8.1 shows the low loss, low permittivity dielectric ceramics for LTCC substrate applications. The microwave dielectric properties of polymer-ceramic composite substrate are shown in Table 8.2. The sintering temperature and microwave dielectric properties of dielectric materials for resonator application are shown in Table 8.3. The dielectric

properties of high permittivity ceramic-metal and polymer-ceramic-metal composite are given in Table 8.4.

Table 8.1 The physical microwave dielectric properties of LMS-glass and LCS- glass composite for LTCC substrate applications.

Material	Sintering Temperature (°C)	% Density	ε_r (9 GHz)	Tan δ (9 GHz)	$\tau_{\varepsilon r}$ (1MHz)
Li_2MgSiO_4 (LMS)	1250 °C/2hrs	92	5.1	0.00050	0.11%
Li_2CaSiO_4 (LCS)	1000 °C/2hrs	70	4.4	0.00600	0.03%
LMS + 1 wt% LBS	925 °C/2hrs	96	5.5	0.00007	0.08%
LMS + 2 wt% LMZBS	875 °C/2hrs	97	5.9	0.00007	0.09%
LCS + 1 wt% LBS	925 °C/2hrs	94	7.1	0.0040	0.05%

Table 8.2 Microwave dielectric properties of CLNT-Polymer composite for substrate applications.

Composite Material	Relative Density (%)	Relative Permittivity (ε_r) (9 GHz)	Dielectric loss (tan δ) (9 GHz)	Coefficient of Thermal Expansion (ppm/°C)	Water absorption (%)
PE- 0.4 V_f CLNT	96.0	7.7	0.004	91	0.07
PS- 0.4 V_f CLNT	97.5	7.4	0.003	29	0.04
Epoxy- 0.3 V_f CLNT	99.0	7.1	0.026	20	0.30

Table 8.3. The microwave dielectric properties of dielectric ceramics useful for practical applications.

Material	Sintering Temperature (°C)	ε_r	$Q_u$xf (GHz)	τ_f (ppm/°C)
$Li_2MgTi_3O_8$ (LMT)	1075	27.20	42000	(+) 3.20
$Li_2(Mg_{0.9}Zn_{0.1})Ti_3O_8$	1075	27.01	62000	(+) 1.20
$Li_2(Mg_{0.2}Zn_{0.8})Ti_3O_8$	1075	25.77	66500	(-) 10.50
$Li_2ZnTi_3O_8$ (LZT)	1075	25.56	72000	(-) 11.20
$Li_2(Mg_{0.95}Ca_{0.05})Ti_3O_8$	1075	28.38	40000	(+) 14.20
$Li_2(Zn_{0.95}Ca_{0.05})Ti_3O_8$	1075	27.06	51100	(-) 2.24
LMT + 1 LMZBS	950	25.21	55000	(+) 1.10
LMT + 3 LMZBS	925	24.54	44000	(+) 0.25
LZT + 1 LMZBS	925	24.31	58000	(-) 14.4
LZT + 3 LMZBS	900	23.24	31300	(-) 15.6
$Ca[(Li_{1/3}Nb_{2/3})_{0.8}Ti_{0.2}]O_{3-\delta}$ (CLNT)	1175	38.6	21200	(+) 4.00
$Ca[(Li_{1/3}Ta_{2/3})_{0.7}Ti_{0.3}]O_{3-\delta}$ (CLTT)	1200	36.0	29500	(-) 3.00
CLNT + 5 wt% LBS	950	30.5	14700	(-) 18
CLTT + 12 wt% BZBS	950	32.0	9000	(-) 41
$Ca[(Li_{1/3}Nb_{2/3})_{0.75}Ti_{0.25}]O_{3-\delta}$ + 5 wt% LBS	950	33.0	11500	(-) 2.0
$Ca[(Li_{1/3}Ta_{2/3})_{0.6}Ti_{0.4}]O_{3-\delta}$ + 5 wt% BZBS	950	34.9	6500	(-) 6.0

Table 8.4 Dielectric properties of high permittivity composites for capacitor applications.

Composite Material	Sintering Temperature (°C)	Relative Permittivity (ε_r) (1 MHz)	Dielectric loss (tan δ) (1 MHz)	Electrical Conductivity σ (S/cm)
CLNT + 0.3 V_f Ag	1150	260	0.002	10^{-7}
CLNT + 5 wt% LBS + 0.16 V_f Ag	925	129	0.002	10^{-7}
CLNT + 5 wt% LBS + 0.17 V_f Ag	925	272	0.003	10^{-7}
CLNT + 5 wt% LBS + 0.18 V_f Ag	925	4×10^{5}	0.10	10^{-2}
Epoxy + 0.3 V_f CLNT	-	72.3	0.065	2.51×10^{-6}
Epoxy + 0.3 V_f CLNT + 0.26 V_f Ag	-	142	0.15	2.05×10^{-5}

The dielectric materials presented in this thesis extends from low permittivity for substrate applications to high permittivity for resonator and capacitor applications. The scope for the extension of work described in this thesis lies mainly in two areas: Tape casting and fabrication of antennas. First one is the tape casting of LTCC dielectric ceramics reported in the present investigation. Design and fabrication of microstrip antenna using the tape would be of great scientific and technological importance. It is intresing to study the variation of antenna properties with the permittivity and loss tangent of the various substrates. Hence fabrication of antennas on ceramic polymer composites and investigating there properties are another topic to be pursued.

Present work reports several temperature stable, low loss, high permittivity ceramics. Design and fabrication of dielectric resonator antennas having different geometries (Hemispherical and Conical) using these ceramics and polymer-ceramic composite is also to be investigated. The $Li_2Mg_{1-x}Zn_xTi_3O_8$ ceramics shows excellent microwave dielectric properties at a low sintering temperature of 1075 °C. The effect of different

synthesis methods such as hydrothermal, sol-gel, citrate-gel and co-precipitation on the sinterability and microwave dielectric properties of these ceramics and the possible substitution of Mg and Zn with Ni, Mn, Co and Cu are also to be investigated.

List of publications

Patent

1. M. T. Sebastian**, Sumesh George**, P. S. Anjana, "Low loss Low Temperature Co-fired Ceramics for millimeter wave applications" (Ref. No. 0104NF2008).

Publications

2. **Sumesh George**, J. J. and M. T. Sebastian, "Gaint permittivity of of Bismuth Zinc Niobate-Silver composite". ***J. Am. Ceram. Soc.*** 2007; 90: 3522.
3. **Sumesh George**, N. Santha and M. T. Sebastian, "Percolation Phenomenon in Barium Samarium Titanate-Silver composite" ***J. Phys. Chem. Solids***. 2009; 70, 107.
4. **Sumesh George**, M. T. Sebastian **"**Effect of sintering temperature on the percolation threshold and the dielectric properties $Ca[(Li_{1/3}Nb_{2/3})_{1-x}Ti_x]O_{3-\delta}$ – Ag composite" ***Comp. Sci. and Tech.*** 2008; 68, 2461.
5. **Sumesh George**, M. T. Sebastian "Effect of lithium based glass addition on the microwave dielectric properties of $Ca[(Li_{1/3}Nb_{2/3})_{1-x}Ti_x]O_{3-\delta}$ ceramics" ***J. All. Comp.*** 2008; 473, 336.
6. **Sumesh George**, M. T. Sebastian, "Enhanced permittivity by the adhesion of conducting and low loss insulating ceramics in polystyrene" ***J. Appl. Poly. Sci***. 2009;114, 1682.
7. **Sumesh George**, M. T. Sebastian **"**Three-phase polymer–ceramic–metal composite for embedded capacitor applications" ***Comp. Sci. and Tech.*** 2009; 69, 1298.
8. **Sumesh George**, P. S. Anjana, V. Deepu, P. Mohanan and M. T. Sebastian, "Low temperature sintering and microwave dielectric properties Li_2MgSiO_4 ceramic for LTCC based devices" ***J. Am. Ceram. Soc.*** 2009; 92, 1244.
9. S. Butee, A. Kulkarni, Om Prakash, R.P.R.C. Aiyar**, Sumesh George,** M.T.Sebastian, "High Q Microwave Dielectric Ceramics in $(Ni_{1-x}Zn_x)Nb2O6$ System" ***J. Am. Ceram. Soc.*** 2009; 92, 1047.
10. H. Padmakumar, **Sumesh George**, J. K. Thomas, S. Solomon, "Synthesis, structural analysis and microwave dielectric properties of $Bi_xLn_{1-x}TiTaO_6$ (Ln = Ce, Pr and Nd) Ceramics" ***J. Mater. Sci: Mater. Elect.*** 2009; (in press).

11. S**umesh George,** S. Raman , P. Mohanan and M. T. Sebastian**,** **"**Novel low loss low permittivity glass-ceramic composites for LTCC applications" ***Int. J. Appl. Ceram. Soc***. 2009; (in press).

12. **Sumesh George**, V. Deepu, P. Mohanan and M. T. Sebastian, "Influence of $Ca[(Li_{1/3}Nb_{2/3})_{0.8}Ti_{0.2}]O_{3-\delta}$ filler on the microwave dielectric properties of polyethylene and polystyrene for microelectronic applications" ***J. Ploy. Engg. Sci***. 2009; (in press).

13. **Sumesh George**, P. S. Anjana, J. Krupka, S. Uma, J. Philip and M. T. Sebastian, "Dielectric, mechanical, and thermal properties of low permittivity polymer-ceramic composites for microelectronic applications" ***Int. J. Appl. Ceram. Soc***. 2009; (in press).

14. P. S. Anjana, **Sumesh George** and M. T. Sebastian, "Giant permittivity of CeO_2- $La_{0.5}Sr_{0.5}CoO_{3-\delta}$ composite" ***J. Phys. D. Appl. Phys***. 2009; 42, 225502.

15. **Sumesh George**, S. Raman, S. Uma, J. Philip and M. T. Sebastian, "Epoxy based Polymer Ceramic Composites for Microelectronic applications" ***J. Phys. D. Appl. Phys***. 2009; (communicated).

16. **Sumesh George**, and M. T. Sebastian, **"**Low Temperature Sintered $Ca[(Li_{1/3}A_{2/3})_{1-x}M_x]O_{3-\delta}$ [A=Nb, Ta and M=Ti, Zr, Sn] complex perovskites: a review" ***Chapter of the book, Nova publishers, UK***. 2009; (Communicated).

17. **Sumesh George**, and M. T. Sebastian, **"**Novel temperature stable high Q materials for resonator applications" ***Appl. Phys. Lett.*** . 2009; (communicated).

18. J. Chameswary, K. Jithesh, **Sumesh George**, S. Raman, P. Mohanan, and M. T. Sebastian, "PTFE-SWNT Composite for Microwave Absorption Application" ***Mater. Lett.*** 2009; (communicated)**.**

19. **Sumesh George**, V. K Sajith, and M. T. Sebastian, "Effect of borosilicate glass additions on the sinterability and microwave dielectric properties of $Ca[(Li_{1/3}Ta_{2/3})_{1-x}Ti_{x}]O_{3-\delta}$ ceramics" ***J. Mater. Sci: Mater. Elect.*** (2009), (to be communicated).

20. **Sumesh George**, V. K Sajith, S. Raman, P. Mohanan and M. T. Sebastian, "Microwave Dielectric Properties of Li_2MgSiO_4 Ceramics prepared by citrate gel route for LTCC Substrate" ***J. Am. Ceram. Soc.*** (2009), (to be communicated).

International conferences

1. **Sumesh George,** P. S Anjana, Jerzy Krupka and M. T. Sebastian, "Microwave dielectric properties of Polystyrene /Li_2MgSiO_4 composites for microelectronic applications" MMA-2008, China.
2. **Sumesh George,** G. Subodh, and M. T. Sebastian "Modeling Relative Permittivity of Ceramic Polymer Composites" ICAFM, Dec 9-10, 2009, Trivandrum.
3. **Sumesh George** and M. T. Sebastian "Epoxy based composites for substrates and embedded capacitor applications" ICE-2009, Dec-13-17, University of Delhi.
4. **Sumesh George,** V. K. Sajith, P. Mohanan and M. T. Sebastian, "Microwave Dielectric Properties of Low Temperature Sintered Bulk and Nano Li_2MgSiO_4 Ceramics" ISMOT-2009, Dec-16-19, Delhi.
5. M. T. Sebastian, **Sumesh George** and S. Thomas "Low Loss Low Permittivity Silicate Based Dielectric Ceramics for LTCC Applications" ISMOT-2009, Dec-16-19, Delhi.
6. M. T. Sebastian, S. Thomas and **Sumesh George, "**Effect of Filler on the Microwave Dielectric Properties of Polyethylene/Ceramic Composites" IEEE- Kolkatta Dec. 13-16, 2009.
7. **Sumesh George** and M. T. Sebastian, "Microwave dielectric properties of $Ca[(Li_{1/3}Nb_{2/3})_{1-x}Ti_x]O_{3-\delta}$ ceramics with lithium magnesium zinc borosilicate glass" IEEE- Kolkatta Dec. 19-20, 2007.
8. **Sumesh George,** S. Thomas, S. Renjini, T. S. Sasikala, P. S. Anjana and M. T. Sebastian "Effect of lithium borosilicate glass addition on the microwave dielectric properties of low loss ceramics" ICAMC 2007 , Trivandrum.
9. P. S. Anjana, **Sumesh George**, S. Thomas, **G. Subodh**, M. T. Sebastian and P. Mohanan "Effect of filler on the microwave dielectric properties of PTFE/ceramic composites" ICAMC 2007, Trivandrum.
10. M. T. Sebastian, **Sumesh George**, P. S. Anjana, S. Thomas, and G. Subodh, "Polyethylene ceramic composites for electronic packaging applications" p. 161, Microwave 2008, Nov. 21-24 Jaipur.

National Conferences - 4